Structures Research
Report 2013/96918

University of Florida
Civil and Coastal Engineering

University of Florida
Civil and Coastal Engineering

Final Report April 2013

Determination of Multi-Barge Flotilla Impact Loads on Bullnose Structures and Flexible Timber Guide Walls

Principal investigator:
Gary R. Consolazio, Ph.D.

Doctoral research assistant:
John R. Wilkes, P.E.

Department of Civil and Coastal Engineering
University of Florida
P.O. Box 116580
Gainesville, Florida 32611

Sponsor:
Digital Engineering and Imaging, Inc.
U.S. Department of the Army
Point of Contact:
Robert C. Patev, Senior Risk Advisor, Risk Management Center, US Army Corps of Engineers

Contract:
UF Project No. 96918
Digital Engineering and Imaging, Inc. No. 674-01-0198-21
U.S. Dept. of the Army No. W912P8-07-D-0054

DISCLAIMER

The opinions, findings, and conclusions expressed in this publication are those of the authors and not necessarily those of the U.S. Department of the Army or Digital Engineering and Imaging, Inc.

ACKNOWLEDGEMENTS

The authors would like to thank the U.S. Department of the Army and Digital Engineering and Imaging, Inc. for providing the funding that made this research possible.

TABLE OF CONTENTS

LIST OF FIGURES

LIST OF TABLES

Table Page

CHAPTER 1
INTRODUCTION AND BACKGROUND

1.1 Introduction

Throughout the United States, navigational structures located along inland waterways play a vital role in guiding and controlling barge traffic. Structural guard walls and guide walls are commonly used to protect dams (and hydroelectric facilities) from intrusion and damage from barge traffic, and to help guide barge flotillas (also called barge 'tows') into lock chambers. At the terminal ends of such walls are relatively rigid reinforced concrete structures known as bullnoses (Figure 1.1). Bullnose structures are subjected to low-level (service level) impacts from controlled barge flotillas as they align to enter locks as well as less-frequent, but much more severe, high energy impacts (Figure 1.2) from errant (out of control) barge flotillas. Consequently, navigational structures terminating in a bullnose configuration must be designed to adequately resist both service level as well as severe barge impact loading conditions.

a)

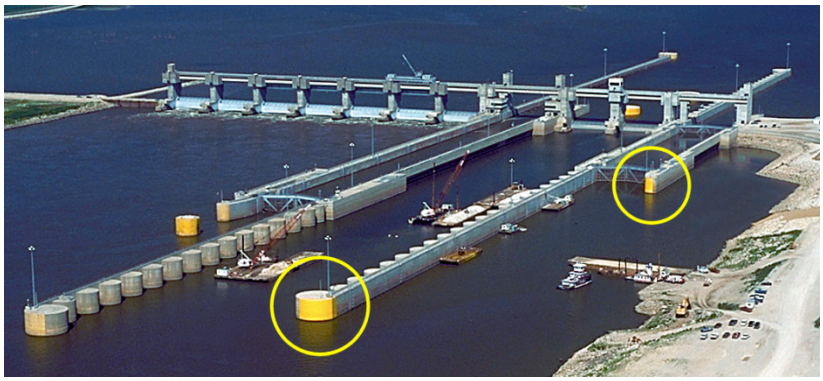

b)

Figure 1.1. Bullnose structures:
a) Sloped-V bullnoses at wall ends, Mississippi River Lock and Dam No. 22;
b) Circular bullnoses at wall ends, Mississippi River Lock and Dam No. 26
(Photo credit: U.S. Army Corps of Engineers)

Figure 1.2. Barge damage caused by high energy impact with a bullnose structure
(Photo credit: U.S. Army Corps of Engineers)

It is well established in the literature that the mass, velocity, and angle of travel of a barge flotilla will determine, in part, the forces that are generated on a structure during a barge impact event. It is also understood that the force-deformation relationship (i.e., the stiffness) of the barge will influence, again in part, the impact load magnitude. However, complicating the process of determining suitable design loads is the fact that a barge flotilla may partially breakup during impact. Flotilla breakup can occur if a sufficient number of wire rope lashings—used to connect adjacent barges together within the flotilla—fail, thus permitting portions of the flotilla to separate and float freely.

In a multi-string (also called multi-column) flotilla, the lashings that connect the impacting string to the rest of the flotilla may fail during impact. In such a scenario, it is important to determine whether the magnitude of impact forces generated is controlled primarily by the kinetic energy (or momentum) of the entire flotilla or just that of the impacting column of barges. Damage to structures such lock walls, guard walls, guide walls, and dams can be further compounded if flotilla breakup results in individual free floating barges. Uncontrolled, free floating barges (Figure 1.3) can significantly impair nearby waterway facilities either directly from structural damage or indirectly by shutting down operations.

Figure 1.3. Individual barges jammed against Marseilles, Illinois Dam after breaking free from remainder of barge flotilla (2013)
(Photo credit: U.S. Coast Guard)

It is therefore highly desirable that methods used to assess impact loads on bullnose structures be capable of accounting for both 1) the high-level, inelastic deformation response of barges that can occur during severe impacts, and 2) the potential for lashing failures and flotilla breakup. Past approaches to quantifying barge flotilla impact loads have involved relatively expensive impact experiments, which were often limited—for safety reasons—to low-energy impact conditions. In such experiments, barge deformations are generally minimal or moderate levels and flotilla breakup is carefully avoided. As a result, there is a scarcity of experimental data available for high energy barge flotilla impacts on bullnose structures. Such data scarcity can lead to conservatism in the formulation of design loads, which may then increase the cost of construction. Given that the U.S. Army Corps of Engineers (USACE) has responsibility for designing bullnose structures (as well as guard and guide walls) to resist high-energy flotilla impact loads, the analytical study documented in this report is undertaken to quantify impact loads on bullnose structures. High-resolution nonlinear dynamic finite element impact simulations are used to quantify impact loads in a manner that accounts for the effects of the impacting barge mass, speed, angle, severe barge deformation, and the potential for lashing failure and flotilla break-up.

An additional area in which improved flotilla impact load data are needed, and which is addressed in this study, is the design of flexible timber guide walls. Of particular interest to the USACE was determining the magnitudes of impact forces that are generated during shallow angle barge impacts on flexible timber guide walls that are constructed from timber piles and reinforced plastic wales (Figure 1.4). Because these structural systems are very flexible in comparison to the stiffness of an impacting barge, impact load prediction equations previously derived from rigid wall studies may be of limited value when attempting to quantify appropriate design loads for flexible timber guide walls. As such, an investigation aimed at quantifying barge impact loads on a typical flexible timber guide wall is included in this study to initiate the process of developing load prediction equations that are appropriate for these types of structural systems.

Figure 1.4. Flexible timber guide wall structure
(Photo credit: U.S. Army Corps of Engineers)

1.2 Objective

The primary objective of this study is to use nonlinear dynamic finite element impact simulation techniques to quantify time-varying (transient) barge flotilla impact forces on both bullnose structures and flexible timber guide wall structures over a range of different impact conditions (flotilla size, flotilla mass, impact speed, impact angle, impact string, impact site [bow, stern], bullnose shape, bullnose slope, wall impact location, soil strength, etc.). A secondary objective is to identify which flotilla parameters (e.g. total flotilla momentum, lead row momentum, impact string momentum, etc.) are best correlated to (i.e., constitute the best predictors of) peak impact load for each type of structure of interest (bullnose, flexible timber guide wall).

1.3 Scope of work

In earlier studies, finite element procedures for modeling individual barges (Consolazio et al. 2010) and large multi-barge flotillas were developed and used to numerically simulate oblique impacts on rigid wall structures (Consolazio et al. 2012) and semi-flexible concrete guide wall structures (Consolazio and Walters 2012). In the present study, the previously developed flotilla modeling procedures are modified and utilized to quantify impact loads for nearly head-on impacts on bullnose structures, and oblique impacts on a flexible timber guide wall structure. High-resolution finite element barge flotilla models employed in this study range in size from one (1) jumbo hopper river barge to fifteen (15) barges. Determination of barge flotilla impact forces is accomplished generally as described below.

1.3.1 Determination of bullnose impact loads

Finite element models of bullnose structures of various shapes and sizes (primarily 10 ft diameter, 35 ft diameter, and sloped-V) are developed based on the assumption that the foundations of the bullnose structures are rigid. Bullnose structural models are integrated together with barge flotilla models of various configurations for the purpose of conducting impact analyses. Modifications are made to the ‘deformable’ impacting barge within the flotilla as is necessary for each individual impact condition simulated. Integrated bullnose and barge flotilla models incorporate appropriate contact definitions, frictional parameters, buoyancy effects, gravity, and lashing modeling. Using integrated bullnose and barge flotilla models, seventy-eight (78) impact simulations are conducted to quantify time-varying impact forces.

1.3.2 Determination of flexible timber guide wall impact loads

A finite element modeling technique is developed to represent timber piles in the elastic response range. Material parameters are obtained from relevant literature. A finite element modeling technique is developed to represent the flexural behavior of plastic wales, which are square in cross-section, with internal fiberglass reinforcing bars. Relevant literature is reviewed to determine appropriate material parameters. An overall system model is constructed consisting of piles, wales, thrust blocks, and various components deemed to be structurally relevant. A representative soil profile (layering) is established based on typical conditions in which timber guide walls are installed. Soil parameters are approximated with the goal of producing conservative estimates of barge impact forces. Soil layer parameters are used to compute force-displacement curves for vertical and lateral soil springs that are, in turn, attached to timber pile

elements. The flexible timber guide wall structural model is then integrated together with barge flotilla models of various configurations for the purpose of conducting impact analyses. Integrated flexible timber guide wall and barge flotilla models incorporate appropriate contact definitions, frictional parameters, buoyancy effects, gravity, and lashing modeling. Using integrated flexible timber guide wall and barge flotilla models, thirty (30) impact simulations are conducted to quantify time-varying impact forces.

CHAPTER 2
BARGE FLOTILLA FINITE ELEMENT MODEL

2.1 Introduction

This study is concerned with loads from impact events between barge flotillas and both bullnose structures and timber founded guide walls. Specifically, the barge flotillas under investigation are comprised of fully-loaded jumbo hopper barges. All simulations conducted for this study utilize a highly discretized, high resolution, finite element (FE) model of an impacting barge. This high resolution barge model is, in most cases, attached to lower resolution non-impacting finite element barge models to form a complete flotilla. A barge flotilla (e.g., Figure 2.1) is an assembly of individual barges, typically of similar size and configuration, which are temporarily connected together by a series of wire ropes (also known as lashings).

The maximum size flotilla of interest in this study is a 3x5, which includes a total of fifteen (15) barges comprised of three (3) strings with five (5) barges per string. Additionally, seven other flotilla configurations are modeled: 3x4, 3x3, 2x5, 2x3, 1x5, 1x3 and 1x1 (i.e. a single barge) model.

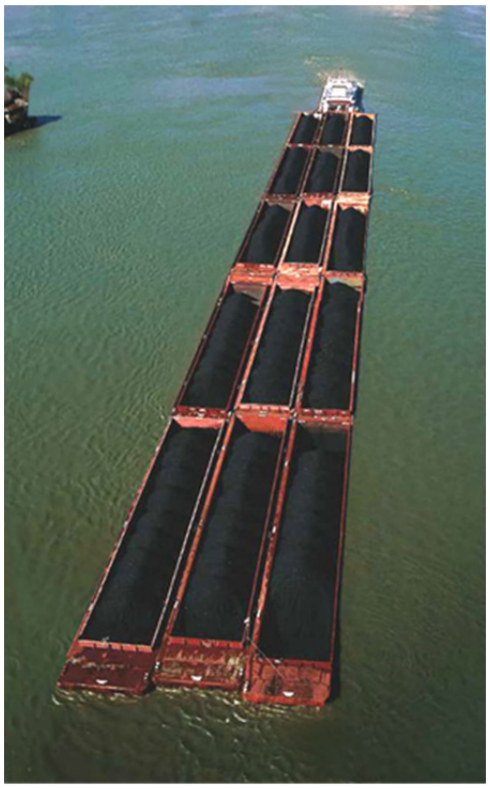

Figure 2.1. Typical 3x5 barge flotilla in transit (after USACE 2007)

Barge flotilla finite element models used in this study are created using the methodology described in *Development of Finite Element Models for Studying Multi-barge Flotilla Impacts* (Consolazio et al. 2012) and *Development of Multi-Barge Flotilla Finite Element Models for Use in Probabilistic Barge Impact Analysis of Flexible Walls* (Consolazio and Walters 2012). These reports provide detailed documentation of the methods used in the development of the barge flotilla models. In the sections that follow, key aspects of the barge flotilla models are

summarized, and noteworthy modifications to the previously developed models, necessary for the present study, are described.

Each barge flotilla model is comprised of a series of jumbo hopper river barges measuring 195 ft long by 35 ft wide and weighing 2000 tons each (where 1 ton = 2000 lbs). Two configurations of this jumbo hopper river barge are employed in each flotilla model: single-raked and double-raked. Single-raked barges are raked (tapered through the depth) at the bow only, whereas double-raked barges are raked at both the bow and stern. Single-raked barges are present at the fore-most and aft-most barge positions of each string of barges while double-raked barges are only present in between the fore- and aft-most barges in each string. A schematic of each jumbo hopper barge is shown in Figure 2.2.

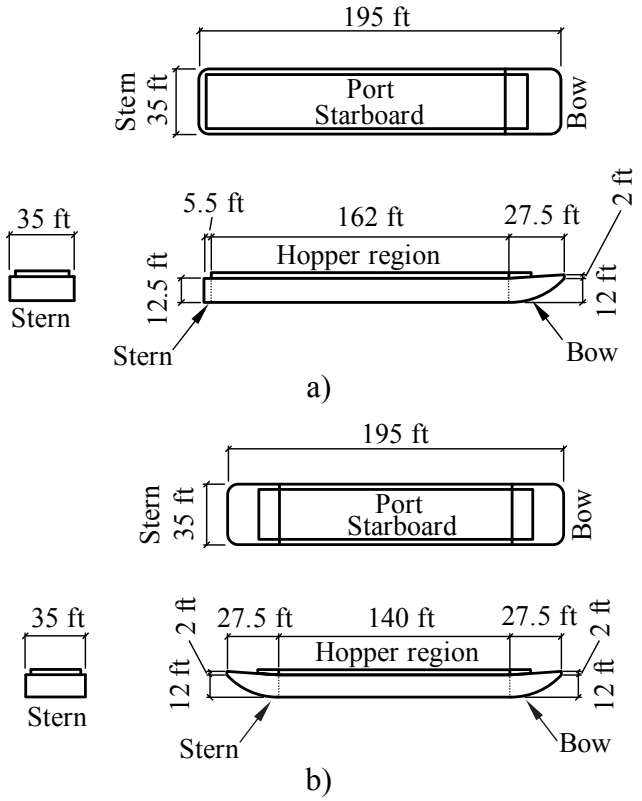

Figure 2.2. Jumbo hopper barge schematics:
a) Single-raked barge; b) Double-raked barge

Two (2) of the eleven (11) flotilla configurations used in this study are illustrated in Figure 2.3. Overall dimensions and weights of all flotilla configurations used in this study are listed in Table 2.1.

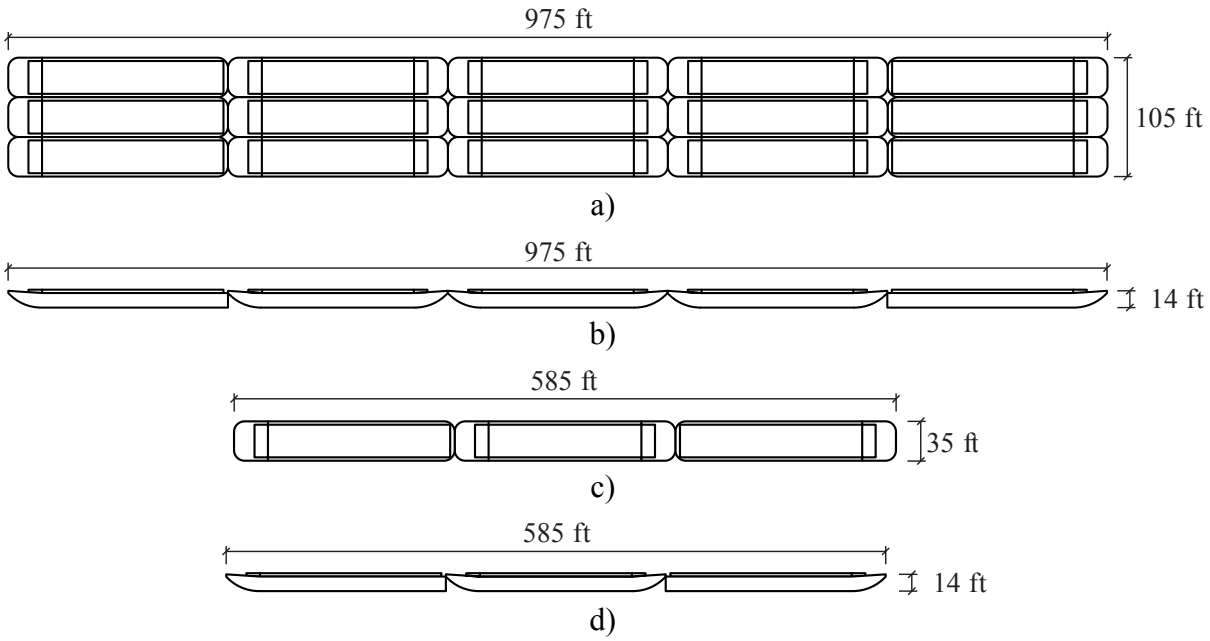

Figure 2.3. Jumbo hopper barge flotilla schematics:
a) 3x5 plan view; b) 3x5 elevation view; c) 1x3 plan view; d) 1x3 elevation view

Table 2.1. Jumbo hopper barge flotilla dimensions and weights

Flotilla Size	Used in Bullnose Impacts	Used in Flexible Timber Guide Wall Impacts	Flotilla Length (ft)	Flotilla Width (ft)	Flotilla Weight (tons)
1 x 1	✓	✓	195	35	2,000
1 x 2		✓	390	35	4,000
1 x 3	✓	✓	585	35	6,000
1 x 5	✓		975	35	10,000
2 x 1		✓	195	70	4,000
2 x 2		✓	390	70	8,000
2 x 3	✓	✓	585	70	12,000
2 x 5	✓		975	70	20,000
3 x 3	✓		585	105	18,000
3 x 4	✓		780	105	24,000
3 x 5	✓		975	105	30,000

2.2 Modeling of barges

Two types of individual barge finite element models are used within each flotilla model (Figure 2.4). A single high-resolution barge, referred to as the *impacting* barge, is the only barge to make physical contact with the target structure (bullnose or flexible timber guide wall). The high level of discretization associated with the impacting barge is necessary to enable accurate representation of the contact interaction between the target structure and impacting barge. The remaining low resolution barges within a given flotilla are referred to as *non-impacting* barges.

The primary role of non-impacting barges is to facilitate modeling the dynamic response resulting from barge-to-barge contact and lashing interactions of adjacent barges during impact. Note that the non-impacting barges never make contact with the target structure.

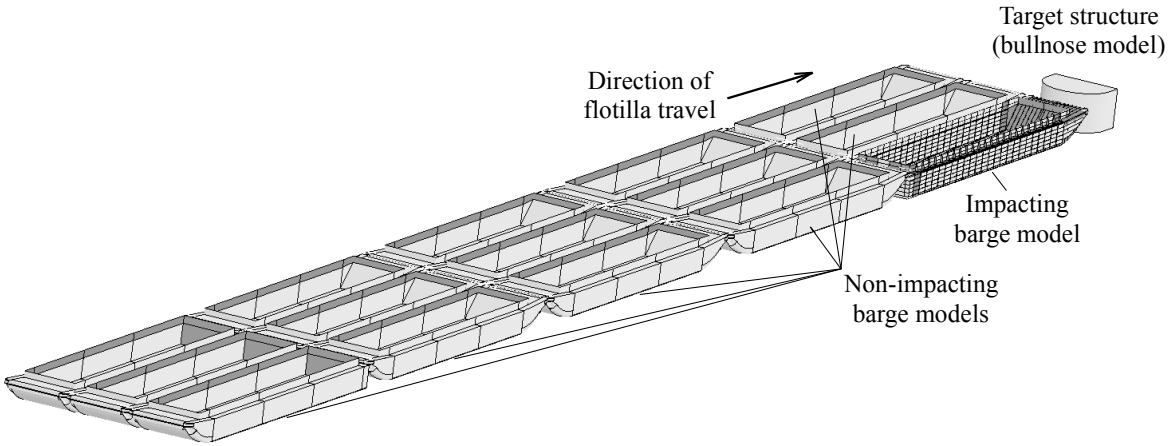

Figure 2.4. Flotilla impact simulation model consisting of a single impacting barge model, multiple non-impacting barge models, and a target structure
(Note: only key geometric edge lines are shown; element mesh not shown for clarity)

2.2.1 Impacting barge

The high resolution impacting barge finite element model is composed of more than 900,000 nonlinear shell elements modeled in LS-DYNA. The barge structural model is consistent with available detailed structural plans and is made up of three barge zones: the bow zone, the stern zone, and the hopper zone. Each zone is discretely modeled with internal structural members and external plate surfaces. Internal structural members consist of angle, channel, or gusset plate sections. Internal member thicknesses and external plate thicknesses vary between 5/16 in. and 5/8 in., as determined from structural plans. Figure 2.5 shows a rendering of the impacting barge. An example of the high level of mesh discretization is demonstrated in Figure 2.6, which shows a rendering of the bow zone of the impacting barge FE model.

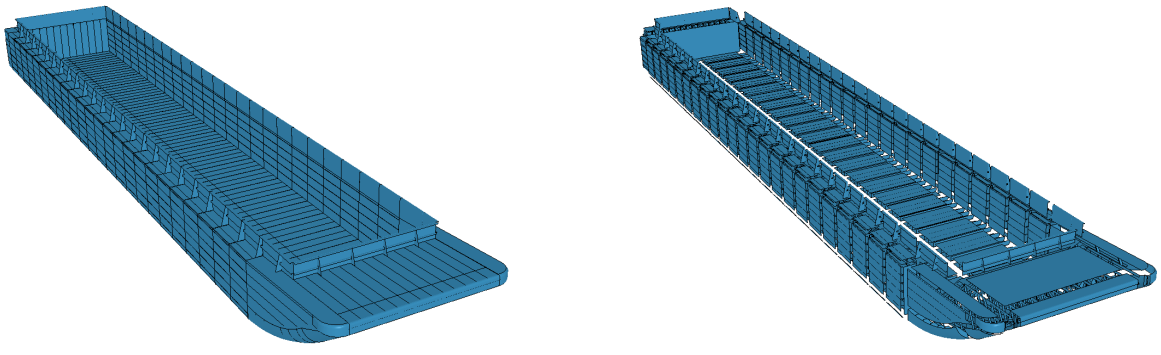

a) b)

Figure 2.5. Jumbo hopper barge finite element model (mesh not shown for clarity):
a) Perspective view; b) Exploded view

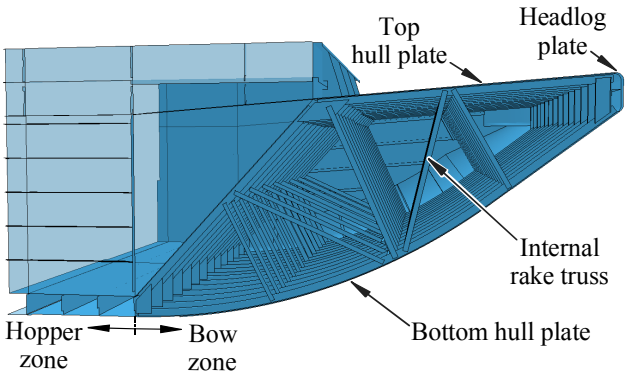

a)

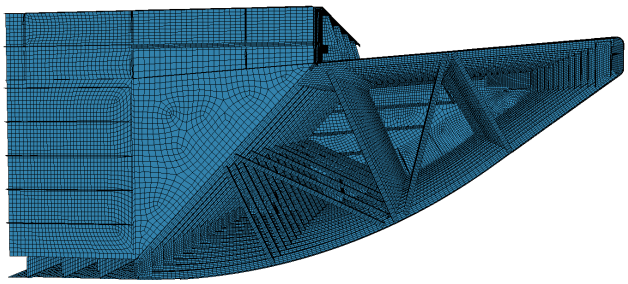

b)

Figure 2.6. Barge bow zone: a) Structural configuration; b) finite element mesh

The high resolution impacting barge model has been given a nonlinear constitutive relationship (effective true stress vs. effective plastic strain) representing A36 structural steel with the Cowper-Symonds strain rate material model and the strain rate parameters described in Consolazio and Walters (2012). All internal structural members and plates are defined by 4-node, fully integrated shell elements with sufficient mesh density to allow local buckling and local material failure to be represented. Material failure is represented in the simulation models by element deletion, and is specified to occur at an effective plastic strain of 0.2 in./in. [Full details regarding the steel material model can be found in Consolazio and Walters (2012)].

2.2.1.1 Modeling high deformation bow impacts

In previous studies (Consolazio et al. 2010, Consolazio et al. 2012, Consolazio and Walters 2012) that utilized the high resolution impacting barge model described above, the conditions that were simulated involved glancing (oblique) impacts on walls, and generally produced only moderate bow or stern corner crushing deformation (typically limited to less than 1 ft in depth). Consequently, a large portion of the impacting barge model (specifically, portions outside the deformation zone) could be 'rigidized' to gain significant numerical efficiency.

In contrast, a key focus of the present study involves quantifying impact forces that are generated during *high energy* bullnose impacts—conditions that are expected to cause large-scale (high-level) barge deformations (Figure 2.7) including plate fracture and inelastic structural member buckling. Consequently, the deformable (i.e., non-rigidized) portion of the impacting barge model that is used in the bullnose simulations is much larger than that which was used in

previous studies. Hence, for bullnose impact simulations, the impacting barge model is modified to permit deformation levels on the order of 10 – 20 ft. For bow impacts, this change requires that all shell elements representing the bow and adjacent hopper region: 1) be fully deformable; 2) make use of the nonlinear material model noted earlier; and 3) be included in contact definitions (so that interactions between various internal structural members can be properly accounted for as buckling occurs). To achieve this outcome, the deformable portion of the barge is configured to include the entire bow and approximately 20 ft of the hopper region (Figure 2.8). A detailed view of the mesh resolution of the deformable portion of the impacting barge model used in bullnose impact conditions is provided in Figure 2.9. In Figure 2.10, a geometric rendering (mesh resolution omitted for clarity) of a barge flotilla configured for bow impact against a circular bullnose model, is provided.

Figure 2.7. Severe bow deformations from barge impact at Mississippi River Lock and Dam No. 9.
(Photo credit: U.S. Army Corps of Engineers)

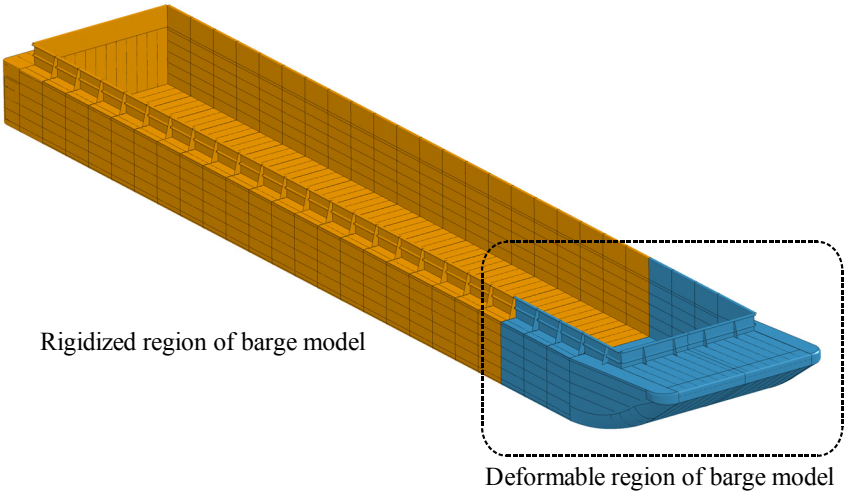

Figure 2.8. Deformable and rigidized portions of impacting barge model (as used in bow impact simulations on bullnose structures)

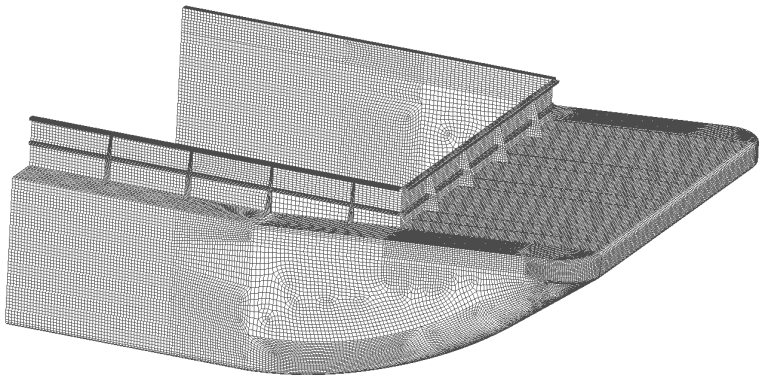

Figure 2.9. Finite element mesh of deformable portion (bow and ~20 ft of hopper) of impacting barge model (as used in bow impact simulations on bullnose structures)

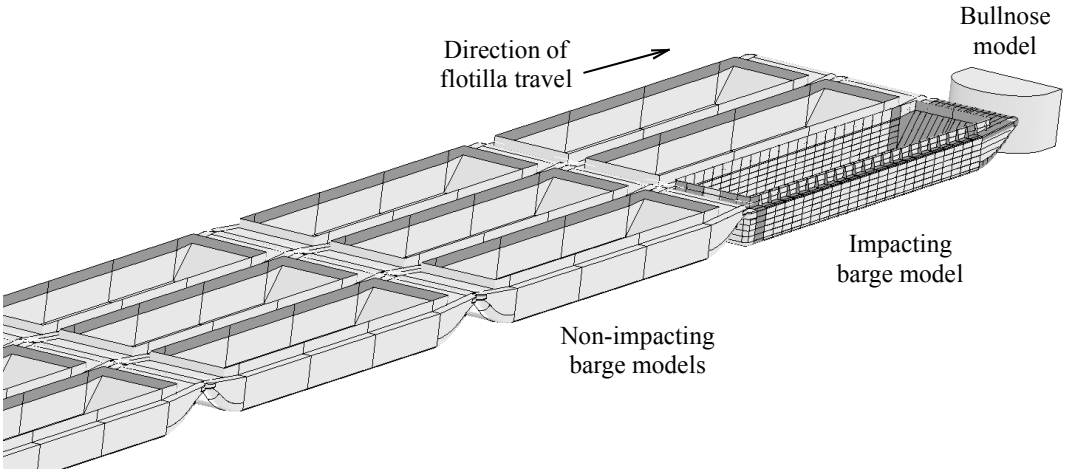

Figure 2.10. Barge flotilla model configured for bow impact against a circular bullnose

2.2.1.2 Modeling high deformation stern (boxed-end) impacts

In addition to simulating bow impact conditions, stern impacts are also simulated in this study. In a stern impact condition, the boxed end of the high resolution impacting barge model makes contact with the bullnose structure (Figure 2.11). Contact force-time histories from stern impact simulations are compared (later in this report) to analogous bow results in an effort to identify which end of the impacting barge produces higher peak impact forces. Developing an impacting barge model for stern impacts involves maintaining correct mesh connectivity (using nodal constraints), establishing appropriate contact definitions in the stern end of the barge, and initializing lashing pretension forces (Consolazio et al 2012, Consolazio and Walters 2012) while simultaneously mixing deformable and rigid materials. In addition to making these changes to the impacting barge model, configuring the overall flotilla model for stern impact conditions further requires rotating all barges in the lead row by 180 degrees (Figure 2.12) and then re-lashing them to the rest of the flotilla in the correct configuration.

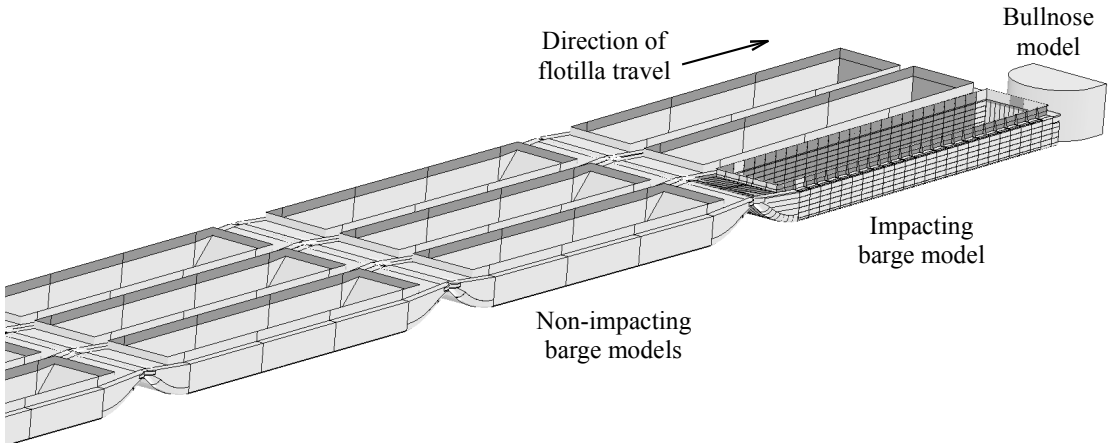

Figure 2.11. Barge flotilla model configured for stern impact against a circular bullnose

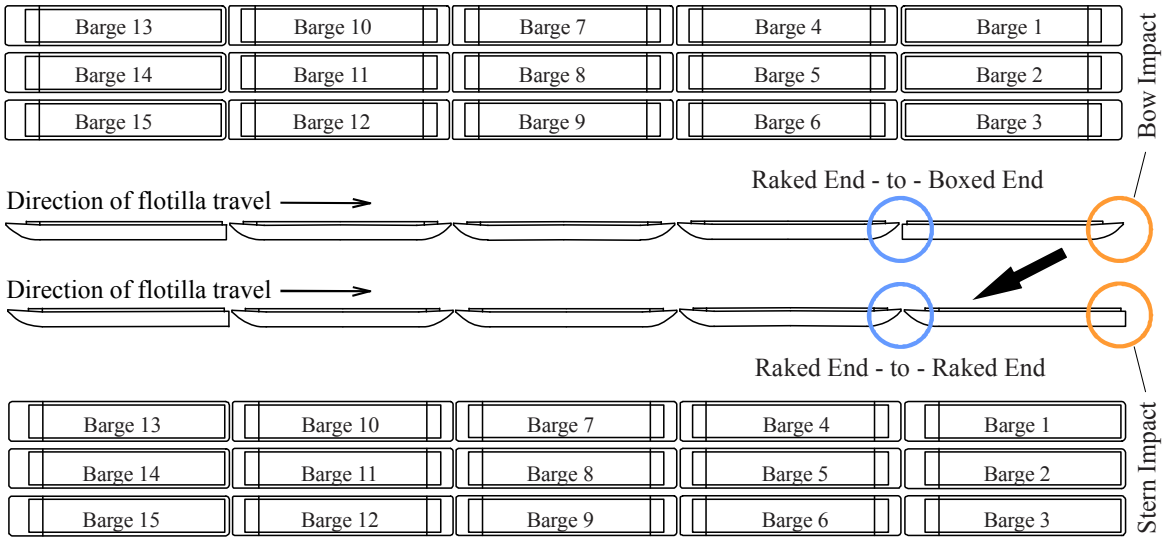

Figure 2.12. Rotation of barges in lead row of flotilla for use in stern bullnose impact simulations

During impact, it is important that the headlog areas on the impacting barge and the non-impacting barge share a sufficient common contact area (Figure 4.6). The contact stiffness of any pair of distinct surfaces is predicated upon the availability of sufficient surface area. In past studies (Consolazio et al. 2012, Consolazio and Walters 2012), headlog extension plates were added to the non-impact barge models to ensure barge-to-barge contact compatibility. In the present study, for stern impact bullnose simulations, additional headlog extension plates are similarly added to the high resolution impacting barge model (Figure 2.14). These plates are installed only for inter-barge contact, and thus play no role in contact with any structures outside of the flotilla.

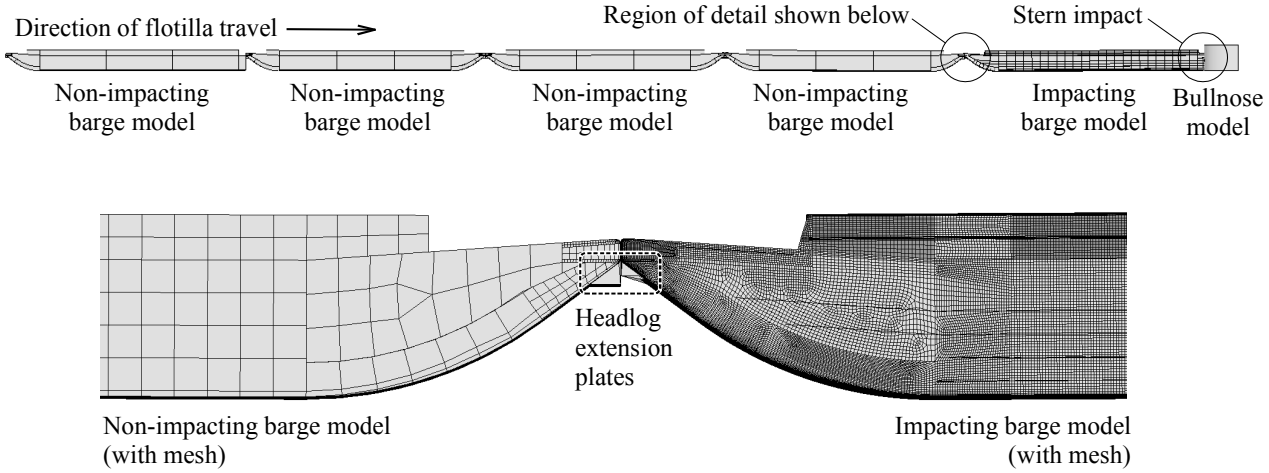

Figure 2.13. Contact between barge bows in stern impact flotilla model (headlog extension plates present in non-impacting barge models [left] and impacting barge model [right])

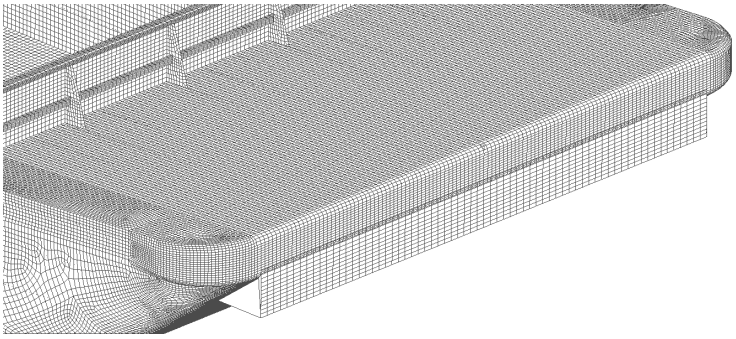

Figure 2.14. Headlog extension plates added to bow of impacting barge model

For stern impacts, all shell elements representing the stern and adjacent hopper region are fully deformable; make use of the nonlinear material model noted earlier; and are included in contact definitions (so that interactions between various internal structural members can be properly accounted for as buckling occurs). To enable modeling of high deformation stern impacts, the deformable portion of the barge is configured to include the stern and approximately 27 ft of the rear hopper region (Figure 2.15). A detailed view of the mesh resolution of the deformable stern portion of the impacting barge model, as used in bullnose impact conditions, is provided in Figure 2.16.

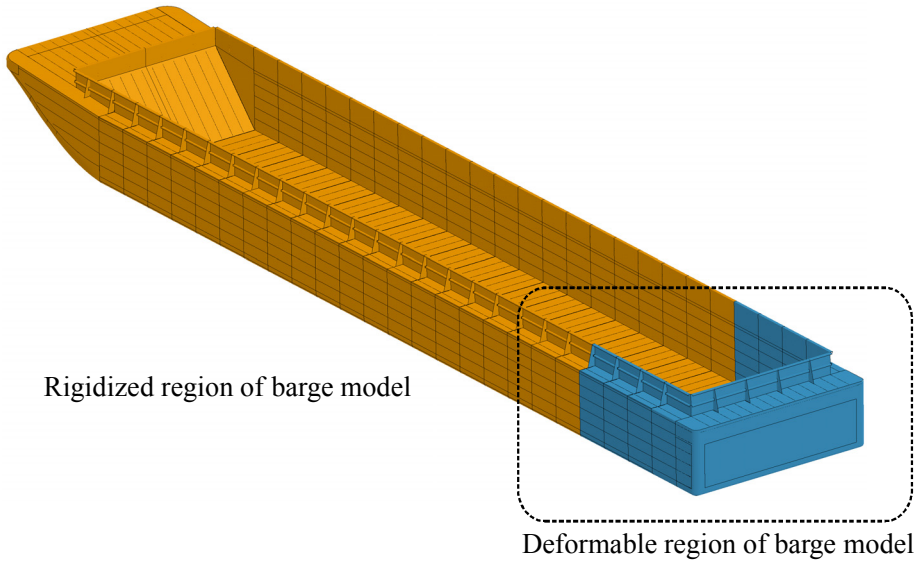

Figure 2.15. Deformable and rigidized portions of impacting barge model (as used in stern impact simulations on bullnose structures)

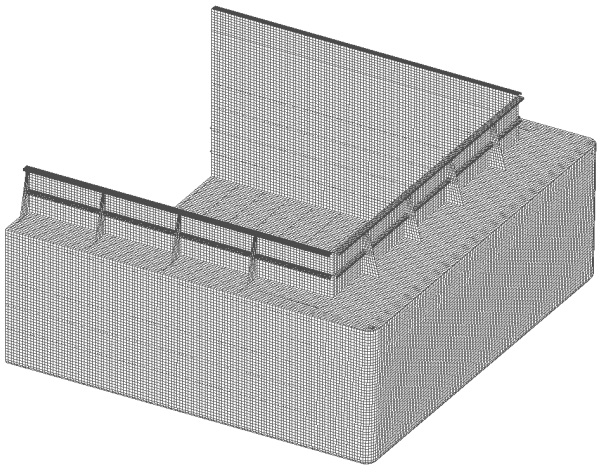

Figure 2.16. Finite element mesh of deformable portion (stern and ~27 ft of hopper) of impacting barge model (as used in stern impact simulations on bullnose structures)

2.2.1.3 Interior String Impacts

A particular area of interest in this study is determining how impact forces generated by exterior string impacts (Figure 2.17a) compare to forces generated by analogous (same speed, same flotilla mass, etc.) interior string impacts (Figure 2.17b). If the flotilla lashings were to possess zero stiffness and zero strength (i.e., break immediately upon impact), then the impact forces for exterior and interior string impacts would be expected to be nearly identical since the characteristics (mass, stiffness, etc.) of the impacting string would be identical in each case. Conversely, if the flotilla lashings were to possess infinite stiffness and infinite strength (i.e., no possibility of breaking), then impact forces for exterior and interior string impacts would again be expected to be very similar since in each case the mass of the entire flotilla would determine

the impact forces generated. However, if the lashings possess finite stiffness and finite strength, as is the case in realistic situations, then the possibility for differences between exterior and interior string impact force arises.

As the impacting string makes contact with the bullnose, it will decelerate as a result of the impact force (load) generated at the bullnose. Simultaneously, momentum will tend to drive the non-impacting strings forward, generating shear forces along the planes that exist between the impacting string and the rest of the flotilla. These shear forces may cause further increase in the force that the impacting string imparts to the bullnose. However, as these shear forces develop, forces in the lashings will also increase. If sufficient shear force is generated, it is possible that all of the lashings along a plane between the impacting string and an adjacent string may fail, thereby separating the two portions of the flotilla. Once such a failure occurs, the non-impact barges would no longer substantially affect the impact force imparted to the bullnose.

Importantly, in an exterior string impact, only lashings along a single plane need to fail to completely separate the impacting string from the momentum of the rest of the flotilla. However, in an interior string impact, twice as many lashings (two planes) must fail in order to separate the impacting string from the rest of the flotilla. Consequently, it is possible that in interior string impacts, the momentum of the non-impacting strings may have a greater effect on force generated against the bullnose than is possible in exterior string impacts. However, ultimately, whether a difference occurs will depend upon the stiffness and strength characteristics of the lashings as well as the stiffness and speed of the barge flotilla. In order to investigate these influences using typical lashing characteristics, flotilla models and impact simulations are conducted for both exterior and interior string impact conditions for a variety of different bullnose shapes, flotilla impact speeds, and barge end conditions (bow, or raked-end, versus stern, or boxed-end). In each such simulation, the appropriate portions of the impacting barge model (bow or stern) are made deformable and are assigned suitable nonlinear constitutive models and contact definitions. Appropriate modifications are also made to the side-to-side contact definitions between the impacting barge and the adjacent non-impacting barge models (these changes are necessary due to the array of different material types that are employed (for efficiency purposes) in the model: deformable, rigid, and a material type referred to as ‘switch-rigidized’).

2.2.2 Non-impacting (decimated) barges

The primary role of each non-impacting finite element barge model is to efficiently represent mass-related inertial properties and the dynamic interactions between barges through contact and lashings. Due to the computational expense of performing an analysis with a nearly one-million element high resolution barge model, it is impractical and unnecessarily inefficient to utilize a fully discretized high resolution deformable barge model at each position within a flotilla to model these effects. Thus, performing an analysis with multiple high resolution barges is neither computationally feasible nor an effective use of computational resources. Therefore, each non-impacting barge is modeled in a way that retains the external geometry of a high resolution barge, as well as the inertial and mass properties, but has a lower mesh resolution (a ‘decimated resolution’) than the high resolution barge finite element model.

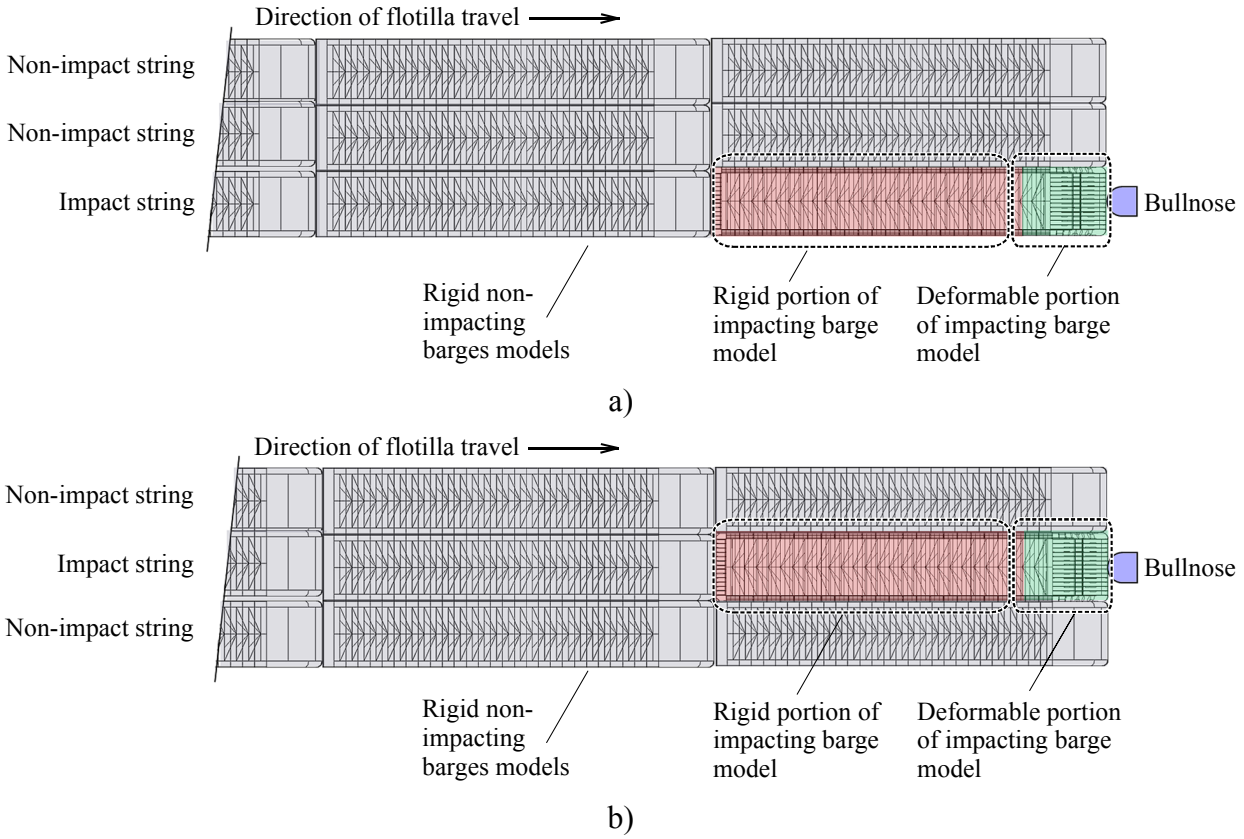

Figure 2.17. Flotilla models configured for bow impact against a 10 ft diameter bullnose: a) Exterior string impact condition; b) Interior string impact condition

Each low resolution ('decimated') non-impacting barge model (Figure 2.18) consists of approximately 4,000 shell elements, as compared to the 900,000 shell elements that are included in the high resolution impacting barge model. Shell elements defining the external geometry of each non-impacting barge are modeled as rigid elements, thus no internal structural elements are required or included. Inertial and mass properties, quantified from the high resolution barge model, are assigned to each rigid non-impacting barge to ensure appropriate dynamic behavior during impact.

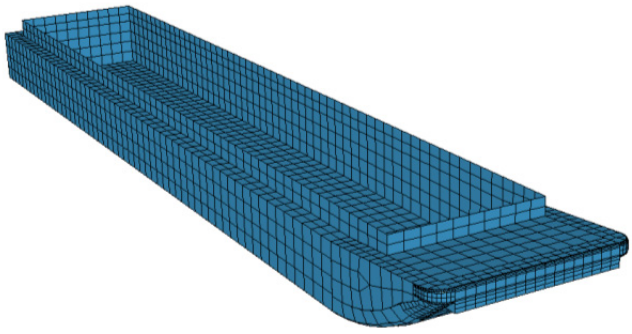

Figure 2.18. Non-impacting barge finite element model (mesh shown)

2.3 Modeling barge interactions

Individual barges within a physical barge flotilla are joined together using wire ropes (or lashings) that wrap around bitts (cylindrical posts) which protrude from the barge deck (Figure 2.19). Lashing configurations used in this study are consistent with those used in the full-scale barge impact tests conducted by the USACE at Gallipolis Locks (Patev et al. 2003) and in previous analytical barge impact studies (Consolazio et al. 2012, Consolazio and Walters 2012). Each wire rope within the finite element model is assigned an appropriate geometric configuration; a set of material properties that represent the nonlinear stiffness of the lashing; and a failure criterion based on ultimate capacity. Depending upon the location of the wire rope within the overall flotilla, an appropriate ultimate tensile of either 90 kips (for 1 in. diameter wire rope) or 120 kips (for 1.25 in. diameter wire rope) is assigned. By including a wire rope (lashing) failure criterion, each flotilla model has the ability to experience either full or partial break-up wherein the individual barges are free to separate from one another and move independently. This feature of the flotilla model is particularly important in terms of quantifying impact loads on rigid bullnose structures, where lashing failures are expected during high energy impacts.

Each pair of adjacent barges within a flotilla is lashed together by wrapping the barge bitts in a specific pattern, referred to as a lashing configuration. Different configurations are used to lash different types of barge pairs (end-to-end, side-to-side, or diagonal) and to resist different loads imposed by common flotilla maneuvers. Lashings are layered on top of each other when more than one configuration is required at the same location. In the largest of the flotilla models considered in the present study (e.g., a 3x5), up to seven different lashing configurations are used to connect individual barges together. For a detailed description of lashing configurations, and the finite element (mathematical) modeling of the lashings, see Consolazio et al. (2012).

Figure 2.19. Typical lashing configuration on barge flotilla

In addition to barges interacting with one another through lashing forces, they also interact by generating contact forces. In the barge flotilla finite element model, contact definitions are defined between each set of adjacent barges. Since all barges except the impacting barge are rigid, the structural stiffness of the non-impacting barge models cannot be related to deformations caused during contact with adjacent barges (since rigid model components cannot undergo deformation). Instead, contact stiffness (and therefore structural stiffness) of each non-impacting barge is accounted for through the use of a prescribed contact stiffness relationship,

which is representative of the stiffness of the high-resolution impacting barge in a particular mode of deformation. To obtain the appropriate contact stiffness relationships, high-resolution finite element models of deformable barges are quasi-statically crushed together (Consolazio et al. 2012). A nonlinear force-deformation relationship (stiffness) is then extracted from the results of each crushing simulation and used to define the barge-to-barge contact stiffness. In this study, force-deformation curves of this type are used to represent raked-end to raked-end (bow-to-bow), raked-end to boxed-end (bow-to-stern), and side-to-side inter-barge contacts. For a detailed description of how finite element crushing simulations are used to establish the various barge-to-barge contact stiffnesses, see Consolazio et al. (2012).

2.4 External loading (gravity and buoyancy)

In each impact simulation conducted in this study, the effects of both gravitational forces and buoyancy forces acting on the barge flotilla are included. Buoyant uplift forces underneath each barge are modeled by introducing individual buoyancy springs over the bottom surface of the barge model. For the high-resolution impacting barge model, approximately 26,400 discrete springs are attached to the barge bottom nodes, whereas each non-impacting barge employs approximately 900 buoyancy springs.

The stiffness of each buoyancy spring is computed by determining the tributary area of the barge bottom surface supported by the spring, and then multiplying this value by the density of water (62.4 lb/ft^3). By using a large number of springs with relatively small tributary areas, the resulting stiffness values are small, thereby precluding the development of unrealistically concentrated buoyant forces during barge motions.

Each buoyancy spring is 200 in. in length and connects to a support node (above the barge) that is freely able to translate in the horizontal plane (Figure 2.20) but restrained against vertical motion. As such, the barge model "hangs" from the collection of buoyancy springs and is able to translate arbitrarily large distances in the horizontal plane (plan view) without resistance. Vertical motions of the barge, however, cause appropriate changes in the distribution of vertical uplift forces, which are based on changes in the submerged depth of the barge. Because the buoyancy springs are always in tension, the vertical support node of each spring "tracks" (in plan view) with the corresponding node at the bottom surface of the barge. Consequently, the buoyancy springs remain vertical at all points in time during the simulation, regardless of the horizontal motions that the flotilla may undergo. This is particularly beneficial should a partial or full flotilla breakup occur during a simulation. Additional aspects of buoyancy modeling, such as calibration of the buoyancy springs and gapping of buoyant springs at the raked barge bow, are described in Consolazio et al. (2012).

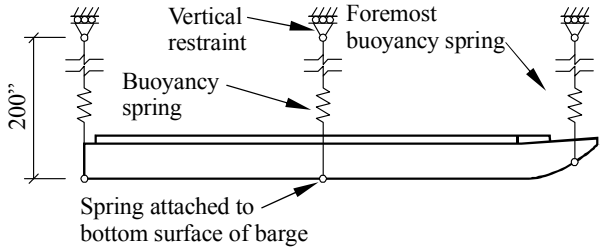

Figure 2.20. Barge buoyancy spring schematic

CHAPTER 3
FINITE ELEMENT MODELING OF RIGID BULLNOSE STRUCTURES

3.1 Introduction

Among the inventory of bullnose structures for which the U.S. Army Corps of Engineers (USACE) is responsible, the majority of such structures have either a circular impact face (Figure 3.1a) or a sloped V-shaped (triangular shaped) impact face (Figure 3.1b). Consequently, in this study, focus is given to quantifying impact forces exerted on such structures from barge flotillas of varying sizes. Bullnose structures with a semi-circular impact face may be followed by a wall with a width equal to the bullnose diameter, or by a wall that is narrower than the bullnose diameter. In this study, for purposes of quantifying impact loads on semi-circular bullnose structures, a semi-circular impact face followed by an equal width wall is used in all circular bullnose cases (Figure 3.2a and Figure 3.2b). From the perspective of predicting conservatively large impact forces, this geometry is more appropriate. Semi-circular bullnoses (for simplicity, referred to as 'circular bullnoses' in much of this report) vary in diameter from one site to another. To cover the range of typical diameters that are contained within the USACE inventory, lower and upper bound diameters of 10 ft and 35 ft are modeled in this study.

In addition to circular bullnoses, the sloped-V bullnose shape, which is commonly utilized along the Mississippi River, is also modeled using finite elements (Figure 3.2c) and included in the impact simulations performed in this study. The primary sloped-V bullnose geometry considered in this study employs a 2:1 (vertical : horizontal) slope on the impact face and is developed from design plans (Figure 3.3) for the Mississippi River Lock and Dam No. 7 (MRLD7). The MRLD7 sloped-V geometry is considered to be reasonably representative of similar structures contained within the USACE inventory. However, two additional variations on the sloped-V geometry are also considered in a small number of separate sensitivity analyses: a sloped-V with a shallower 1:1 front face slope, and a sloped-V with an even shallower 1:2 front face slope. These additional cases are investigated, in limited scope, to examine the sensitivity of impact forces to sloped-V front face slope (additional details are provided later in this chapter).

a) b)

Figure 3.1. Primary types of bullnose structures considered:
a) Circular geometry; b) Mississippi sloped-V geometry (2:1 vertical-to-horizontal slope)

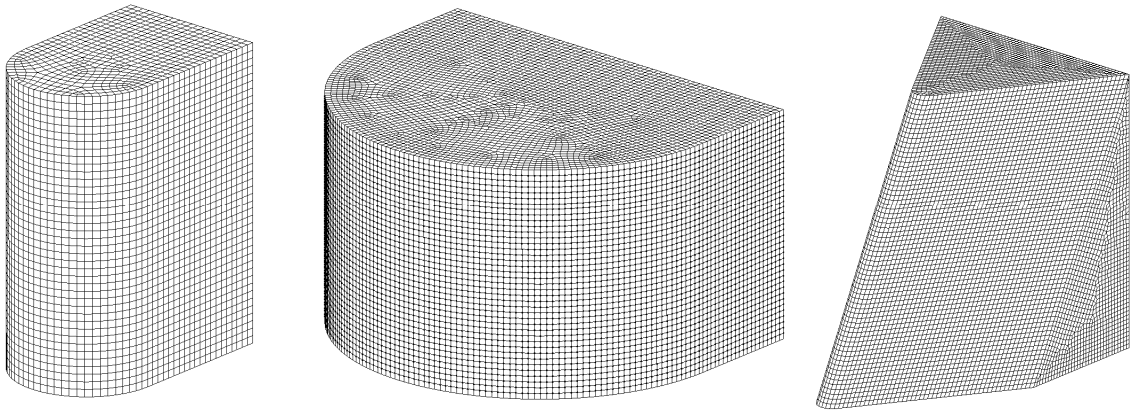

a) b) c)

Figure 3.2. Finite element models of bullnose structures used in impact simulations:
a) 10 ft diameter semi-circular; b) 35 ft diameter semi-circular; c) sloped-V

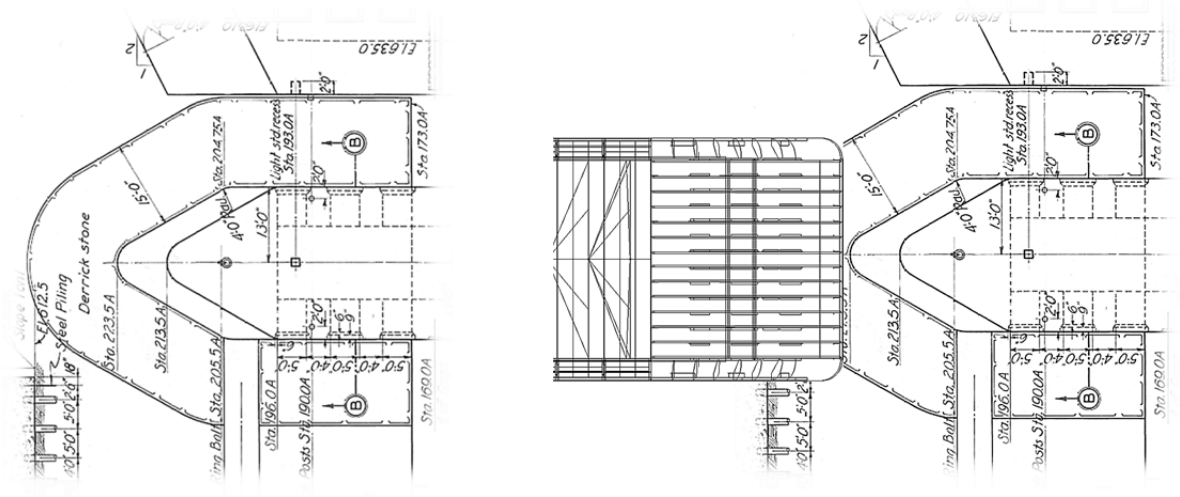

a) b)

Figure 3.3. Mississippi River Lock and Dam No. 7 sloped-V bullnose:
a) Excerpt from structural plans (plan view);
b) Bow of jumbo hopper barge superimposed on bullnose drawing for comparison of scale

Presented in Figure 3.4 are finite element models in which a single high-resolution impacting barge model (discussed in the previous chapter) is combined with each of the primary bullnose shapes. In multi-barge (as opposed to single barge) flotilla impact simulations—the vast majority of cases considered in this study—it is always a single high-resolution impacting barge model that makes direct contact with the bullnose model. As described in the previous chapter, non-impacting barges contribute to the overall impact forces generated on the bullnose, but do not make direct contact with the bullnose model.

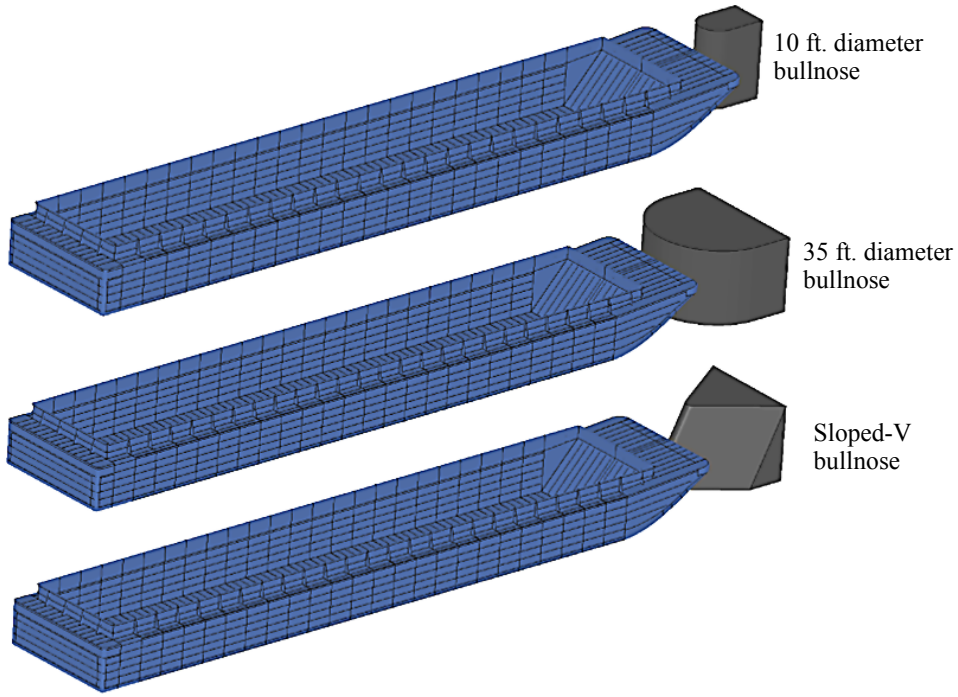

Figure 3.4. Integrated finite element models of a single barge and bullnose
(Note: only key model geometry shown; mesh resolution omitted for clarity)

3.2 Development of bullnose FE models

Given that reinforced concrete bullnose structures are typically much stiffer than the bow or stern structural steel components of hopper barges, in this study, all bullnose structures are modeled—for numerical simulation efficiency reasons—as non-deformable, materially rigid entities. It is important to note that simplification is conservative in nature with respect to the calculation of impact forces (impact loads). Similarly, soil deformation is also conservatively ignored (i.e., soil is treated as rigid), therefore fixed boundary conditions are applied to the base nodes of all bullnose structural models presented herein. The simplifying approximations of treating both bullnose and soil response as rigid are based on an engineering understanding of the relative stiffnesses between an impacting barge and a typical USACE concrete bullnose structure, as well as direct observations from high-energy barge impact incidents that have occurred at various USACE bullnose installations (e.g. Mississippi River Lock and Dam No. 9 [recall Figure 2.7] and numerous similar incidents). Thus, based on these simplifying—but conservative—approximations, all bullnose structures in this study are modeled with 8-node solid brick elements and a mathematically rigid material definition. The 8-node solid brick elements are meshed to be approximately 6” x 6” x 6” in dimension to accurately represent the exterior geometry of the concrete bullnoses while also being no larger than approximately twice the size of the smallest impacting shell elements present in the impacting-face (bow [Figure 2.9] or stern [Figure 2.16]) of the high-resolution impacting barge finite element model.

3.2.1 Semi-circular 10 ft diameter bullnose model

The 10 ft diameter finite element bullnose model (Figure 3.5 and Figure 3.6) is intended to be representative of smaller diameter semi-circular concrete bullnose structures in the USACE

structural inventory. More than 22,000 solid elements, approximately 6" x 6" x 6" in size, and utilizing a rigid material definition, are included in this model. All nodes at the base of the model are fully restrained against translation. A 20 ft vertical height is selected for the bullnose model to ensure that steel shell elements of the impacting barge model cannot 'overtop' (i.e., pass over the top surface of) the bullnose model as a result of steel plate folding and fracturing, or buoyant uplift-motion of the barge during impact. In actual field conditions, partial overtopping may or may not occur, depending upon the physical height of the bullnose, the water level, and the barge tow draft. However, in conducting finite element simulations of impacts against the vertical-faced 10 ft diameter bullnose model, preventing overtopping ensures that conservatively high predictions of impact force are obtained. A 20 ft model height is found to be sufficient to prevent overtopping.

3.2.2 Semi-circular 35 ft diameter bullnose model

The 35 ft diameter finite element bullnose model (Figure 3.7 and Figure 3.8) is intended to be reasonably representative of the maximum diameter semi-circular concrete bullnose structures in the USACE structural inventory. The 35 ft diameter is also chosen as it corresponds to the full width of a jumbo hopper barge. More than 137,000 solid elements, approximately 6" x 6" x 6" in size, and utilizing a rigid material definition, are included in the 35 ft diameter bullnose model. All nodes at the base of the model are fully restrained against translation. As is the case in the 10 ft diameter bullnose model, the 35 ft diameter model also uses a 20 ft vertical height to prevent overtopping of the impacting barge model.

3.2.3 Sloped-V bullnose models

The impact face of the Mississippi sloped-V bullnose (Figure 3.9 and Figure 3.10) features a vertical 2:1 slope and a plan-view shape that is approximately triangular in form, terminating in a 4 ft diameter radial nose. The base and sidewalls of the structure extend 28 ft in width. More than 16,000 8-node solid brick elements, approximately 6" x 6" x 6" in size, and utilizing a rigid material definition, are used to model the sloped-V bullnose. All nodes at the base of the model are fully restrained against translation.

In contrast to the 10 ft and 35 ft diameter bullnoses, both of which employ vertical impact faces, the non-vertical 2:1 slope of the impact face on the sloped-V bullnose will permit the barge to slide (or ride) partially up the bullnose during impact. To ensure that the barge model does not slide to a position beyond the top surface of the sloped-V bullnose model, an increased total bullnose height of 33 ft is used.

As noted earlier, two additional variations on the sloped-V geometry are also considered in a set of sensitivity analyses: a sloped-V with a shallower 1:1 front face slope, and a sloped-V with an even shallower 1:2 front face slope (Figure 3.11). Of interest in considering these alternative structures was determining the influence that impact face slope has on the impact forces generated and the quantity of lashing failures that are produced. While the curvature of the nose (4 ft diameter) and the width of the structure (28 ft) are consistent for all three sloped-V models, the height and length of the modified sloped-V models were increased to allow for substantial sliding of the barge along the face of the bullnose (particularly in high energy impact conditions).

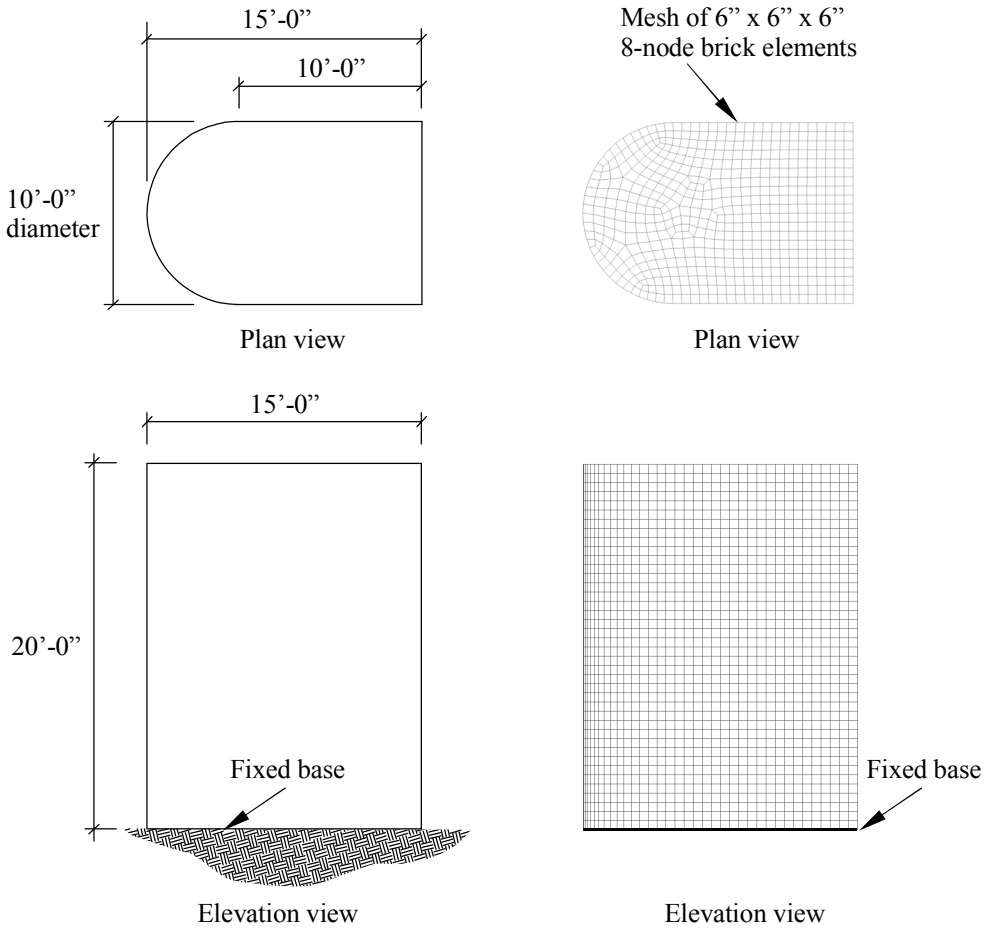

Figure 3.5. Schematic diagrams and finite element mesh of 10 ft. diameter semi-circular bullnose

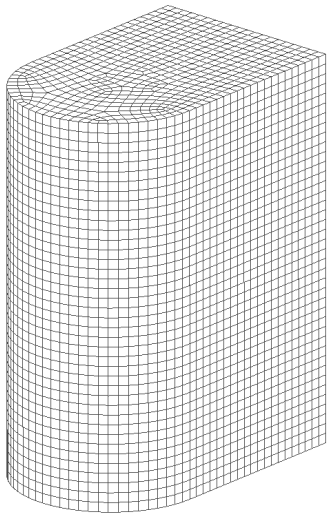

Figure 3.6. Isometric view of 10 ft. diameter semi-circular bullnose finite element model

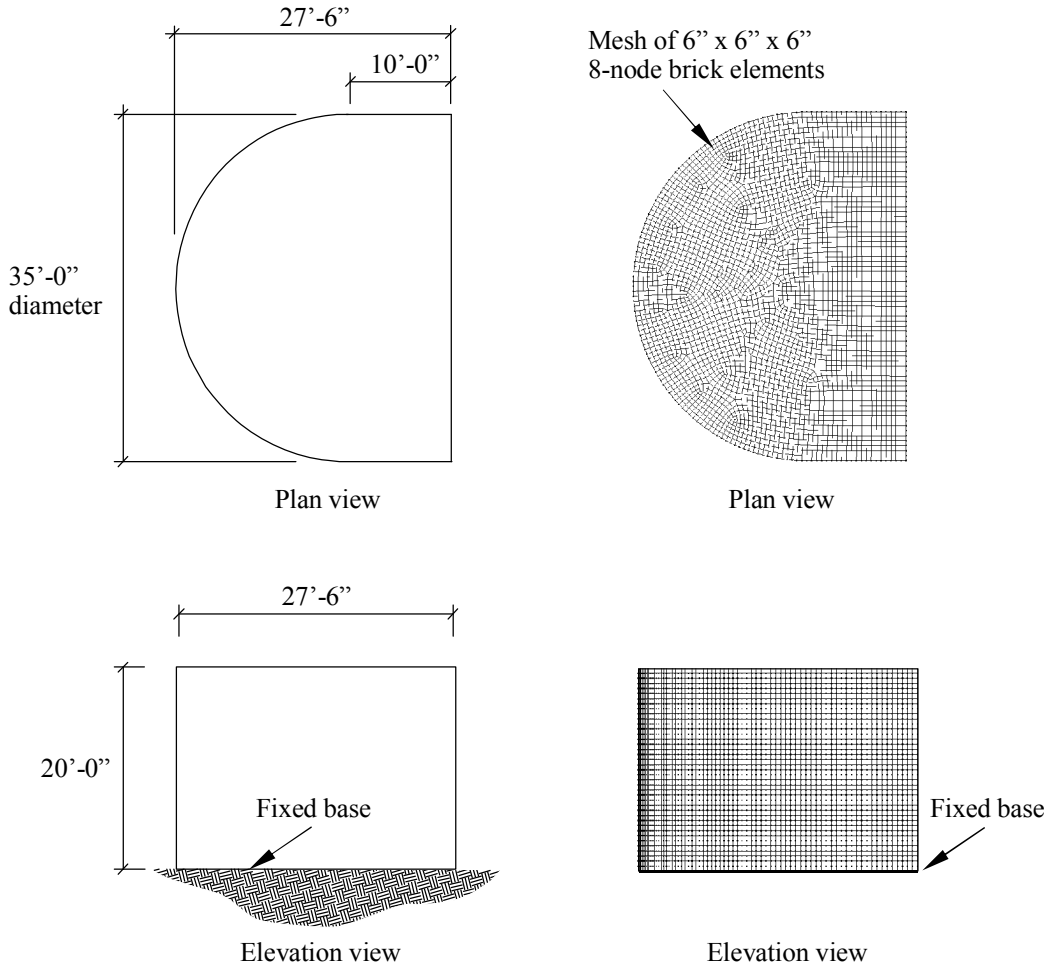

Figure 3.7. Schematic diagrams and finite element mesh of 35 ft diameter semi-circular bullnose

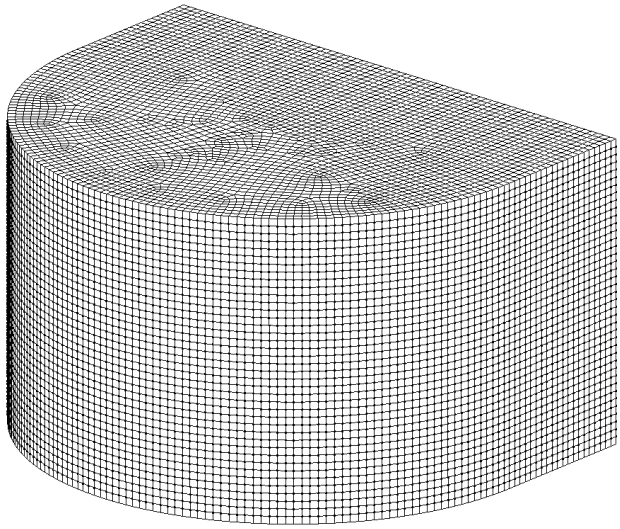

Figure 3.8. Isometric view of 35 ft diameter semi-circular FE bullnose model

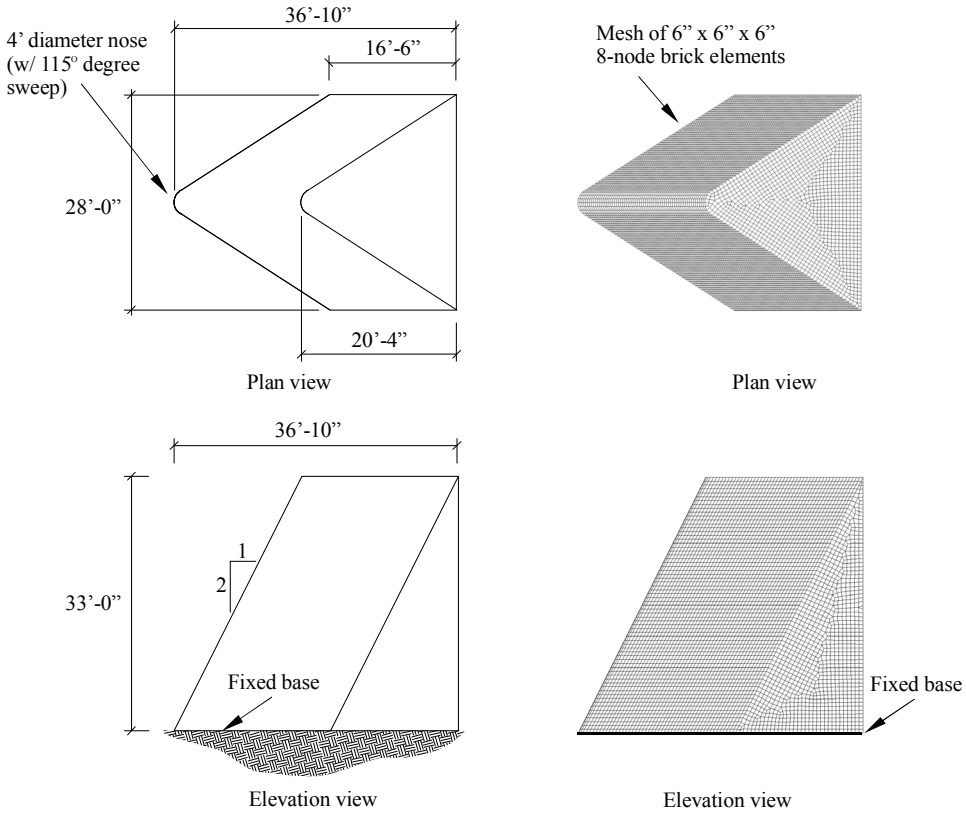

Figure 3.9. Schematic diagrams and finite element mesh of 2:1 sloped-V bullnose

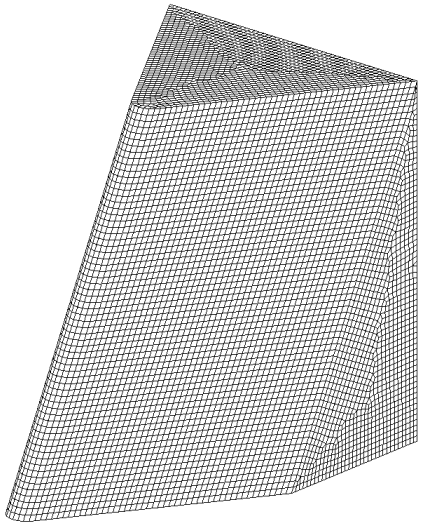

Figure 3.10. Isometric view of 2:1 sloped-V bullnose finite element model

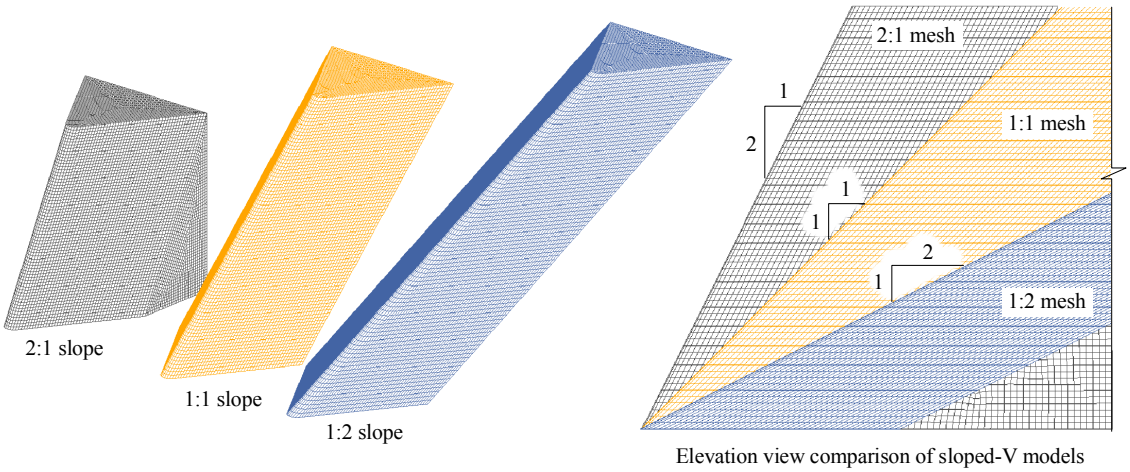

Figure 3.11. Standard and modified sloped-V finite element bullnose models: a) isometric view comparison, b) elevation view comparison

3.2.4 Frictional coefficients assigned to bullnose contact face

During numeric simulation of a barge flotilla impacting any of the bullnose models described above, contact forces are generated at the interface between the steel barge model and the rigid concrete bullnose model. These contact forces possess both normal (perpendicular) and transverse (frictional, or sliding) components with respect to face of the bullnose structure. In this study, as in previous studies (Consolazio et al. 2012, Consolazio and Walters 2012), the frictional parameters assigned to the contact definition between the steel barge model and the rigid concrete bullnose model are 0.55 and 0.45 for static and dynamic coefficients of friction, respectively.

CHAPTER 4
DETERMINATION OF IMPACT FORCES ON BULLNOSE STRUCTURES

4.1 Introduction

To quantify impact forces on bullnose structures, and to investigate the factors that affect these forces, barge flotilla models of varying sizes (recall Table 2.1) are combined with finite element models of the 10 ft diameter (10' ∅) semi-circular, 35 ft diameter (35' ∅) semi-circular, and sloped-V bullnose structures described in the previous chapter. A total of seventy-eight (78) dynamic barge-bullnose impact simulations are conducted, as listed in Table 4.1 (10' ∅), Table 4.2 (35' ∅), and Table 4.3 (sloped-V). Basic parameters that are varied include flotilla configuration (number of strings, number of rows), flotilla mass, impact speed, bullnose shape, impacting barge end (bow, stern), and impacting barge string (exterior, interior). For selected cases, additional parameters are also investigated, including impact angle (Table 4.2, Table 4.3), lateral impact offset (Table 4.3), and modified face slopes (1:1 and 1:2) for sloped-V bullnoses (Table 4.3).

4.2 Overview of impact force results

Impact forces computed in this study are dynamic contact forces between the high-resolution deformable impacting barge model and the surface of the bullnose structure. Unless otherwise noted, all impact forces reported in this chapter for bullnose structures are two-dimensional *resultant forces in the horizontal plane*, and are low-pass filtered at approximately 10 Hz so that the quantified impact forces are not unduly influenced by higher frequency oscillations present in the finite element results. Peak (maximum) impact forces for all cases are summarized in Tables 4.1 - 4.3 and time-histories of horizontal resultant force (as well as vertical force) are provided in Appendix A. The naming convention used to identify each bullnose impact case is also described in detail in the introduction to Appendix A.

Barge-bullnose impact conditions, particularly those involving high levels of flotilla momentum, are relatively long duration events, particularly in comparison to shallow angle (oblique, glancing blow) barge impacts on wall structures. Critical design forces for bullnose impacts are associated with 'head-on' (0° angle) impact conditions in which the flotilla is decelerated and eventually brought to rest (or breaks up). In high momentum cases, the time duration required to bring a flotilla *fully to rest* is far longer than the time required to simply *redirect* a flotilla off a wall impacted at a shallow angle. Consequently, due to the lengthy time duration of each bullnose impact event, and due to the large number of impact conditions simulated in this study (Tables 4.1 - 4.3), it is impractical to conduct all simulations to a point of zero force (i.e., flotilla fully at rest). Instead, each impact simulation is conducted with the intent of quantifying the maximum (peak) generated, not with the intent of capturing the entire time-history of load. For some impact conditions, the entire force-time history will be captured; in other cases, only the portion of the time history needed to quantify peak force will be captured.

Table 4.1. Semi-circular 10’ ∅ bullnose impact conditions and results (14 cases)

Flotilla Size	Impact Speed	Bullnose Shape	Impact End	Impact String	Impact Angle	Impact Offset	Impact Force (kip)	Lashings reaching ≥ 90% utilization
1 x 1	4 FPS	10’ ∅	Bow	Single	0°	0’	1119 †	–
1 x 1	4 FPS	10’ ∅	Stern	Single	0°	0’	777	–
1 x 3	4 FPS	10’ ∅	Bow	Single	0°	0’	1313 †	0
1 x 5	4 FPS	10’ ∅	Bow	Exterior	0°	0’	1335 †	0
2 x 3	4 FPS	10’ ∅	Bow	Exterior	0°	0’	1429 †	2
2 x 5	4 FPS	10’ ∅	Bow	Exterior	0°	0’	1427 †	1
3 x 3	2 FPS	10’ ∅	Bow	Exterior	0°	0’	1304 †	0
3 x 3	4 FPS	10’ ∅	Bow	Exterior	0°	0’	1413 †	2
3 x 5	2 FPS	10’ ∅	Bow	Exterior	0°	0’	1249 †	1
3 x 5	2 FPS	10’ ∅	Bow	Interior	0°	0’	1480 †	0
3 x 5	6 FPS	10’ ∅	Bow	Exterior	0°	0’	1653 †	3
3 x 5	6 FPS	10’ ∅	Bow	Interior	0°	0’	1477 †	3
3 x 5	9 FPS	10’ ∅	Bow	Exterior	0°	0’	1861	4
3 x 5	9 FPS	10’ ∅	Bow	Interior	0°	0’	1555	0

Notes:
Flotilla sizes are described as number of strings ‘by’ number of rows
FPS = feet per second; USACE definitions of impact speed : usual: 0.5 – 2 FPS; unusual: 2 – 4 FPS, extreme: 4 – 6 FPS
† Indicates data used in the development of impact force prediction equations (see Section 4.10)

Table 4.2. Semi-circular 35’ ∅ bullnose impact conditions and results (28 cases)

Flotilla Size	Impact Speed	Bullnose Shape	Impact End	Impact String	Impact Angle	Impact Offset	Impact Force (kip)	Lashings reaching ≥ 90% utilization
1 x 1	2 FPS	35’ ∅	Bow	Single	0°	0’	1022 †	–
1 x 1	2 FPS	35’ ∅	Stern	Single	0°	0’	836	–
1 x 1	6 FPS	35’ ∅	Bow	Single	0°	0’	1610 †	–
1 x 1	6 FPS	35’ ∅	Stern	Single	0°	0’	1374	–
1 x 1	10 FPS	35’ ∅	Bow	Single	0°	0’	1750	–
1 x 3	2 FPS	35’ ∅	Bow	Single	0°	0’	1260 †	0
1 x 3	6 FPS	35’ ∅	Bow	Single	0°	0’	1637 †	0
1 x 5	2 FPS	35’ ∅	Bow	Single	0°	0’	1317 †	0
1 x 5	6 FPS	35’ ∅	Bow	Single	0°	0’	1642 †	0
2 x 3	2 FPS	35’ ∅	Bow	Exterior	0°	0’	1323 †	1
2 x 3	6 FPS	35’ ∅	Bow	Exterior	0°	0’	1669 †	3
2 x 5	2 FPS	35’ ∅	Bow	Exterior	0°	0’	1326 †	1
2 x 5	6 FPS	35’ ∅	Bow	Exterior	0°	0’	1816 †	2
3 x 3	2 FPS	35’ ∅	Bow	Exterior	0°	0’	1341 †	2
3 x 3	2 FPS	35’ ∅	Bow	Interior	0°	0’	1601 †	1
3 x 3	6 FPS	35’ ∅	Bow	Exterior	0°	0’	1836 †	12 [8] ‡
3 x 5	2 FPS	35’ ∅	Bow	Exterior	0°	0’	1586 †	0
3 x 5	2 FPS	35’ ∅	Stern	Exterior	0°	0’	1303	0
3 x 5	2 FPS	35’ ∅	Bow	Interior	0°	0’	1604 †	1
3 x 5	2 FPS	35’ ∅	Stern	Interior	0°	0’	1520	3
3 x 5	6 FPS	35’ ∅	Bow	Exterior	0°	0’	1983 †	3
3 x 5	6 FPS	35’ ∅	Stern	Exterior	0°	0’	1618	3
3 x 5	6 FPS	35’ ∅	Bow	Interior	0°	0’	1996 †	4
3 x 5	6 FPS	35’ ∅	Stern	Interior	0°	0’	1773	4
3 x 5	6 FPS	35’ ∅	Bow	Exterior	30°	0’	1871	3
3 x 5	6 FPS	35’ ∅	Bow	Interior	30°	0’	2080	5
3 x 5	9 FPS	35’ ∅	Bow	Exterior	0°	0’	2676	3
3 x 5	9 FPS	35’ ∅	Bow	Interior	0°	0’	2108	2

Notes:
Flotilla sizes are described as number of strings ‘by’ number of rows
FPS = feet per second; USACE definitions of impact speed : usual: 0.5 – 2 FPS; unusual: 2 – 4 FPS, extreme: 4 – 6 FPS
† Indicates data used in the development of impact force prediction equations (see Section 4.10)
‡ Of twelve (12) lashings that reached ≥ 90% utilization, eight (8) reached complete failure (i.e. 100% utilization)

Table 4.3. Sloped-V bullnose impact conditions and results (36 cases)

Flotilla Size	Impact Speed	Bullnose Shape	Impact End	Impact String	Impact Angle	Impact Offset	Impact Force (kip)	Lashings reaching ≥ 90% utilization
1 x 1	2 FPS	2:1 Sloped-V	Bow	Single	0°	0’	488 †	–
1 x 1	2 FPS	2:1 Sloped-V	Stern	Single	0°	0’	424	–
1 x 1	6 FPS	2:1 Sloped-V	Bow	Single	0°	0’	937 †	–
1 x 1	6 FPS	2:1 Sloped-V	Stern	Single	0°	0’	604	–
1 x 3	2 FPS	2:1 Sloped-V	Bow	Single	0°	0’	629 †	0
1 x 3	6 FPS	2:1 Sloped-V	Bow	Single	0°	0’	1204 †	0
1 x 5	2 FPS	2:1 Sloped-V	Bow	Single	0°	0’	789 †	0
1 x 5	6 FPS	2:1 Sloped-V	Bow	Single	0°	0’	1192 †	0
2 x 3	2 FPS	2:1 Sloped-V	Bow	Exterior	0°	0’	890 †	0
2 x 3	6 FPS	2:1 Sloped-V	Bow	Exterior	0°	0’	1221 †	1
2 x 5	2 FPS	2:1 Sloped-V	Bow	Exterior	0°	0’	910 †	0
2 x 5	6 FPS	2:1 Sloped-V	Bow	Exterior	0°	0’	1362 †	1
3 x 3	2 FPS	2:1 Sloped-V	Bow	Exterior	0°	0’	900 †	1
3 x 3	2 FPS	2:1 Sloped-V	Bow	Interior	0°	0’	902 †	0
3 x 3	6 FPS	2:1 Sloped-V	Bow	Exterior	0°	0’	1336 †	3
3 x 4	5 FPS	2:1 Sloped-V	Bow	Exterior	0°	0’	1210 †	1
3 x 5	2 FPS	2:1 Sloped-V	Bow	Exterior	0°	0’	991 †	1
3 x 5	2 FPS	2:1 Sloped-V	Stern	Exterior	0°	0’	885	0
3 x 5	2 FPS	2:1 Sloped-V	Bow	Interior	0°	0’	994 †	0
3 x 5	2 FPS	2:1 Sloped-V	Stern	Interior	0°	0’	909	6
3 x 5	6 FPS	2:1 Sloped-V	Bow	Exterior	0°	0’	1935 †	3
3 x 5	6 FPS	2:1 Sloped-V	Stern	Exterior	0°	0’	1462	3
3 x 5	6 FPS	2:1 Sloped-V	Bow	Interior	0°	0’	1654 †	2
3 x 5	6 FPS	2:1 Sloped-V	Stern	Interior	0°	0’	1463	2
3 x 5	6 FPS	2:1 Sloped-V	Bow	Exterior	0°	5’	1739	2
3 x 5	6 FPS	2:1 Sloped-V	Bow	Exterior	0°	10’	1818	5
3 x 5	6 FPS	2:1 Sloped-V	Bow	Exterior	0°	15’	1105	12 [4] ‡
3 x 5	6 FPS	2:1 Sloped-V	Bow	Exterior	10°	0’	1744	4
3 x 5	6 FPS	2:1 Sloped-V	Bow	Exterior	20°	0’	1808	4
3 x 5	6 FPS	2:1 Sloped-V	Bow	Exterior	30°	0’	1635	3
3 x 5	6 FPS	1:1 Sloped-V	Bow	Exterior	30°	0’	1871	2
3 x 5	6 FPS	1:1 Sloped-V	Bow	Exterior	0°	0’	2144	3
3 x 5	6 FPS	1:2 Sloped-V	Bow	Exterior	30°	0’	1397	2
3 x 5	6 FPS	1:2 Sloped-V	Bow	Exterior	0°	0’	1178	3
3 x 5	9 FPS	2:1 Sloped-V	Bow	Exterior	0°	0’	2098	1
3 x 5	9 FPS	2:1 Sloped-V	Bow	Interior	0°	0’	2190	2

Notes:
Flotilla sizes are described as number of strings ‘by’ number of rows
FPS = feet per second; USACE definitions of impact speed : usual: 0.5 – 2 FPS; unusual: 2 – 4 FPS, extreme: 4 – 6 FPS
† Indicates data used in the development of impact force prediction equations (see Section 4.10)
‡ Of twelve (12) lashings that reached ≥ 90% utilization, four (4) reached complete failure (i.e. 100% utilization)

In Figures 4.1 – 4.5, various aspects of a representative bullnose impact condition, specifically bullnose impact case ‘3x3 – 4 FPS – 10’ ∅ – Bow – Exterior’ (Table 4.1), are presented. In Figure 4.1, the 3x3 barge flotilla is integrated together with a 10’ ∅ bullnose model and given an initial velocity of 4 FPS in the direction toward the bullnose. As indicated in Figure 4.2, the flotilla model consists of one (1) deformable impacting barge model, and eight (8) non-impacting barge models. Impact forces are computed at the interface between the impacting barge model and the bullnose model. Because this case is an ‘exterior string’ impact condition, the centerline of the exterior barge string is aligned with the centerline of the 10’ ∅ bullnose.

Computed time histories of horizontal resultant (i.e., ‘impact’) force and vertical force are presented in Figure 4.3, where it is evident that entire impact event is captured for this particular case (i.e., zero impact force at approximately t = 6 sec. indicate that the flotilla has essentially been brought to rest). The peak impact force (1413 kips, see Table 4.1) occurs relatively early in the impact event and is followed by a sustained period of reduced force (~1000 kips). In

Figures 4.4 and 4.5, visualizations of barge deformation during the impact are presented. Maximum bow deformation (i.e., 'crush depth') for the impacting barge occurs at approximately t = 5 sec. and is equal to approximately 6.5 ft. While not quite as severe as the bow damage shown earlier in the photograph in Figure 1.2, the overall finite element bow deformation patterns indicated in Figures 4.4 and 4.5 are similar in nature. In Figure 4.5, significantly yielded portions of the barge bow are rendered in red—where 'significantly yielded' is characterized by plastic strains exceeding ten (10) times the yield strain of steel—and reveal widespread hull plate folding and inelastic buckling of internal structural members (consistent with Figure 1.2).

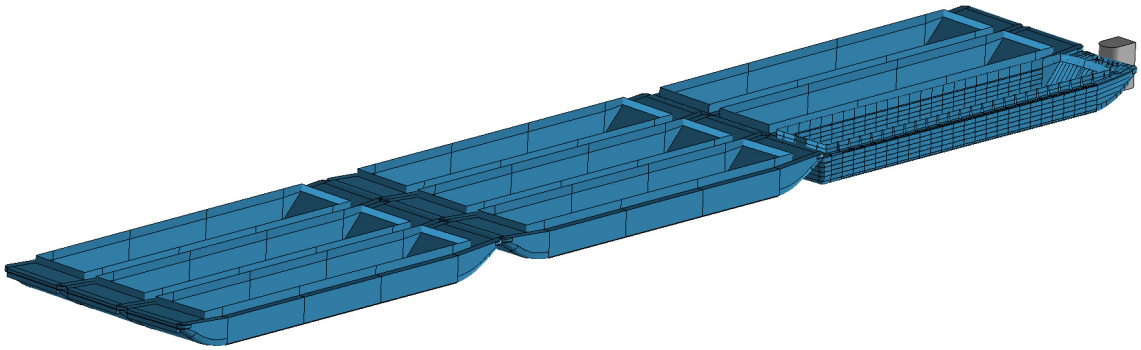

Figure 4.1. Finite element model: 3x3 – 4 FPS – 10' ∅ – Bow – Exterior

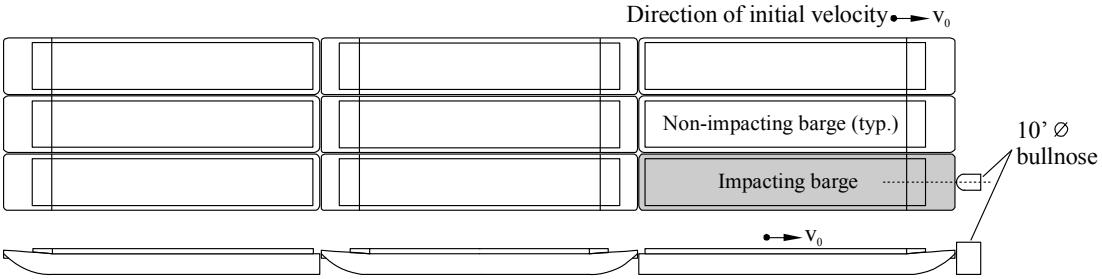

Figure 4.2. Schematic diagram: 3x3 – 4 FPS – 10' ∅ – Bow – Exterior

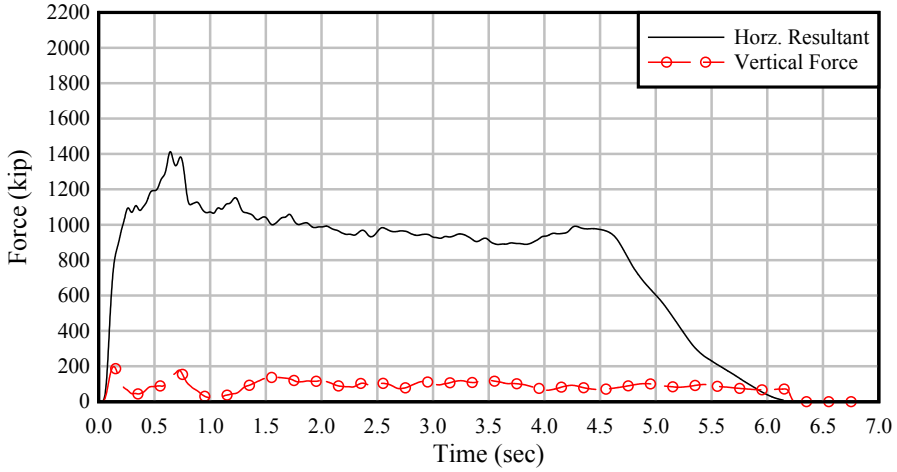

Figure 4.3. Impact force-time history for case: 3x3 – 4 FPS – 10' ∅ – Bow – Exterior

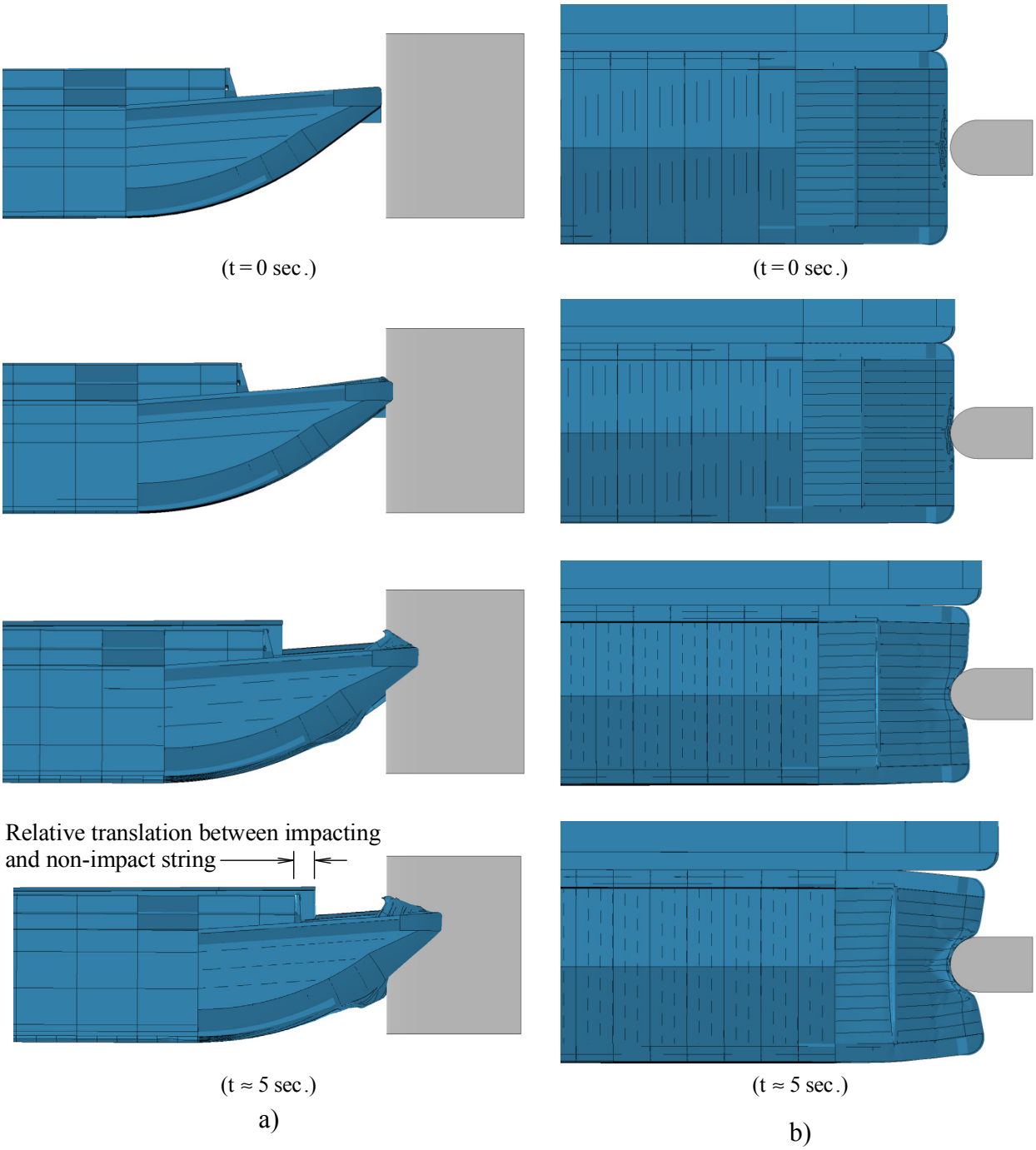

Figure 4.4. Barge bow deformation and relative sliding between strings:
a) Elevation view; b) Plan view
(Case: 3x3 – 4 FPS – 10’ ∅ – Bow – Exterior)

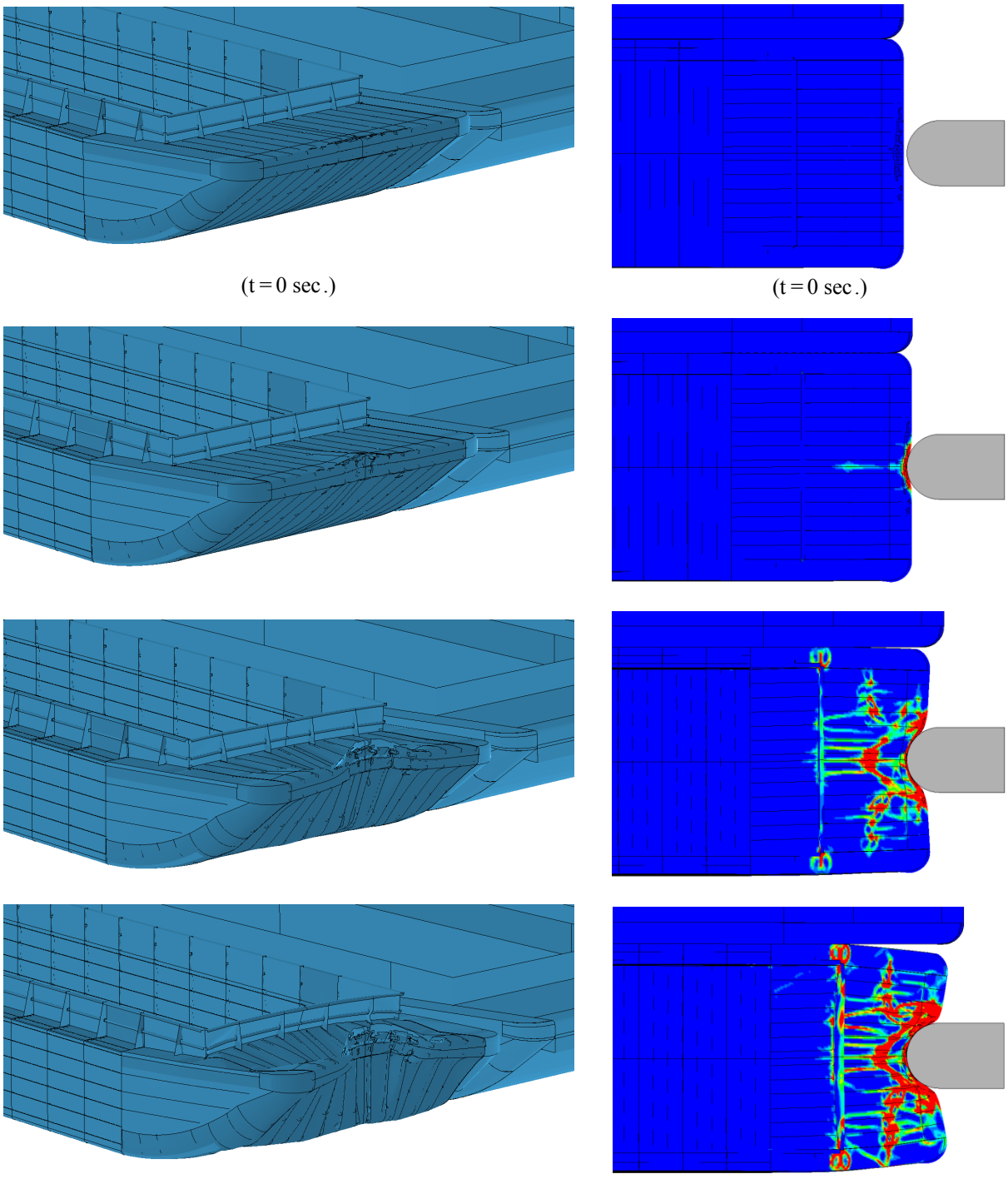

Figure 4.5. Barge bow deformation and plastic strain:
a) Isometric view of deformation;
b) Plastic strains, ε_p (blue = 0; red = $\varepsilon_p \geq 10 \times \varepsilon_y$ where $\varepsilon_y = F_y/E$ = steel yield strain)
(Case: 3x3 – 4 FPS – 10' ∅ – Bow – Exterior)

Because the impacting exterior barge string is connected to two adjacent non-impacting barge strings (recall Figure 4.2) through wire rope lashings, the momentum of the non-impacting strings contributes to the impact force that is generated on the bullnose. At the bottom of Figure 4.4a, relative motion (translation) between the impacting string (foreground) and the non-impacting strings (background) is evident. From t = 0 sec. to approximately t = 2 sec., relative translational motion between the impacting and non-impacting strings grows from zero to approximately 2 ft., then holds constant until the impact event ends. Simulation results indicate that during impact, tensile forces in two of the lashings that connect the impacting barge to surrounding barges exceeded 90% of their respective capacities. One of these lashings, spanning between the impacting string and the adjacent non-impacting string 'failed' (defined as exceeding 90% of ultimate capacity) at approximately t = 0.5 sec. into the impact event. Later in this chapter, the role of non-impacting string momentum in impact force generation will be presented in more detail by comparing impact forces from exterior string impacts to analogous interior string impacts.

4.3 Impact force sensitivity to bullnose geometry

Numerous prior studies conducted for the purpose of quantifying barge impact loads on bridge piers (e.g., Consolazio et al. 2008, Consolazio et al. 2009, Getter and Consolazio 2011) have clearly established that the 'geometry'—specifically the shape (circular, rectangular, etc.) and size (diameter or width)—of an impacted structural surface strongly influences the magnitude of force that is generated during a barge impact. For example, wide flat structural surfaces generate impact forces that are much larger than narrow rounded surfaces. As is discussed in detail in Consolazio et al. (2008), the underlying reason for the differences in impact force relates directly to the number of internal stiffening trusses (inside the barge bow) that are structurally engaged (e.g., buckled) during an impact event. Wide and flat surfaces (e.g. rectangular waterline pier footings) simultaneously engage a large number of internal stiffening trusses during impact and consequently result in very large forces. In contrast, narrow and round surfaces engage fewer internal trusses, and thus result in forces that are smaller in magnitude.

Given these past observations, it is anticipated that similar relationships between impact force and surface geometry apply to bullnose structures as well. Hence, to assess impact force sensitivity to bullnose geometry, cases involving combinations of 3x3 and 3x5 barge flotillas impacting 10' ∅, 35' ∅, and sloped-V bullnoses are considered (Figure 4.6) for selected exterior and interior string impact conditions. As expected, in Figures 4.7 - 4.9, a predictable relationship between impact force and bullnose shape is clearly apparent. For otherwise identical conditions (flotilla size, impact speed, etc.), impacts on sloped-V bullnoses produce the smallest forces; impact forces for 10' ∅ semi-circular bullnoses are larger; and forces for 35' ∅ bullnoses are largest. While not surprising, these results do suggest that—if desirable and warranted—the development of impact force prediction equations that incorporate geometric parameters (e.g., bullnose diameter) may at least be feasible.

Finally, it must be noted that the sloped-V bullnose should be thought of as having a variable, and 'momentum-dependent', characteristic width, rather than a fixed width of 4' (i.e., the diameter of the nose). As initial impact momentum increases—e.g. due to increasing flotilla size or mass—the triangular 'V-shape' of the bullnose will produce zones of barge crushing (deformation) that increase in width. Hence, while a characteristic width of 4' may be an appropriate predictor of impact force for low to moderate momentum impacts, for severe impacts, a larger 'effective' characteristic width may be needed to accurately predict peak impact

force. Relationships between peak impact force and flotilla momentum, presented later in this chapter (Section 4.10), will confirm this observation in that for severe impact conditions, impact forces generated on sloped-V bullnoses can exceed those generated on 10’ ∅ bullnoses.

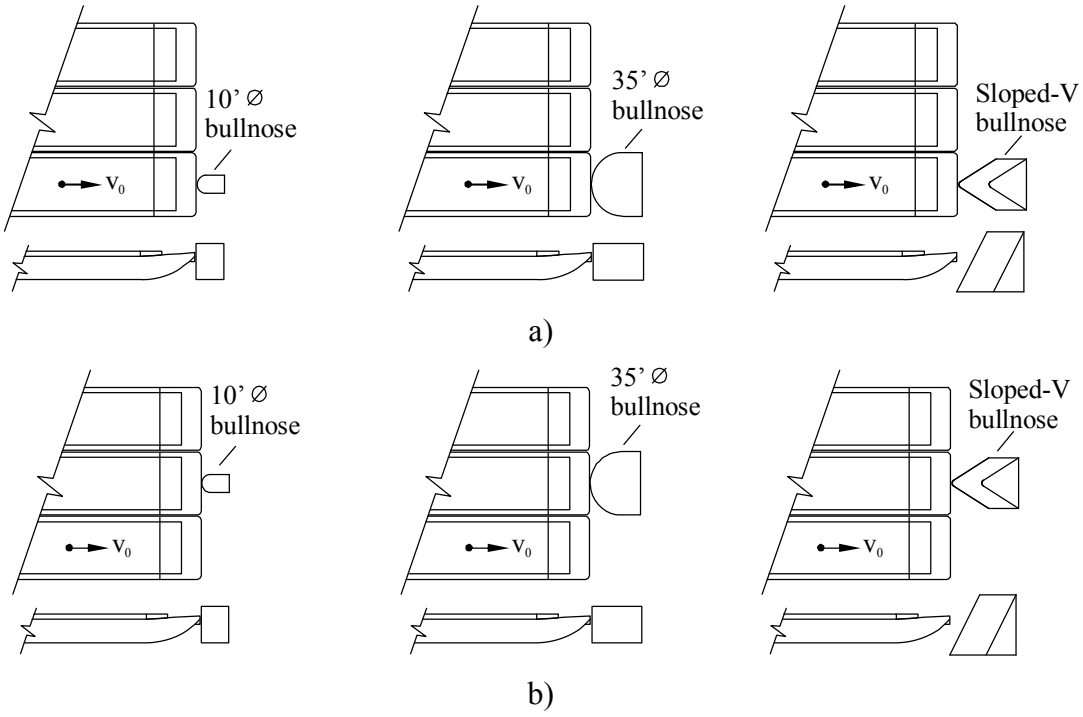

Figure 4.6. Investigation of impact force sensitivity to bullnose shape:
a) 10’ ∅, 35’ ∅, and sloped-V bullnoses (exterior string impacts)
b) 10’ ∅, 35’ ∅, and sloped-V bullnoses (interior string impacts)

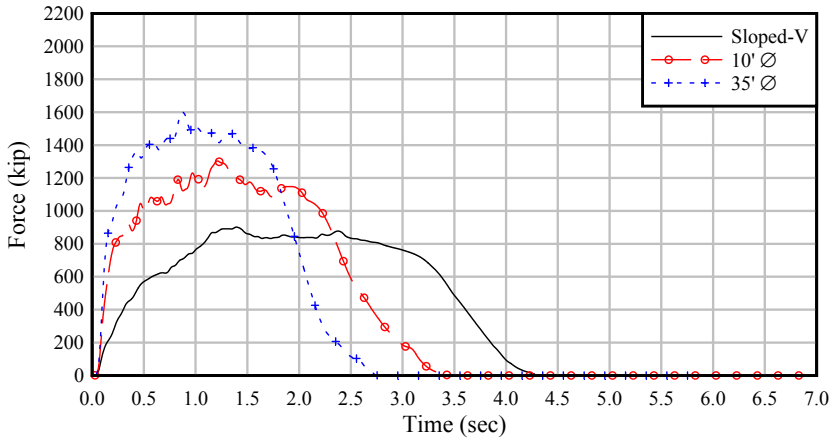

Figure 4.7. Sensitivity to bullnose shape:
3x3 – 2 FPS – [Sloped-V, 10’ ∅, 35’ ∅] – Bow – Interior

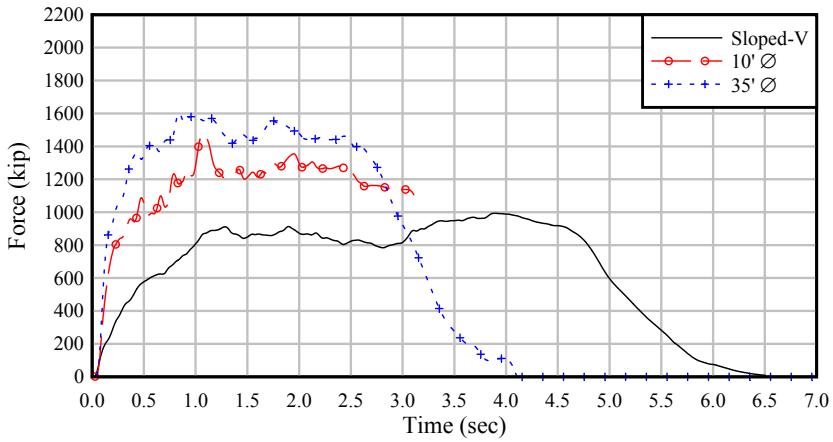

Figure 4.8. Sensitivity to bullnose shape:
3x5 – 2 FPS – [Sloped-V, 10’ ∅, 35’ ∅] – Bow – Interior

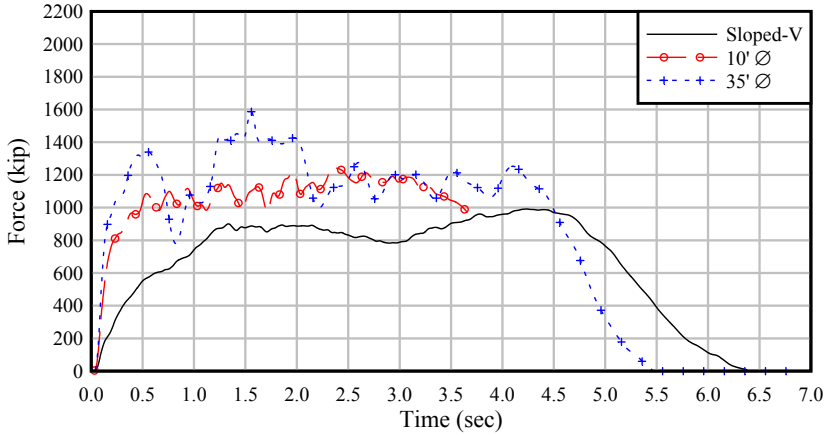

Figure 4.9 Sensitivity to bullnose shape:
3x5 – 2 FPS – [Sloped-V, 10’ ∅, 35’ ∅] – Bow – Exterior

4.4 Impact force sensitivity to bow versus stern impacts

Flotilla impacts on bullnose structures most frequently involve the bow, or raked-end, of a barge making contact with a bullnose. However, conditions involving the stern, or boxed-end, of a barge making contact are also possible. To determine whether larger impact forces are generated by bow or stern impact conditions, simulation results spanning a range of different impact conditions are considered. In Tables 4.1 - 4.3, for every case in which the ‘impact end’ is indicated as ‘stern’, there is a corresponding case for which the impact end is indicated as ‘bow’—with all other impact parameters (flotilla size, impact speed, etc.) being identical. As these tables indicate, stern impacts fall into one of two categories: single barge (1x1) stern impacts on all bullnoses (10’ ∅, 35’ ∅, and sloped-V); and 3x5 flotilla stern impacts on the 35’ ∅ and sloped-V bullnoses. In the latter category, both interior string and exterior string stern impacts are simulated. By comparing impact forces from bow (Figure 4.10a) and stern

(Figure 4.10b) impacts, the data in Tables 4.1 - 4.3 reveal that bow impacts universally generate larger impact forces than stern impacts.

In Figures 4.11 - 4.16, bow and stern impact force-time histories, for selected single barge impacts and 3x5 flotilla impacts, are compared. In all cases, peak stern impact forces are smaller than corresponding peak bow impact forces. Based on this finding, stern impact forces are considered 'non-controlling' (or non-critical) relative to corresponding bow impact forces, and are therefore omitted from the development of force prediction equations discussed later in this chapter.

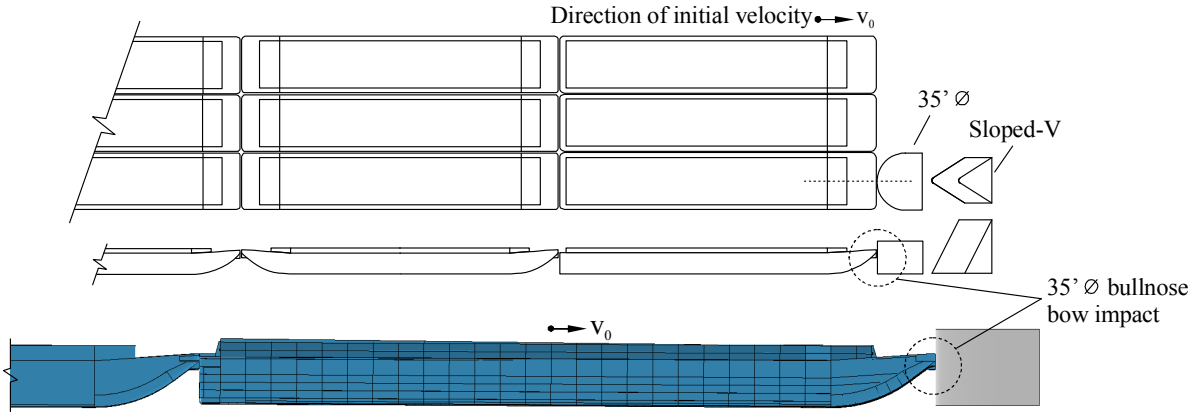

a)

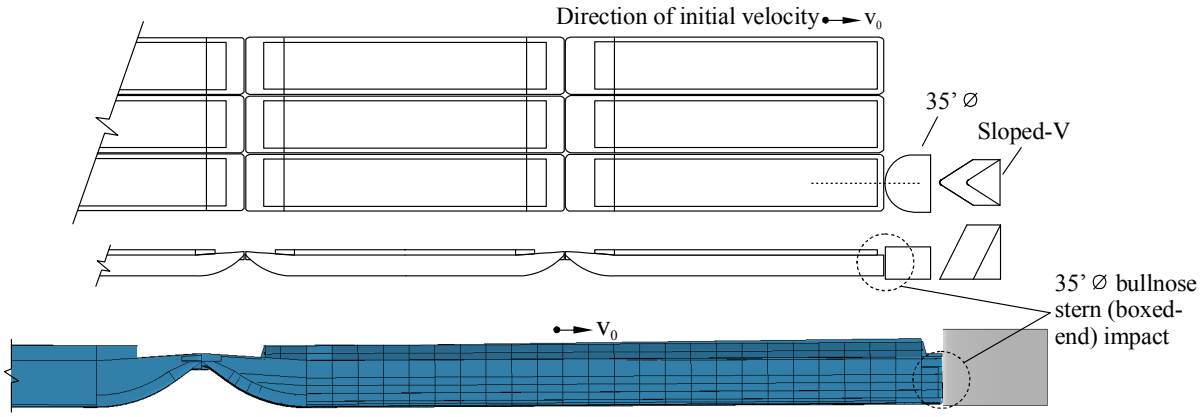

b)

Figure 4.10. Investigation of impact force sensitivity to bow versus stern impact:
a) Bow impact schematic and partial finite element model;
b) Stern (boxed-end) impact schematic and partial finite element model

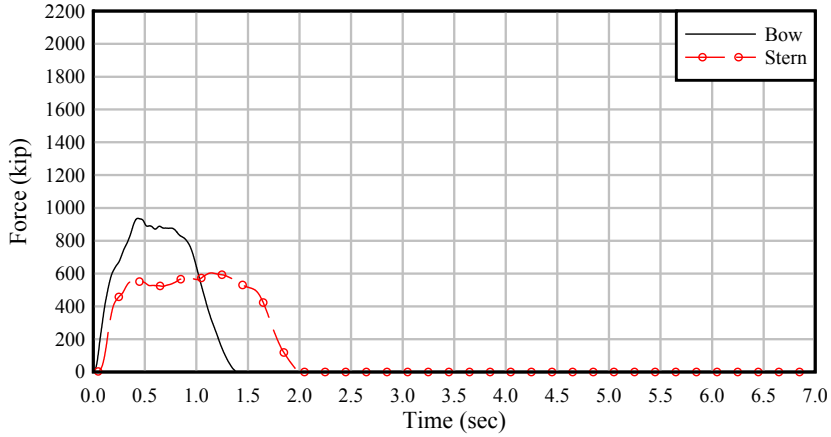

Figure 4.11. Sensitivity to bow versus stern impact:
1x1 – 6 FPS – Sloped-V – [Bow, Stern] – Single barge

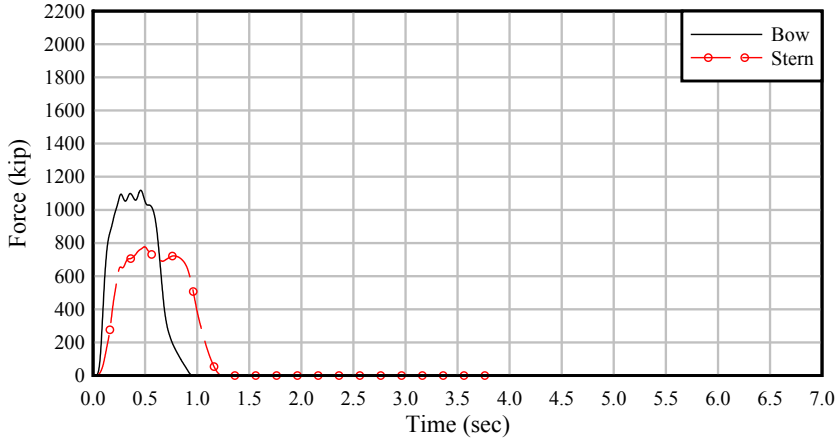

Figure 4.12. Sensitivity to bow versus stern impact:
1x1 – 4 FPS – 10’ ∅ – [Bow, Stern] – Single barge

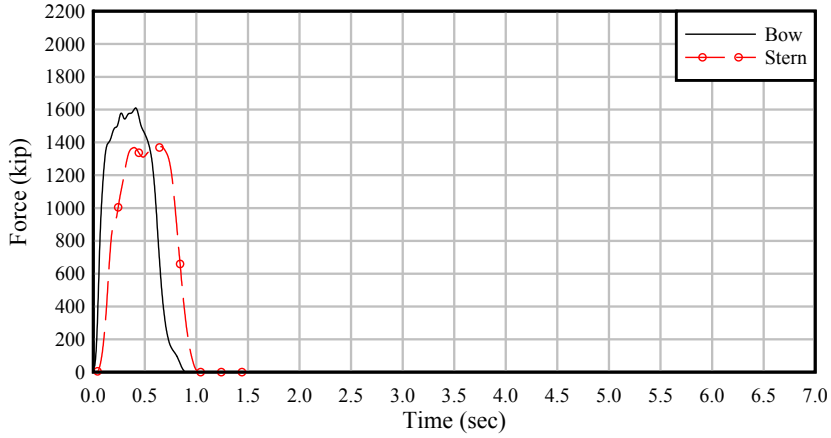

Figure 4.13. Sensitivity to bow versus stern impact:
1x1 – 6 FPS – 35’ ∅ – [Bow, Stern] – Single barge

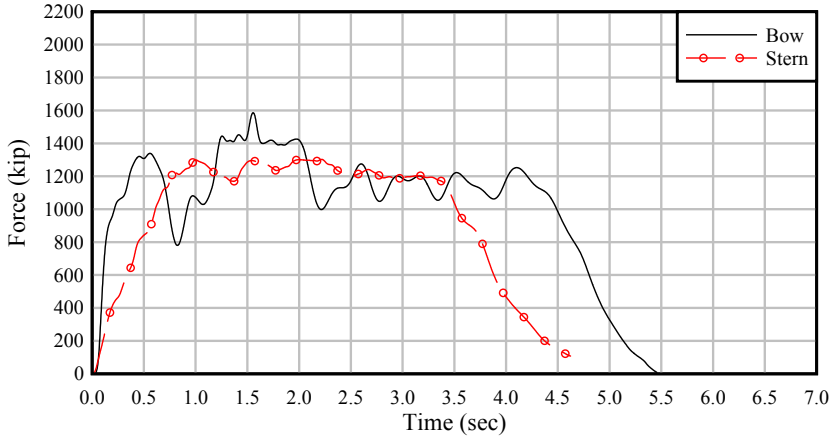

Figure 4.14. Sensitivity to bow versus stern impact:
3x5 – 2 FPS – 35’ ∅ – [Bow, Stern] – Exterior

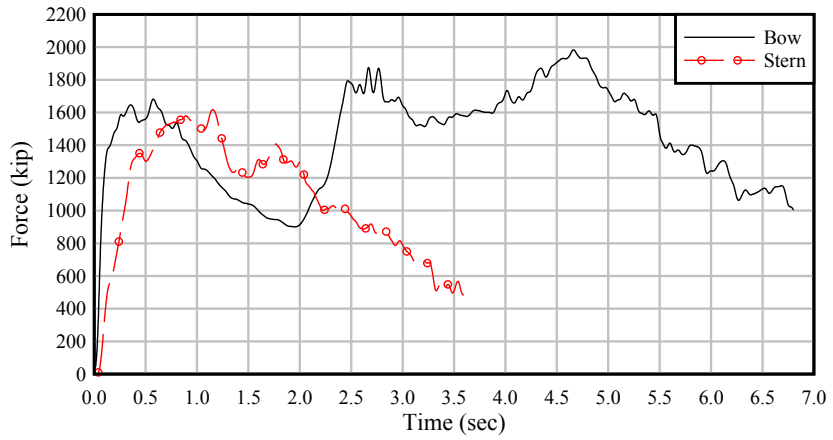

Figure 4.15. Sensitivity to bow versus stern impact:
3x5 – 6 FPS – 35’ ∅ – [Bow, Stern] – Exterior

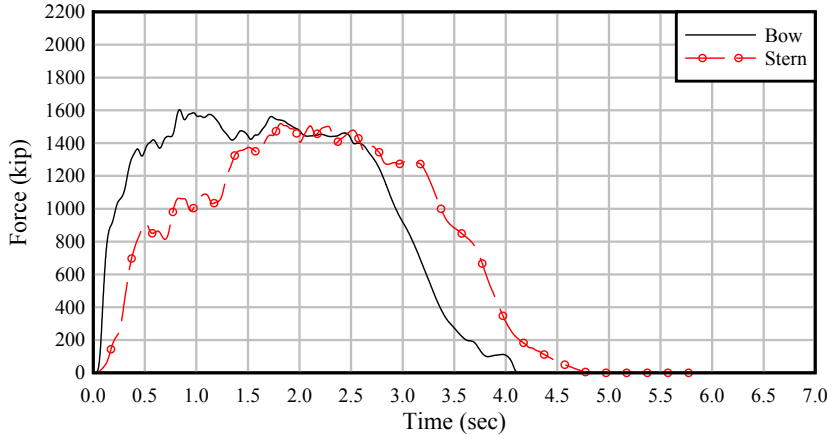

Figure 4.16. Sensitivity to bow versus stern impact:
3x5 – 2 FPS – 35’ ∅ – [Bow, Stern] – Interior

4.5 Impact force sensitivity to interior versus exterior string impacts

For impact conditions involving flotillas with three (or more) barge strings, it is of interest to determine how forces from exterior string impacts (Figure 4.17a-b) compare to forces from interior string impacts (Figure 4.17c-d). In an exterior string impact, the impacting string and the non-impacting strings are separated by a single shear plane that runs along the length of the flotilla. Lashings span across this shear plane and connect the non-impacting strings (and their momentum) to the impacting string. In an interior string impact situation, however, there are *two* such shear planes—and therefore approximately twice as many lashings—that connect the non-impacting strings to the impacting string. It is therefore of interest to determine whether interior string impacts generate larger impact forces than exterior string impacts. Such an increase, if exhibited, would presumably be attributable to the momentum of the non-impacting strings being 'better connected'—through twice as many lashings—to the impacting string.

In Table 4.4, peak impact forces for *bow* impacts of 3x3 and 3x5 flotillas on 10' ∅, 35' ∅, and sloped-V bullnoses are compared for exterior and interior string impact conditions. Additionally, in Figures 4.18 - 4.25, detailed force-time histories for these same cases are presented and compared. In Table 4.4, positive (+) values of % force-change (last column) indicate cases for which an interior string impact condition generates a larger force than the corresponding exterior string condition. The data in Table 4.4 indicate that—at least for the cases studied here—low speed (2 FPS) interior string impacts produce forces that are roughly 0 - 20% larger than corresponding exterior forces (as expected), but high speed (6 FPS) interior string impacts produce forces that are roughly 0 - 15% *smaller* than corresponding exterior forces.

Based on the data generated and available in this study, no clear correlation between impact string (exterior vs. interior) and impact force is evident. Determination as to which configuration will produce a larger impact force appears to be a more subtle reflection of the specifics of the overall impact event (bullnose shape, flotilla shape, motions of barge during impact, lashing forces, etc.). Consequently, data from *both* types of impact conditions (exterior and interior string impacts) are used later in this chapter in the development of force prediction equations.

Table 4.4. Comparison of peak bow impact forces from interior and exterior string impacts

Flotilla Size	Impact Speed	Bullnose Shape	Exterior string impact force (kip)	Interior string impact force (kip)	Interior vs. exterior impact force change
3 x 5	2 FPS	10' ∅	1249	1480	+ 18.5%
3 x 5	6 FPS	10' ∅	1653	1477	- 10.6%
3 x 3	2 FPS	35' ∅	1341	1601	+ 19.4%
3 x 5	2 FPS	35' ∅	1586	1604	+ 1.1 %
3 x 5	6 FPS	35' ∅	1983	1996	+ 0.7 %
3 x 3	2 FPS	Sloped-V	900	902	+ 0.2%
3 x 5	2 FPS	Sloped-V	991	994	+ 0.3%
3 x 5	6 FPS	Sloped-V	1935	1654	- 14.5%

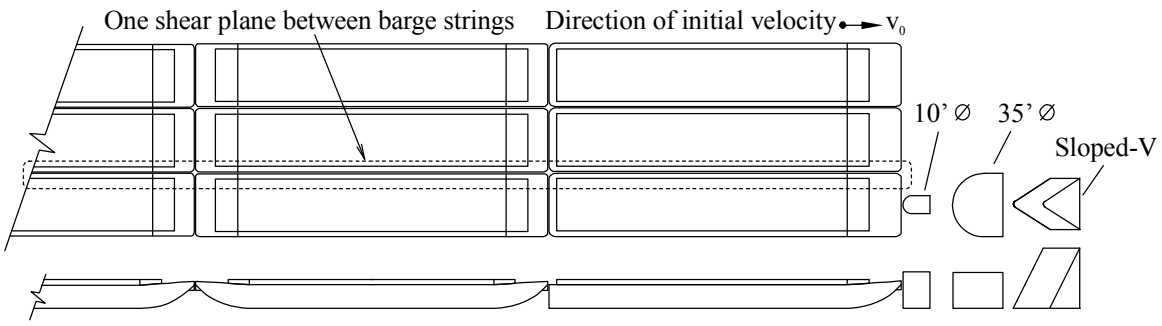

a)

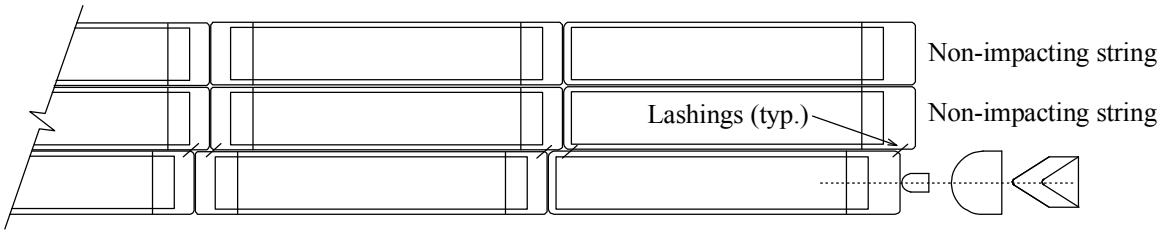

b)

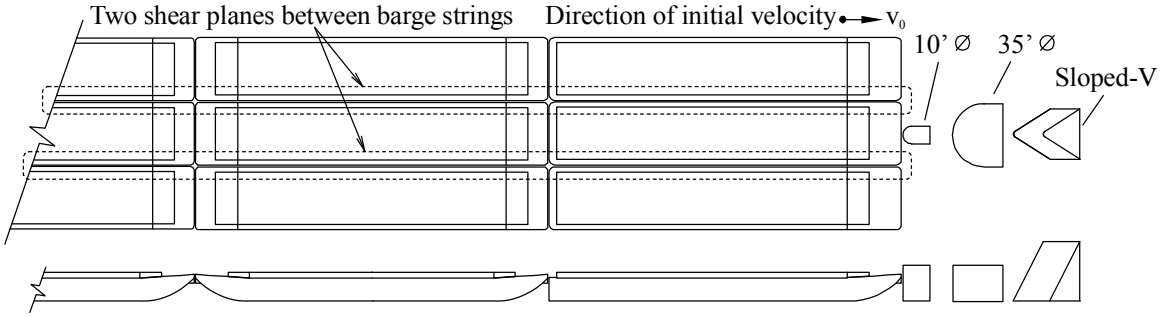

c)

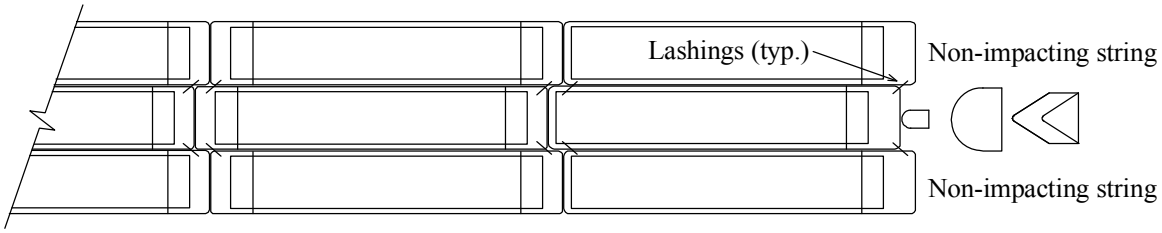

d)

Figure 4.17. Investigation of impact force sensitivity to impacting string:
a) Exterior string configuration *prior* to impact; b) Exterior string configuration *during* impact;
c) Interior string configuration *prior* to impact; d) Interior string configuration *during* impact
(Note: lashings in figure are 'iconic' only and to not indicate actual number of lashing elements)

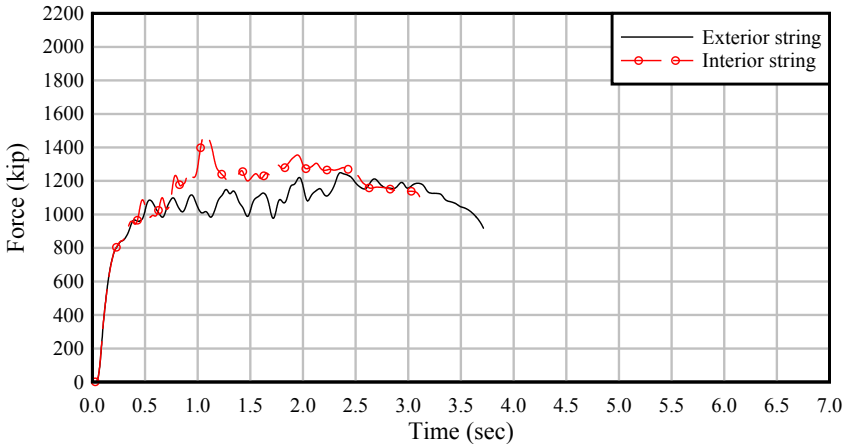

Figure 4.18. Sensitivity to impact string:
3x5 – 2 FPS – 10’ ∅ – Bow – [Exterior, Interior]

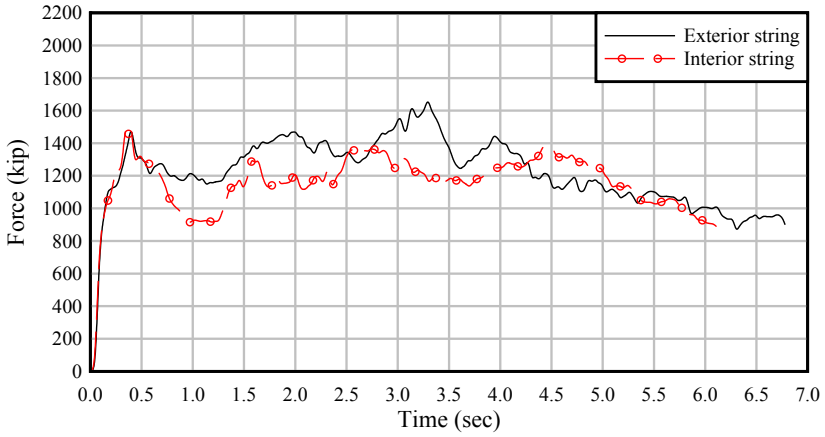

Figure 4.19. Sensitivity to impact string:
3x5 – 6 FPS – 10’ ∅ – Bow – [Exterior, Interior]

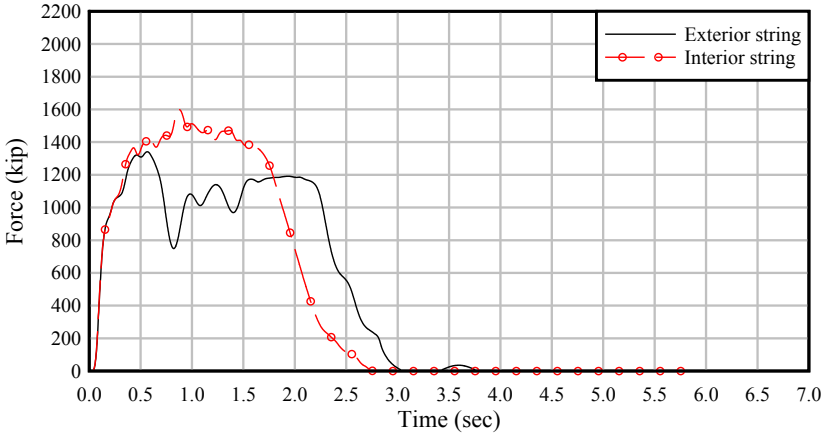

Figure 4.20. Sensitivity to impact string:
3x3 – 2 FPS – 35’ ∅ – Bow – [Exterior, Interior]

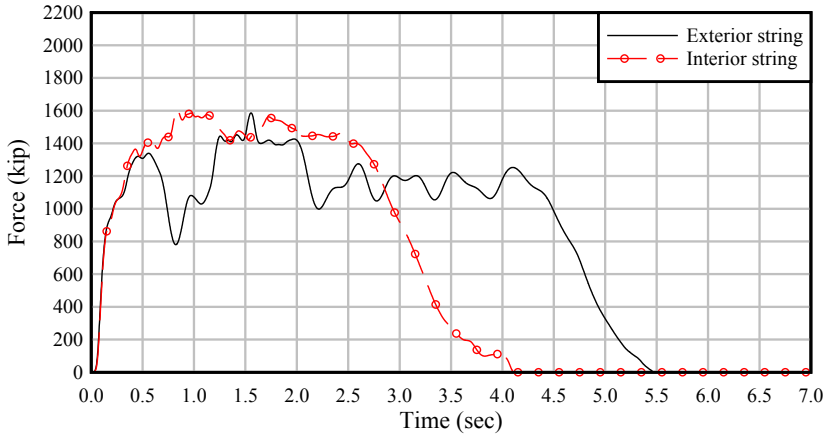

Figure 4.21. Sensitivity to impact string:
3x5 – 2 FPS – 35’ ∅ – Bow – [Exterior, Interior]

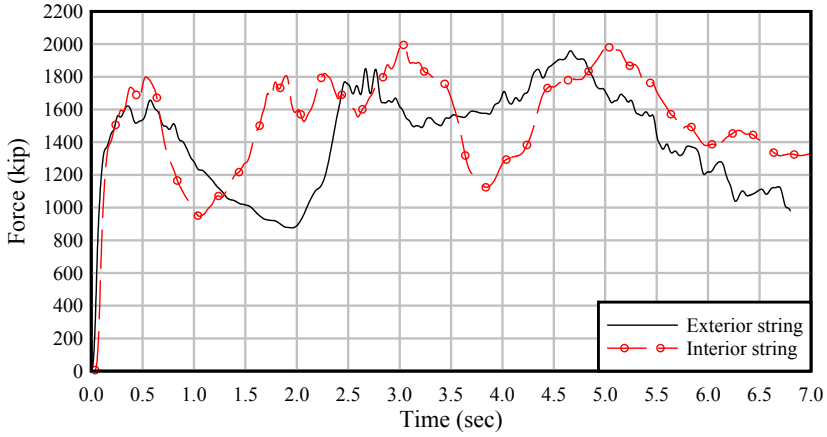

Figure 4.22. Sensitivity to impact string:
3x5 – 6 FPS – 35’ ∅ – Bow – [Exterior, Interior]

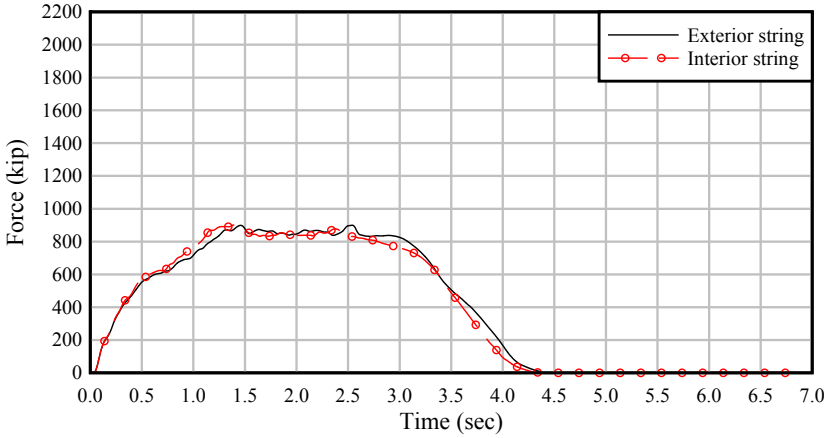

Figure 4.23. Sensitivity to impact string:
3x3 – 2 FPS – Sloped-V – Bow – [Exterior, Interior]

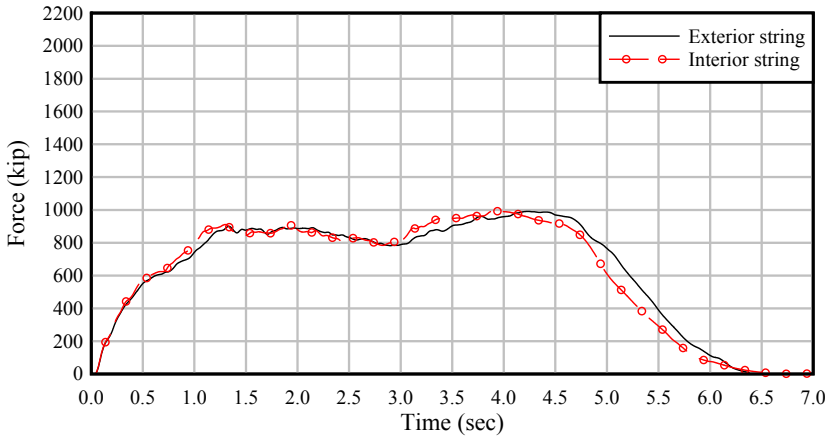

Figure 4.24. Sensitivity to impact string:
3x5 – 2 FPS – Sloped-V – Bow – [Exterior, Interior]

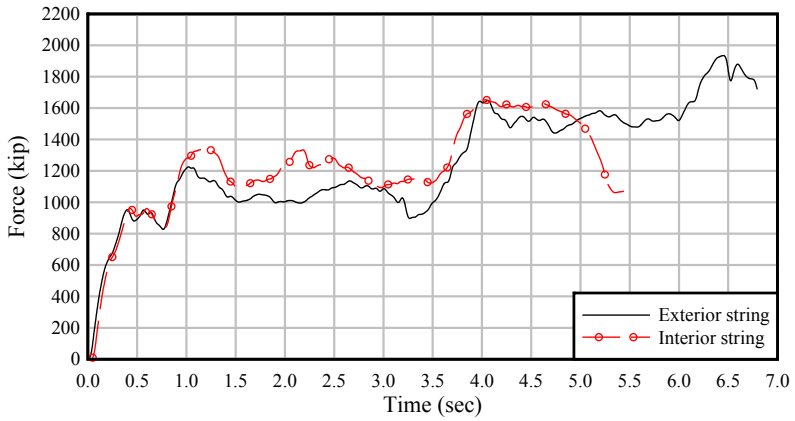

Figure 4.25. Sensitivity to impact string:
3x5 – 6 FPS – Sloped-V – Bow – [Exterior, Interior]

4.6 Impact force sensitivity to impact angle for 35' diameter bullnose

For the 35' ∅ semi-circular bullnose, the sensitivity of impact force to impact angle is investigated for both exterior and interior string impact conditions (Figure 4.26). In Figures 4.27 - 4.28, force-time histories are compared for impact angles of 0° and 30°. The force data clearly indicate that no significant relationship is exhibited between impact angle and peak force for this bullnose. For semi-circular bullnoses, rotating the impact surface through angles of less than ~30° has no effect for small deformation levels, and only minimal effect at large deformation levels (where the barge may interact with the 'flat' sidewalls of the bullnose).

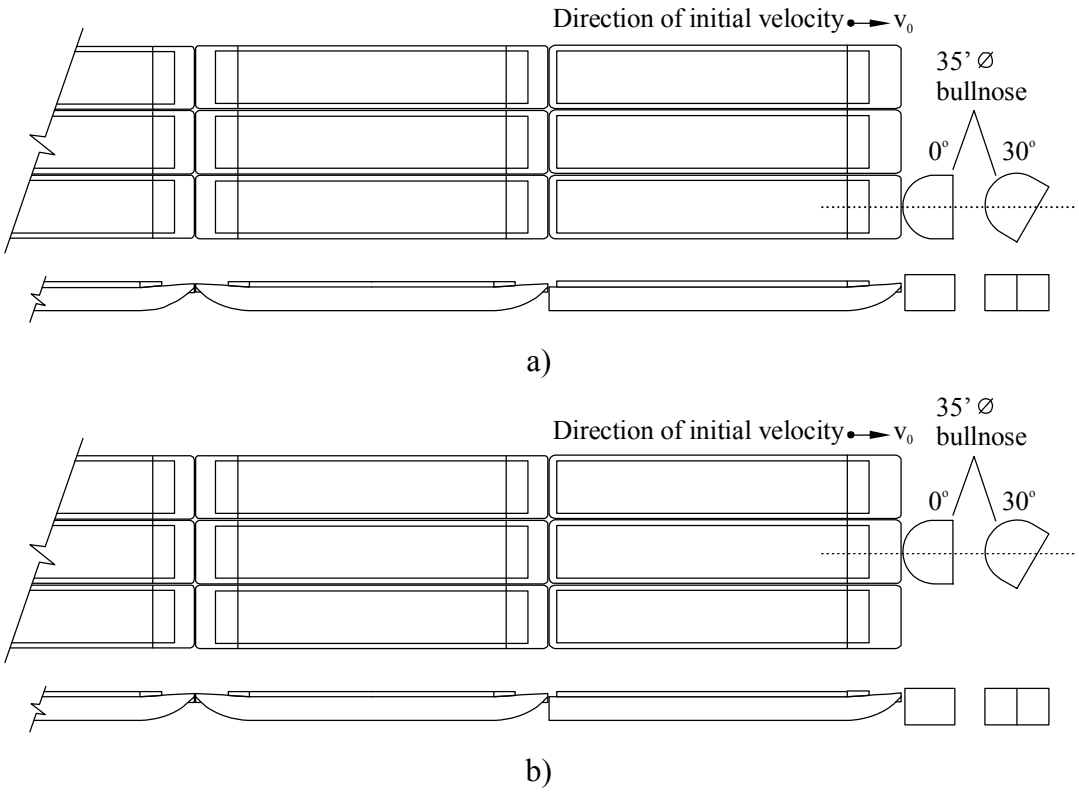

Figure 4.26. Investigation of impact force sensitivity to impact angle for 35' ∅ bullnose: a) Exterior string impacts; b) Interior string impacts;

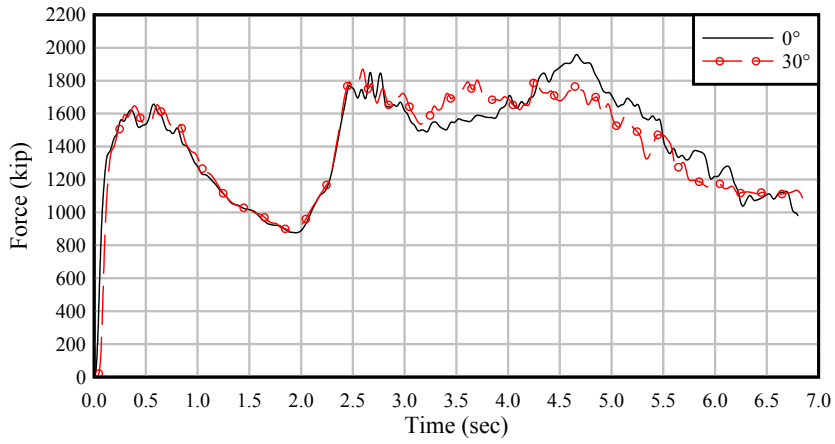

Figure 4.27. Sensitivity to impact angle:
3x5 – 6 FPS – 35' ∅ – Bow – Exterior – [0°, 30°]

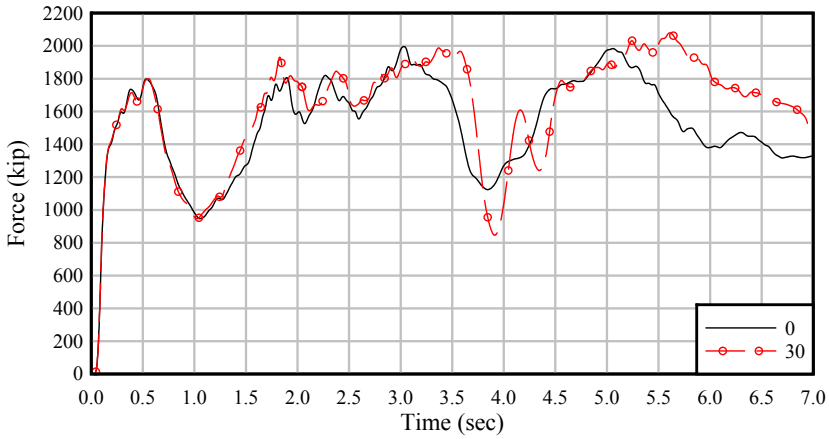

Figure 4.28. Sensitivity to impact angle:
3x5 – 6 FPS – 35’ ∅ – Bow – Interior – [0°, 30°]

4.7 Impact force sensitivity studies: sloped-V bullnose

In the following sections, impact force the sensitivities to various system parameters (impact angle, lateral impact offset, and impact face slope) are investigated for the sloped-V bullnose.

4.7.1 Impact angle

Since the sloped-V bullnose has a ‘rounded-triangle’ shape that differs from the semi-circular geometry discussed above, the sensitivity of impact force to impact angle is investigated for the sloped-V using exterior string 3x5 barge impacts conducted at 0°, 10°, 20°, and 30° (Figure 4.29). Force-time histories for all impact angles are compared in Figure 4.30. Peak forces produced by all impact angles are very similar in magnitude, hence impact forces for the sloped-V do not appear to exhibit angle sensitivity (i.e., dependency).

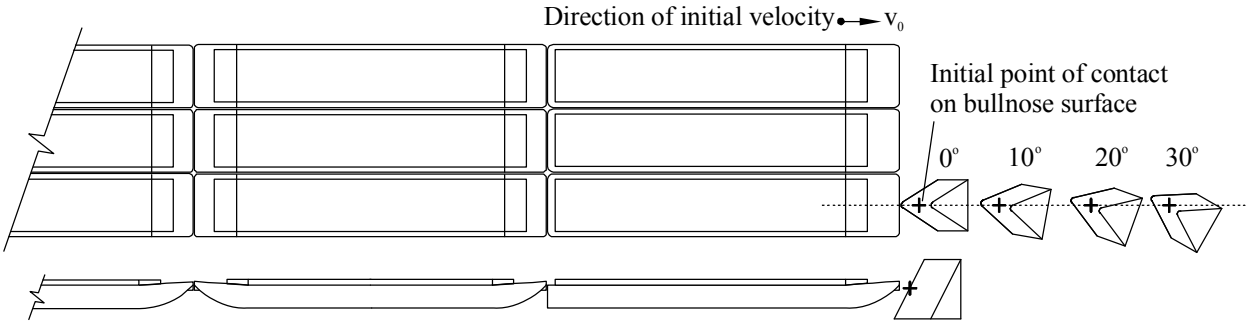

Figure 4.29. Investigation of impact force sensitivity to impact angle for the 2:1 sloped-V bullnose

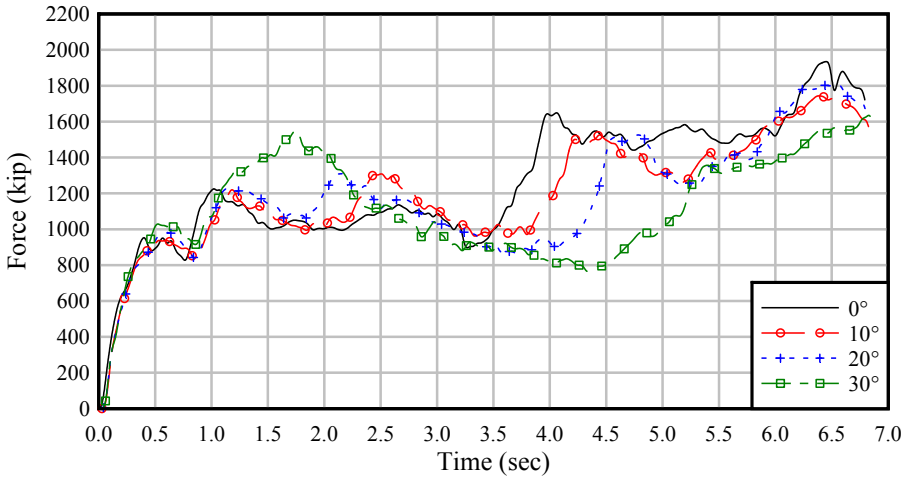

Figure 4.30. Sensitivity to impact angle:
3x5 – 6 FPS – 2:1 Sloped-V – Bow – Exterior – [0°, 10°, 20°, 30°]

4.7.2 Off-center impacts

To ensure that conservatively large values of impact force are quantified for the sloped-V bullnose, the sensitivity of impact force to lateral offset is investigated using 3x5 exterior string bow impacts (Figure 4.31). Simulations are conducted at lateral offset distances—relative to the barge centerline—of 5', 10', and 15'. Force-time histories for these cases are compared to the centerline impact condition in Figure 4.32. While the centerline condition produces the largest peak impact force, offsets of 5' and 10' produce peak forces that are moderately smaller. In contrast, however, an offset of 15' produces a *substantially reduced* peak impact force. At an offset of 15', the bullnose center line, and therefore the initial point of contact, is very close to the outside edge of the impacting barge. Consequently, when the rounded geometry of the barge corner interacts with the rounded (and sloped) face of the bullnose, the impacting barge is *redirected* off of one side of the bullnose (Figure 4.33) rather than becoming 'snagged' at the tip of the triangular bullnose (which would abruptly decelerate and halt the flotilla). Hence, because the flotilla is redirected rather that halted, the peak force is greatly reduced and the force-time history is more typical of the shallow angle (oblique) glancing blows investigated in previous studies (e.g., Consolazio et al. 2012). Consequently, because the centerline (zero offset) impact condition produces the largest peak force, only data for centerline impact cases will be used later in this chapter in the development of force prediction equations.

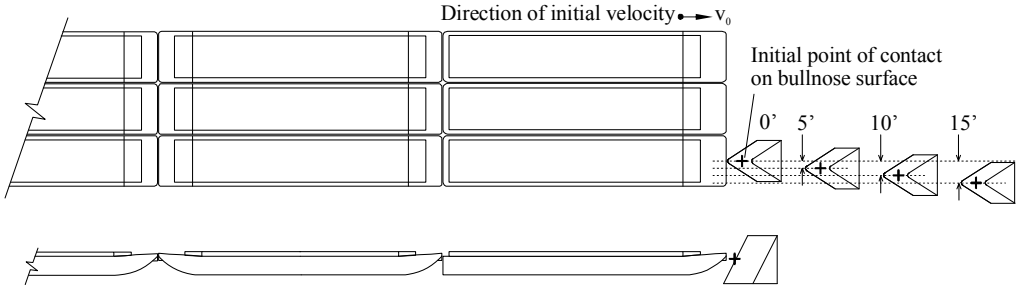

Figure 4.31. Investigation of impact force sensitivity to lateral offset for 2:1 sloped-V bullnose

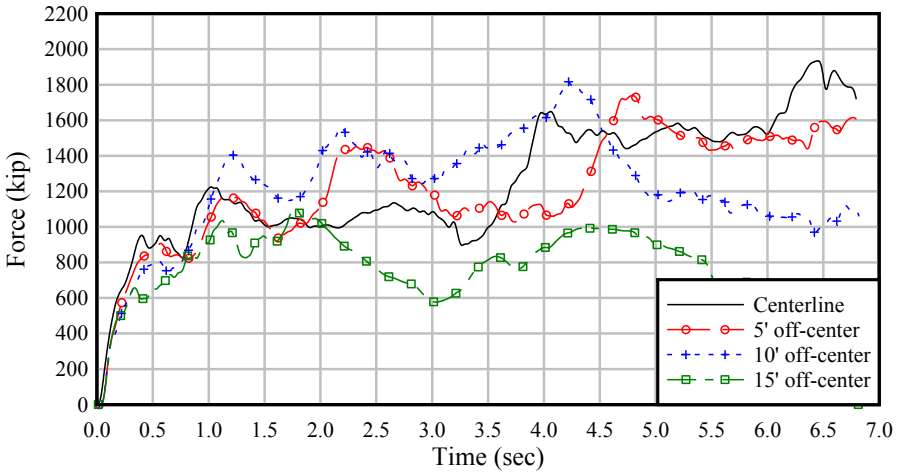

Figure 4.32. Sensitivity to lateral offset:
3x5 – 6 FPS – 2:1 Sloped-V – Bow – Exterior – [0', 5', 10', and 15' offsets]

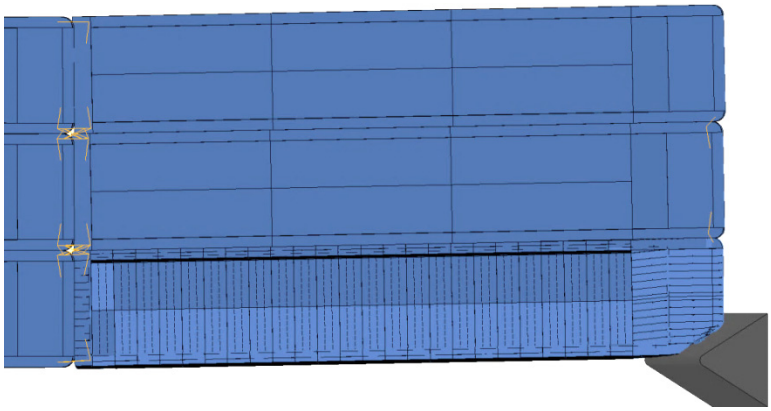

Figure 4.33. Flotilla redirection at approximately 3 sec. after initial contact:
3x5 – 6 FPS – 2:1 Sloped-V – Bow – Exterior – 15' off-center

4.7.3 Face slope

For the sloped-V bullnose, it is of interest to determine whether reducing the slope of the impact face (Figure 4.34) might produce favorable reductions in impact force and potential for flotilla breakup (which is related to lashing failure). Hence, a slope-sensitivity investigation is carried out by simulating 3x5 exterior string impacts on sloped-V bullnoses having slopes of: 2:1 (baseline slope); 1:1 (intermediate slope); and 1:2 (shallow slope). Horizontal impact forces plotted in Figure 4.35 indicate that reducing the face slope to 1:1 appears to have little effect, but that further reducing the slope to 1:2 reduces the peak horizontal force by roughly one half (50%). However, vertical forces (Figure 4.36) trend in the opposite direction: reducing the face slope *increases* the downward force acting on the bullnose. Such results are expected because reductions in the slope of the impact face increase the ability of the impacting barge to 'slide up' the face of the bullnose—a behavior which reduces horizontal force but increases vertical force.

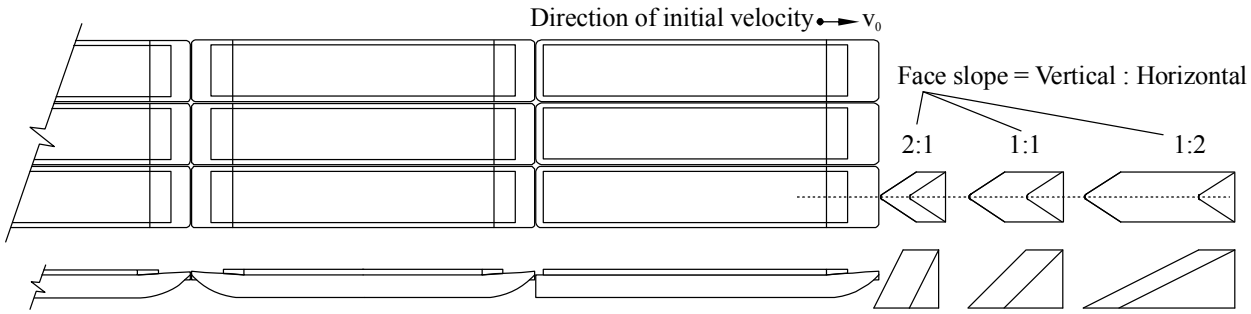

Figure 4.34. Investigation of impact force sensitivity to face slope for sloped-V bullnose

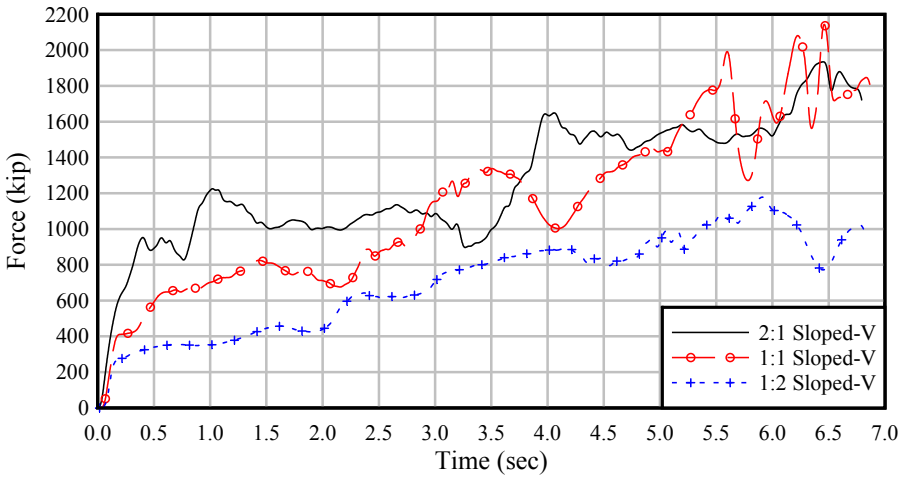

Figure 4.35. Horizontal force sensitivity to face slope of sloped-V bullnose:
3x5 – 6 FPS – [2:1 Sloped-V, 1:1 Sloped-V, 1:2 Sloped-V] – Bow – Exterior

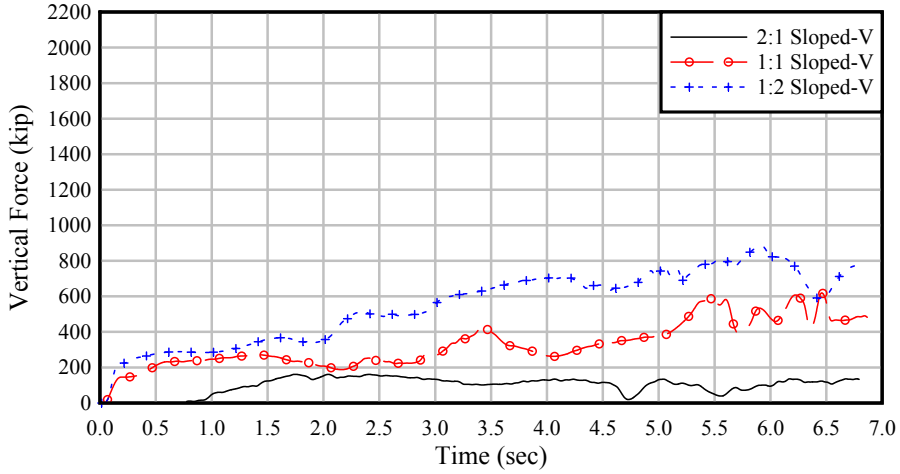

Figure 4.36. Vertical force sensitivity to face slope of sloped-V bullnose:
3x5 – 6 FPS – [2:1 Sloped-V, 1:1 Sloped-V, 1:2 Sloped-V] – Bow – Exterior
(Note: positive values indicate downward force on the bullnose)

With regard to the potential effects of face slope on flotilla breakup, in each of the three impact cases studied (2:1, 1:1, 1:2), three (3) lashings in the flotilla model reached or exceeded 90% of their respective ultimate capacities (note that the three lashing that reached this condition were not the same in all three impact cases). However, in all three of the impact cases studied, even complete failure of three lashings in question would not create a condition in which a barge is able to float freely away from the rest of the flotilla. Hence, results from this investigation suggest no measurable change in likelihood of flotilla breakup.

4.8 Impact force sensitivity to number of barge strings

The sensitivity of impact forces to the number of barge strings is investigated using flotillas of two lengths: three (3) rows, and five (5) rows (Figure 4.37). For each length, the number of barge strings (i.e., the flotilla width) is incremented from 1, to 2, to 3. Two-string ('two-wide') flotillas consist of a single impacting string and a single non-impacting string (connected together through lashings), whereas three-string ('three-wide') flotillas consist of an impacting string and two non-impacting strings. As such, adding additional strings to a single string flotilla can be viewed as adding additional non-impacting mass (and therefore non-impacting momentum).

Force-time histories for selected cases are presented in Figures 4.38 - 4.43. Each plot compares force levels produced by impact conditions that are identical in every way *except* in the number of barge strings present in the flotilla. The most evident trend in these figures is that significant changes of impact *duration* are produced by changing the number of strings. Although not universally true, the impact durations are roughly proportional to the total number of strings in the flotilla.

With regard to impact force *magnitudes* (i.e., peak impact forces), several of the comparisons presented (e.g., Figure 4.38, 4.40, 4.41, and 4.43) suggest a relationship between peak force and number of strings. In particular, Figures 4.41 and 4.43 clearly indicate that increasing the number of strings (and thereby increasing the flotilla mass) results in an increase in peak impact force. However, these figures also reveal that the incremental force increases produced by adding additional strings are smaller than the baseline force level produced by a single string impact. This suggests that the mass and momentum associated with non-impacting strings contributes to impact force, but—perhaps due to lashing flexibility—not as strongly as the mass and momentum of the impacting string.

4.9 Impact force sensitivity to number of barge rows

The sensitivity of impact forces to the number of barge rows is investigated using flotillas with one (1) string, two (2) strings, and three (3) strings (Figure 4.44) by incrementing the number of barge rows by two (2) to produce flotillas with three (3) and five (5) rows. Force-time histories for selected cases are presented in Figures 4.45 - 4.53. Each plot compares force levels produced by impact conditions that are identical in every way *except* in the number of barge rows. The most evident trend in these figures is that significant changes of impact duration are produced by adding rows (as was the case when strings were added, as discussed in the previous section). Impact durations appear to be roughly proportional to the number of rows in the flotilla.

With regard to impact force magnitudes, several cases indicate a possible relationship between peak force and number of rows. For example, Figures 4.50, 4.51, and 4.53 indicate that increasing the number of rows from three (3) to five (5) increases the peak impact forces, although not in direct proportion to the number of added rows.

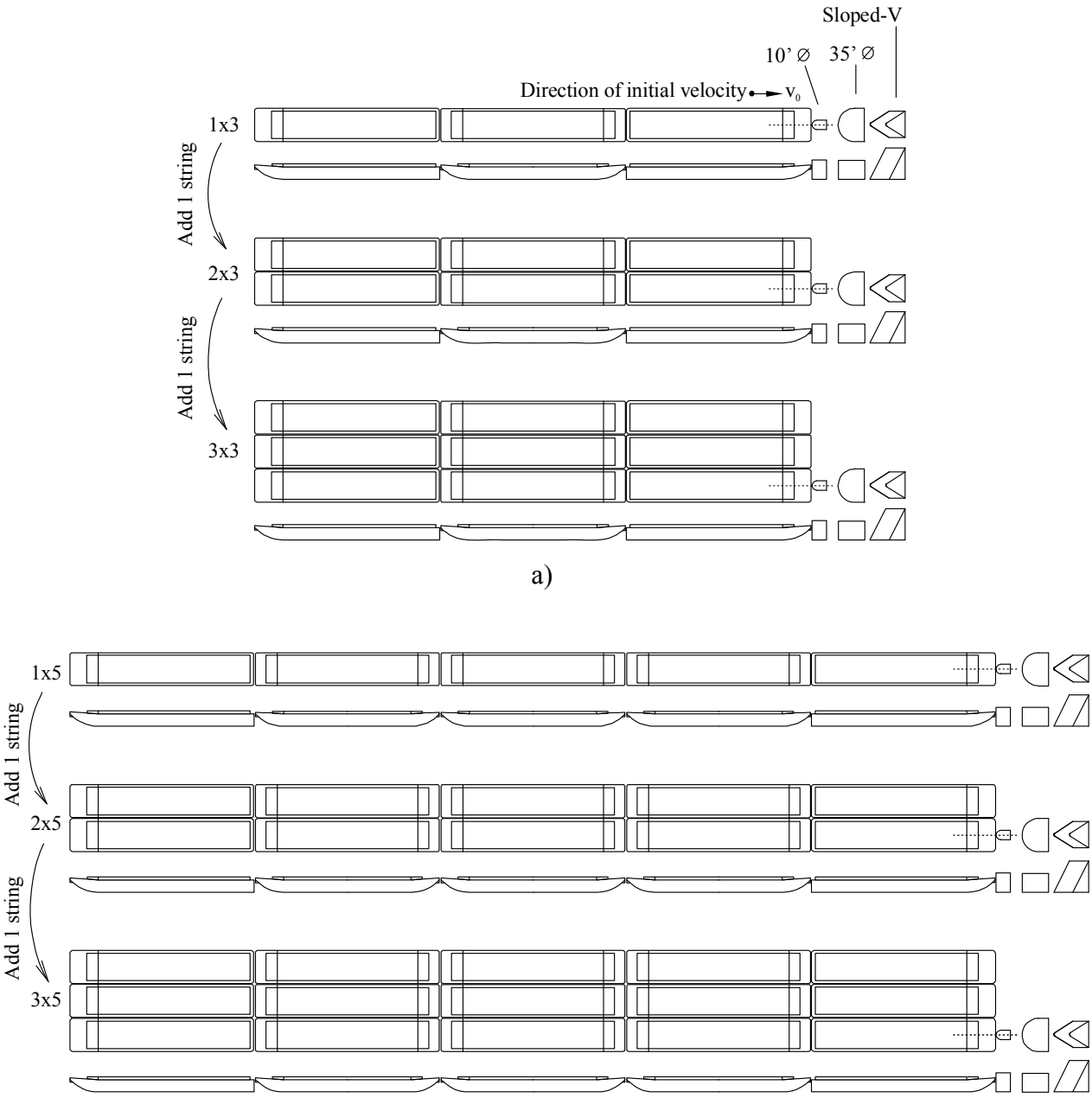

Figure 4.37. Investigation of impact force sensitivity to number of flotilla strings:
a) Incremental addition of strings to a three row flotilla;
b) Incremental addition of strings to a five row flotilla;

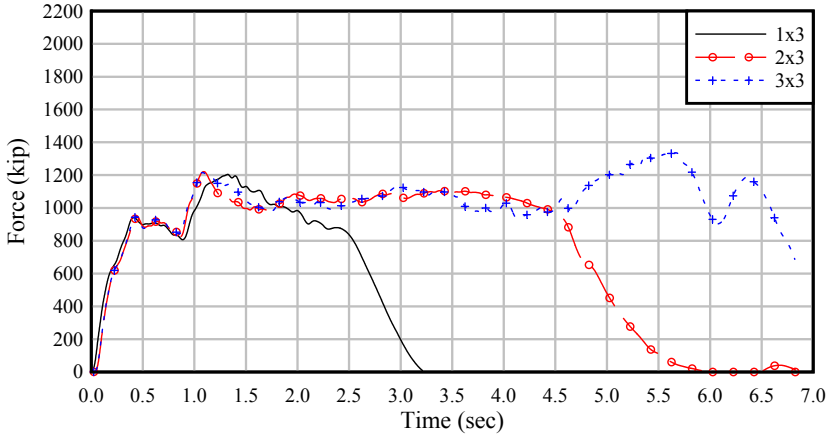

Figure 4.38. Sensitivity to number of strings:
[1, 2, 3] strings x 3 rows – 6 FPS – Sloped-V – Bow – Exterior

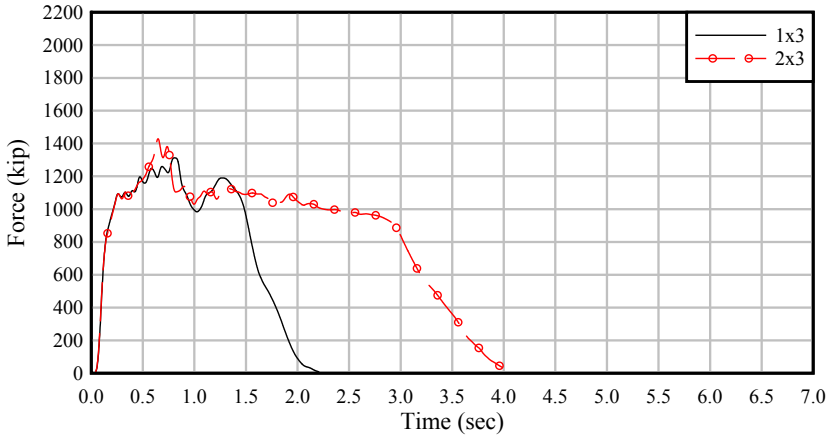

Figure 4.39. Sensitivity to number of strings:
[1, 2] strings x 3 rows – 4 FPS – 10’ ∅ – Bow – Exterior

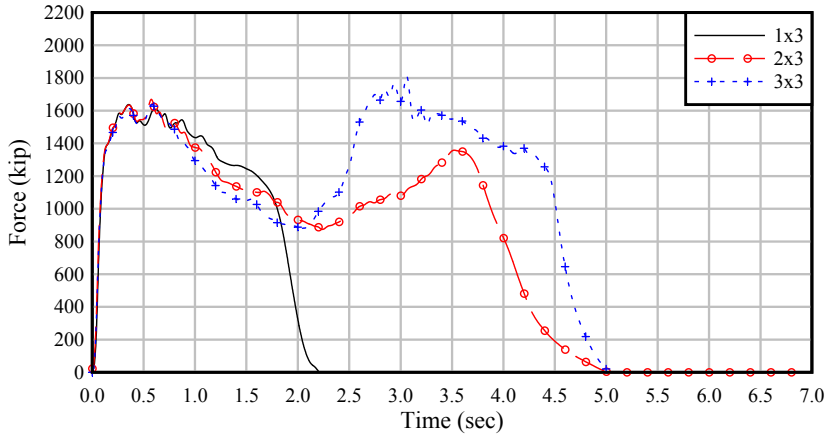

Figure 4.40. Sensitivity to number of strings:
[1, 2, 3] strings x 3 rows – 6 FPS – 35’ ∅ – Bow – Exterior

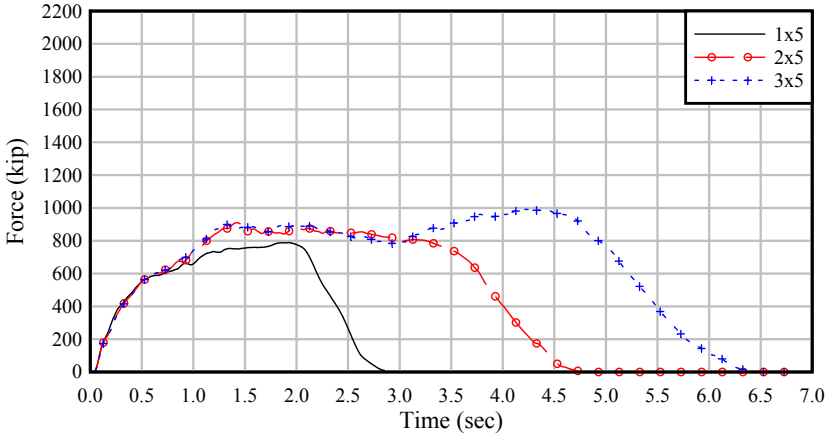

Figure 4.41. Sensitivity to number of strings:
[1, 2, 3] strings x 5 rows – 2 FPS – Sloped-V – Bow – Exterior

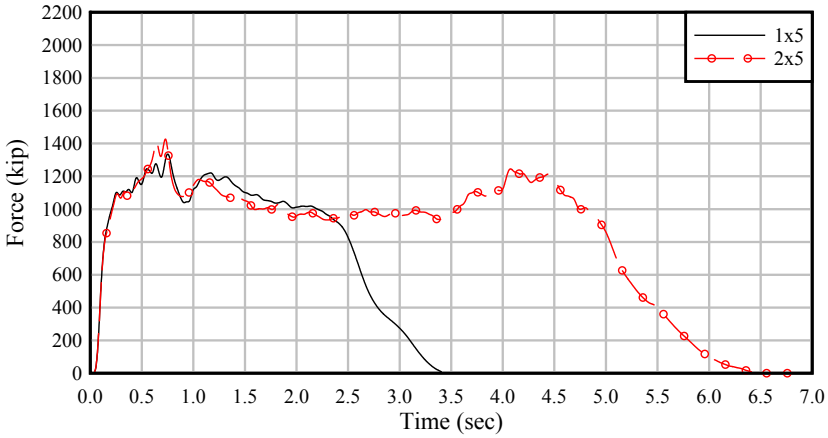

Figure 4.42. Sensitivity to number of strings:
[1, 2] strings x 5 rows – 4 FPS – 10’ ∅ – Bow – Exterior

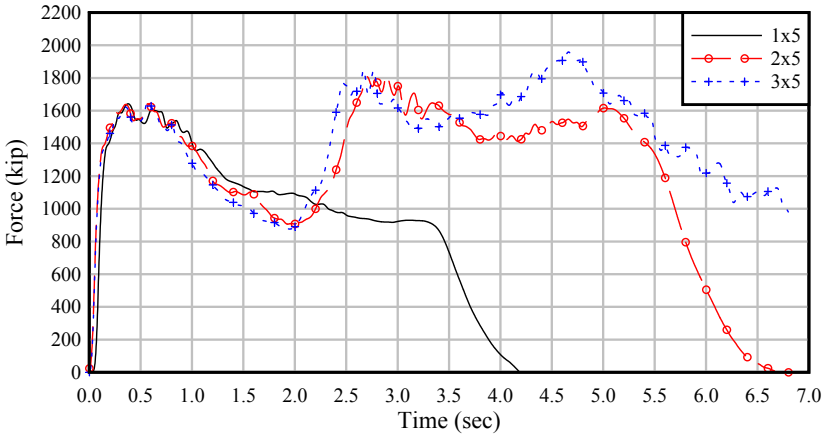

Figure 4.43. Sensitivity to number of strings:
[1, 2, 3] strings x 5 rows – 6 FPS – 35’ ∅ – Bow – Exterior

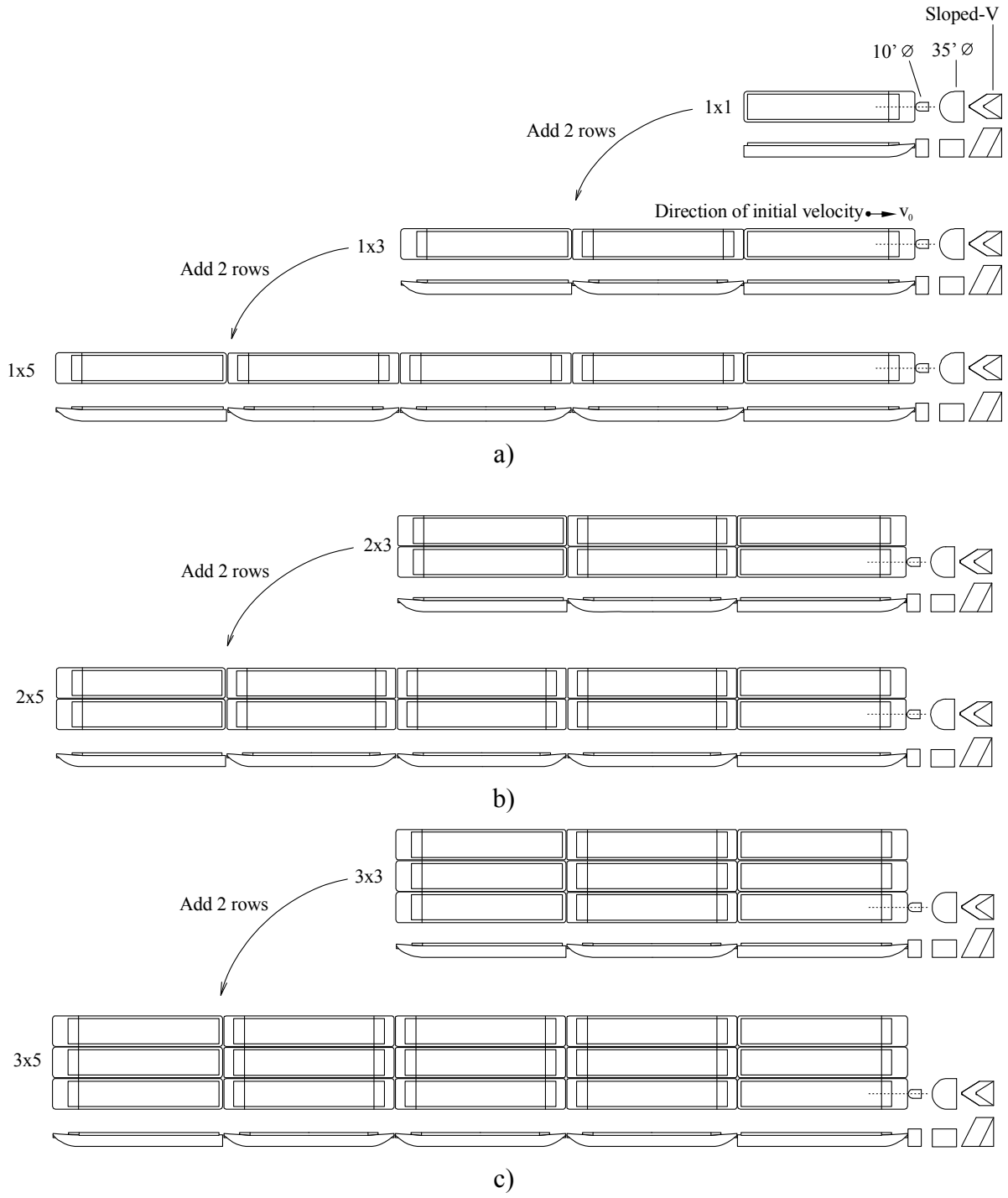

Figure 4.44. Investigation of impact force sensitivity to number of flotilla rows:
a) Incremental addition of rows to a one string flotilla;
b) Incremental addition of rows to a two string flotilla;
c) Incremental addition of rows to a three string flotilla

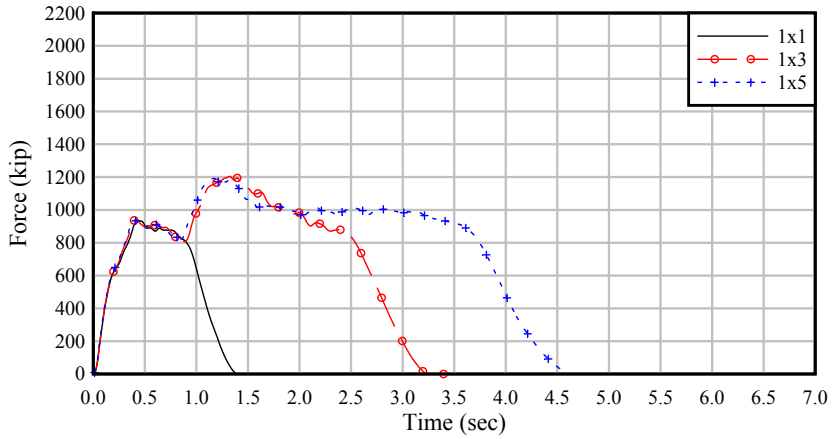

Figure 4.45. Sensitivity to number of rows:
1 string x [1, 3, 5] rows – 6 FPS – Sloped-V – Bow – Single string

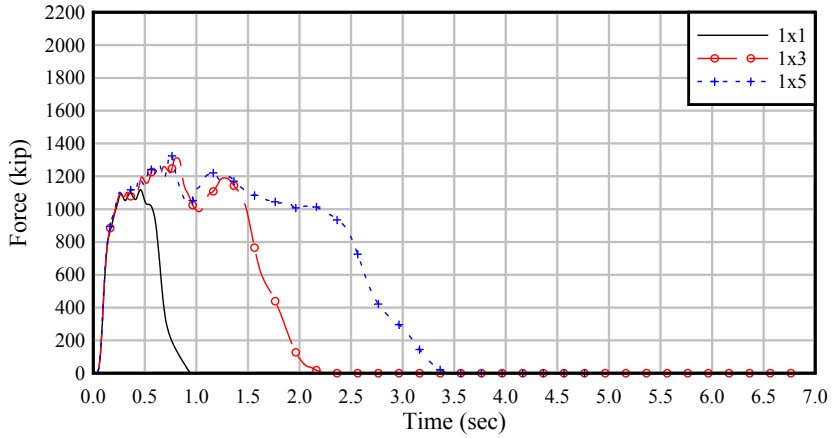

Figure 4.46. Sensitivity to number of rows:
1 string x [1, 3, 5] rows – 4 FPS – 10’ ∅ – Bow – Single string

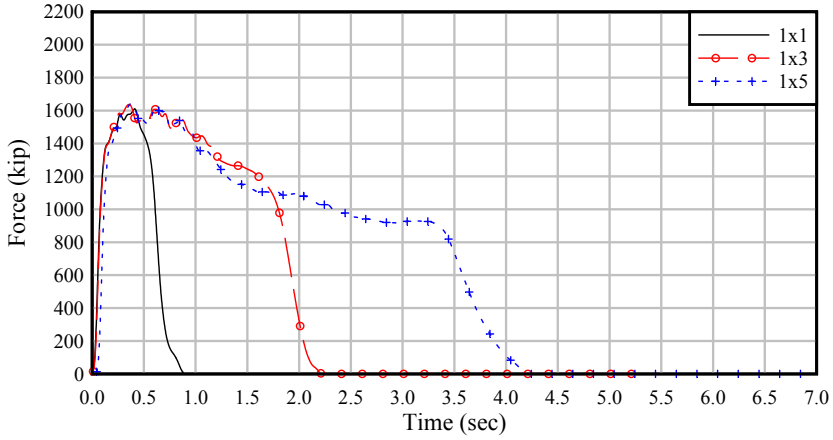

Figure 4.47. Sensitivity to number of rows:
1 string x [1, 3, 5] rows – 6 FPS – 35’ ∅ – Bow – Single string

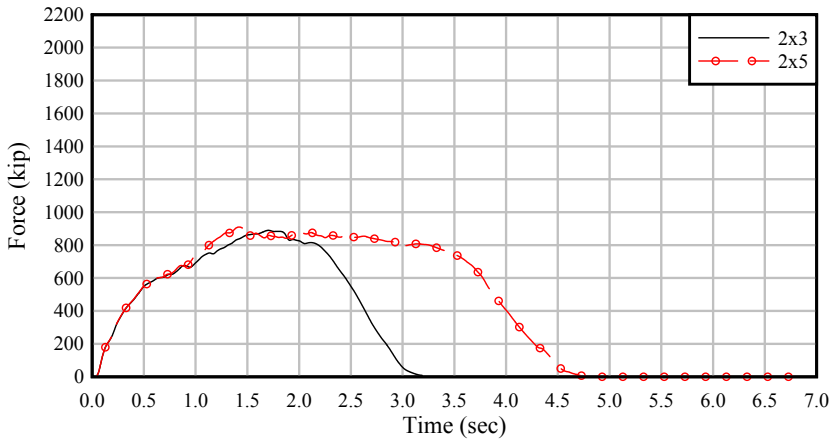

Figure 4.48. Sensitivity to number of rows:
2 strings x [3, 5] rows – 2 FPS – Sloped-V – Bow – Exterior

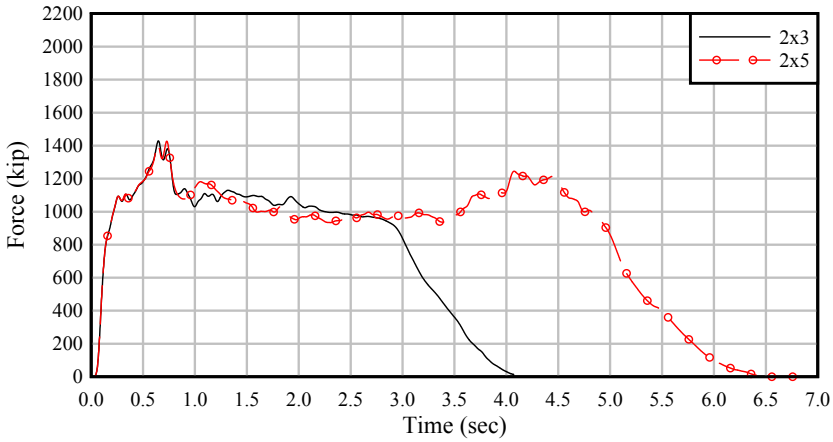

Figure 4.49. Sensitivity to number of rows:
2 strings x [3, 5] rows – 4 FPS – 10’ ∅ – Bow – Exterior

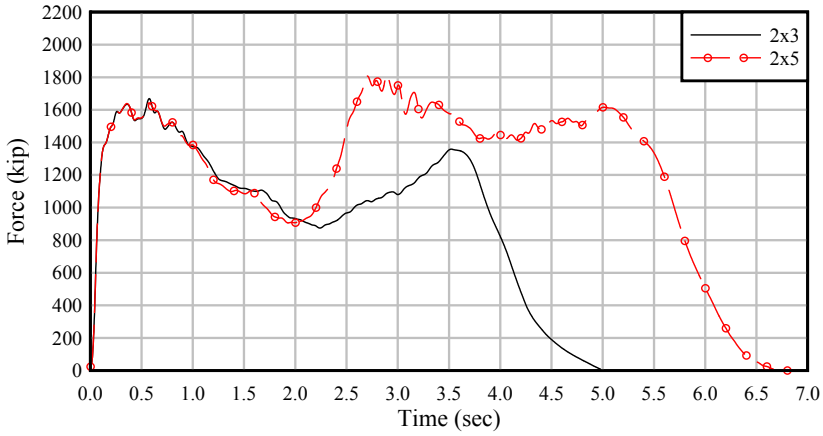

Figure 4.50. Sensitivity to number of rows:
2 strings x [3, 5] rows – 6 FPS – 35’ ∅ – Bow – Exterior

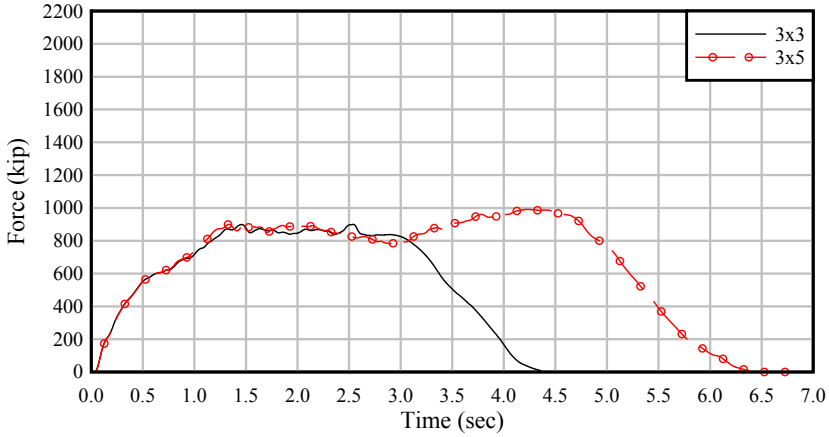

Figure 4.51. Sensitivity to number of rows:
3 strings x [3, 5] rows – 2 FPS – Sloped-V – Bow – Exterior

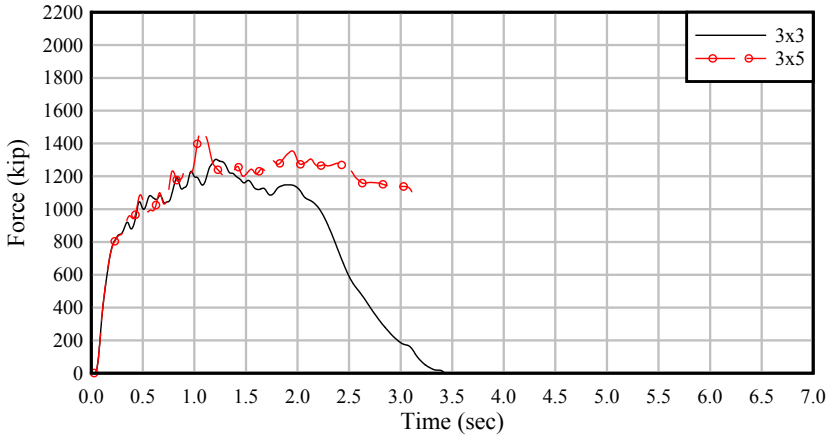

Figure 4.52. Sensitivity to number of rows:
3 strings x [3, 5] rows – 2 FPS – 10’ ∅ – Bow – Interior

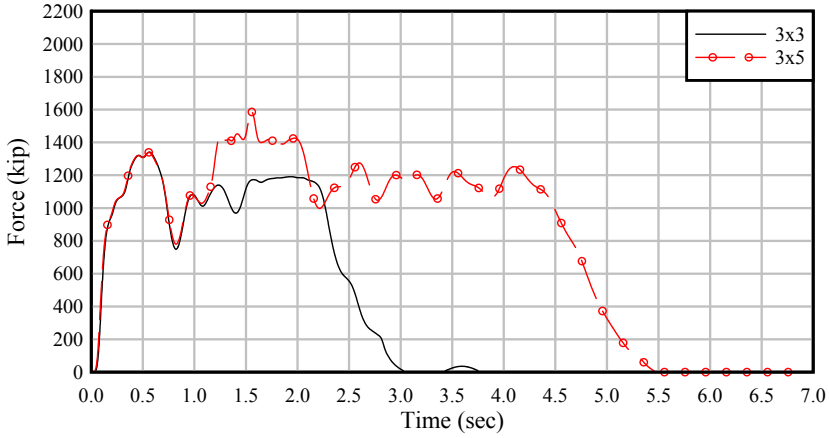

Figure 4.53. Sensitivity to number of rows:
3 strings x [3, 5] rows – 2 FPS – 35’ ∅ – Bow – Exterior

4.10 Empirical prediction of impact load for bullnose structures

Development of empirical impact load (i.e. impact force) prediction equations for bullnose structures is based on correlating peak two-dimensional resultant horizontal impact forces, reported in Tables 4.1 - 4.3, to total flotilla momentum ($p = m \times v$, where m = total flotilla mass and v = flotilla velocity [speed]). However, not all data reported in Tables 4.1 - 4.3 are used in the forming the load prediction equations. Impact cases that are known to produce non-controlling (or non-critical) impact forces are excluded from the development process so as not to bias the resulting curve-fits (between load and momentum) in an unconservative manner. Specifically, the non-controlling cases that are excluded consist of: all stern impacts (10' ∅, 35' ∅, and 2:1 sloped-V); all angled impacts (35' ∅ and sloped-V); and all laterally off-center impacts (sloped-V). Additionally, since the 1:1 sloped-V and 1:2 sloped-V bullnoses do not represent any USACE structures known to currently exist, impact data from these cases are also excluded. Finally, data from the limited number of high-speed (9 FPS and 10 FPS) impact cases are excluded because these speeds are well beyond the USACE 'extreme impact' definition of 4 - 6 FPS.

Using all remaining ('non-excluded') data from Tables 4.1 - 4.3, impact forces for the 10' ∅ bullnose (Figure 4.54), the 35' ∅ bullnose (Figure 4.55), and the 2:1 sloped-V bullnose (Figure 4.56) are linearly related—using least squares regression—to total flotilla momentum. (Coefficients of determination, R^2, for the linear fits are provided in the Figures 4.54 - 4.56). Aside from a small number of data points corresponding to very low momentum levels (single barge [1x1] impact cases), overall, the data presented for each bullnose clearly suggest a linear relationship between force and momentum. This assertion is strengthened by the fact that, based on the number of data points (impact cases) for each bullnose type, and based on the Pearson correlation coefficient (R) for each bullnose, the probability that each of these linear fits is statistically meaningful is computed to be ≥99%.

In Figure 4.57, best-fit linear load prediction lines for all three bullnose shapes are presented together. Comparing the lines for the 10' ∅ and 35' ∅ bullnoses, the latter clearly has a steeper slope indicating that, for a particular momentum level ($m \times v$), larger impact loads will be exerted on a 35' ∅ bullnose than on a 10' ∅ bullnose. This is expected, since—as discussed in Section 4.3—impact against a 35' ∅ bullnose will structurally engage a larger number of internal stiffening trusses in the impacting barge than will a 10' ∅ bullnose.

The fact that the 10' ∅ and 35' ∅ bullnose lines converge to approximately the same force at very low momentum levels (Figure 4.57) is also expected. Both the 10' ∅ and 35' ∅ bullnoses have a vertical impact face, and a semi-circular plan-view shape. For a semi-circular bullnose with a vertical face, the initial zone of contact with an impacting barge will be a very narrow strip (essentially a line) extending vertically across headlog of the barge bow. (In plan view, it will appear as though there is a single point of contact between the barge bow and the bullnose). Importantly, for such a case, the shape of the *initial* contact zone does *not* depend on the diameter of the bullnose. Only as barge deformations grow larger, and the zone of contact spreads, does the diameter of the bullnose influence the impact force level. Hence, at *very low momentum levels*, where barge deformations are minimal, the zones of contact for 10' ∅ and 35' ∅ bullnoses are nearly identical, and therefore the impact forces that are produced are nearly identical, as Figure 4.57 indicates.

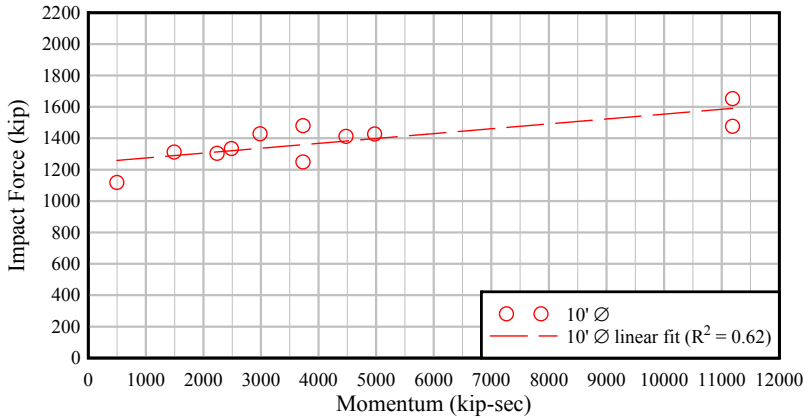

Figure 4.54. Linear relationship between impact force and momentum for 10’ Ø bullnose (11 impact cases)

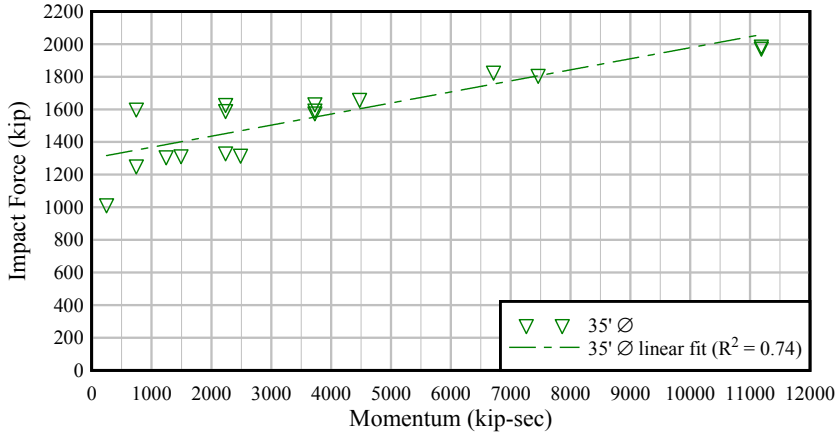

Figure 4.55. Linear relationship between impact force and momentum for 35’ Ø bullnose (17 impact cases)

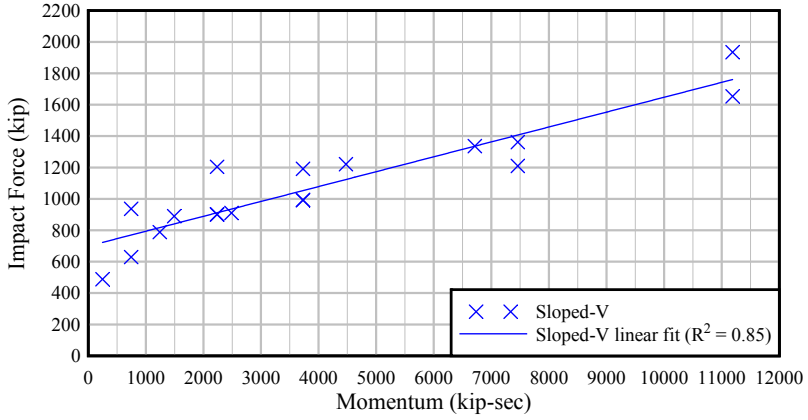

Figure 4.56. Linear relationship between impact force and momentum for sloped-V bullnose (18 impact cases)

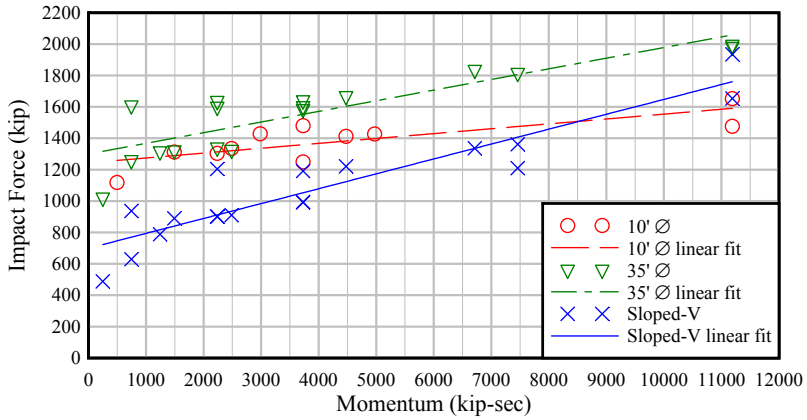

Figure 4.57. Linear relationships between impact force and momentum for 10' ∅, 35' ∅, and sloped-V bullnoses individually

In contrast to the semi-circular bullnoses, the sloped-V bullnose produces significantly smaller impact forces at low momentum levels (Figure 4.57). Although the sloped-V impact face features a semi-circular 4' diameter shape, it is also sloped, not vertical. As a result, the initial zone of contact between a barge and the sloped-V bullnose is a localized *point* on the underside of the barge bow, not a vertical line spanning across the entire barge headlog. As a consequence of this reduced area of contact and deformation, smaller impact forces are generated during low to moderate momentum impacts on the sloped-V bullnose.

However, at higher levels of momentum, impact forces for the sloped-V bullnose exceed those of the 10' ∅ bullnose (Figure 4.57). As discussed in Section 4.3, the sloped-V bullnose should be thought of as having a 'momentum-dependent' characteristic width, rather than a fixed width (diameter) of 4'. As impact momentum increases, the triangular 'V-shape' of the bullnose produces a zone of barge deformation that increases in width, consequently also increasing the impact forces that are generated. Hence, the fact that sloped-V impact forces exceed 10' ∅ impact forces for high momentum impacts, as shown in Figure 4.57, is expected.

In Figure 4.58, impact force data for the 10' ∅, 35' ∅, and 2:1 sloped-V bullnoses are aggregated (combined) together and linearly related—using least squares regression—to total flotilla momentum. Based on the number of data points (46) and the Pearson correlation coefficient (R=0.66), the probability that this aggregated linear fit is statistically meaningful is computed to be ≥99%. The least squares regression process yields—after rounding off the coefficients—the following empirical impact load prediction equation:

$$F = 1050 + 0.07(mv) \tag{4.1}$$

where F is the impact force (kip), m is the total mass of all barges in the flotilla, and v is the impact velocity. Since Eqn. (4.1) is an empirical fit, it is important to note that the momentum term mv must have units of kip-sec.

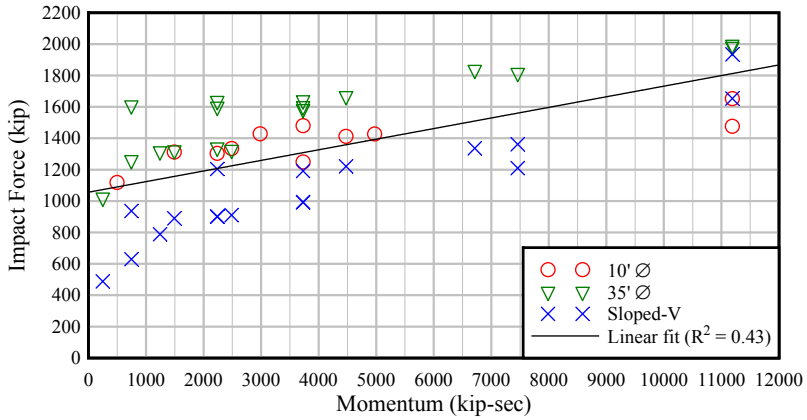

Figure 4.58. Linear relationship between impact force and momentum for 10’ ∅, 35’ ∅, and sloped-V bullnoses in aggregate (46 impact cases)

Since Eqn. (4.1) is formed using least squares linear regression, it is by definition intended to represent the mean relationship between impact force and momentum. If it is instead necessary to introduce design *conservatism* (a ‘factor of safety’) directly into the load prediction equation itself—as opposed to introducing conservatism through, e.g. load factors, or a probabilistic calculation framework—then a suitable confidence bound (e.g, 95% or 99%) could be applied and a modified load prediction equation formed using the data presented in Figure 4.58.

Finally, the intent in aggregating the 10’ ∅, 35’ ∅, and 2:1 sloped-V impact data and forming Eqn. (4.1) is to provide a *single* representative load prediction equation that can be considered applicable to a range of different bullnose types currently in use by the USACE. If, however, it is deemed warranted to form load prediction equations that are specific to particular bullnose types (e.g. sloped-V) or particular geometric parameters (e.g., semi-circular bullnose diameter), updated load prediction equations can be formed in the future using the data generated in this study.

CHAPTER 5
FINITE ELEMENT MODELING OF FLEXIBLE TIMBER GUIDE WALL STRUCTURE

5.1 Introduction

In addition to quantifying barge impact loads on bullnose structures, an additional area of focus in this study is quantifying the loads generated by shallow angle barge impacts on flexible timber guide wall structures. Such structures are used by the USACE as components of broader navigational control structures on a large number of inland waterways. The general type of guide wall structure considered in this study is constructed using plumb and battered timber piles and fiberglass reinforced plastic beams connected with steel bolts. For purposes of finite element modeling and impact simulation, a specific structure—one of the guide walls at the Catfish Point control structure 2 (Figure 5.1), located in southern Louisiana—is selected for this study. It is anticipated that impact loads quantified for this wall should be representative of loads that would be generated on similarly constructed flexible timber guide walls. Additionally, load data obtained from barge impact simulations involving this flexible timber guide wall will compliment data previously determined (experimentally and analytically) for much stiffer navigational structures such as concrete guide walls, concrete rigid walls, and concrete bullnoses.

a)

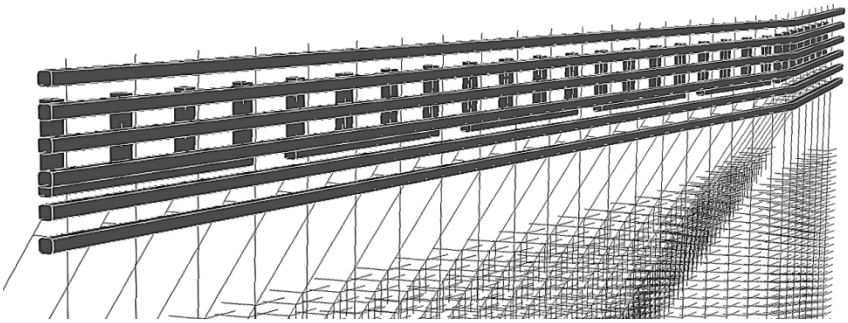

b)

Figure 5.1. Catfish Point flexible timber guide wall control structure 2:
a) Site photo (Photo credit: U.S. Army Corps of Engineers);
b) Finite element model (piles and soil springs rendered as lines)

Data pertaining to the geometry and structural configuration of the guide wall modeled in this study are taken from site plans (Figure 5.2a) titled 'Catfish Point Control Structure: North and South Guidewalls Replacement'. The specific portion of the project site that is selected for finite element model development is the northwest wall of structure 2. As Figure 5.2b illustrates, the wall consists of two parts: a 100' long primary wall, and an end 'flare' (angled at 15 deg.) that is 38'-6" long. A cross-sectional plan for the wall is reproduced in Figure 5.3 from which structural data, needed for model development, are obtained. As the cross-section indicates, the wall utilizes 12" diameter circular timber piles (both plumb and battered) to generate lateral resistance to impact loads. Fiberglass reinforced recycled plastic flexural elements, approximately square in cross-section, are used to form the impact face of the wall, as well as for thrust blocks and girts on the back (non-impact) side of the wall.

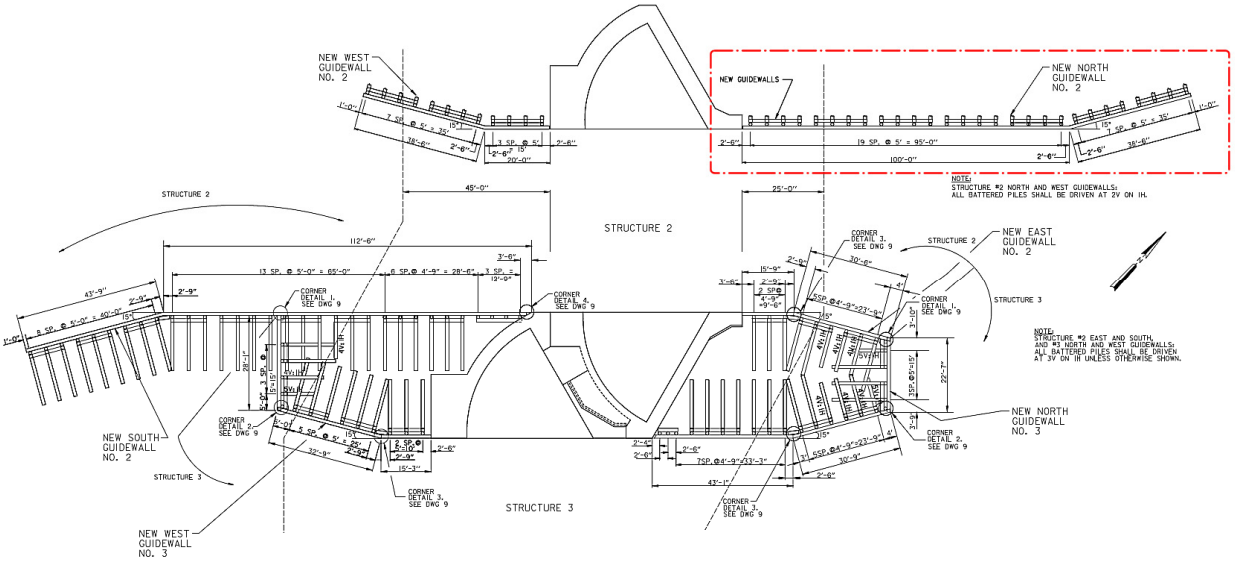

a)

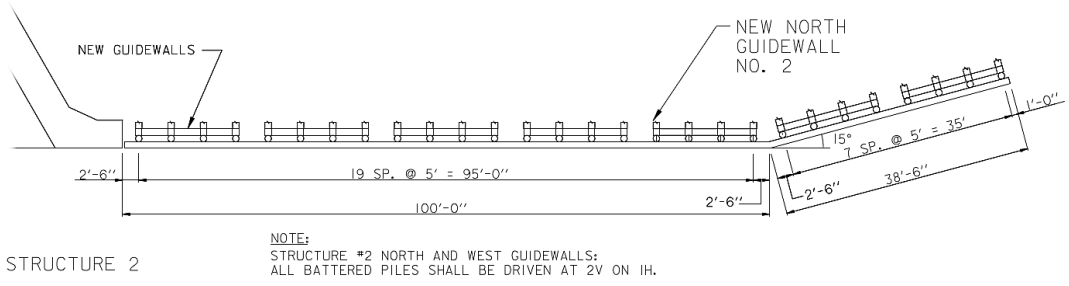

b)

Figure 5.2. Catfish Point control structure 2 and partial structure 3:
a) Partial site plan; b) Guide selected for finite element model development
(From plans titled 'Catfish Point Control Structure: North and
South Guidewalls Replacement' dated 2005, USACE)

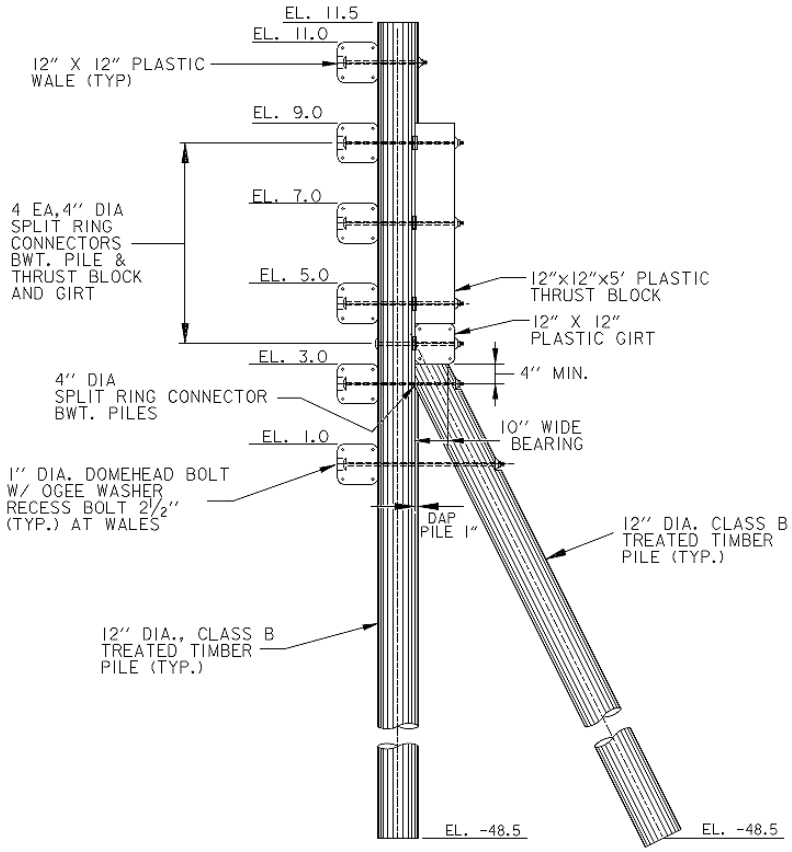

Figure 5.3. Cross section of flexible timber guide wall used in Catfish Point structure 2 (from plans titled 'Catfish Point Control Structure: North and South Guidewalls Replacement' dated 2005, USACE)

In Figure 5.4, an alternate plan view of the wall is provided. In this figure, the wall is rotated 180 deg. such that barges impacting the structure will approach from left to right, encountering first the flare, then the primary wall. In both the flare and the primary wall, each set of four pile 'groups' (where a pile 'group' consists of the combination of a single plumb pile and a single battered pile [see Figure 5.3]) is tied together with a horizontal girt on the backside of the wall. Also visible on the back side of the finite element wall model in Figure 5.4 are the battered piles extending away from the impact face.

In Figure 5.5, various isometric views of the complete wall model are presented. In Figure 5.5a, the piles—which are modeled using beam elements—are rendered with 'beam prisms' to give a realistic sense of pile diameter and geometry. In Figure 5.5b, the beam elements representing the piles are rendered instead simply as lines (although the beam element cross-sectional properties still represent the physical pile diameters). Additionally, the wall model rendered in Figure 5.5b includes nonlinear spring elements that are used to represent lateral and vertical soil stiffness (additional details are given later in this chapter).

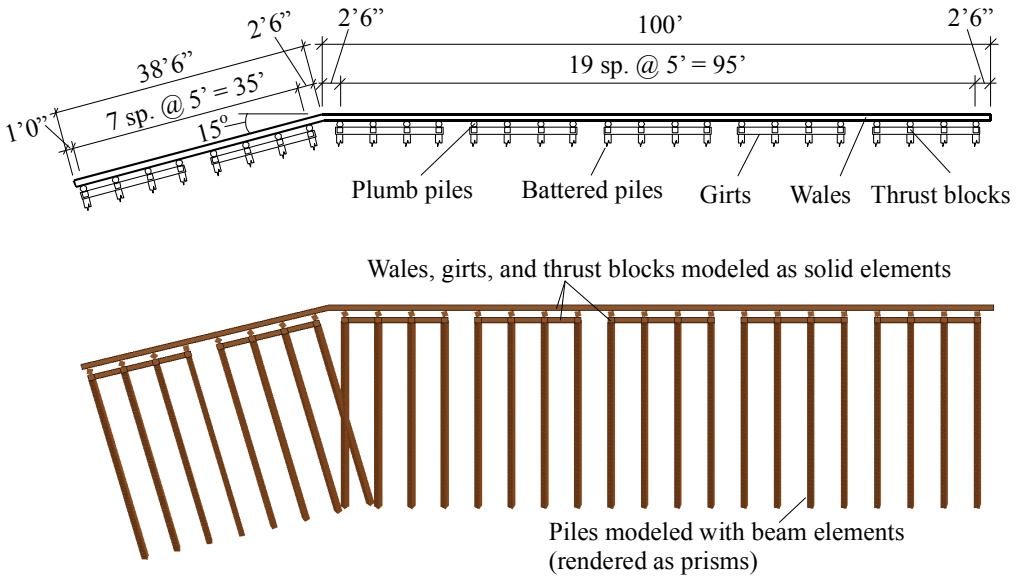

Figure 5.4. Plan view and geometry of flexible timber guide wall
(schematic diagram and rendering of the corresponding finite element model)

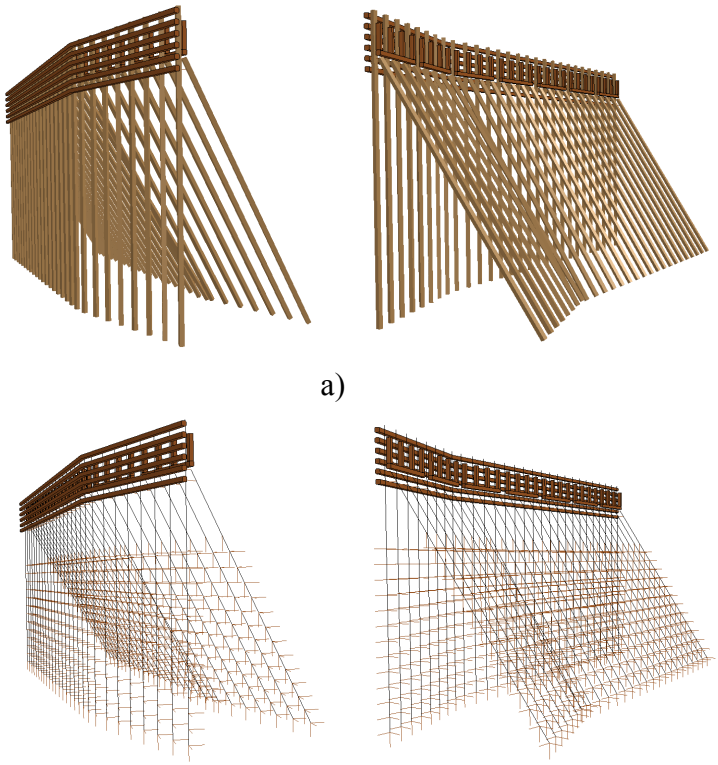

a)

b)

Figure 5.5. Isometric views of the complete flexible timber guide wall finite element model:
a) without soil spring elements; with piles rendered as 'prisms' of appropriate diameter;
b) with soil springs and pile elements rendered as lines

5.2 Structural components of flexible timber guide wall model

As shown in Figure 5.6a, the flexible timber guide wall structure is comprised of timber piles (plumb and battered), horizontal wales, horizontal girts, vertical thrust blocks, and steel bolts. Components of the corresponding finite element model are illustrated in Figure 5.6b and are discussed in detail in the sections that follow. It is important to note that since the intent of this study is to *conservatively* quantify impact loads that are *representative* of forces generated on structures of similar construction and configuration to the wall modeled herein, all structural components in the finite element model use linear elastic material properties. The assumption of linear elastic behavior ensures that individual structural components (e.g. timber piles) do not fail during impact. Including such failure would cap (limit) the impact force in a manner that would be specific to the cross-sectional dimensions and ultimate strengths of the materials involved, and therefore would become structure specific. Instead, since representative and conservative estimates of impact force are desired, linear elastic material behavior is employed for all structural components (note that soil stiffness is treated as nonlinear elastic, as discussed later).

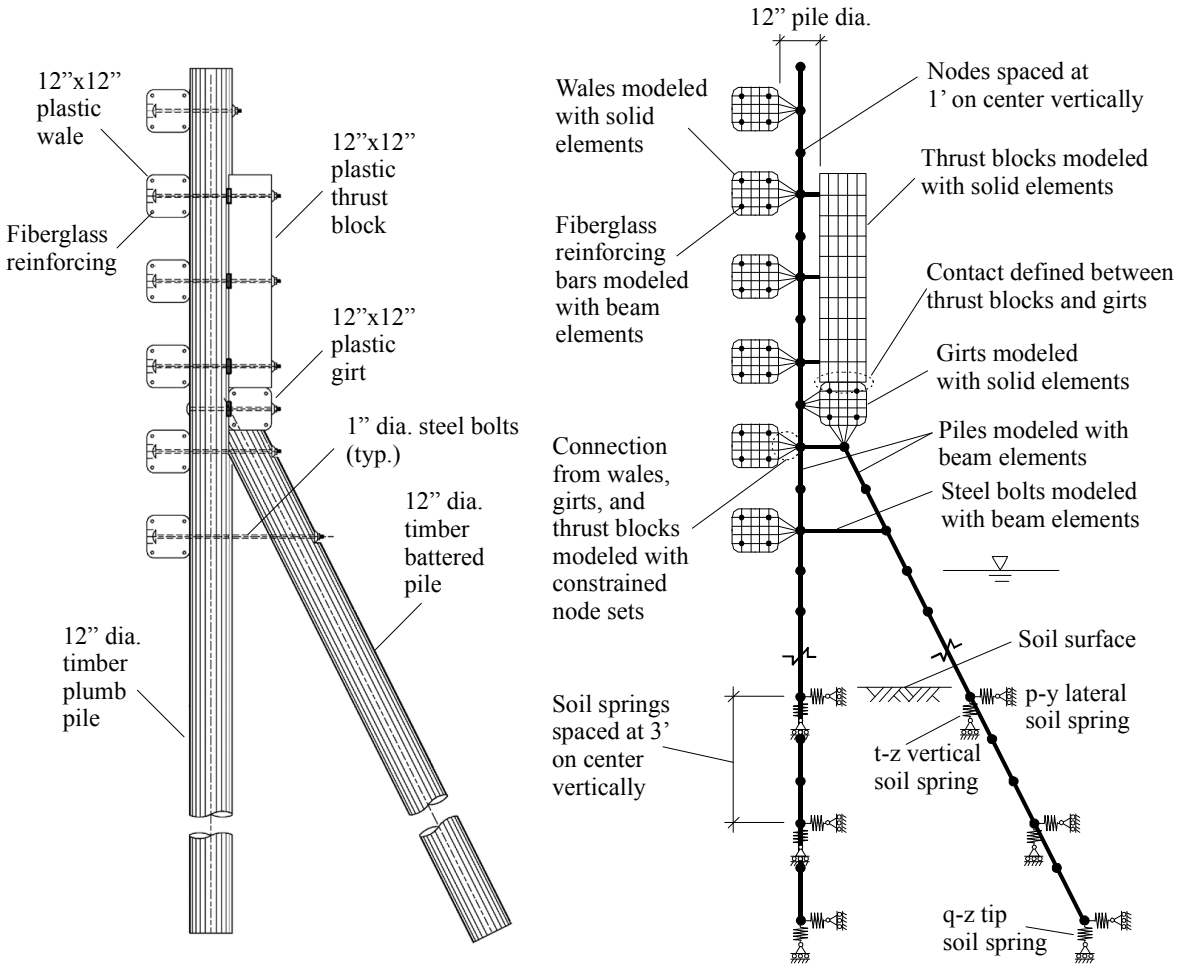

Figure 5.6. Flexible timber guide wall:
a) structural components; b) finite element model

5.2.1 Modeling timber piles

The 12” dia. class B treated timber piles, both plumb and battered, are modeled using resultant beam elements. As such, the beam elements (and nodes) are positioned along the centerlines of the piles. Nodes to which the pile elements connect are evenly spaced at vertical intervals of 1’-0” (Figure 5.6b) throughout the pile lengths. Section stiffness of the beam elements is specified by assigning a cross-section area and moments of inertia based on the 12” circular cross-sectional shape, and by specifying an elastic modulus of 1,600 ksi (as recommended by the Timber Piling Council).

5.2.2 Modeling fiberglass-reinforced recycled plastic beams

All wales, girts, and thrust blocks in the wall are constructed from 12”x12” recycled plastic beams that include four 1.25” dia. embedded fiberglass reinforcing bars (Figure 5.7a). In the finite element model (Figure 5.7b), the geometric shapes of the recycled plastic components are discretely modeled using solid 8-node brick elements, the majority of which measure 2.4” x 2.4” x 6” (where the 6” dimension is oriented along the longitudinal axis of each member). Fiberglass reinforcing bars embedded within the recycled plastic beams are modeled as resultant beam elements, each 6” in length. In total, approximately 54,000 solid recycled plastic elements and 8,600 fiberglass beam elements are used in the complete wall model. Because the fiberglass reinforcing bar elements share common nodes with the solid mesh of the recycled plastic elements, composite action of the fiberglass and plastic is represented (with strain compatibility enforced at the interface between the two materials).

Contract documents for construction of the Catfish Point control structure state various performance requirements for the fiberglass-reinforced recycled plastic beams. The key requirement that applies to this study is that the flexural stiffness (EI) of the composite plastic and fiberglass section must be at least 4.90×10^8 lb-in^2. By conducting a numeric simulation of a three-point flexural bending test on a finite element model of a 5’-0” long wale section, the flexural stiffness (EI) of the finite element model (Figure 5.7b) was determined to be 4.97×10^8 lb-in^2.

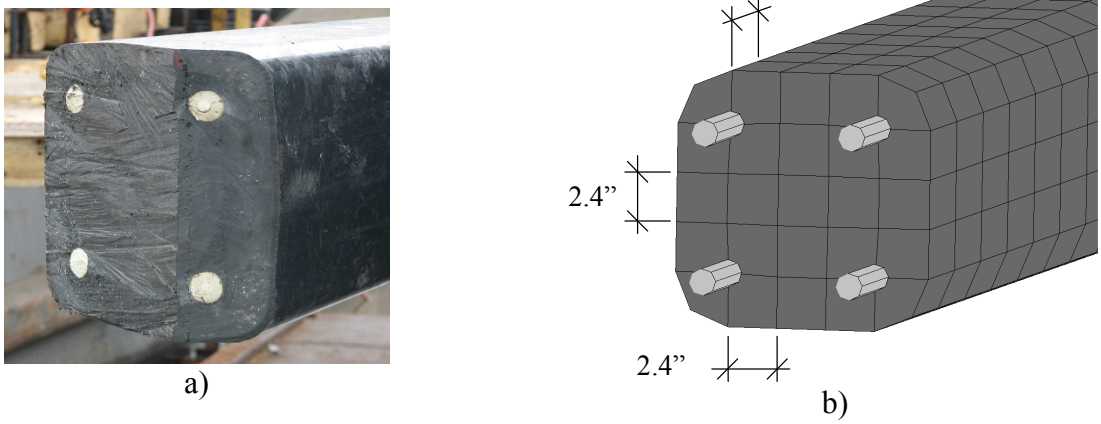

a) b)

Figure 5.7. Recycled plastic beam with fiberglass reinforcing bars:
a) Catfish Point Control Structure (Photo credit: U.S. Army Corps of Engineers);
b) Finite element model

When the finite element wall model is integrated together with a barge flotilla model for purposes of conducting an impact simulation, the only parts of the wall that the barge will make contact with are the surfaces (outer solid-element 'faces') of the wales. Hence, configuring an integrated barge-wall finite element model (Figure 5.8) involves defining contact between the exterior faces of the solid elements used to model the plastic wales (Figure 5.7b), and nodes on the starboard corner of the impacting barge model (Figure 5.8). The parameters that are assigned to the contact definition between the plastic wales and the steel barge are 0.30 and 0.20 for static and dynamic coefficients of friction, respectively.

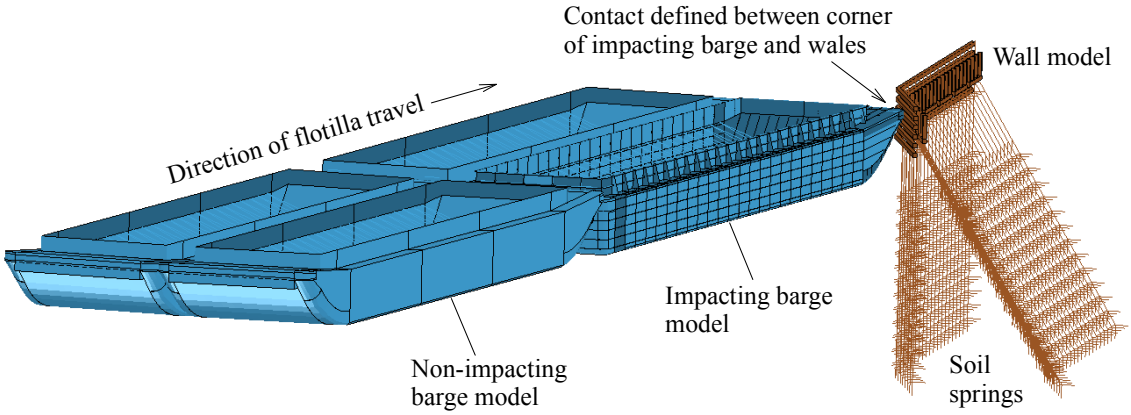

Figure 5.8. Definition of contact between barge flotilla model and guide wall model

5.2.3 Modeling connections

Connections between the various components of the flexible timber guide wall are made using 1" diameter steel bolts of varying lengths (Figure 5.6a). Tensioned through-bolts are used to pull the reinforced plastic components (wales, girts, and thrust blocks) into direct bearing against the timber piles. Additional bolts serve to pull the battered piles toward, or into contact with, the plumb piles. In Figure 5.9, photographs of various connection types are provided together with a summary of the finite element modeling procedures that are used to approximate the behavior of the connections.

Because the reinforced plastic elements are discretely modeled using meshes of solid elements, but the timber piles are modeled with resultant (centerline) beam elements, special care is required at all locations where solid (plastic) elements directly bear against beam (pile) elements. In each such location, the resistance of the bolted connection to rotation of the plastic beam (about its longitudinal axis) is primarily determined not by the flexural stiffness of the 1" dia. steel bolts, but by the bearing (contact) stresses—caused by tension in the bolt—that exist at the interface between the plastic beam and the timber pile. As noted earlier, modeling detailed failure mechanisms in the wall is not a focus of this study, hence a modeling simplification of these bolted-bearing connections is appropriate. As Figure 5.9c indicates, each bolted-bearing connection between a reinforced plastic beam and a timber pile is formed using a 'constrained node set' (also called a 'nodal rigid body'). Each of these constrained sets is arranged in either a vertical 'fan' pattern, or a horizontal 'fan' pattern. On one side of each fan are four (4) nodes of the solid element plastic mesh (wale, girt, thrust block) that would be in direct bearing (contact)

with the timber pile. At the other end of each fan (nodal rigid body) is a single node located on the timber pile centerline (and to which a pile beam element is connected).

Thus, in this finite element modeling approximation of the bolted-bearing connections, the flexural stiffness of each timber pile beam element is connected to (constrained to) the nodes of the plastic mesh that would be in direct bearing (with the pile) in the physical system. This modeling approach is numerically efficient, and sufficiently accurate for modeling the elastic structural response of walls subjected to barge impact loading. (In contrast, if modeling and analysis of wall *failure* were the intent, this connection modeling method might require modification and increased complexity).

In the two locations in the wall cross-section where steel bolts are used to tie the timber piles directly to each other (see bottom right of Figure 5.9c), the bolts are modeled not with constrained node sets, but instead with linearly elastic beam elements having the cross-sectional and material properties of 1" dia. steel bolts. A limited-scope sensitivity study indicated, however, that barge impact loads generated against the wall model (for the conditions simulated in this study) are not highly sensitive to the properties of these elastic bolts.

a)

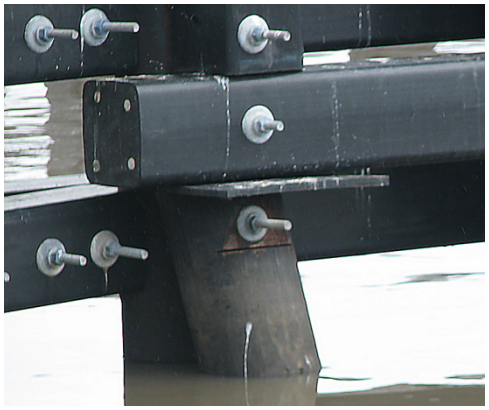

b)

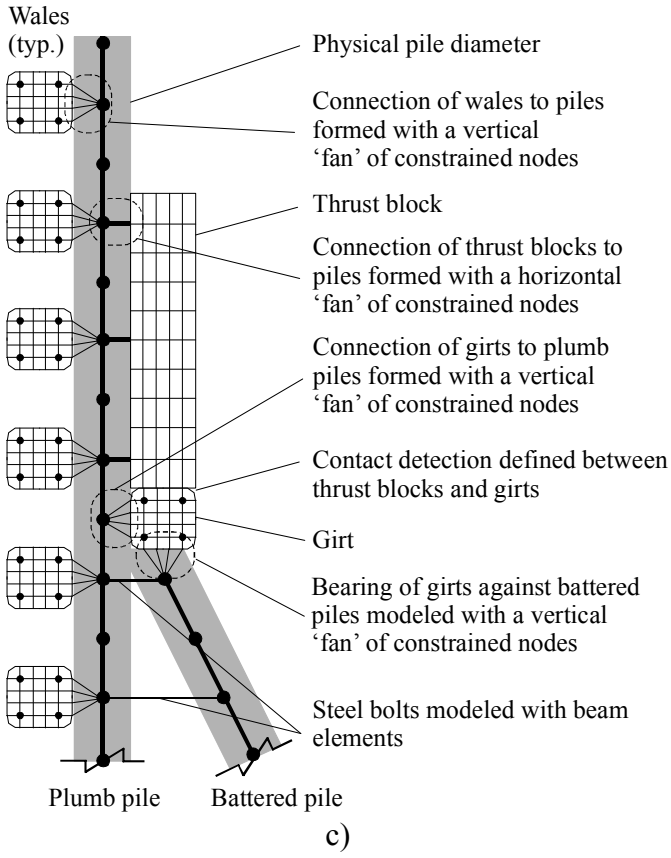

c)

Figure 5.9. Connection of fiberglass reinforced recycled plastic members to timber pile: a) Connection of wale to pile; b) intersection of battered pile, girt, and thrust block; c) finite element model of system

5.3 Soil components of flexible timber guide wall finite model

Lateral and vertical soil resistance acting on the timber pile elements is represented in the finite element model using nonlinear elastic spring elements that are attached to pile nodes at 3'-0" vertical spacings (recall Figure 5.6b). The USACE (New Orleans District office) provided soil data for three sites: Calcasieu Lock (Calcasieu), Northwest of Larose (LGM), and West Closure Complex (WCC). Data for each site include lateral soil stiffness definitions in the form of force-displacement (p-y) curves at three-foot (3'-0") vertical intervals as well as associated soil-layer profiles and strength parameters (Table 5.1). Of the three sites, the LGM site has the greatest stiffness in the upper elevations of the profile. These higher soil stiffness levels, illustrated with typical p-y curves in Figure 5.10, are due to a surface layer of 'cemented silt' (c-phi soil) over subterranean layers of soft clay (Figure 5.11). Maximizing soil stiffness near the tops of the piles is likely to result in the stiffest soil-structure response, and therefore conservatively high predictions of barge impact forces. Consequently, the LGM soil profile is selected for integration into the finite element wall model. Relative to the finite element wall model, the elevation of the top of the soil (indicated as 'top elevation' 0 ft in Table 5.1) is 13'-0" below the centerline of the bottom wale in the wall.

At pile nodes below the soil surface (and at a spacing of 3'-0", recall Figure 5.6b), three nonlinear elastic soil springs are attached: a lateral p-y spring; a lateral p-x spring; and either a vertical t-z (skin) spring or a vertical q-z (tip) spring (at the pile tip). Lateral force-displacement curves (p-y and p-x) are formed directly from the p-y data provided by the USACE. Vertical skin stiffness curves (t-z) and tip resistance curves (q-z) are formed using the soil strength parameters provided by the USACE (Table 5.1), the timber pile dimensions, empirically estimated soil properties (Table 5.2), and procedures employed by the FB-MultiPier software package. Skin (t-z) soil resistance is modeled as nonlinear and elastic (e.g., Figure 5.12a), and tip resistance (q-z) is modeled as nonlinear, elastic, and compression-only (no tension) (e.g., Figure 5.12b).

Table 5.1. Soil strength parameters
(Source: USACE, New Orleans District office)

Site	Layer	Top Elev. (ft)	Bottom Elev. (ft)	Soil Type	Effective Unit Weight, γ (pcf)	Undrained Cohesion, S_u (psf)	Friction Angle, ϕ (°)	k (pci)
Calcasieu	1	0	5	Soft Clay (Matlock)	90	180	–	–
	2	5	25	Soft Clay (Matlock)	108	325.44	–	–
	3	25	45	Sand (Reese)	122	–	30	–
	4	45	90	Soft Clay (Matlock)	115	999.36	–	–
LGM	1	0	13	Silt (Cemented c-phi)	110	200	15	30
	2	13	25	Soft Clay (Matlock)	103	400	–	–
	3	25	42	Soft Clay (Matlock)	108	500	–	–
	4	42	60	Soft Clay (Matlock)	105	600-800	–	–
WWC	1	0	10	Soft Clay (Matlock)	90	180	–	–
	2	10	20	Silt (Cemented c-phi)	110	200	15	30
	3	20	30	Soft Clay (Matlock)	103	220-380	–	–
	4	30	40	Soft Clay (Matlock)	105	380-500	–	–
	5	40	56	Soft Clay (Matlock)	103	500-650	–	–

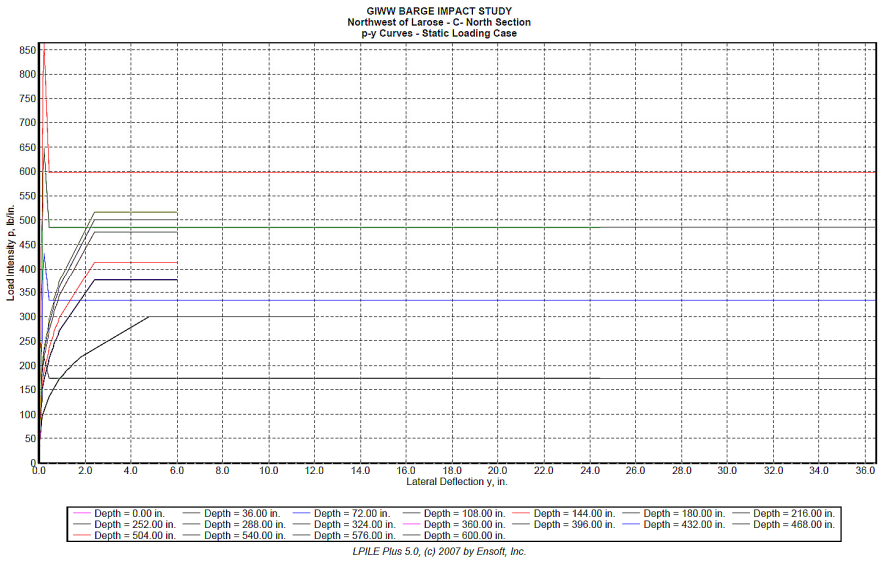

Figure 5.10. P-y curves for Northwest of Larose (LGM)
(Source: USACE, New Orleans District office)

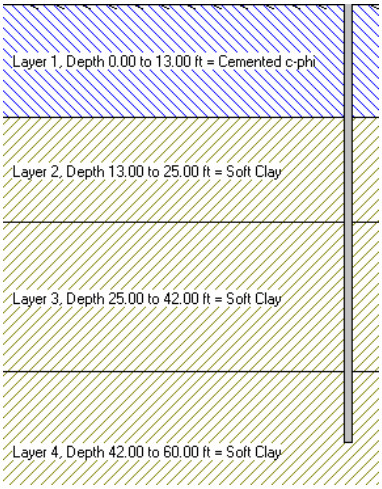

Figure 5.11. LGM Soil-layer profile illustration (generated from LPILE software)
(Data source for soil profile generation: USACE, New Orleans District office)

Table 5.2. Summary of estimated LGM soil properties for calculating t-z and q-z curves

Parameter	Layer 1	Layer 2	Layer 3	Source
Initial Shear Modulus (G)	4.74 ksi	3.61 ksi	7.25 ksi	Correlation with Su & depth (*NCHRP Synthesis 368*)
Poisson's ratio (ν)	0.4	0.4	0.4	Representative design values
Ultimate Unit Skin Friction (τ_u)	Top of layer: 200 psf Layer bottom: 310 psf	400 psf	500 psf	Estimated from S_u and ϕ
Axial Bearing Failure Load, Q	-	-	7.5 kip	Estimated from overburden pressure (*Timber Pile Design and Construction Manual*)

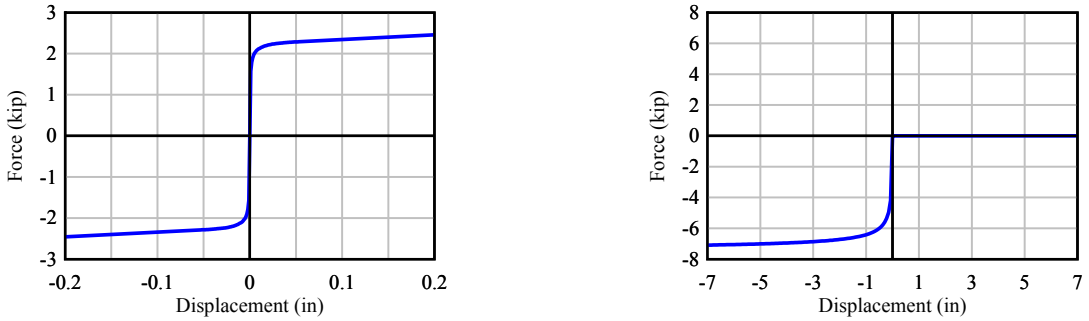

a) b)

Figure 5.12. Typical vertical soil force-displacement curves used in finite element model: a) Skin resistance t-z curve at 6' below soil surface; b) Tip resistance q-z curve at pile tip

Each soil stiffness curve (p-x, p-y, t-z, and q-z) in the finite element model is represented by a single spring element, oriented in either the x, y, or z directions, which is assigned a nonlinear constitutive (force-displacement) curve. In total, approximately 2,300 nonlinear soil spring elements (Figure 5.13), each 36" in length, are used in the flexible timber guide wall model. Each soil spring is connected at one end to a timber pile node, and at the other end to an 'anchor node'. At each anchor node, translational constraints are used to ensure that the soil element axes remains aligned with the appropriate global coordinate axis (x for p-x springs; y for p-y springs, and z for t-z and q-z springs). (See Consolazio et al. 2012 for additional details).

Finally, although the 'Northwest of Larose' (LGM) soil profile is selected as the baseline soil condition for this study, additional sensitivity studies—in which the soil stiffnesses are doubled—are also conducted to quantify the influence that soil stiffness has on impact loads.

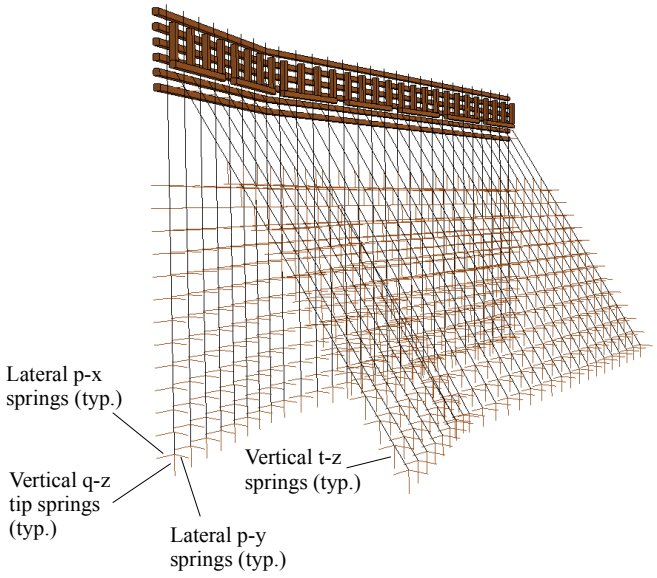

Figure 5.13. Lateral and vertical soil springs integrated into finite element guide wall model

CHAPTER 6
DETERMINATION OF IMPACT FORCES ON FLEXIBLE TIMBER GUIDE WALLS

6.1 Introduction

To quantify barge impact loads on the flexible timber guide wall system, the guide wall model discussed in the previous chapter is merged, in varying configurations, with six (6) distinct barge flotilla models (recall Table 2.1) to form integrated barge-wall impact models (Figure 6.1). In total, thirty (30) dynamic impact simulations are conducted (Table 6.1).

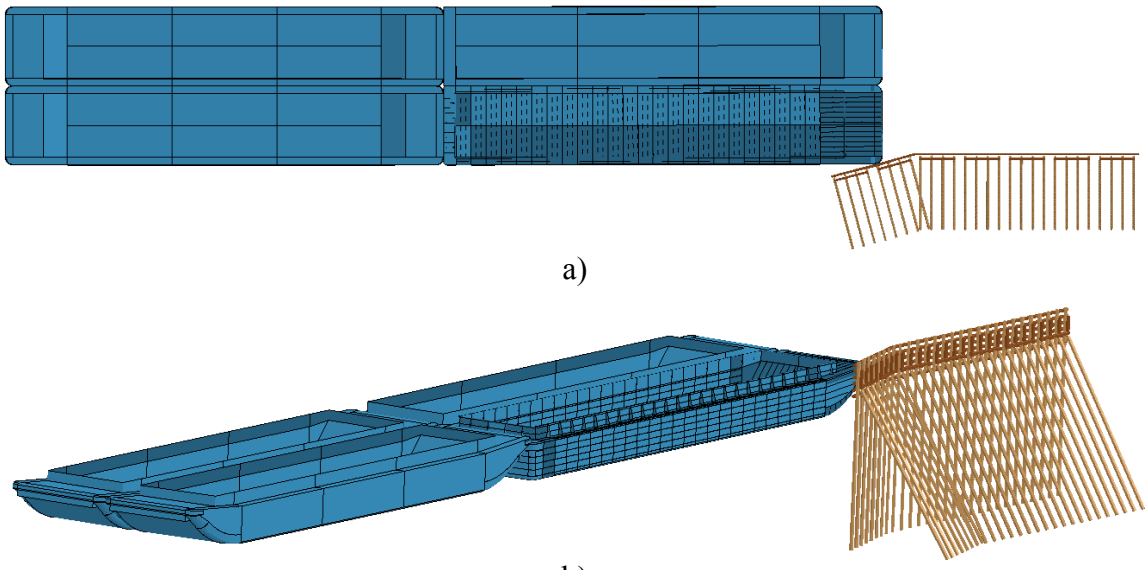

a)

b)

Figure 6.1. Integrated barge and flexible timber guide wall model (soil elements not shown): a) Plan view; b) Isometric view

Two different impact locations on the flexible timber guide wall model are simulated: impacts on the flare (end-treatment) at the 4th pile line from the flare-to-wall connection (Figure 6.2a); and impacts on the primary wall at the 1st pile line from the flare-to-wall connection (Figure 6.2b). Impacts on the flare are conducted at angles of 15° and 25° whereas impacts on the primary wall are conducted only at 15°. Approximately twice as many impacts are conducted on the flare (Table 6.1) because a wider range of impact angles are considered feasible on the flare. In addition, particularly for high severity (high energy, high momentum, longer duration) impacts, the flare impact point is expected to be marginally stiffer than the wall impact point. In the flare case, during impact the barge moves *toward* the geometrically-stiffened region where the flare and the wall connect (Figure 6.3), whereas in the wall impact case, the barge moves *away from* this area. Due to the increased stiffness, high severity impacts on the flare are expected to generate marginally larger forces than impacts on the wall, therefore, for conservatism, a greater number of flare impacts are conducted.

Table 6.1. Flexible timber guide wall impact conditions and results

Flotilla Size	Impact Speed	Impact Angle On Flare	Impact Angle On Wall	Soil Stiffness	Impact Location	Impact force (kip)
1 x 1	2 FPS	25°	-	SSx1	Flare	76
1 x 1	4 FPS	-	15°	SSx1	Wall	133
1 x 1	4 FPS	15°	-	SSx2	Flare	124
1 x 2	2 FPS	15°	-	SSx1	Flare	68
1 x 2	4 FPS	-	15°	SSx1	Wall	148
1 x 2	4 FPS	25°	-	SSx2	Flare	214
1 x 3	2 FPS	15°	-	SSx1	Flare	71
1 x 3	2 FPS	-	15°	SSx2	Wall	85
1 x 3	2 FPS	25°	-	SSx2	Flare	135
1 x 3	4 FPS	-	15°	SSx1	Wall	132
1 x 3	4 FPS	15°	-	SSx2	Flare	146
1 x 3	4 FPS	25°	-	SSx1	Flare	191
2 x 1	2 FPS	15°	-	SSx1	Flare	83
2 x 1	2 FPS	25°	-	SSx1	Flare	147
2 x 1	2 FPS	25°	-	SSx2	Flare	172
2 x 1	4 FPS	-	15°	SSx1	Wall	167
2 x 1	4 FPS	15°	-	SSx2	Flare	192
2 x 1	4 FPS	25°	-	SSx1	Flare	255
2 x 2	2 FPS	15°	-	SSx1	Flare	100
2 x 2	2 FPS	25°	-	SSx1	Flare	163
2 x 2	2 FPS	25°	-	SSx2	Flare	187
2 x 2	4 FPS	-	15°	SSx1	Wall	176
2 x 2	4 FPS	15°	-	SSx2	Flare	211
2 x 2	4 FPS	25°	-	SSx1	Flare	312
2 x 2	4 FPS	25°	-	SSx2	Flare	333
2 x 2	6 FPS	15°	-	SSx1	Flare	248
2 x 2	6 FPS	-	15°	SSx1	Wall	250
2 x 2	6 FPS	15°	-	SSx2	Flare	267
2 x 3	2 FPS	-	15°	SSx2	Wall	119
2 x 3	6 FPS	-	15°	SSx1	Wall	247

Notes:
Flotilla sizes are described as number of strings 'by' number of rows
FPS = feet per second; USACE definitions of impact speed : usual: 0.5 – 2 FPS; unusual: 2 – 4 FPS, extreme: 4 – 6 FPS
Soil conditions: SSx1 = baseline soil stiffness (see Chapter 5); SSx2 = Amplified soil stiffness (baseline stiffness 'times 2')
Impact forces are peak dynamic values imparted normal to (perpendicular to) the impacted surface (flare or primary wall) of the structure

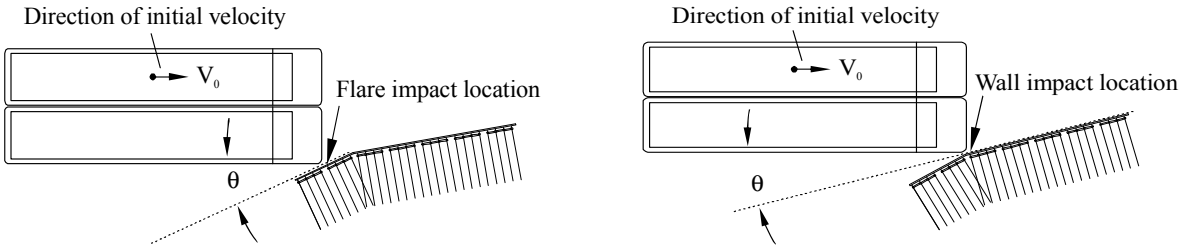

a) b)

Figure 6.2. Impact locations on flexible timber guide wall model:
a) flare impact at 4th pile line from the flare-to-wall connection;
b) wall impact at 1st pile line from the flare-to-wall connection

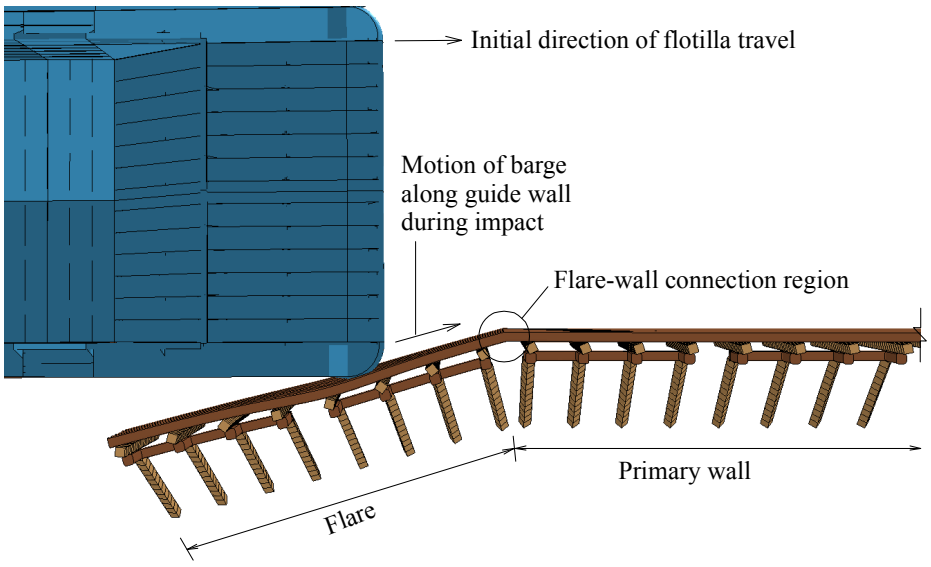

a)

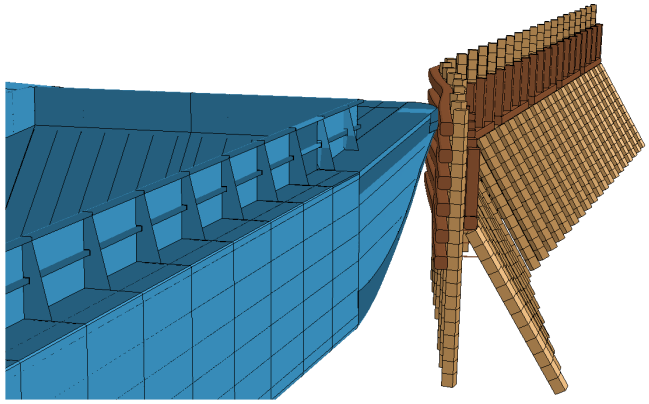

b)

Figure 6.3. Motion of barge along guide wall model during flare impact simulation (Note: for visualization purposes, displacements are scaled by 2.0; soil elements are not shown; and pile elements below soil surface (mud-line) are not shown): a) Plan view; b) Isometric view

6.2 Overview of impact force results

Impact forces presented in this chapter are dynamic contact forces between the high-resolution deformable impacting barge model and the wales of the flexible timber guide wall model (Figure 6.3b). All forces are in the horizontal plane and have been resolved into the direction *normal to* (perpendicular to) the impacted surface (flare or primary wall) of the guide wall structure. Furthermore, all results are low-pass filtered at approximately 10 Hz so that the quantified impact forces are not unduly influenced by higher frequency oscillations present in the finite element results.

Of primary interest is quantifying the peak (maximum) barge impact forces (Table 6.1) that are generated on the flexible timber guide wall for various simulated impact conditions. Due to the flexibility of the guide wall, during impact the force may momentarily drop to zero, then

increase again imparting a second pulse of force to the structure. Whether one, two, or more pulses of force are generated depends on the specifics of the impact condition (flotilla size, impact speed, impact angle, etc.) being analyzed. For example, in Figure 6.4, the time history of impact force the for case '1x2 – 2 FPS – 15° – SSx1 – Flare' (see Appendix B for the impact case nomenclature) is presented in two forms: the complete impact event history, and a force-time history truncated after the first pulse. Due to energy dissipation that occurs during the initial loading pulse, the maximum force level reached during the second pulse is less than the first. An inspection of results from additional flexible timber guide wall impact simulations conducted in this study reveals the same trend, but with an even greater reduction of force level from first peak to second peak. Additionally, subsequent force pulses may not even occur, depending on the impact conditions being simulated.

Thus, in order to accurately but also *efficiently* quantify peak impact forces for the flexible timber guide wall, all simulations in this study are configured to automatically terminate when the impact force (contact force) drops to zero, even if subsequent pulse of reloading might occur. In addition, for clarity and consistency of presentation in this chapter, *all* impact force-time histories are truncated after the initial pulse and the peak impact force is (appropriately) quantified as the maximum force generated during the initial pulse.

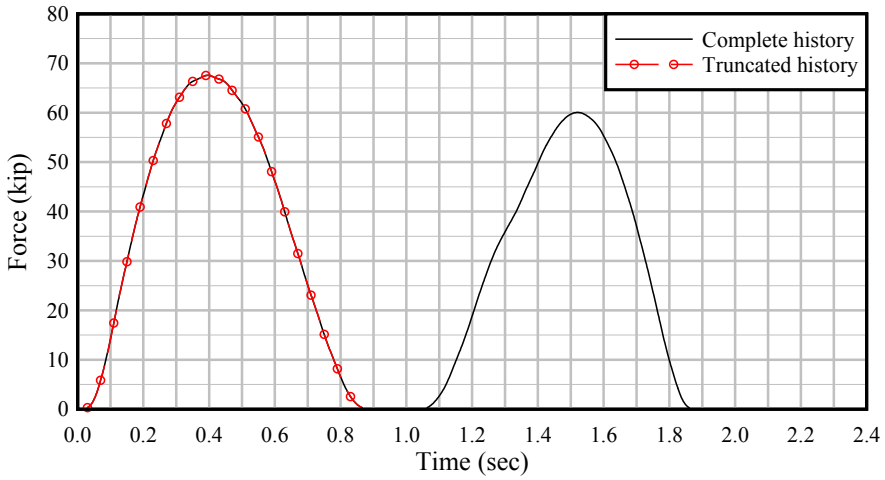

Figure 6.4. Impact force-time history for case: 1x2 – 2fps – 15° – SSx1 – Flare

6.3 General trends in the impact force results

In Figure 6.5 'initial pulse' impact force-time histories for all thirty (30) impact simulations are presented and segregated by impact location (either flare or wall). Evident from the figure is that—with only two notable exceptions—force-time histories from flare and wall impacts span approximately the same range of force level and force duration. No clearly distinguishing trends between flare impacts and wall impact forces are identifiable from Figure 6.5. This is desirable in that it suggests the feasibility of developing a *single load prediction equation* that can be considered applicable to the entire structure (flare and wall); as opposed to having to develop individual flare and wall load prediction equations. The two notable 'outliers' in Figure 6.5 are cases that produce impact forces in excess of 300 kips. As Table 6.1 indicates, these cases are '2x2 – 4 FPS – 25°– SSx1 – Flare' and '2x2 – 4 FPS – 25° – SSx2 – Flare', both steep angle (25°) relatively high severity impacts on the flare. Since no

corresponding impact conditions (2x2 – 4 FPS – 25°) are simulated for the wall impact point, it is unclear whether similarly large (>300 kip) impact forces would be obtained in such cases. It is, however, probable wall impacts under such conditions would produce marginally smaller forces due to the reduced stiffness of the primary wall relative to the flare.

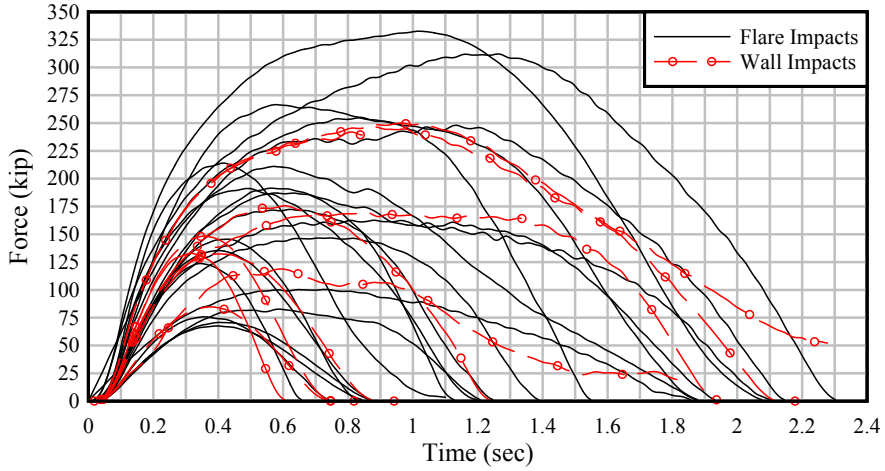

Figure 6.5. Impact force-time histories segregated by impact location

In Figure 6.6, the impact force-time histories are segregated by impact angle. No clearly discernible trends separate the data for 15° and 25° impact angles. This is not surprising, however, since impact severity is related not only to impact angle, but also (strongly) to impact momentum ($m \times v$) which involves both the mass (m) and speed (v) of the impacting flotilla. Consequently, in Figure 6.7 where force results are segregated by impact speed, as expected, general trends become apparent. As impact speed increases from 2 FPS to 4 FPS, impact force magnitudes also generally increase, although there is spread (and overlap) in the data due to variations in impact angles, number of barge strings, and number of barge rows. For the limited number of 6 FPS impacts that are conducted, all at the shallower 15° impact angle (Table 6.1), the force data fall within the spread (scatter) of the 4 FPS results.

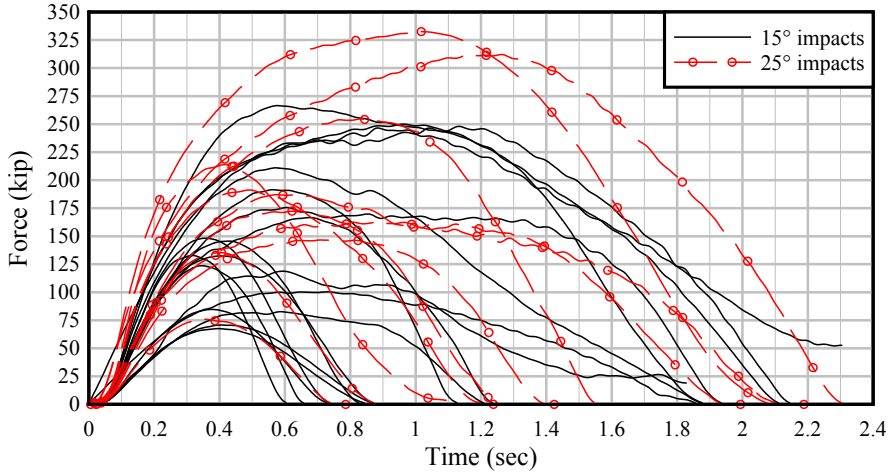

Figure 6.6. Impact force-time histories segregated by impact angle

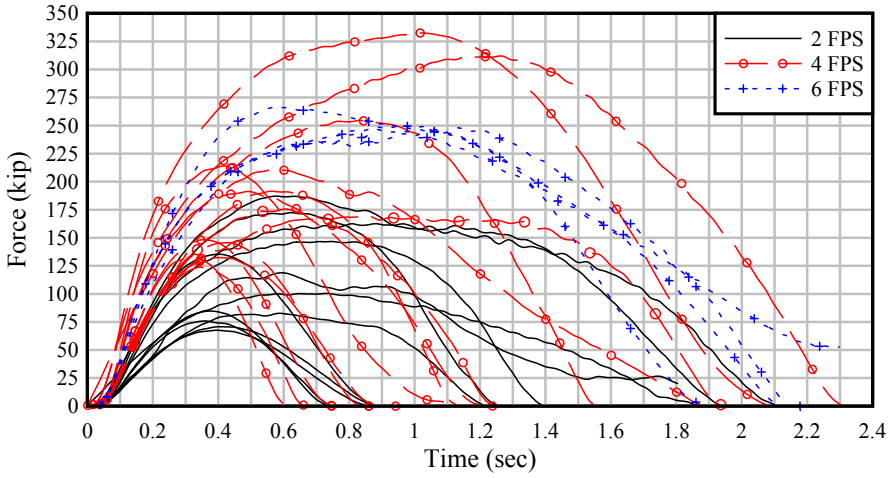

Figure 6.7. Impact force-time histories segregated by impact speed

In Figure 6.8, where the results are segregated by the number of strings in the flotilla, clear trends (correlations) between barge mass (number of strings) and impact force become evident. Doubling the number of strings in each flotilla doubles the mass, and therefore doubles the momentum of the flotilla. In Figure 6.8, doubling the momentum clearly produces significant increases in both impact force magnitude and duration.

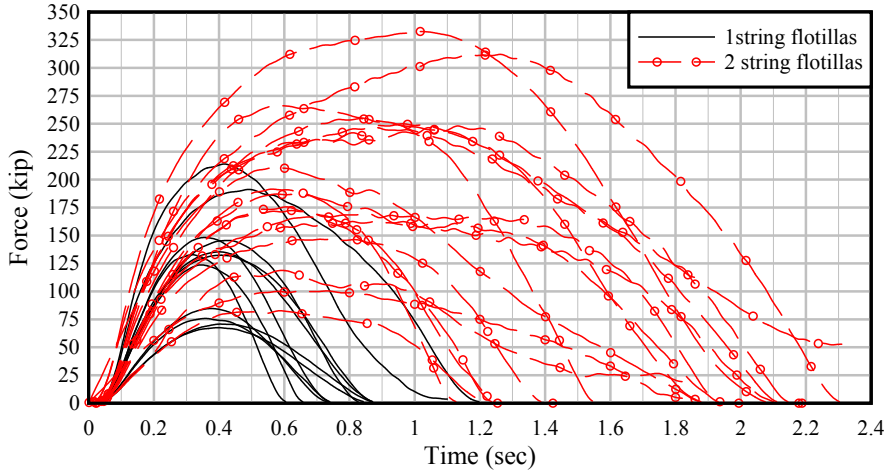

Figure 6.8. Impact force-time histories segregated by number of flotilla strings

Based on the trends shown in Figure 6.7 for impact speed, and Figure 6.8 for impact mass, it is evident that development of an impact force prediction equation will need to involve flotilla momentum. However, in a previous study (Consolazio and Walters 2012) focusing on shallow angle (glancing) flotilla impacts on relatively stiff *prestressed concrete* guide walls, it was determined that barge impact forces were correlated much more strongly to the momentum of the *lead row* of the flotilla than to the total momentum of the entire flotilla. Specifically, it was found that in multiple row flotillas, redirection of the lead row of barges accounts for the greatest proportion of the impact load generated. This finding, however, was related to the much greater

stiffness of the reinforced concrete guide wall in comparison to the smaller barge flotilla stiffness (in a 'bending' mode of deformation, where the lashings allow for 'flexing' of the flotilla). Given that the flexible timber guide wall structure of interest in present study is less stiff (i.e., more flexible) than the concrete guide wall previously investigated, it must be determined whether peak impact forces will again be best correlated to lead row impact momentum, or whether total flotilla momentum will better predict peak impact forces.

In Figure 6.9, the flexible timber guide wall impact results are segregated by the number of rows (1, 2, or 3) in the impact flotillas considered. If the two previously noted 'outlier' cases are ignored in Figure 6.9, then the remainder of the data indicate that maximum impact forces of approximately 250 kip are achieved *regardless* of whether the flotillas have a single (1) row, two (2) rows, or three (3) rows. Importantly, this suggests that lead row momentum may be a better predictor of peak impact force than total flotilla momentum (as in Consolazio and Walters 2012). Later in this chapter, the relative strengths of correlation between impact force, lead row momentum, and total momentum will be quantified and presented.

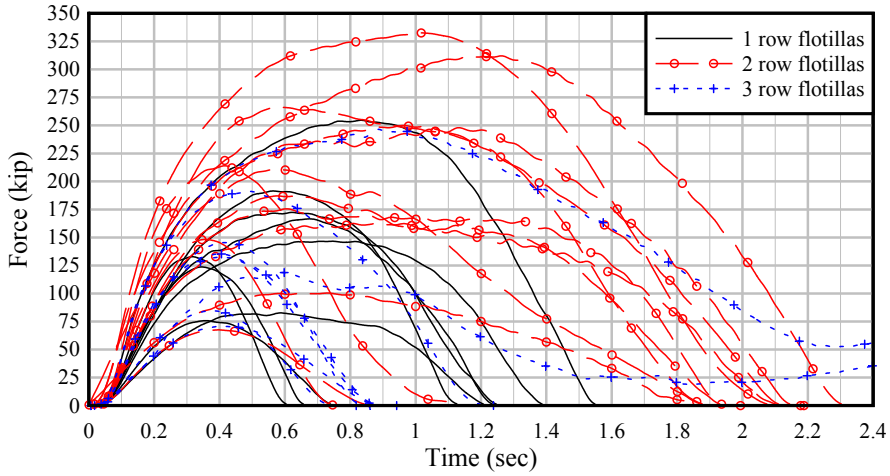

Figure 6.9. Impact force-time histories segregated by number of flotilla rows

In the following sections, the sensitivity of impact force to soil stiffness and flotilla configuration (number of strings and number of rows) is discussed in greater detail, with specific data comparisons for selected illustrative cases. Following these discussions, the development of an impact force prediction equation for the flexible timber guide wall is presented.

6.4 Impact force sensitivity to soil stiffness

As discussed in Chapter 5, the flexible timber guide wall model is based on a soil profile (i.e., stratification and properties) from a single representative site ('Northwest of Larose', LGM). Given that predicting conservatively large impact forces is a goal of this study, the LGM site is selected (from among available data) with the intent of maximizing soil stiffness, and therefore maximizing impact forces. However, it is still of interest to quantify the influence that further increases in soil stiffness (in excess of the LGM profile) might have on computed barge impact forces. As such, impact simulations in this study (Table 6.1) are conducted on the flexible timber guide wall model using two different soil conditions: one referred to as SSx1 ('soil stiffness times 1'), and the other referred to as SSx2 ('soil stiffness times 2'). Soil condition SSx1 corresponds to the baseline LGM soil model described in Chapter 5 whereas SSx2

corresponds to a 100% increase (i.e., a doubling) of the soil stiffness. For additional discussion of the basis for using a 100% increase in soil stiffness to investigate impact force sensitivity to soil conditions, see Consolazio et al. (2010).

The effects of increasing soil stiffness in the flexible timber guide wall model are illustrated in Figures 6.10 – 6.12 for impact cases involving varying flotilla sizes (2x1 and 2x2), varying impact speeds (2 FPS and 6 FPS), and varying impact angles (15° and 25°). In each case, increasing the soil stiffness by 100% produces only a modest increase in impact force (and a modest reduction in duration). The fact that the impact forces do not increase in proportion to soil stiffness indicates that, at least for the representative soil profile used in this study, the *structural* stiffness of the guide wall (related to the flexibility of the timber piles) has more influence on impact force magnitude than does soil stiffness. However, to help ensure that impact force data—generated to enable development of a load prediction equation—are reasonably conservative, approximately one-third (1/3) of the flexible timber guide wall impact simulations (Table 6.1) are conducted using the amplified soil stiffness condition SSx2.

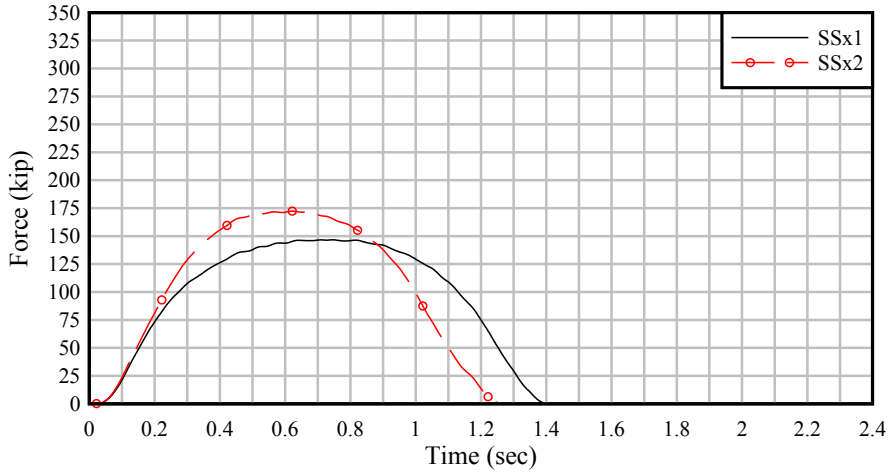

Figure 6.10. Sensitivity to soil stiffness: 2x1 – 2 FPS – 25° – Flare – [SSx1, SSx2]

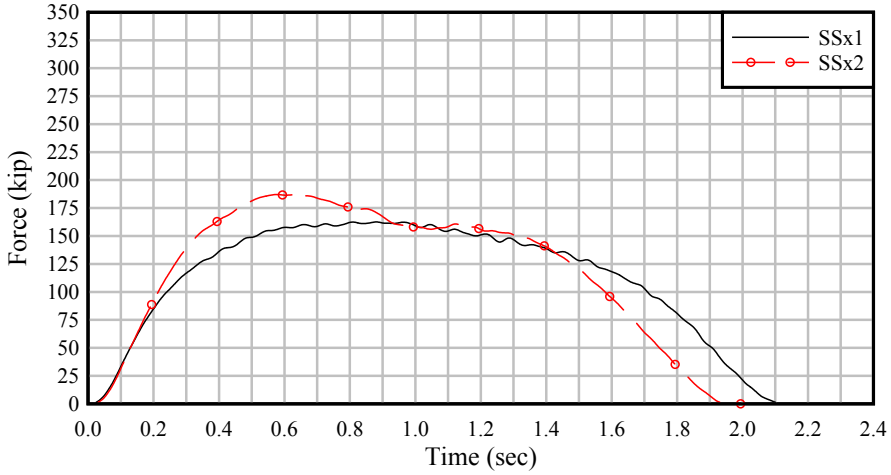

Figure 6.11. Sensitivity to soil stiffness: 2x2 – 2 FPS – 25° – Flare – [SSx1, SSx2]

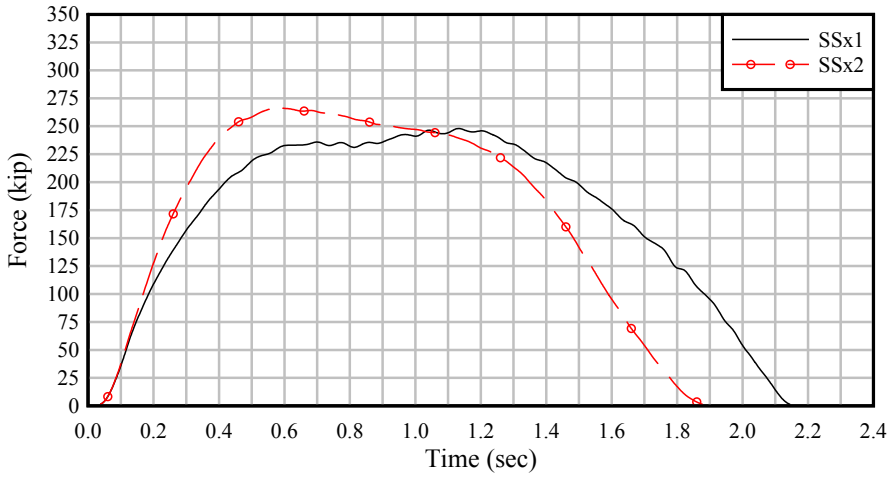

Figure 6.12. Sensitivity to soil stiffness: 2x2 – 6 FPS –15° – Flare – [SSx1, SSx2]

6.5 Impact force sensitivity to number of barge strings

The sensitivity of impact forces to the number of barge *strings*—either 1 or 2—present in the impacting flotilla is illustrated in Figures 6.13 – 6.18. The cases selected for presentation include flotillas with varying numbers of rows, varying impact speeds, varying impact angles, varying impact locations, and varying soil stiffnesses. Each plot compares force levels produced by two impact conditions that are identical in every way *except* in the number of barge strings. Evident from these figures is the fact that significant changes of both impact force magnitude and impact force duration are produced by changing the number of strings in the flotilla (and thereby changing the mass, both of the lead row of the flotilla, as well as the overall flotilla). However, the data also illustrate a variable level of sensitivity to the number of strings. In some cases, doubling the number of strings (i.e., the impacting mass) doubles the peak impact force (and the impact force duration), while in other cases doubling the mass produces only a modest increase in impact force. In order to account for this variability, least squares curve fitting will be used later in this chapter to establish a reasonable correlation between momentum and impact force.

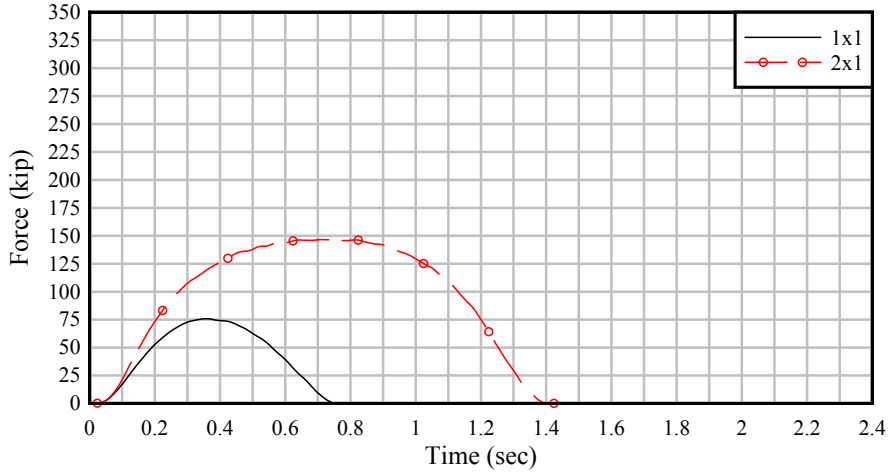

Figure 6.13. Sensitivity to number of strings: [1, 2] strings x 1 row – 2 FPS – 25° – SSx1 – Flare

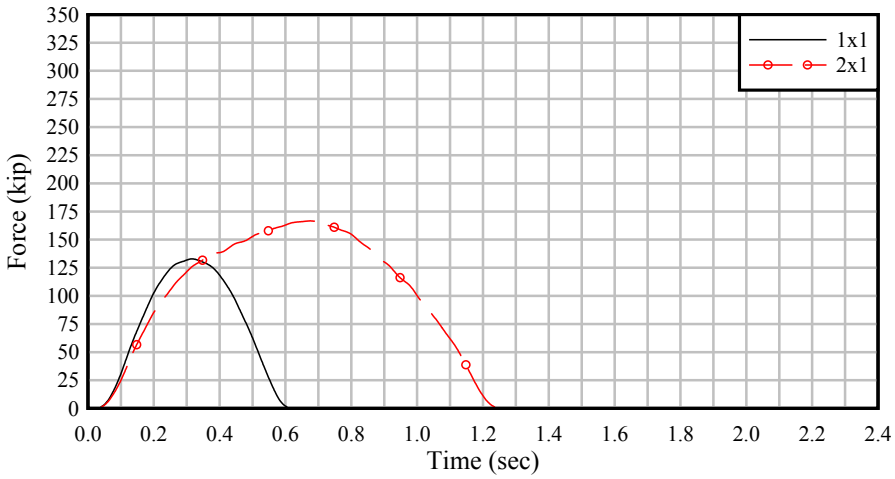

Figure 6.14. Sensitivity to num. of strings: [1, 2] strings x 1 row – 4 FPS – 15° – SSx1 – Wall

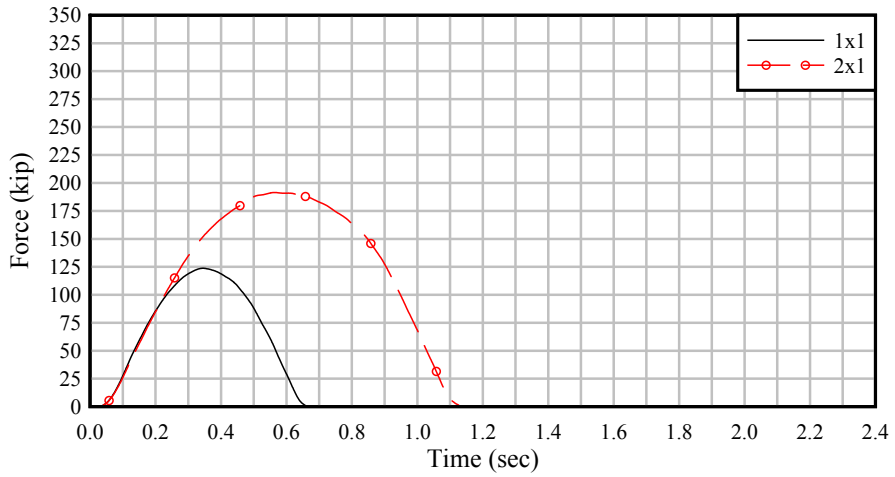

Figure 6.15. Sensitivity to num. of strings: [1, 2] strings x 1 row – 4 FPS – 15° – SSx2 – Flare

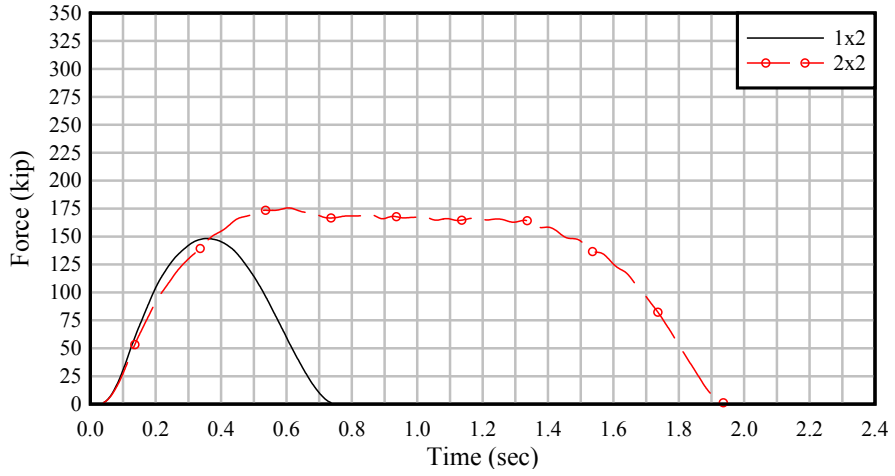

Figure 6.16. Sensitivity to num. of strings: [1, 2] strings x 2 rows – 4 FPS – 15° – SSx1 – Wall

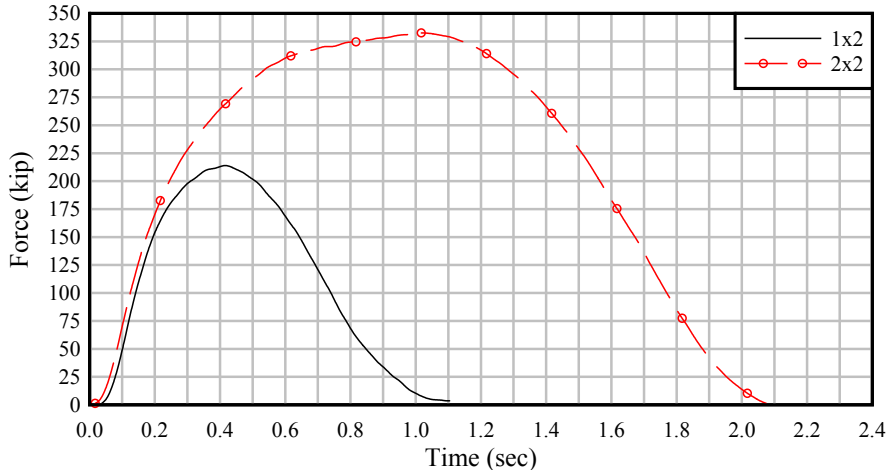

Figure 6.17. Sensitivity to num. of strings: [1, 2] strings x 2 rows – 4 FPS – 25° – SSx2 – Flare

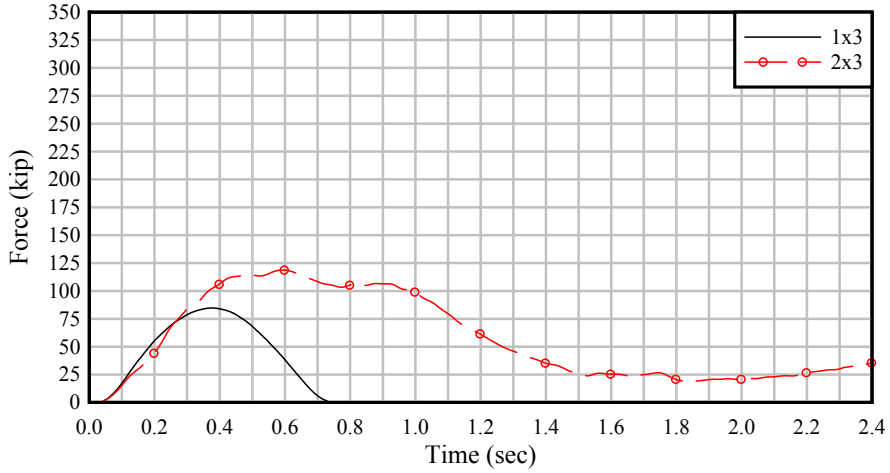

Figure 6.18. Sensitivity to num. of strings: [1, 2] strings x 3 rows – 2 FPS – 15° – SSx2 – Wall

6.6 Impact force sensitivity to number of barge rows

The sensitivity of impact forces to the number of barge *rows*—either 1, 2, or 3—present in the impacting flotilla is illustrated in Figures 6.19 – 6.23. The cases selected for presentation include flotillas with varying numbers of strings, varying impact speeds, varying impact angles, varying impact locations, and varying soil stiffnesses. Each plot compares force levels produced by two impact conditions that are identical in every way *except* in the number of barge rows. In most of the comparisons presented, the number of barge rows is doubled (increasing the flotilla mass by 100%), but in Figure 6.23 the number of rows (and mass) is increased by 50%, and in Figure 6.20 the number of rows (and mass) is increased by 200%. Across this reasonably wide spectrum of impact conditions, the data presented in Figures 6.19 – 6.23 reveal that changing the number of rows in the impacting flotilla has only a modest effect on the peak impact forces generated. As such, the general suggestion introduced earlier (in relation to Figure 6.9) that *lead row* momentum—rather than total flotilla momentum—may be the strongest predictor of impact force, is greatly strengthened by the specific data comparisons presented in Figures 6.19 – 6.23.

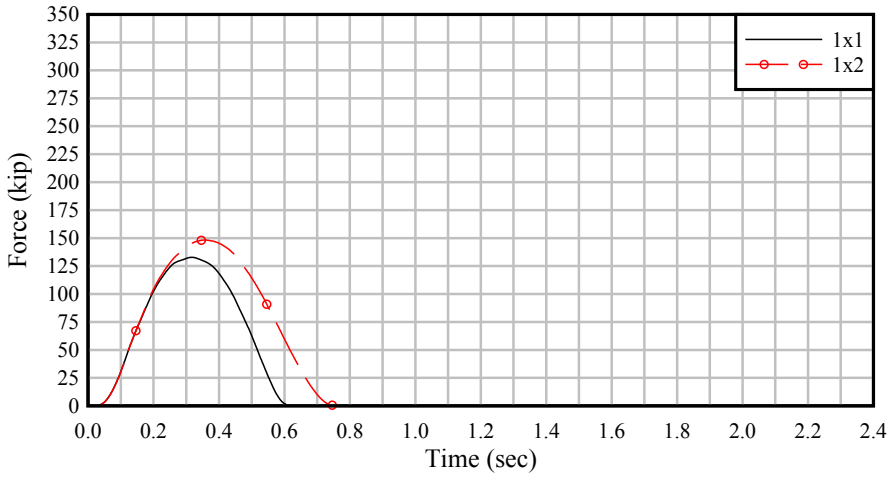

Figure 6.19. Sensitivity to num. of rows: 1 string x [1, 2] rows – 4 FPS – 15° – SSx1 – Wall

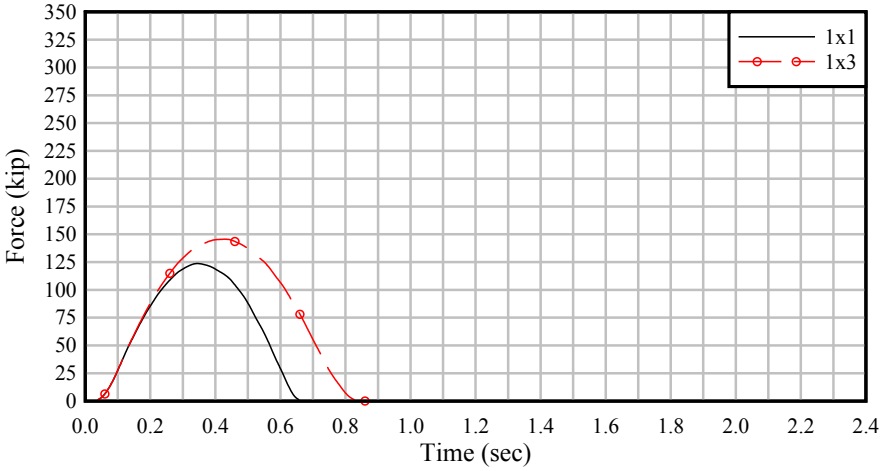

Figure 6.20. Sensitivity to num. of rows: 1 string x [1, 3] rows – 4 FPS – 15° – SSx2 – Flare

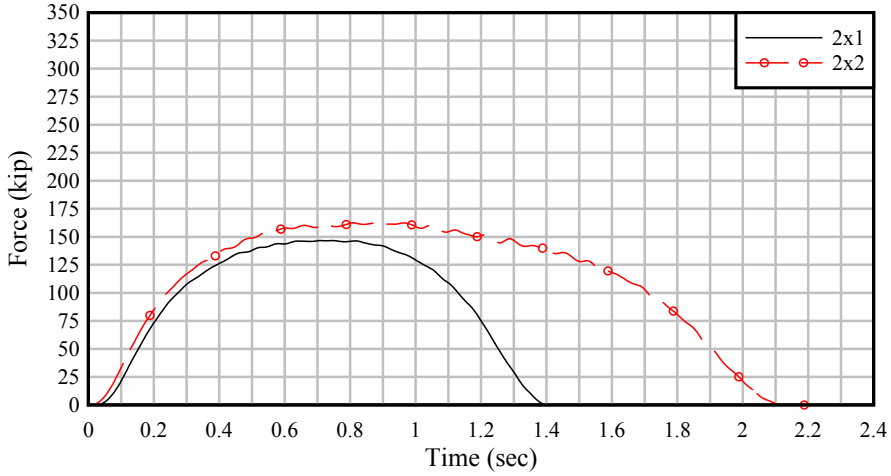

Figure 6.21. Sensitivity to num. of rows: 2 strings x [1, 2] rows – 2 FPS – 25° – SSx1 – Flare

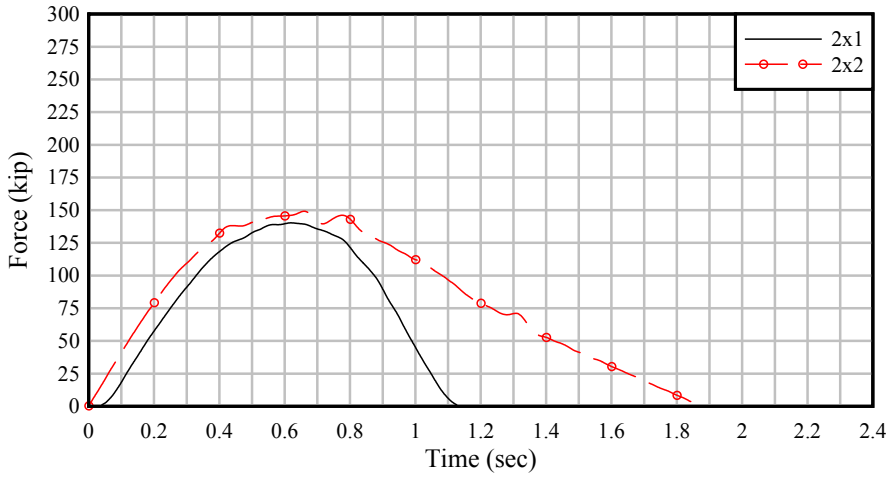

Figure 6.22. Sensitivity to num. of rows: 2 strings x [1, 2] rows – 4 FPS – 15° – SSx2 – Flare

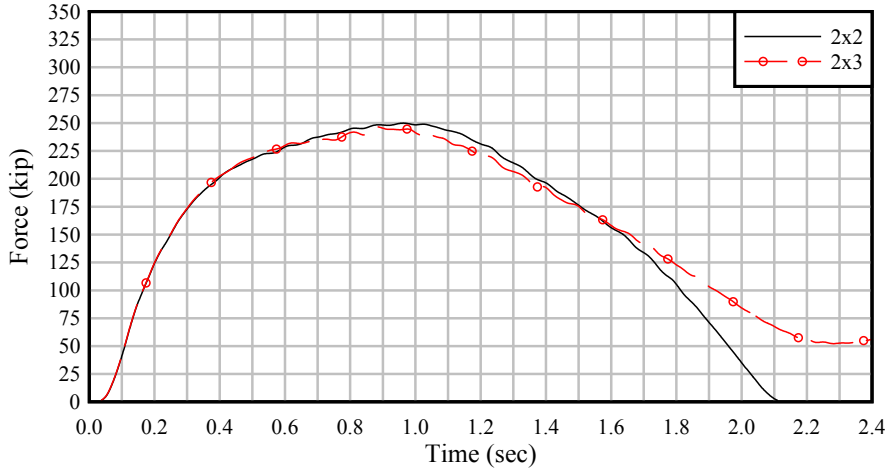

Figure 6.23. Sensitivity to num. of rows: 2 strings x [2, 3] rows – 6 FPS – 15° – SSx1 – Wall

6.7 Empirical prediction of impact load for the flexible timber guide wall

The trends and sensitivities discussed in the sections above suggest that development of an impact load prediction equation for the flexible timber guide wall system should be based on correlating peak impact forces to flotilla mass (either lead row or total), flotilla speed, and impact angle. In Figure 6.24, peak (normal) impact forces for all flexible timber guide wall impact simulations (Table 6.1) are linearly related—using least squares regression—to total flotilla momentum (specifically, the component of momentum normal to the impacted surface of the structure; either flare or primary wall). Considering the coefficient of determination for this fit, R^2=0.69, impact force is considered moderately correlated to total normal flotilla momentum. However, if—as suggested in the previous section—peak normal impact forces are related instead to the normal component of momentum of only the *lead row* of barges in the flotilla, then a substantially stronger correlation (R^2=0.89) is observed (Figure 6.25).

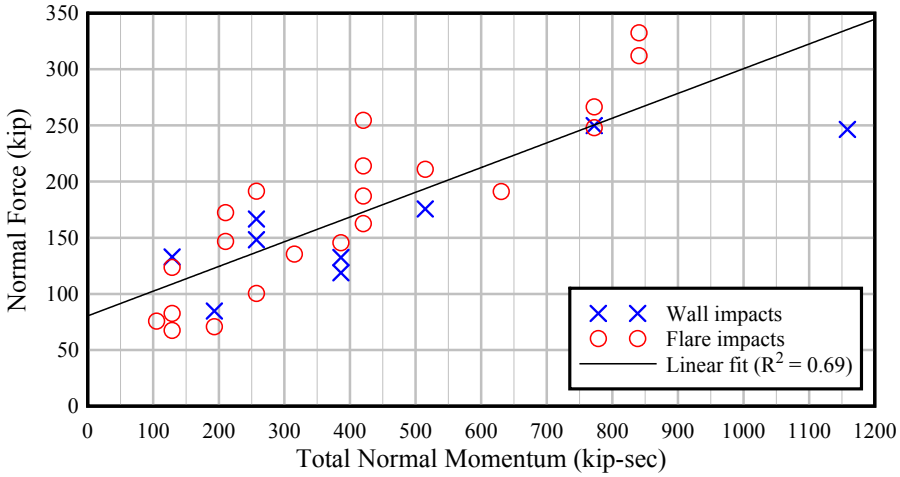

Figure 6.24 Relationship between impact force (normal to wall) and total momentum (normal to impacted surface of wall)

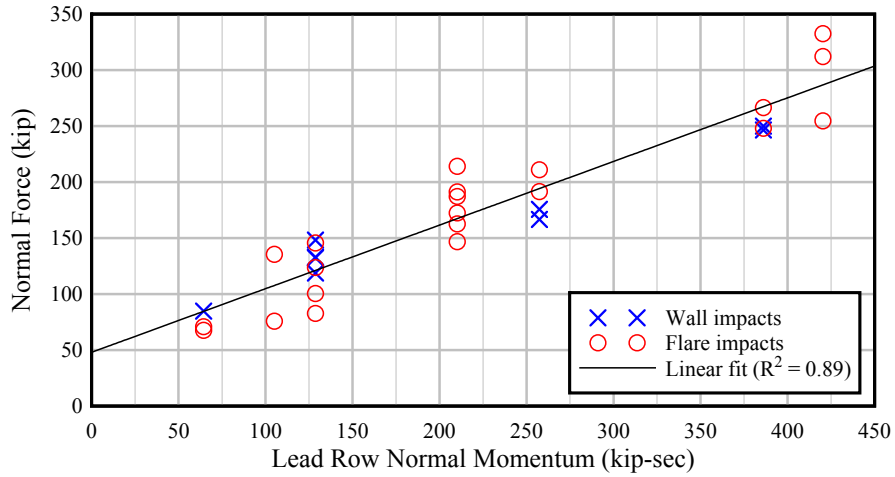

Figure 6.25 Relationship between impact force (normal to wall) and lead row momentum (normal to impacted surface of wall)

In this case (Figure 6.25), least squares regression yields the following empirical impact load prediction equation:

$$F = 48 + 0.57\left(m_{LR}v\right)\sin(\theta) \tag{6.1}$$

where F is the normal impact force (kip), m_{LR} is the mass of all barges in the *lead row* of the flotilla, v is the impact velocity (in the longitudinal direction), and θ is the impact angle. Since Eqn. (6.1) is an empirical fit, it is important to note that the momentum term $m_{LR}v$ must have units of kip-sec. It is also noteworthy that in Figure 6.25, linear trends are exhibited by both the flare impact data points as well as the wall impact data points, indicating that Eqn. (6.1) is applicable to either flare or wall impact locations, as long as the appropriate impact angle θ (relative to the impacted surface) is used.

As Figure 6.24 and Figure 6.25 indicate, impact forces for the flexible timber guide wall are moderately correlated to total flotilla momentum but strongly correlated to lead row momentum. This finding is consistent with previous work (Consolazio and Walters 2012) despite the flexible timber guide wall being significantly more flexible than the previously investigated concrete walls. The reason for the strong correlation to lead row momentum—even in the flexible timber guide wall—appears to be consistent with past findings: due to flotilla flexing during impact, redirection (rotation) of the lead row of barges accounts for the greatest proportion of the impact load generated. This concept is illustrated in Figure 6.26 for the impact case '2x2 – 4 FPS – 15° – SSx2 – Flare' (Table 6.1).

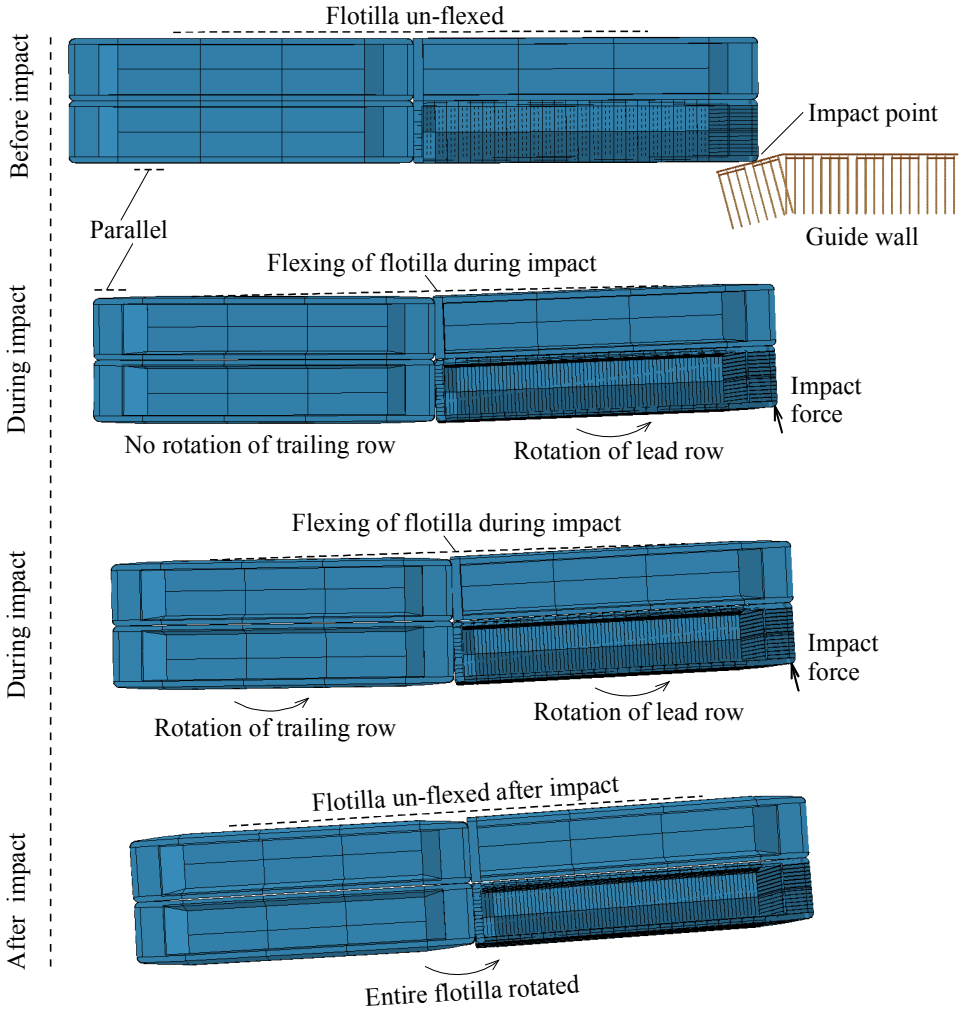

Figure 6.26 Redirection and flexure of barge flotilla during impact
(Note: for visualization purposes, displacements are scaled by 10.0)

During initial impact (i.e., contact), barges in the lead row of the flotilla rotate (in response to contact force), but barges in the trailing row (or rows) remain un-rotated due to inertial resistance. The relative rotation between lead row and trailing row(s) is enabled by the flexibility of the lashings, and produces a transient (short duration) flexural deformation in the

flotilla. As the impact event continues, however, the lashing forces eventually rotate the trailing rows and flexure in the flotilla is relieved (after which the entire flotilla has been rotated). Hence, it appears lead row momentum (resolved in the direction normal to the impacted surface) is the best predictor of impact forces for shallow-angle (glancing) impacts on guide structures of wide ranging stiffnesses.

Finally, since Eqn. (6.1) is formed using least squares linear regression, it is by definition intended to represent the mean relationship between impact force and lead row momentum. If it is instead necessary to introduce design *conservatism* (a 'factor of safety') directly into the load prediction equation itself—as opposed to introducing conservatism through, e.g. load factors, or a probabilistic calculation framework—then a suitable confidence bound (e.g, 95% or 99%) could be applied and a modified load prediction equation formed using the data summarized in Table 6.1.

CHAPTER 7
SUMMARY AND CONCLUSIONS

The primary objective of this study has been to use nonlinear dynamic finite element impact simulation techniques to quantify barge flotilla impact force-time histories (i.e., transient forces) and peak impact forces (for use in static analysis and design) for bullnose structures, and for a flexible timber guide wall structure. Barge flotilla impact forces have been quantified over a wide range of different conditions including variations in: flotilla configuration, flotilla mass, impact speed, impact angle, lateral impact offset, impacting barge string, impacting barge end, bullnose type, bullnose slope, wall impact location, and soil stiffness.

Finite element models for three bullnose types commonly employed by the USACE have been developed: 10 ft diameter semi-circular (10' ∅), 35 ft diameter semi-circular (35' ∅), and sloped-V. Each bullnose model has been integrated together with barge flotilla models of varying configurations to conduct dynamic impact simulations over a range of different impact conditions. In total, seventy-eight (78) barge-bullnose impact simulations have been conducted, for which peak values of force, as well as time histories of force, have been quantified, reported, and discussed. A number of different sensitivity studies have been conducted for the purpose of identifying parameters that strongly influence impact force magnitudes. Key findings from the barge-bullnose impact sensitivity studies include: 1) barge bow (headlog) impacts consistently generate impact forces that are larger than corresponding stern (boxed-end) impact forces; 2) peak impact forces for semi-circular bullnoses are a function of diameter, with increased diameters producing increased forces; 3) peak impact forces for sloped-V bullnoses are smaller than semi-circular bullnose forces for low-momentum impact conditions, but grow significantly larger for high-momentum conditions. Using peak impact force data from a subset of the seventy-eight (78) impact simulations, an empirical impact load prediction equation for bullnose structures has been developed and presented.

In addition, a finite element model of a flexible timber guide wall structure has been developed that includes: timber piles; fiberglass-reinforced recycled-plastic wales, girts, and thrust blocks; and simplified representations of steel-bolted connections. A representative soil profile (layering) has been established and used to compute force-displacement curves for vertical and lateral soil springs that attach to timber pile elements in the finite element model. The flexible timber guide wall model has been integrated together with barge flotilla models to conduct impact analyses. In total, thirty (30) impact simulations have been conducted, for which peak values of force, as well as time histories of force, have been quantified, reported, and discussed. Sensitivity studies have been conducted and presented for the purpose of identifying parameters that strongly influence impact force magnitudes. Key findings from the sensitivity studies include: 1) the momentum of the *lead-row* of the impacting barge flotilla (resolved to be normal to the impacted wall surface) is a better predictor of peak impact force than is *total* flotilla momentum normal to the wall; and 2) peak impact forces appear to be more strongly influenced by wall stiffness (e.g., piles) than soil stiffness (at least for the soil profile used in this study). Using peak impact force data from all thirty (30) impact simulations, an empirical impact load prediction equation for the flexible timber guide wall structure has been developed and presented.

REFERENCES

Consolazio, G. R., McVay, M. C., Cowan, D. R., Davidson, M. T., and Getter, D. J., "Development of improved bridge design provisions for barge impact loading." *Structures Research Report No. 51117*, Engineering and Industrial Experiment Station, Univ. of Florida, Gainesville, FL, 2008.

Consolazio, G. R., Davidson, M. T., and Cowan, D. R., "Barge bow force-deformation relationships for barge-bridge collision analysis." *Transportation Research Record 2131*, Transportation Research Board, Washington, DC, 3–14, 2009.

Consolazio, G.R., Davidson, M.T., and Getter, D.J., *Development and support of dynamic numerical modeling of aberrant rake barges impacting hurricane protection structures subjected to forces from a hurricane environment*, Final report to U.S. Army Corps of Engineers, Structures Research Report 2010/83710, University of Florida, Department of Civil and Coastal Engineering, 112 p., 2010.

Consolazio, G.R., Walters, R.A., Harper, Z.S., *Development of Finite Element Models for Studying Multi-Barge Flotilla Impacts*, Final report to U.S. Army Corps of Engineers, Structures Research Report 2012/87754, University of Florida, Department of Civil and Coastal Engineering, 61 p., 2012.

Consolazio, G.R., Walters, R.A., *Development Of Multi-Barge Flotilla Finite Element Models For Use In Probabilistic Barge Impact Analysis Of Flexible Walls*, Final report to U.S. Army Corps of Engineers, Structures Research Report 2012/94753, University of Florida, Department of Civil and Coastal Engineering, 79 p., 2012.

FB-MultiPier, *FB-MultiPier User's Manual*. Florida Bridge Software Institute, University of Florida, Gainesville, Florida, 2013.

Getter, D. J., and Consolazio, G. R., "Relationships of barge bow force-deformation for bridge design: Probabilistic consideration of oblique impact scenarios." *Transportation Research Record 2251*, Transportation Research Board, Washington, DC, 3-15, 2011.

LSTC, *LS-DYNA Keyword User's Manual: Version 971*, Livermore Software Technology Corporation, Livermore, CA, 2009.

U.S. Army Corps of Engineers, *2007 Flood Control and Navigation Maps: Mississippi River*, U.S. Army Corps of Engineers, Washington D.C., 2007.

APPENDIX A
IMPACT FORCE-TIME HISTORIES FROM BULLNOSE SIMULATIONS

Individual force-time histories for all barge-bullnose impact simulations conducted in this study are plotted on the following pages. Each plot includes separate traces for the *two-dimensional (2-D) resultant impact force in the horizontal plane*, and the vertical component of impact force. All impact forces presented herein correspond to the contact force-time histories between the high-resolution impacting (deformable) barge model and the bullnose model. Also note that all forces presented in this appendix have been low-pass filtered using the procedure described earlier in this report.

The nomenclature used in each figure caption, to identify the impact condition that is plotted, is of the form:

NSxNR – SPEED FPS – BULLNOSE – END – STRING – MISC

where:

NS	=	number of barge strings (barge columns) in the flotilla
NR	=	number of barge rows in the flotilla
SPEED	=	impact speed in ft/sec (FPS)
BULLNOSE	=	bullnose structure impacted by barge flotilla:
		10’ ∅ : 10 ft semi-circular bullnose
		35’ ∅ : 35 ft semi-circular bullnose
		2:1 sloped-V : standard sloped-V bullnose
		1:1 sloped-V : modified sloped-V bullnose
		1:2 sloped-V : modified sloped-V bullnose
END	=	[Bow, Stern] : end of barge flotilla that impacts bullnose
STRING	=	[Exterior, Interior] : string of barge flotilla that impacts bullnose
MISC	=	miscellaneous conditions:
		impact is at an angle (specified in degrees)
		off-center : impact location is off-center from centerline of barge string

For additional information regarding the barge-bullnose impact conditions for which impact forces are plotted in this appendix, see Chapter 4.

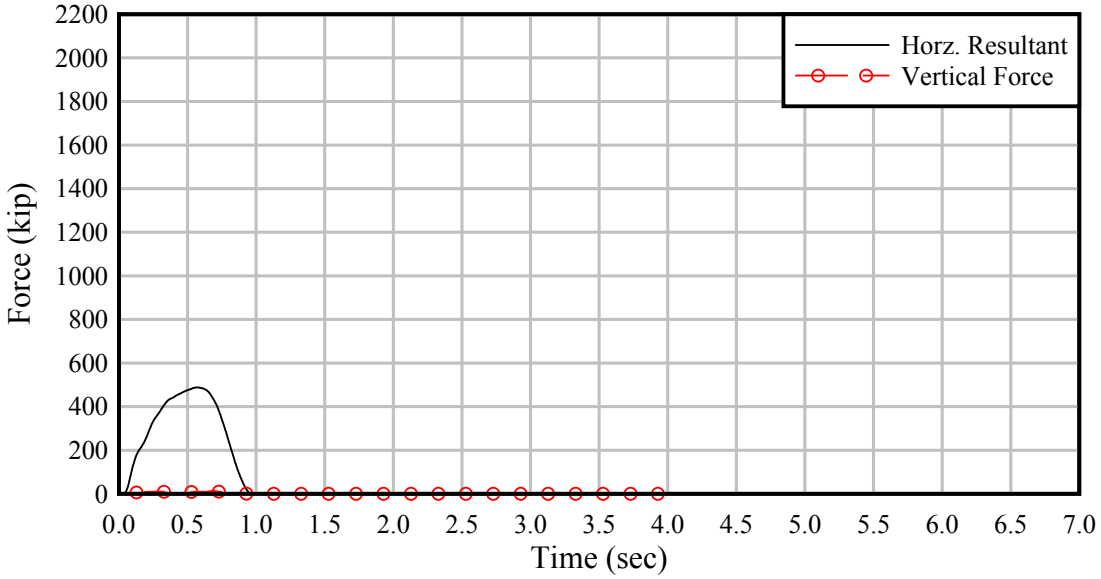

Figure A.1. 1x1 – 2 FPS – 2:1 Sloped-V – Bow – Exterior

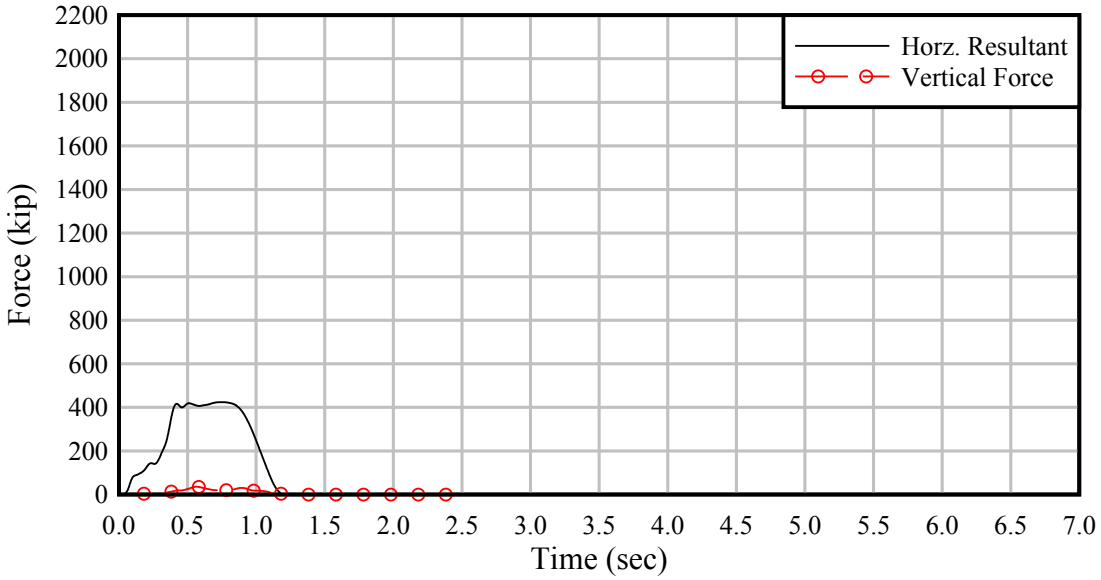

Figure A.2. 1x1 – 2 FPS – 2:1 Sloped-V – Stern – Exterior

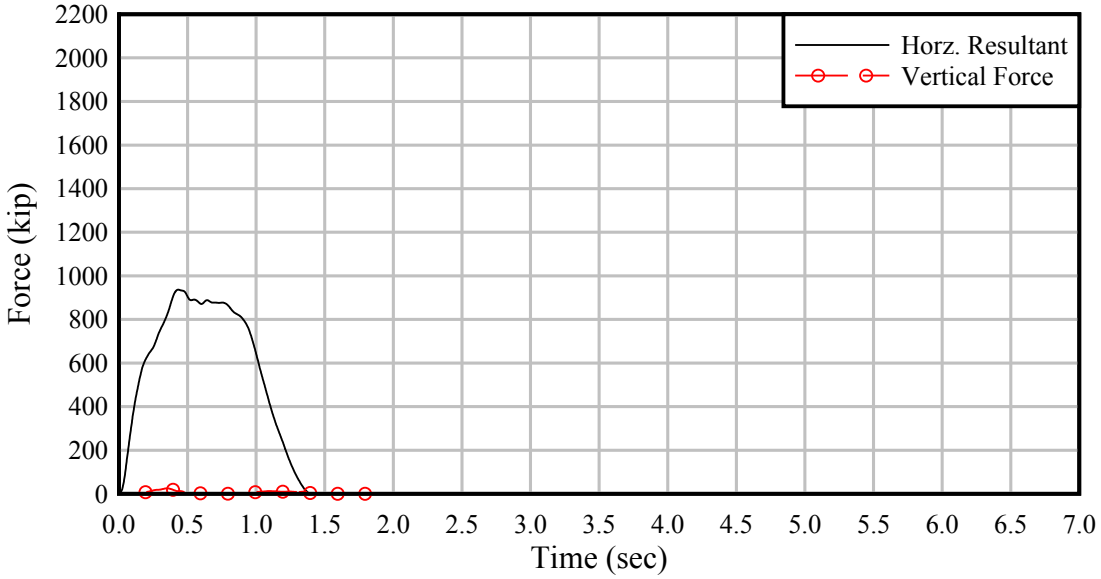

Figure A.3. 1x1 – 6 FPS – 2:1 Sloped-V – Bow – Exterior

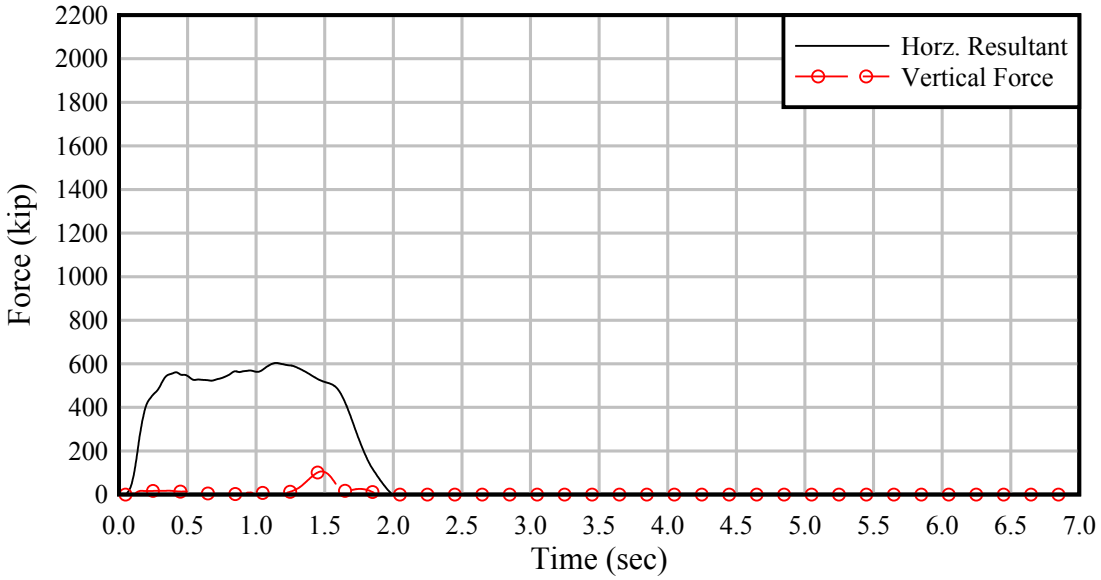

Figure A.4. 1x1 – 6 FPS – 2:1 Sloped-V – Stern – Exterior

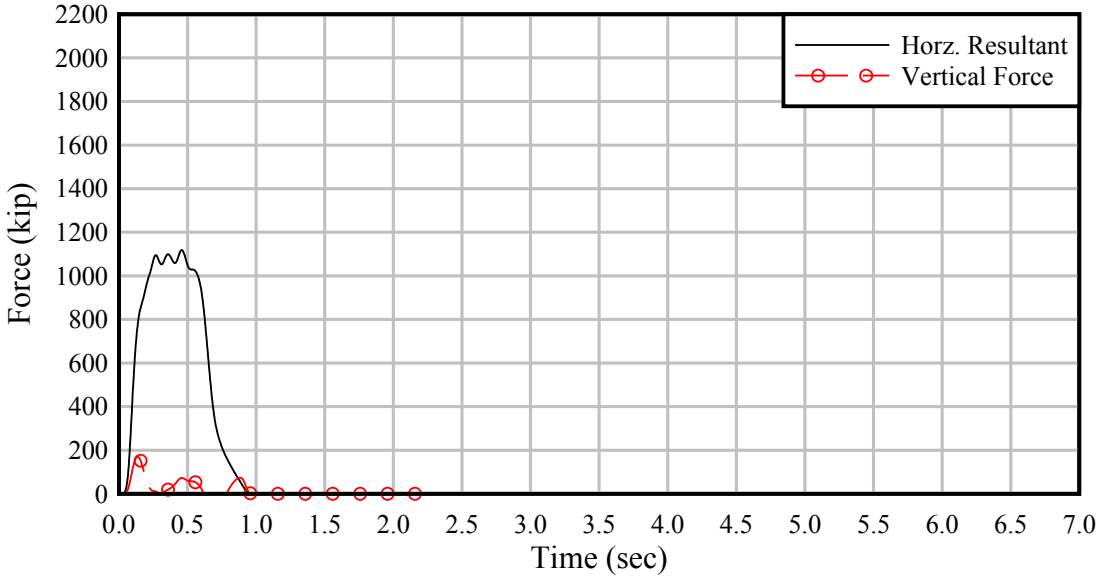

Figure A.5. 1x1 – 4 FPS – 10’ ∅ – Bow – Exterior

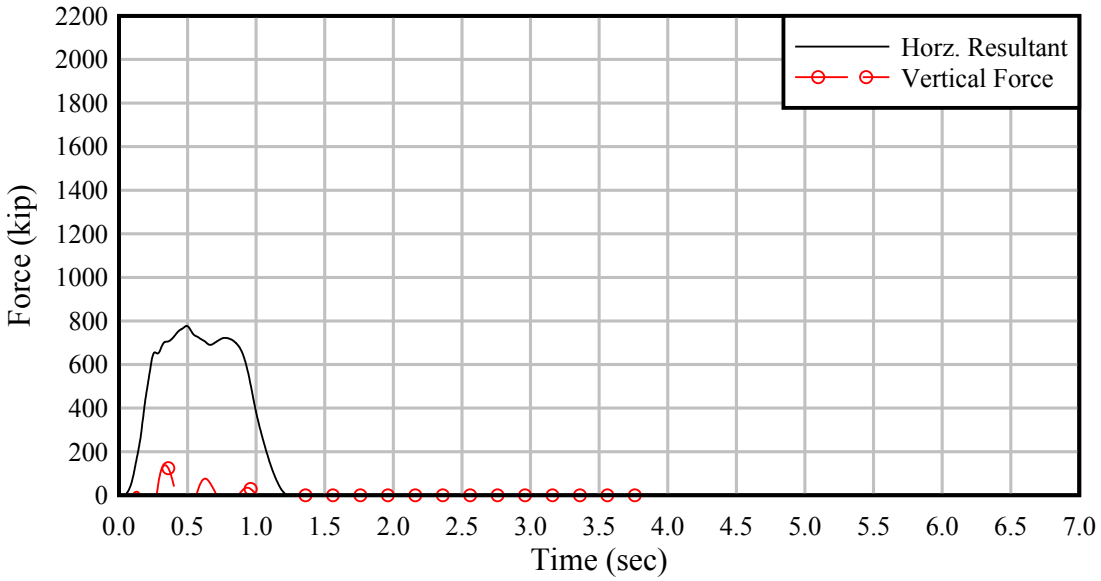

Figure A.6. 1x1 – 4 FPS – 10’ ∅ – Stern – Exterior

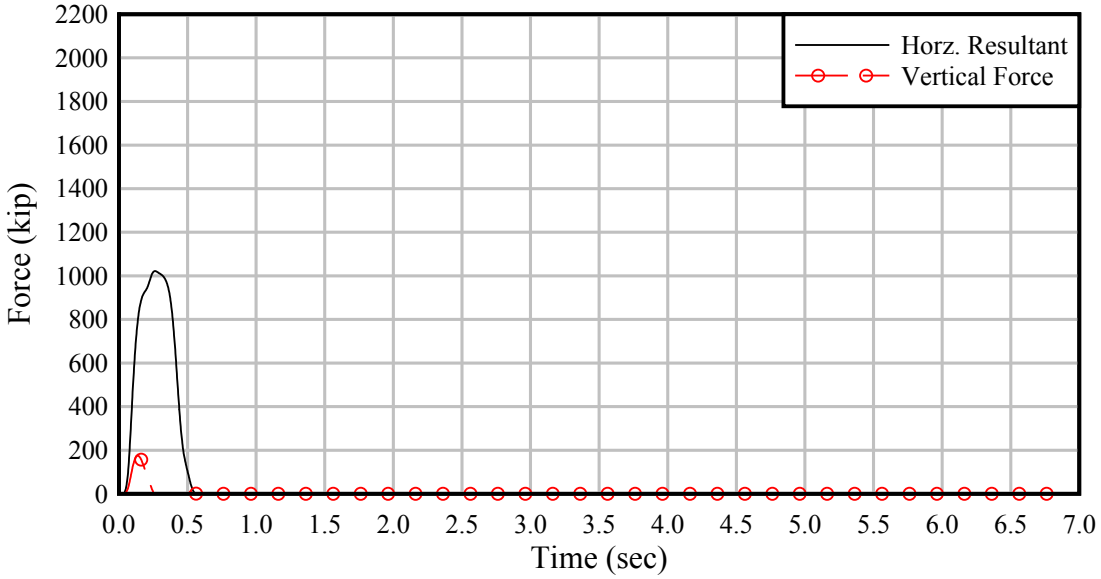

Figure A.7. 1x1 – 2 FPS – 35’ ∅ – Bow – Exterior

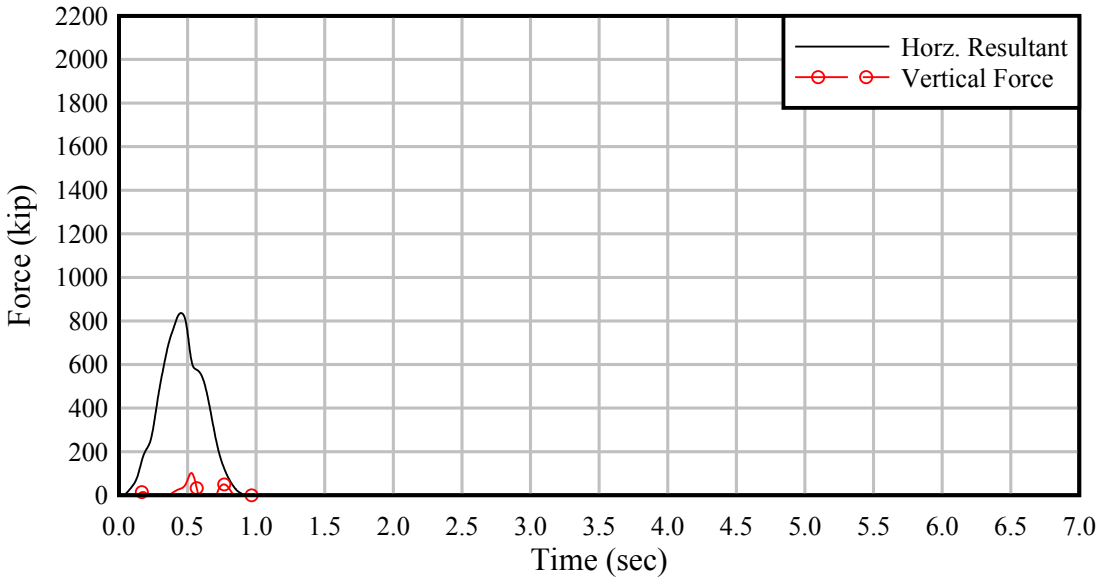

Figure A.8. 1x1 – 2 FPS – 35’ ∅ – Stern – Exterior

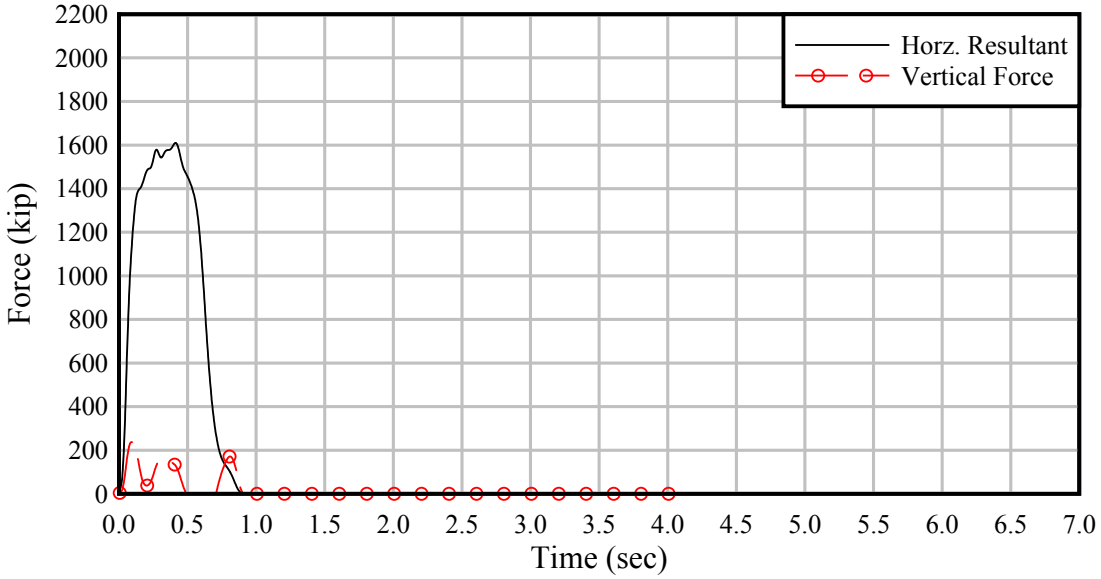

Figure A.9. 1x1 – 6 FPS – 35’ ∅ – Bow – Exterior

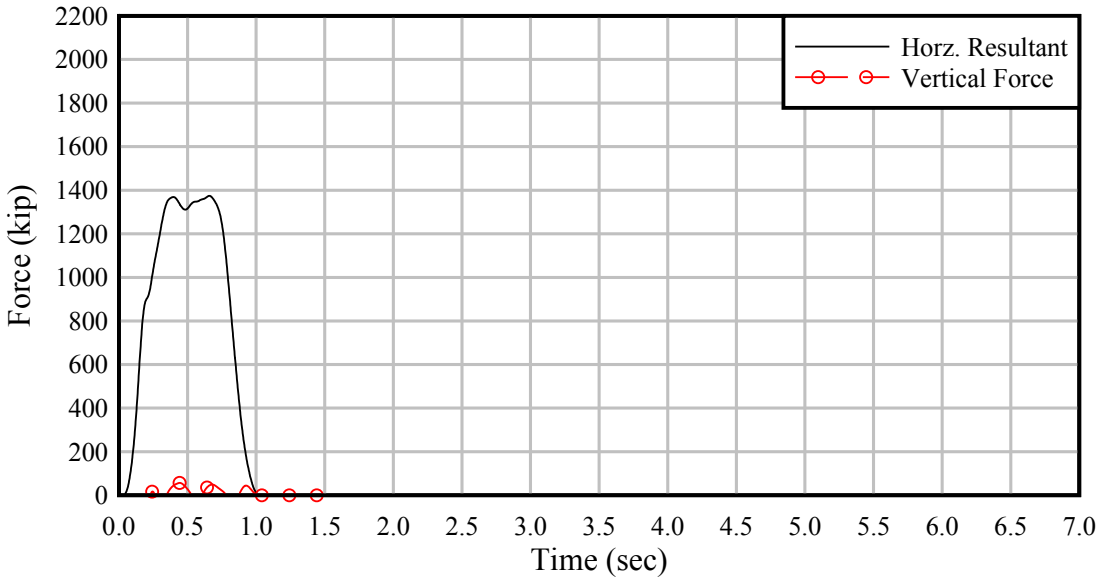

Figure A.10. 1x1 – 6 FPS – 35’ ∅ – Stern – Exterior

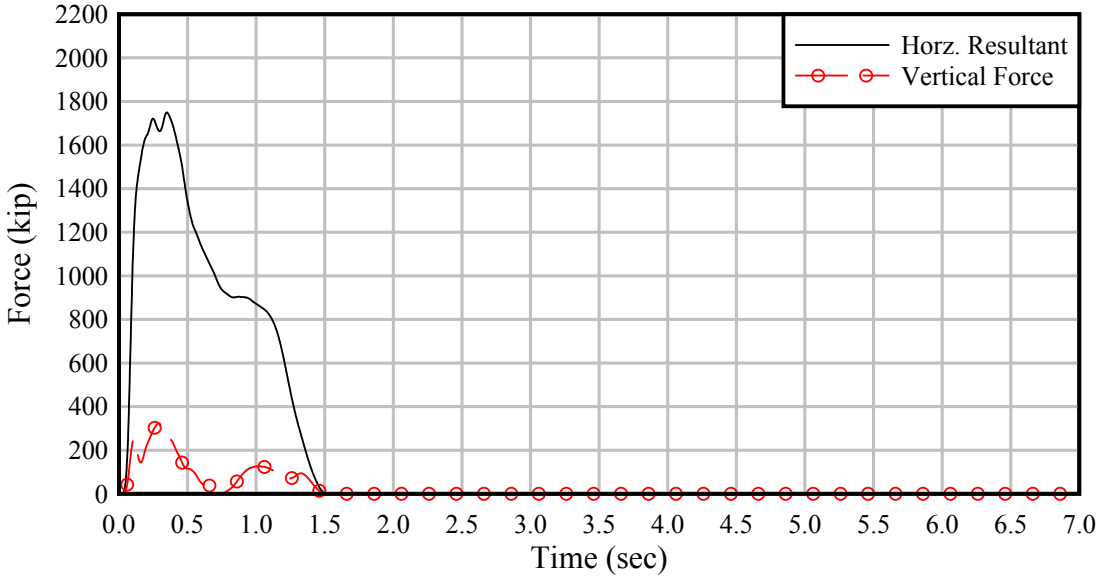

Figure A.11. 1x1 – 10 FPS – 35’ ∅ – Bow – Exterior

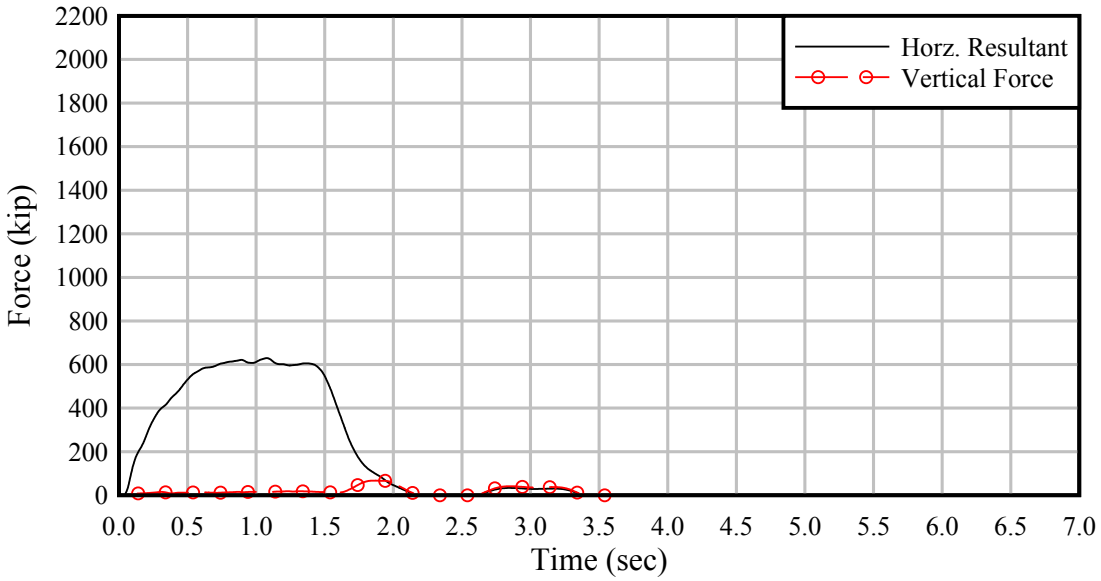

Figure A.12. 1x3 – 2 FPS – 2:1 Sloped-V – Bow – Exterior

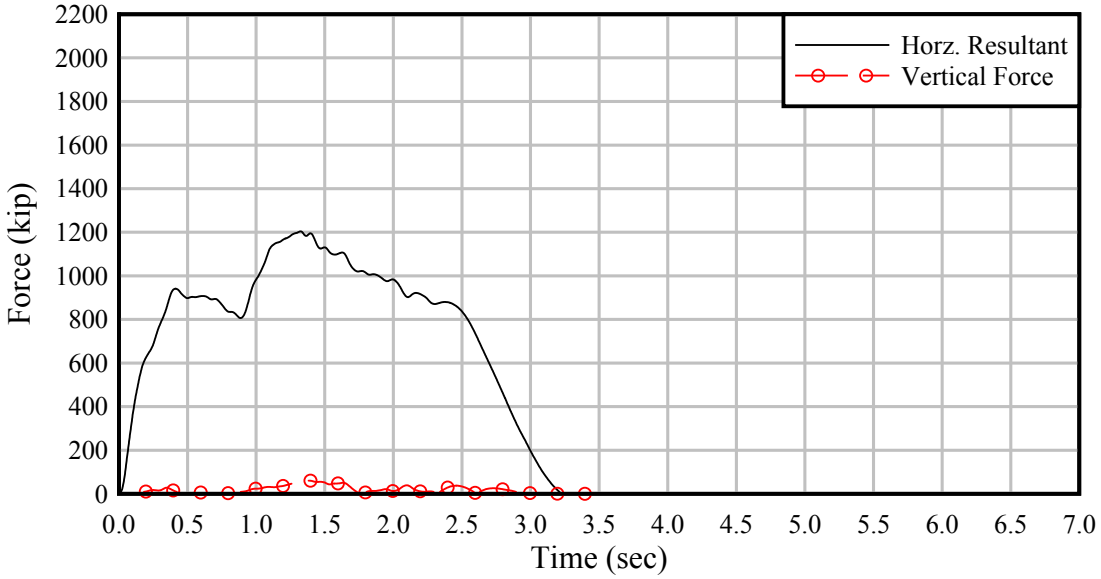

Figure A.13. 1x3 – 6 FPS – 2:1 Sloped-V – Bow – Exterior

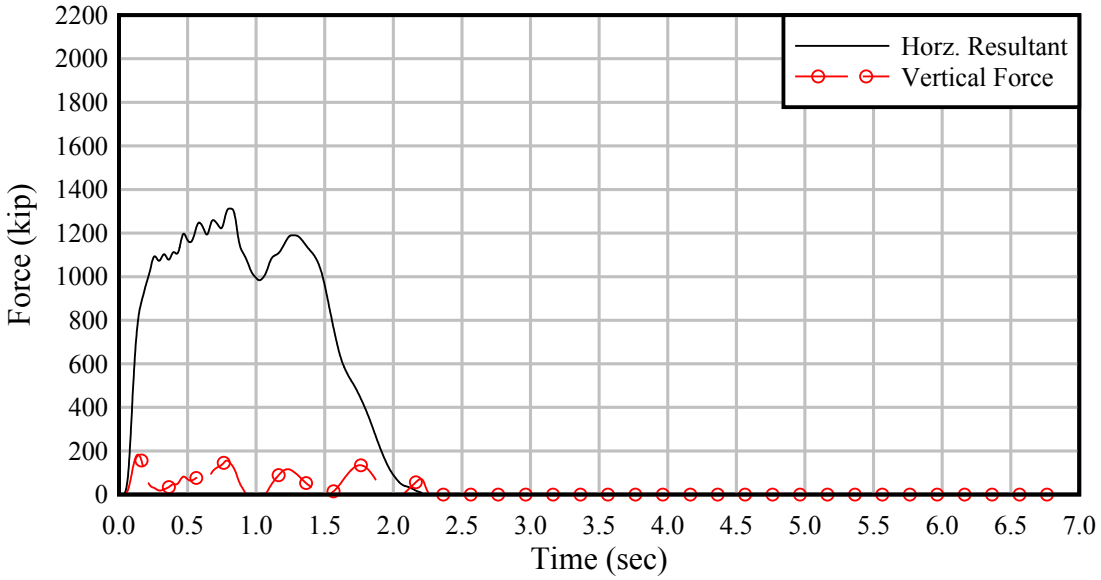

Figure A.14. 1x3 – 4 FPS – 10’ ∅ – Bow – Exterior

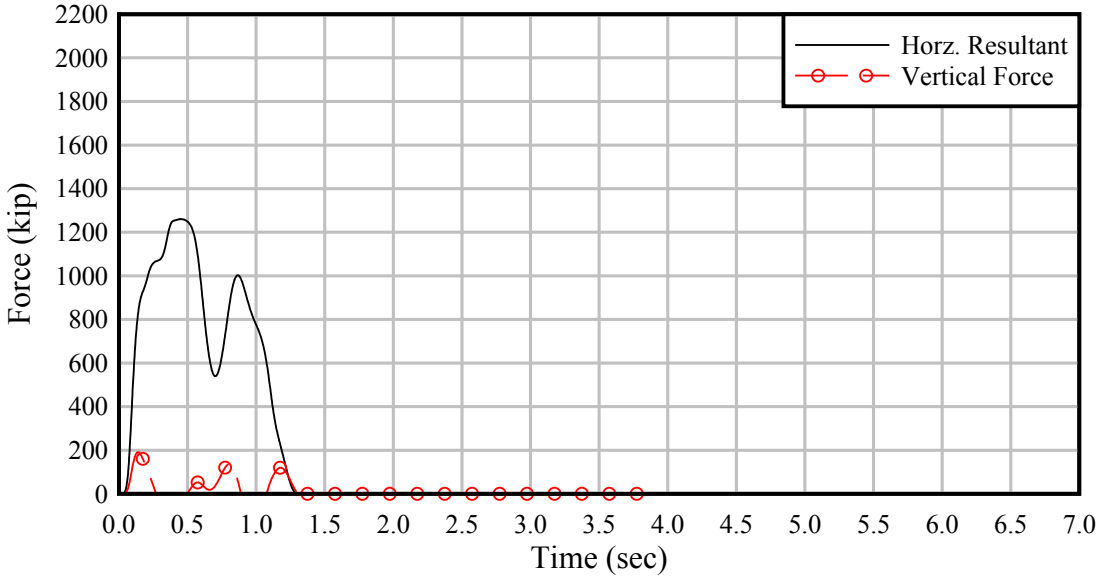

Figure A.15. 1x3 – 2 FPS – 35’ ∅ – Bow – Exterior

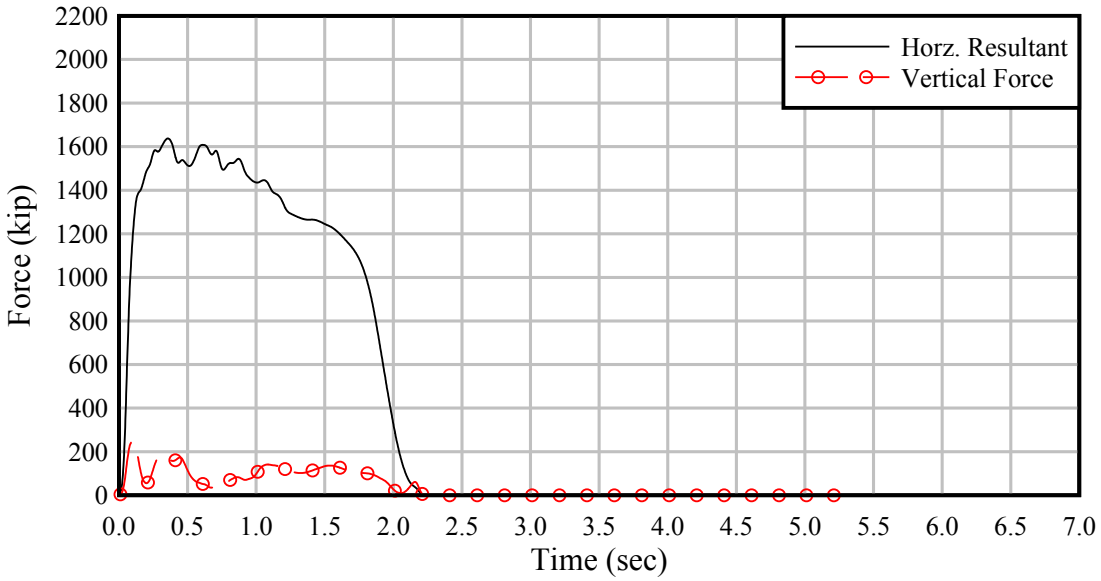

Figure A.16. 1x3 – 6 FPS – 35’ ∅ – Bow – Exterior

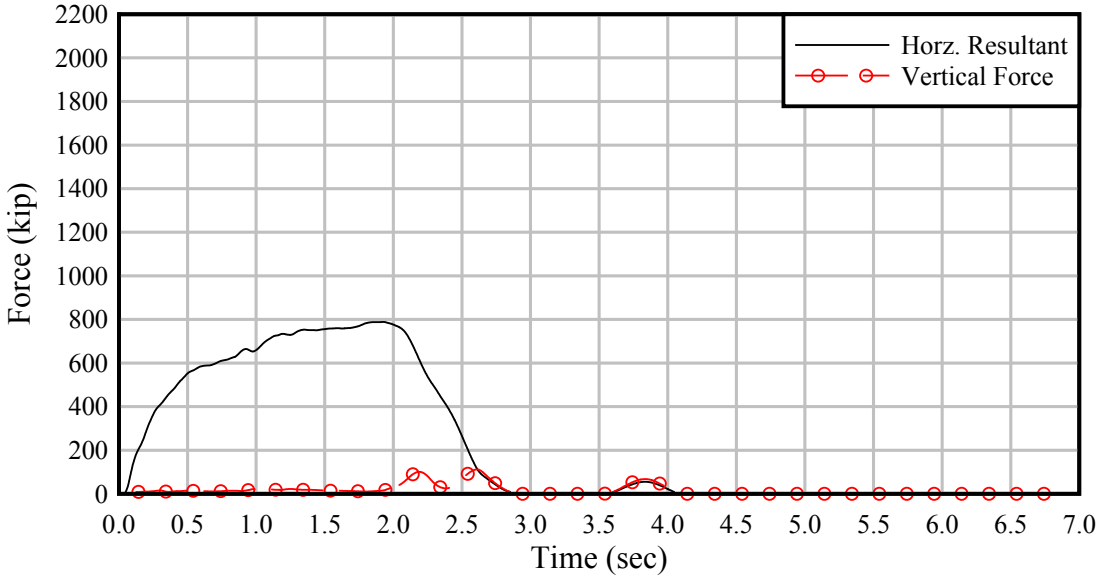

Figure A.17. 1x5 – 2 FPS – 2:1 Sloped-V – Bow – Exterior

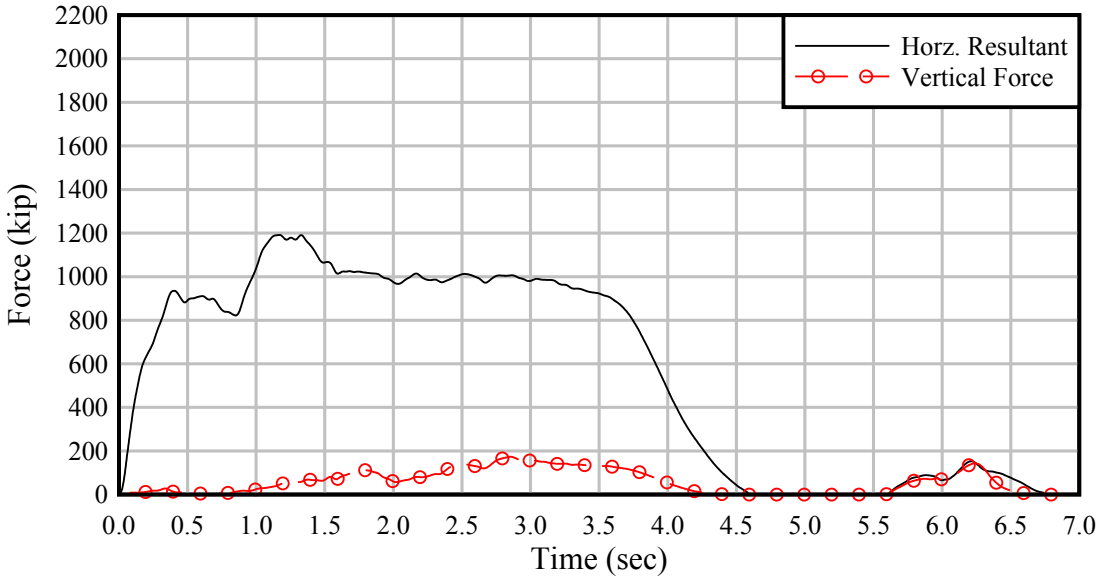

Figure A.18. 1x5 – 6 FPS – 2:1 Sloped-V – Bow – Exterior

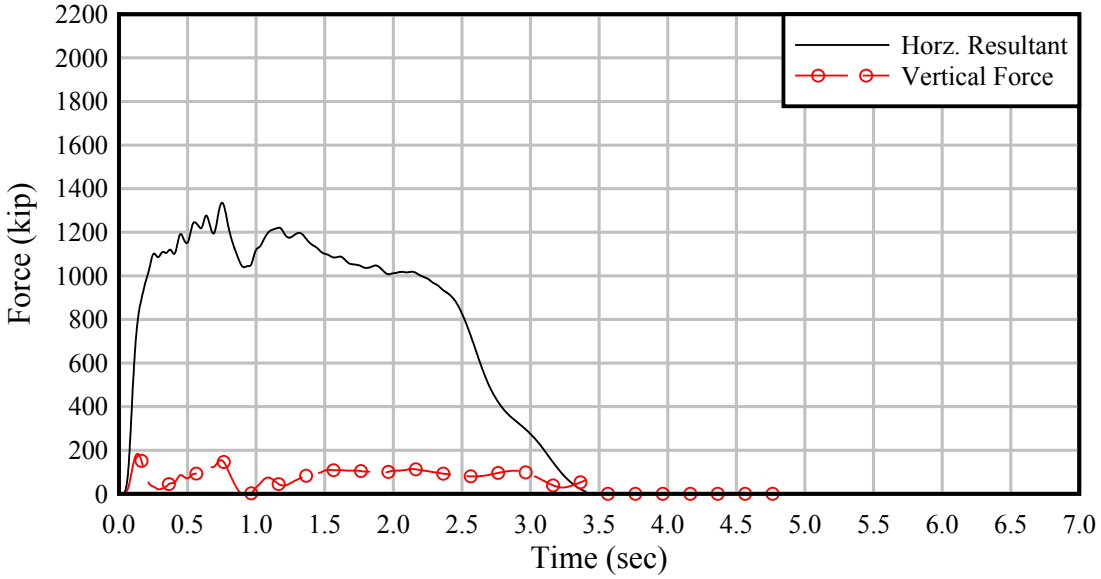

Figure A.19. 1x5 – 4 FPS – 10’ ∅ – Bow – Exterior

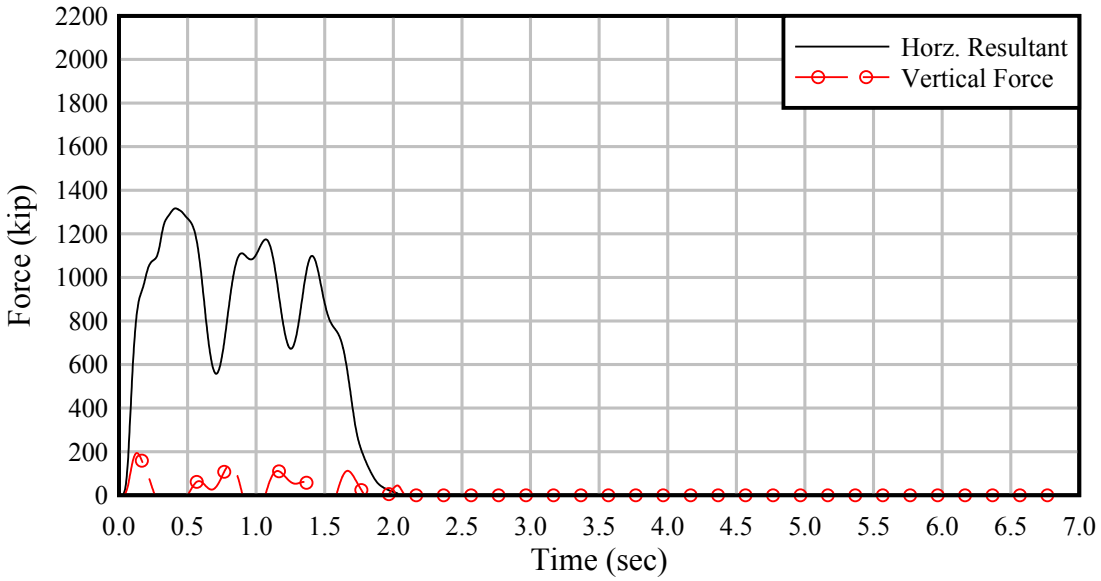

Figure A.20. 1x5 – 2 FPS – 35’ ∅ – Bow – Exterior

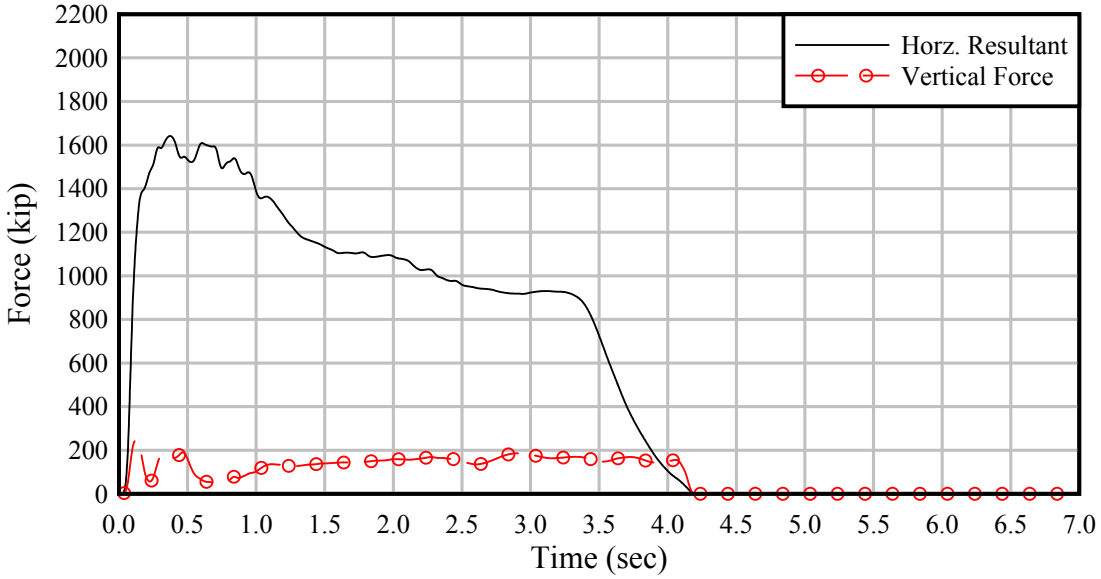

Figure A.21. 1x5 – 6 FPS – 35’ ∅ – Bow – Exterior

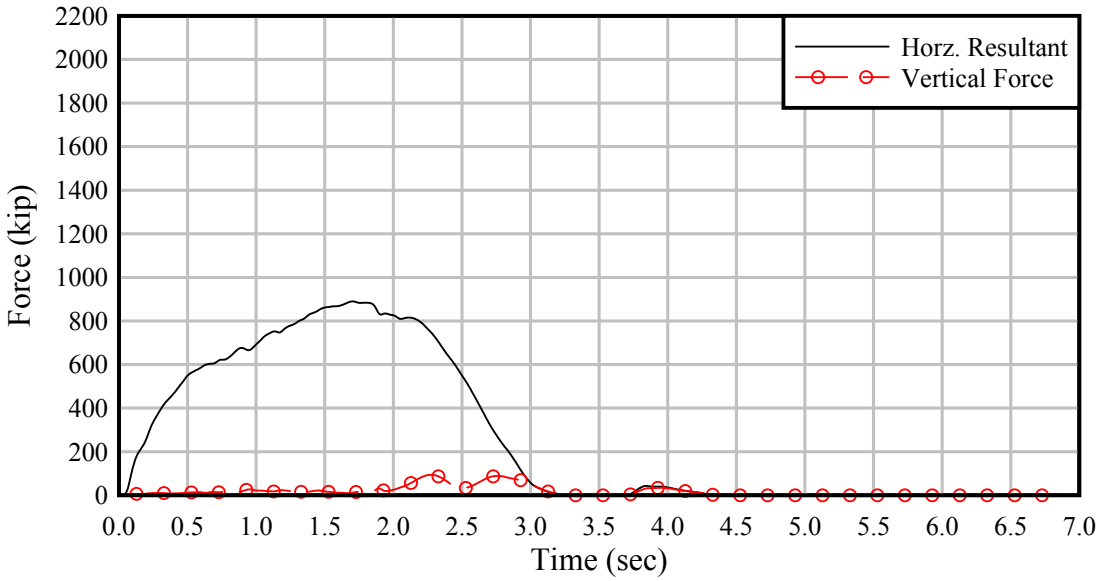

Figure A.22. 2x3 – 2 FPS – 2:1 Sloped-V – Bow – Exterior

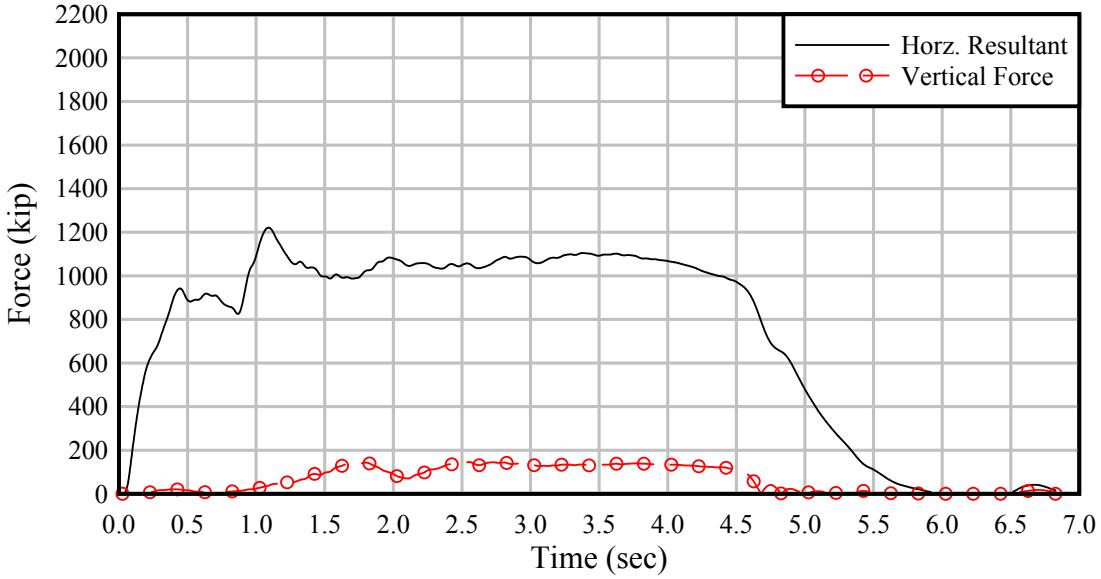

Figure A.23. 2x3 – 6 FPS – 2:1 Sloped-V – Bow – Exterior

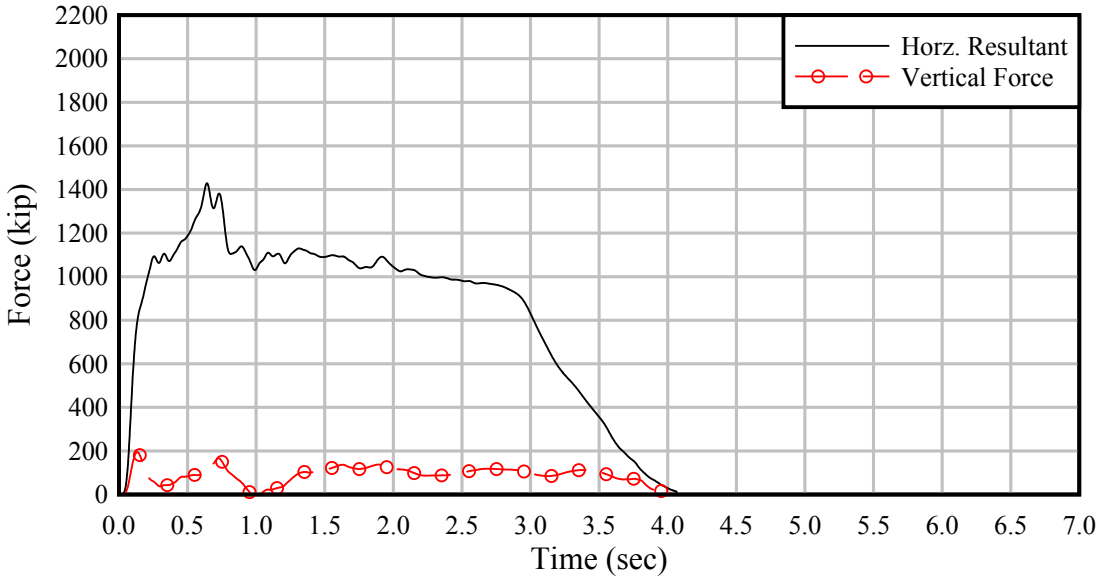

Figure A.24. 2x3 – 4 FPS – 10’ ∅ – Bow – Exterior

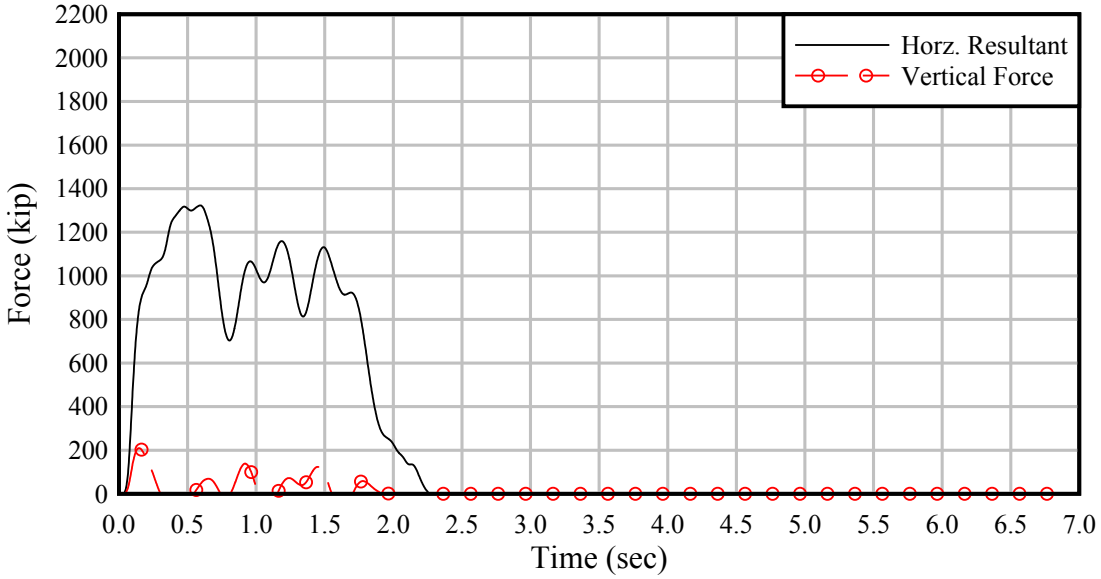

Figure A.25. 2x3 – 2 FPS – 35’ ∅ – Bow – Exterior

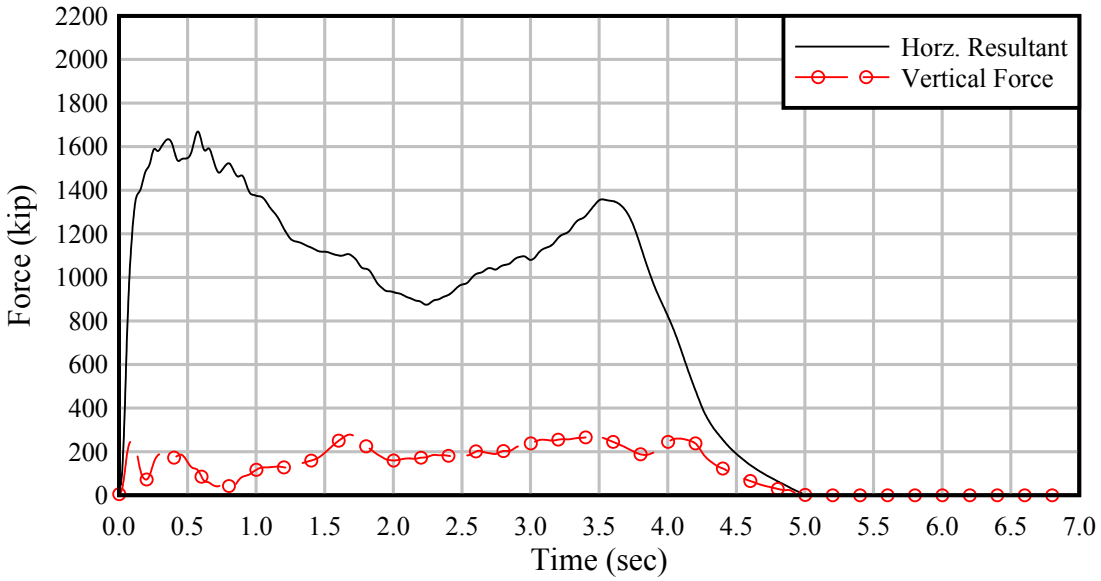

Figure A.26. 2x3 – 6 FPS – 35’ ∅ – Bow – Exterior

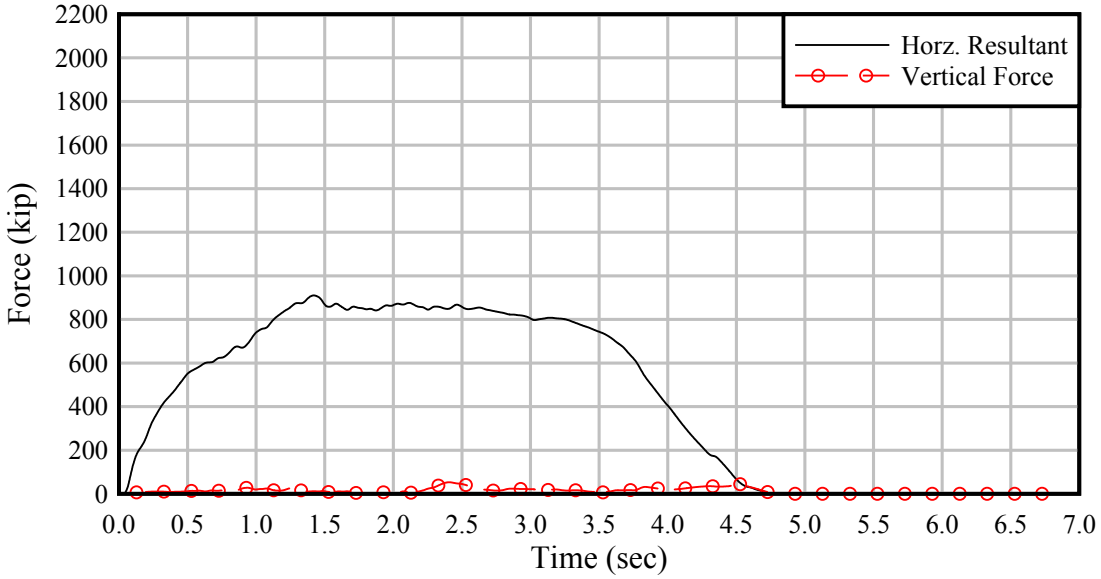

Figure A.27. 2x5 – 2 FPS – 2:1 Sloped-V – Bow – Exterior

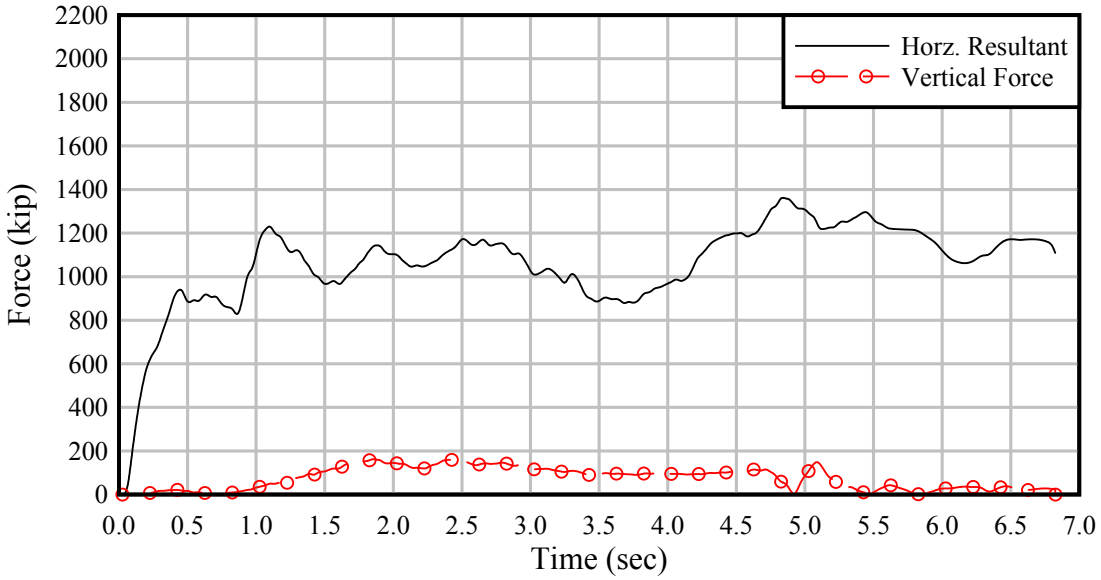

Figure A.28. 2x5 – 6 FPS – 2:1 Sloped-V – Bow – Exterior

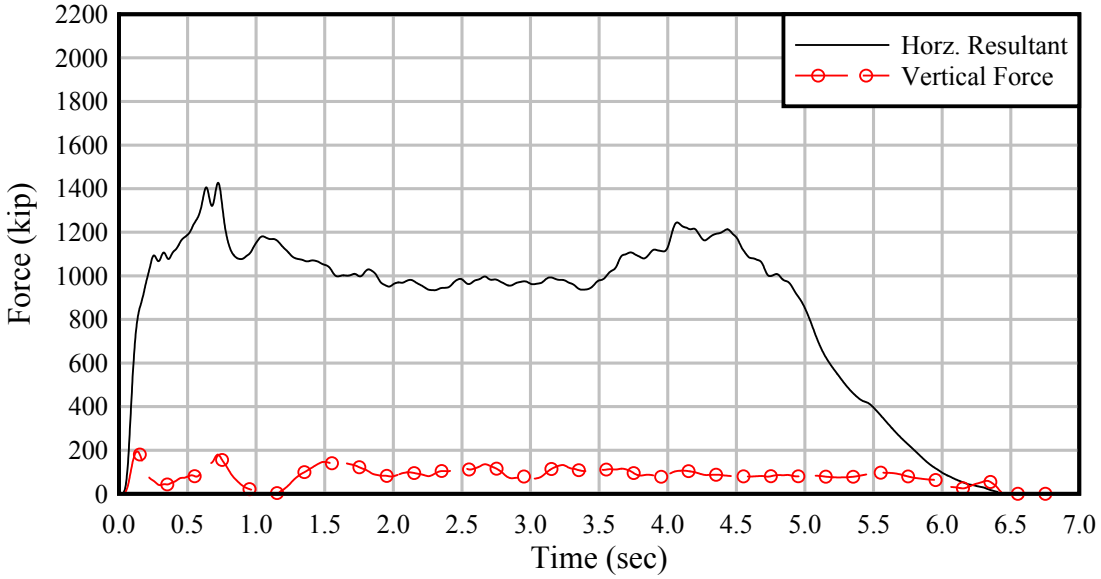

Figure A.29. 2x5 – 4 FPS – 10’ ∅ – Bow – Exterior

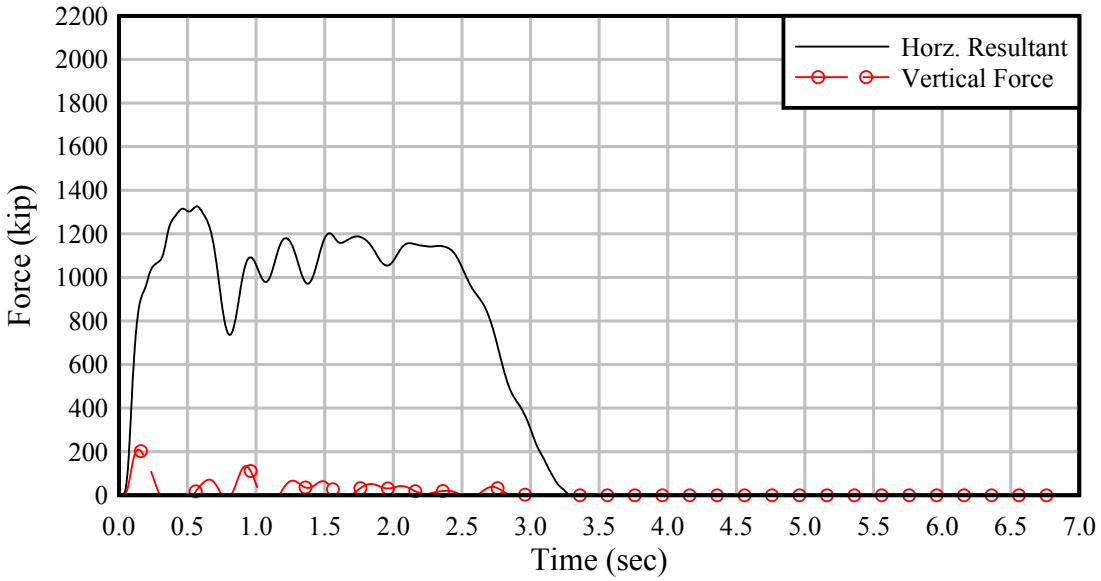

Figure A.30. 2x5 – 2 FPS – 35’ ∅ – Bow – Exterior

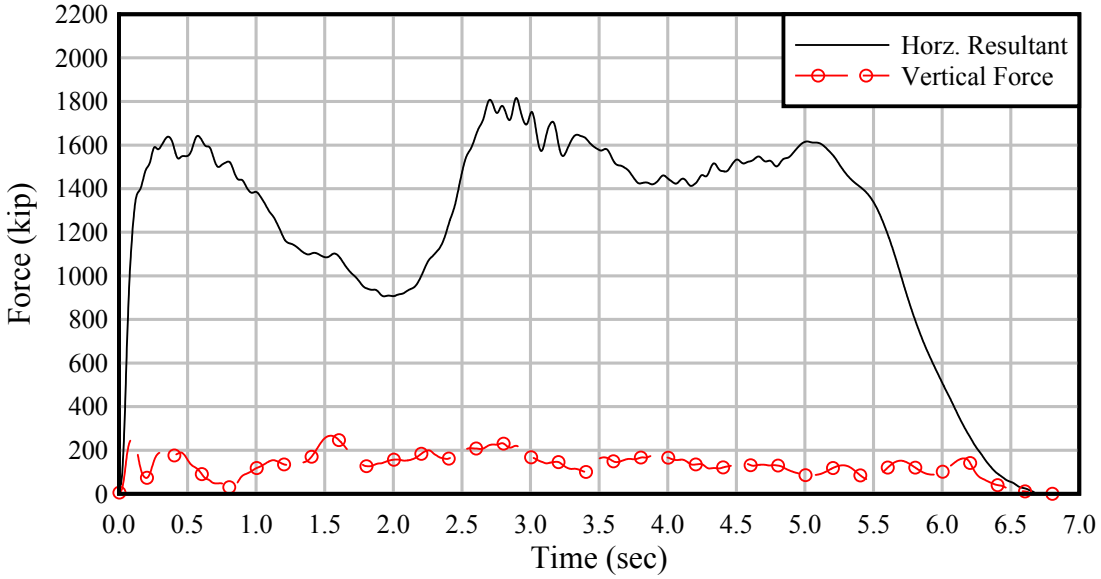

Figure A.31. 2x5 – 6 FPS – 35’ ∅ – Bow – Exterior

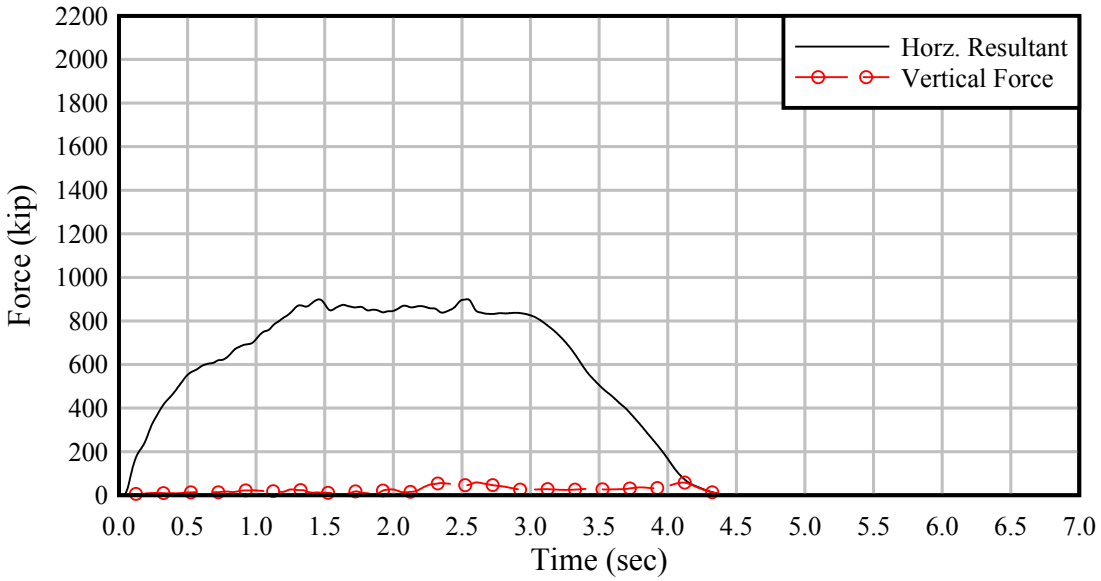

Figure A.32. 3x3 – 2 FPS – 2:1 Sloped-V – Bow – Exterior

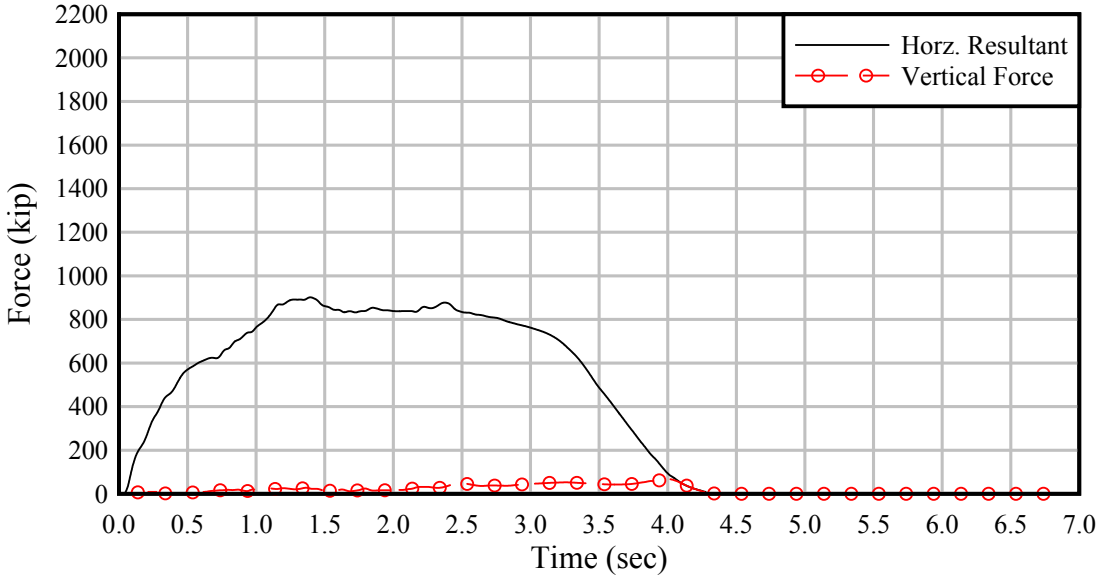

Figure A.33. 3x3 – 2 FPS – 2:1 Sloped-V – Bow – Interior

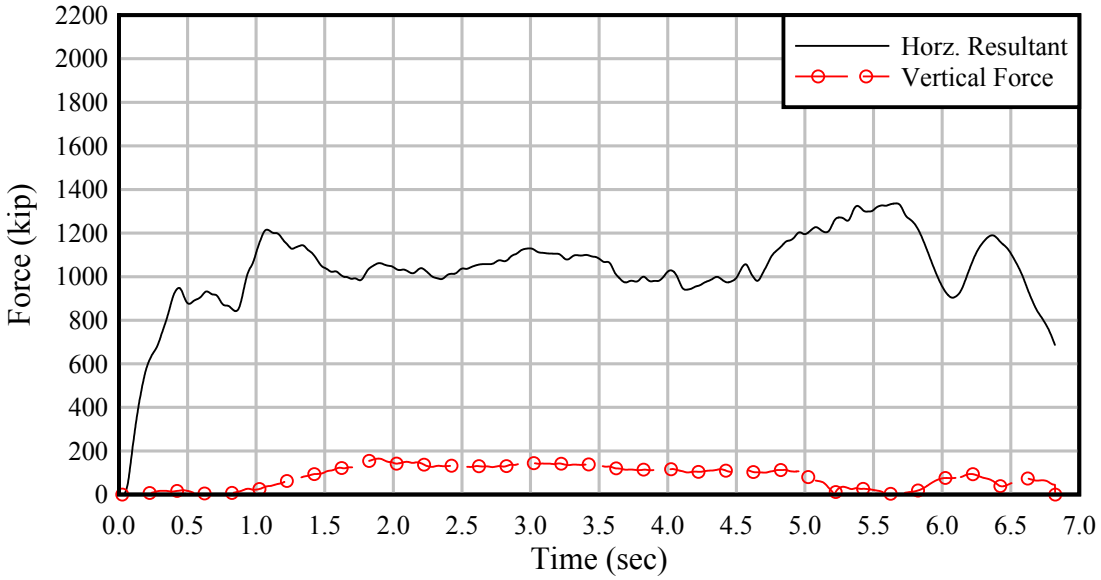

Figure A.34. 3x3 – 6 FPS – 2:1 Sloped-V – Bow – Exterior

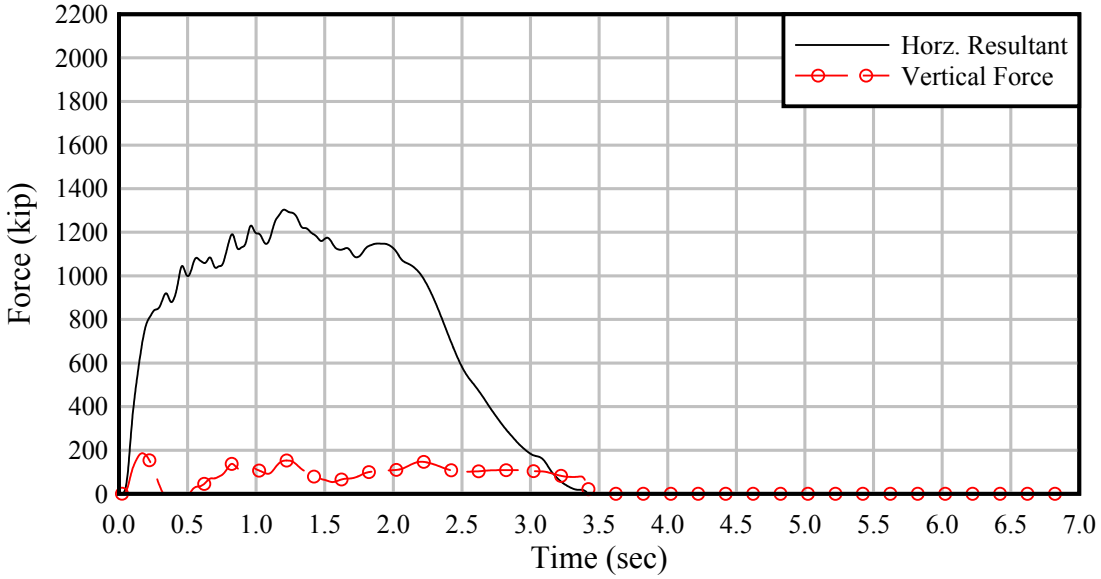

Figure A.35. 3x3 – 2 FPS – 10’ ∅ – Bow – Interior

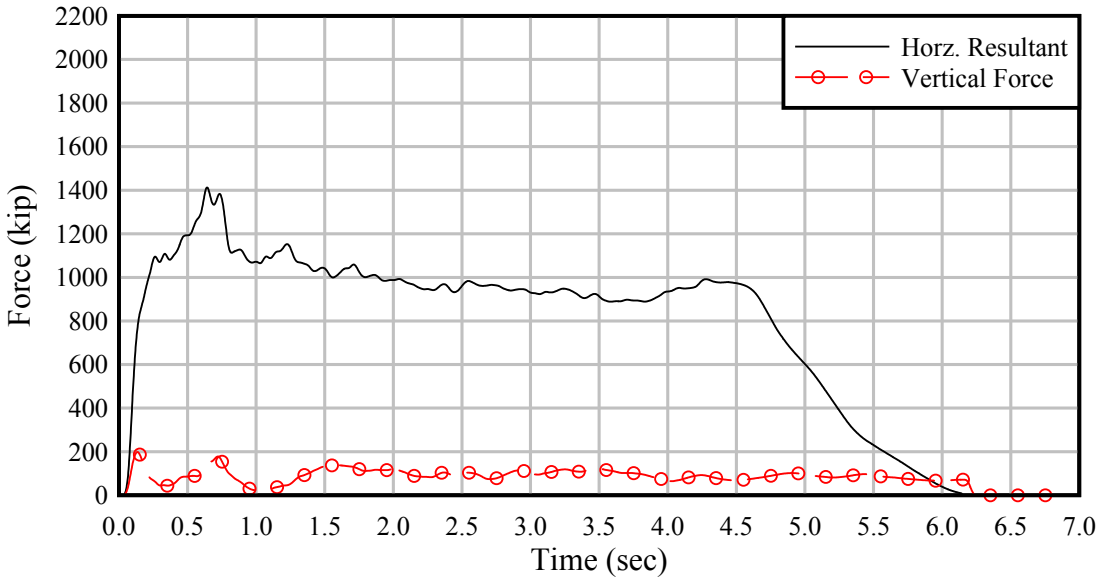

Figure A.36. 3x3 – 4 FPS – 10’ ∅ – Bow – Exterior

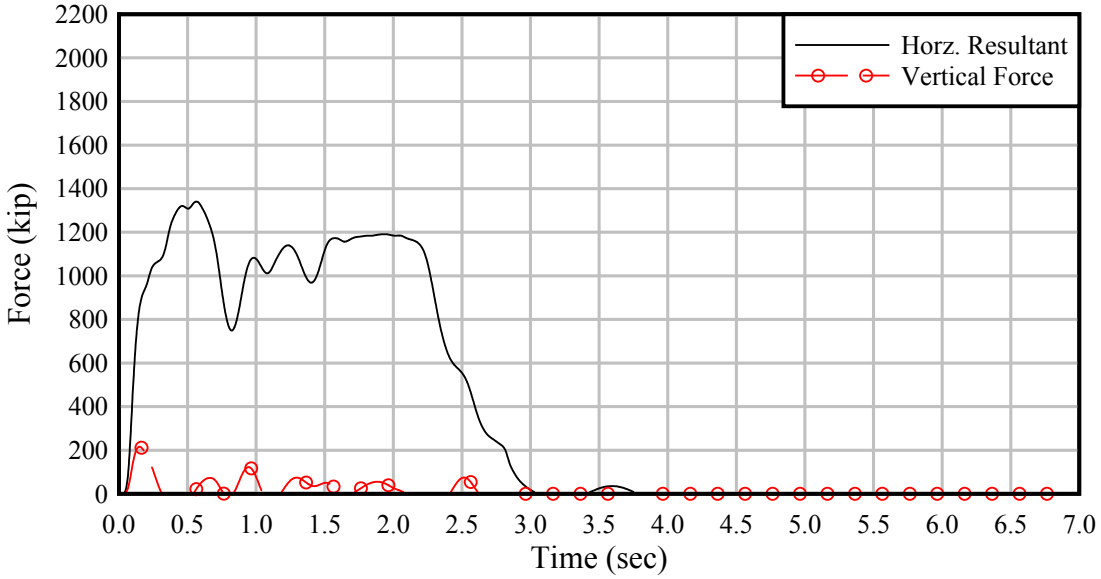

Figure A.37. 3x3 – 2 FPS – 35’ ∅ – Bow – Exterior

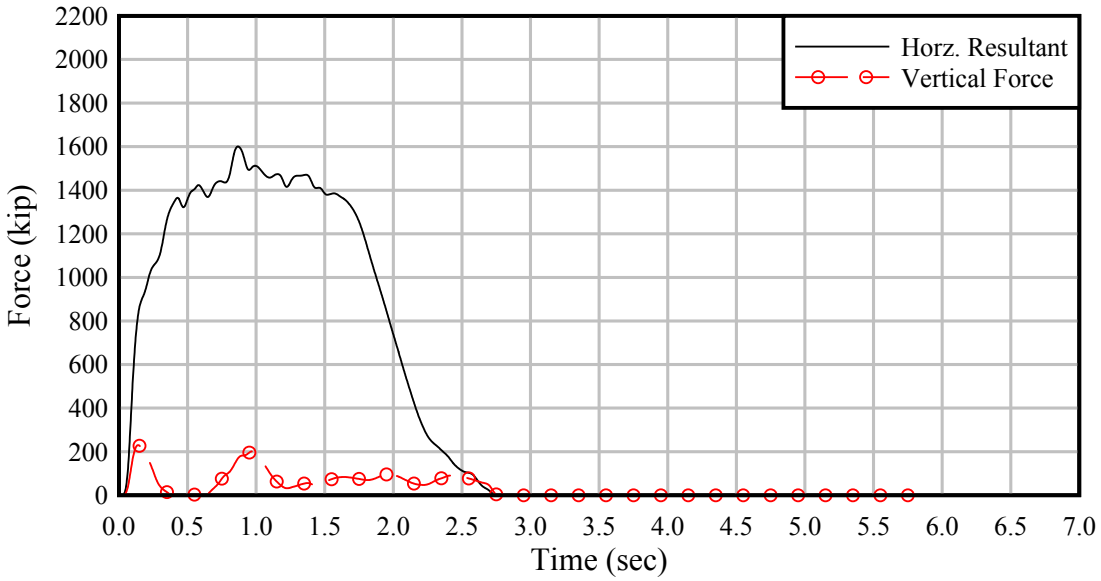

Figure A.38. 3x3 – 2 FPS – 35’ ∅ – Bow – Interior

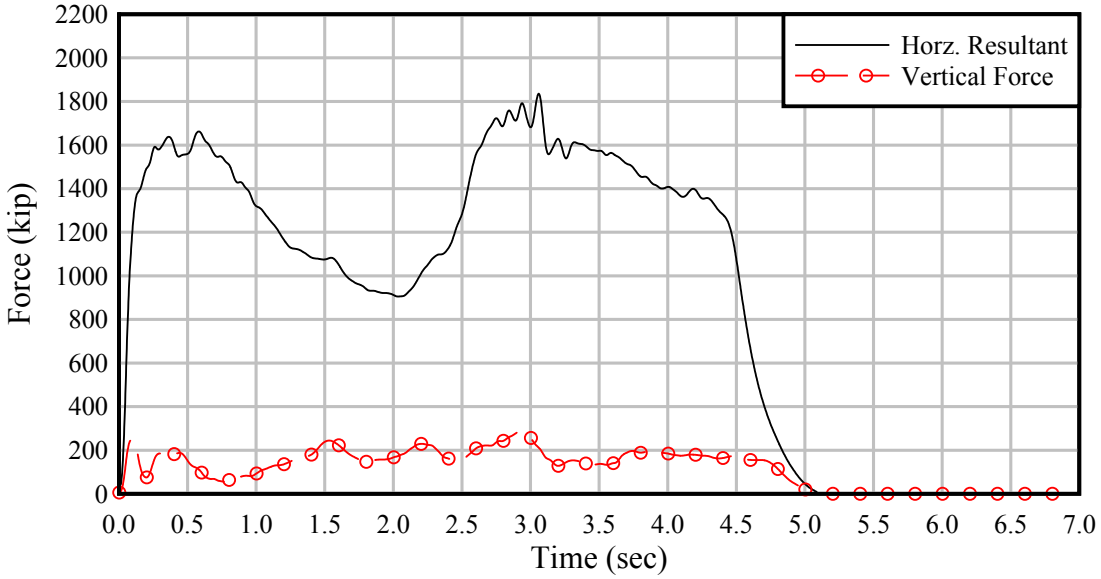

Figure A.39. 3x3 – 6 FPS – 35’ ∅ – Bow – Exterior

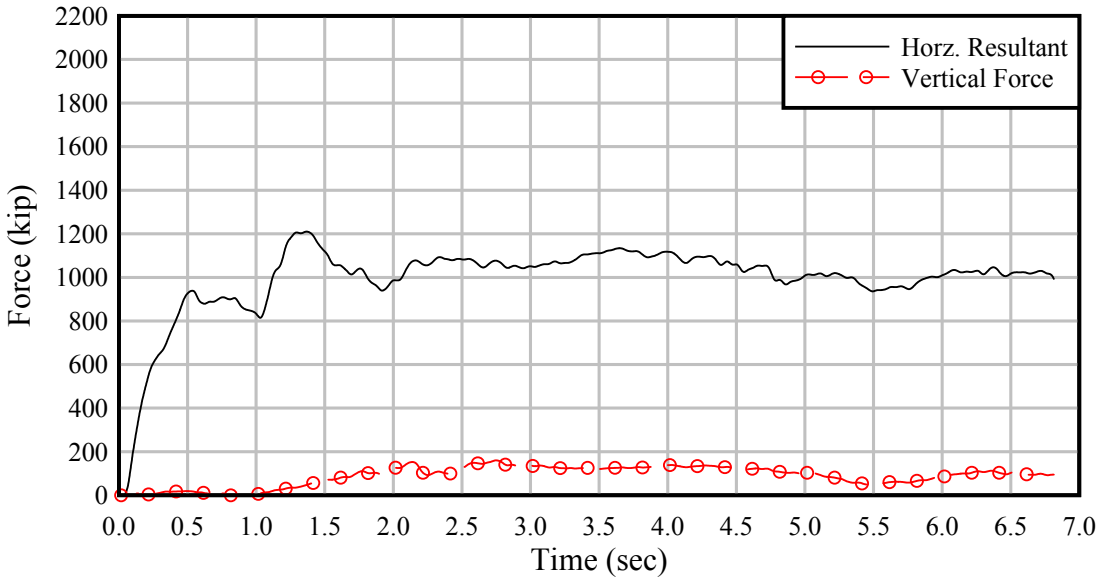

Figure A.40. 3x4 – 5 FPS – 2:1 Sloped-V – Bow – Exterior

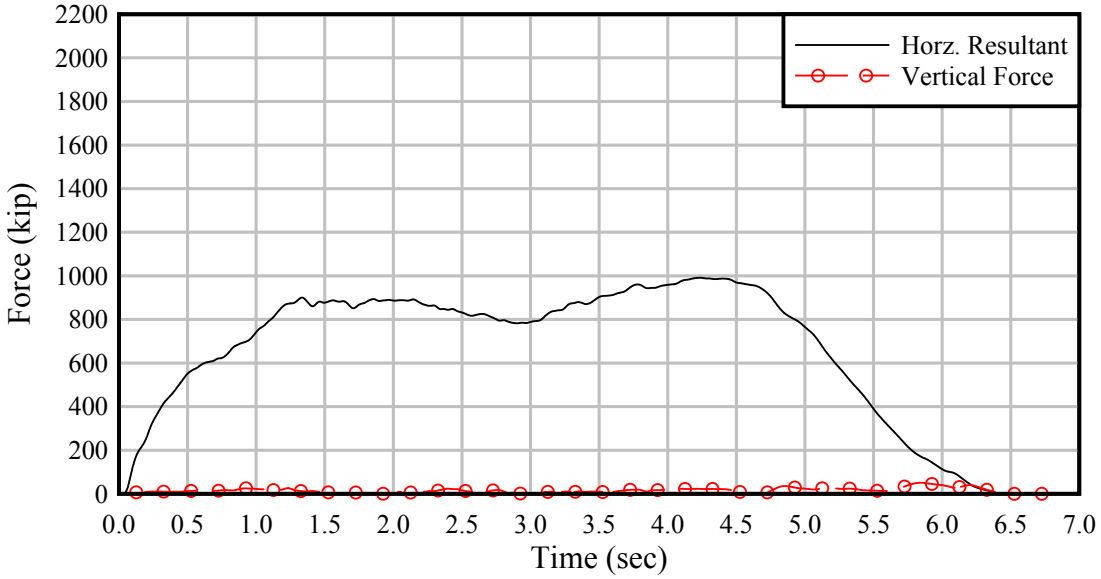

Figure A.41. 3x5 – 2 FPS – 2:1 Sloped-V – Bow – Exterior

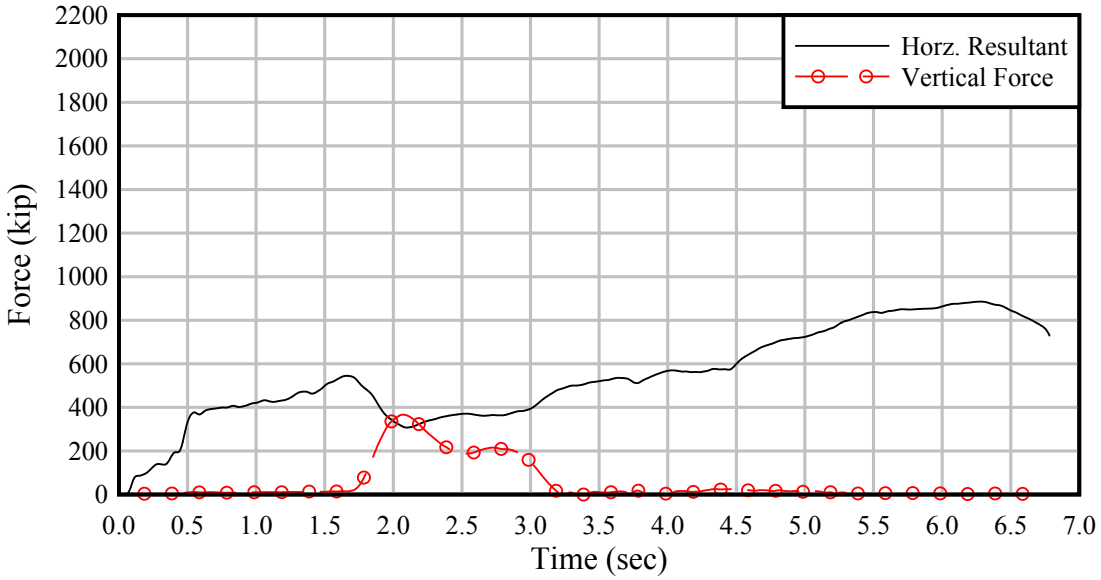

Figure A.42. 3x5 – 2 FPS – 2:1 Sloped-V – Stern – Exterior

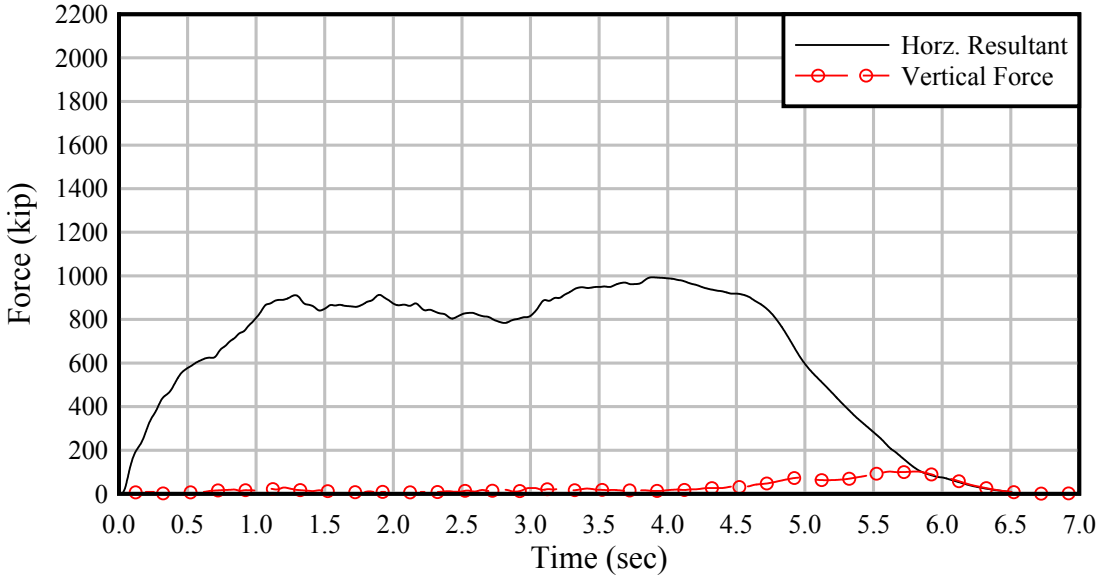

Figure A.43. 3x5 – 2 FPS – 2:1 Sloped-V – Bow – Interior

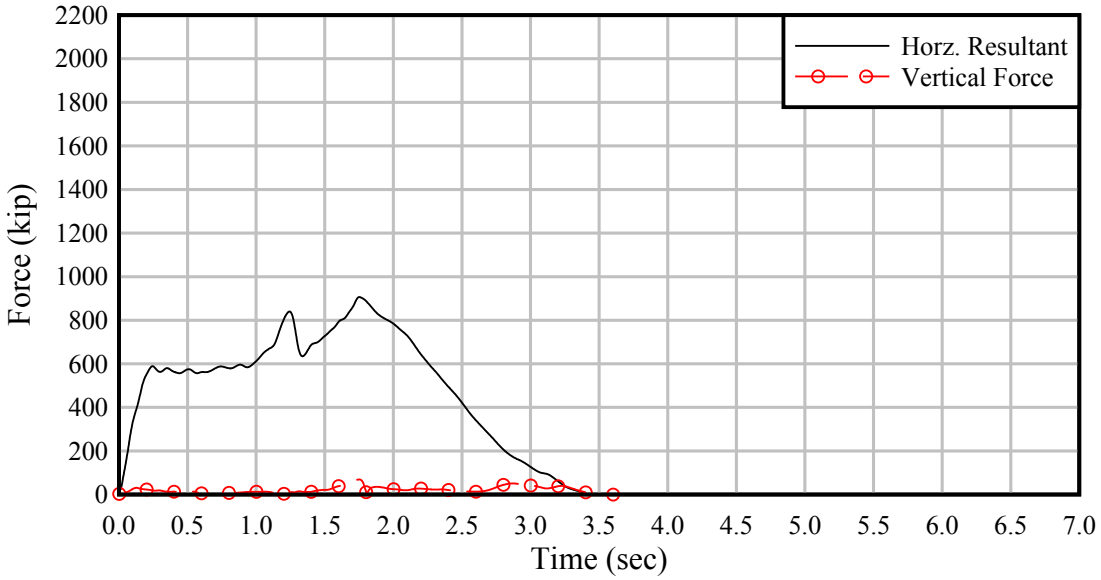

Figure A.44. 3x5 – 2 FPS – 2:1 Sloped-V – Stern – Interior

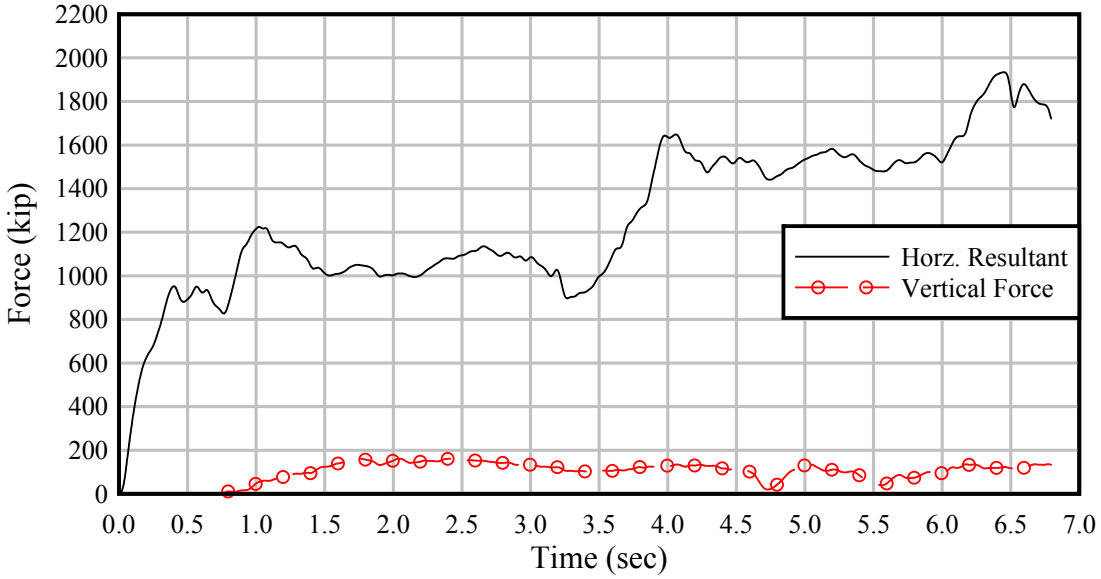

Figure A.45. 3x5 – 6 FPS – 2:1 Sloped-V – Bow – Exterior

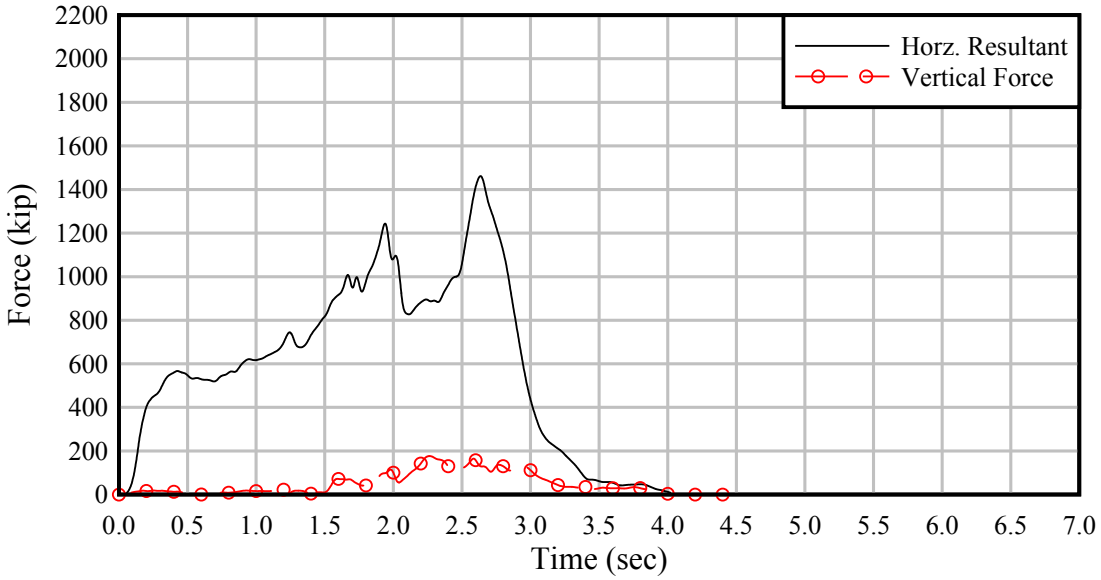

Figure A.46. 3x5 – 6 FPS – 2:1 Sloped-V – Stern – Exterior

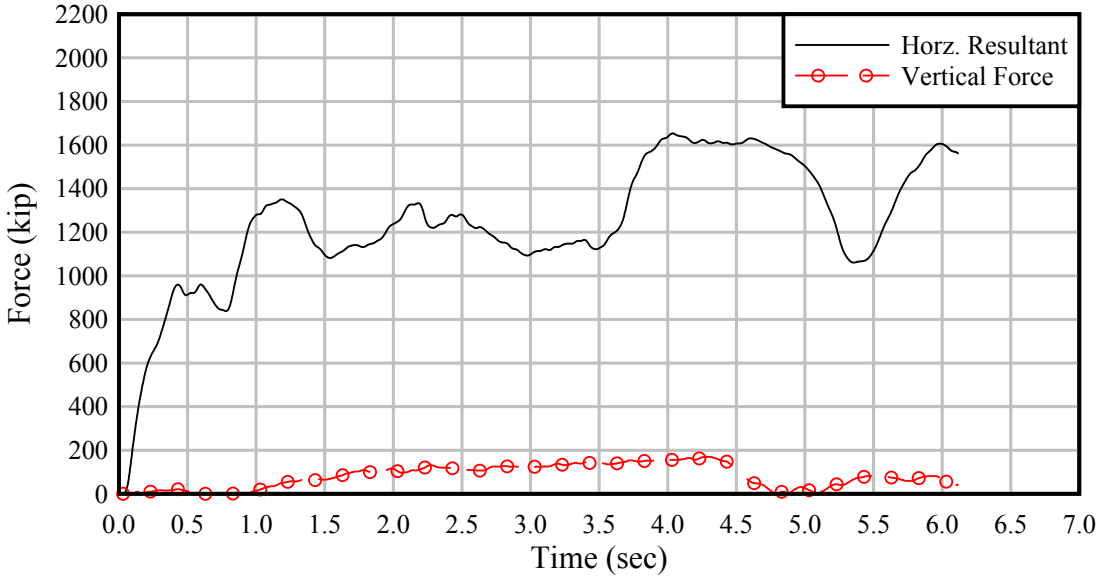

Figure A.47. 3x5 – 6 FPS – 2:1 Sloped-V – Bow – Interior

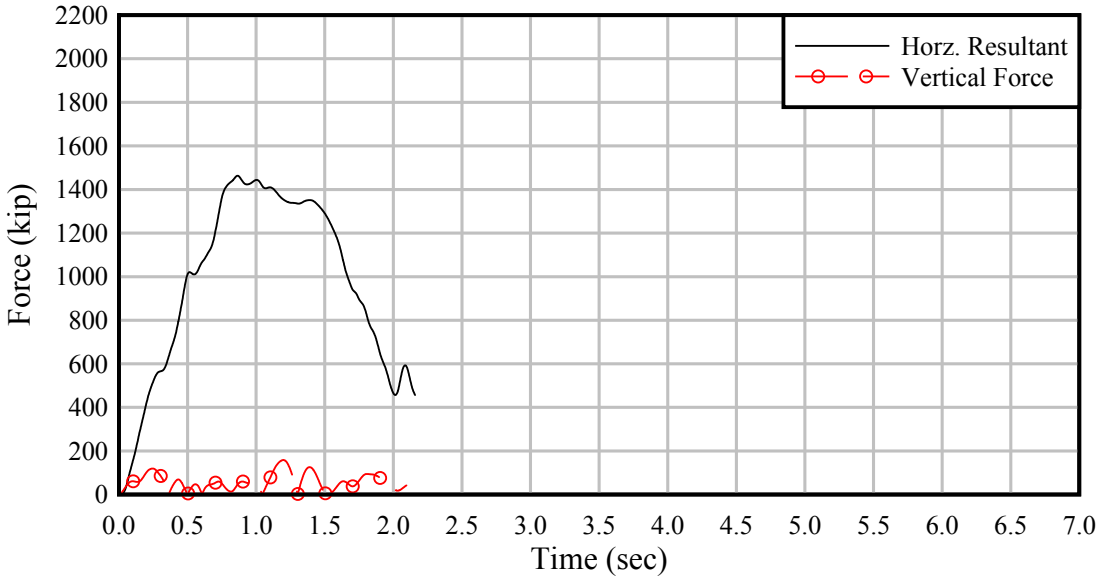

Figure A.48. 3x5 – 6 FPS – 2:1 Sloped-V – Stern – Interior

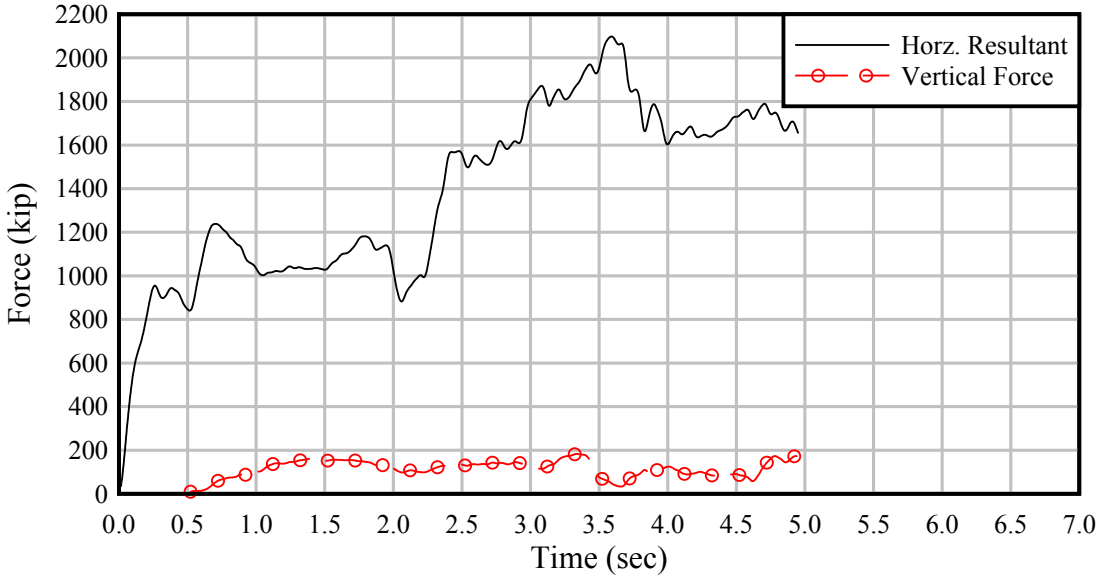

Figure A.49. 3x5 – 9 FPS – 2:1 Sloped-V – Bow – Exterior

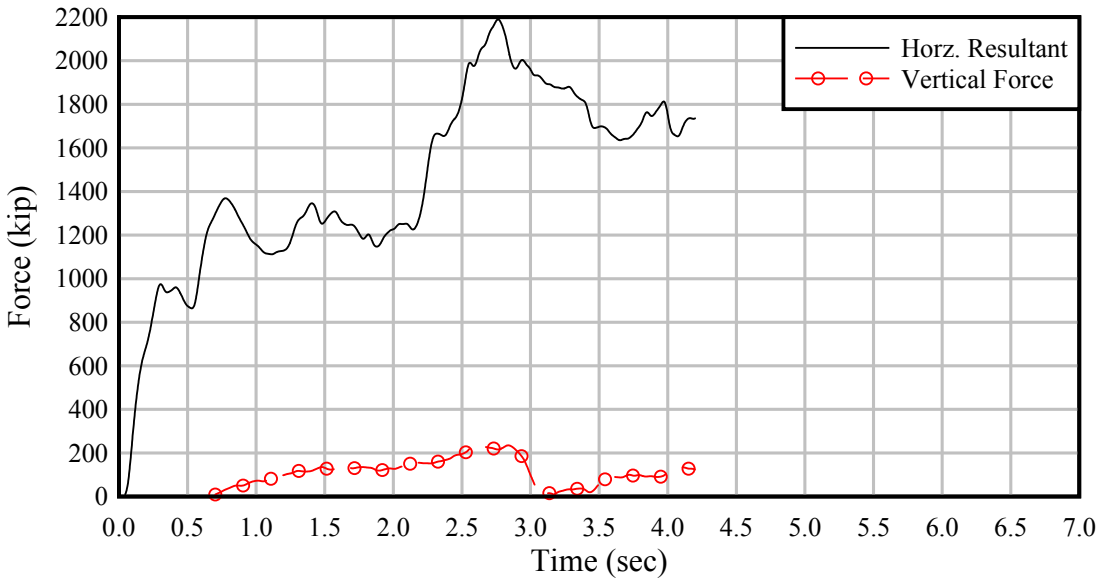

Figure A.50. 3x5 – 9 FPS – 2:1 Sloped-V – Bow – Interior

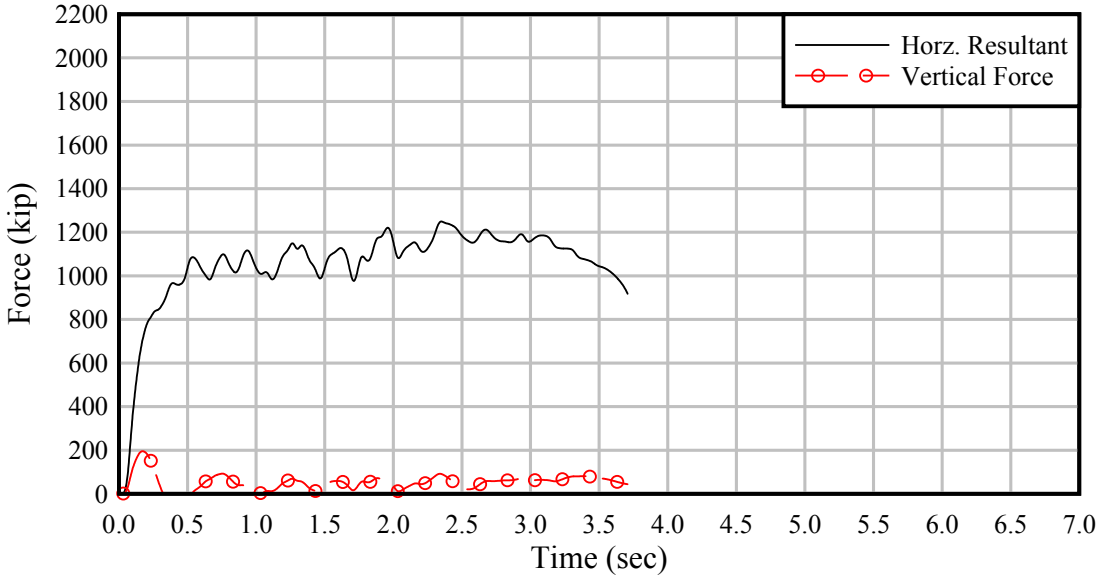

Figure A.51. 3x5 – 2 FPS – 10’ ∅ – Bow – Exterior

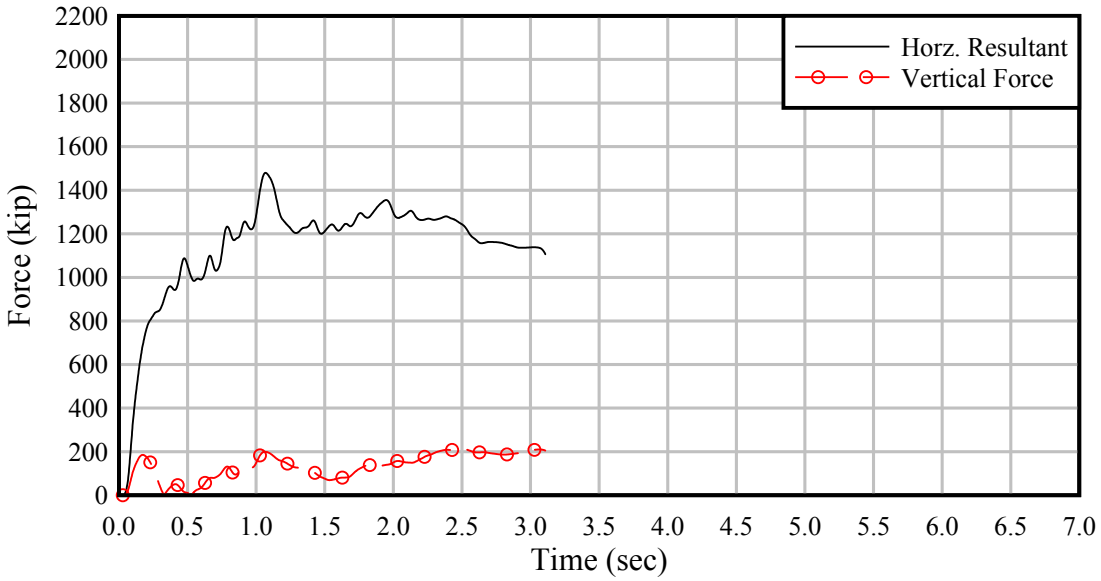

Figure A.52. 3x5 – 2 FPS – 10’ ∅ – Bow – Interior

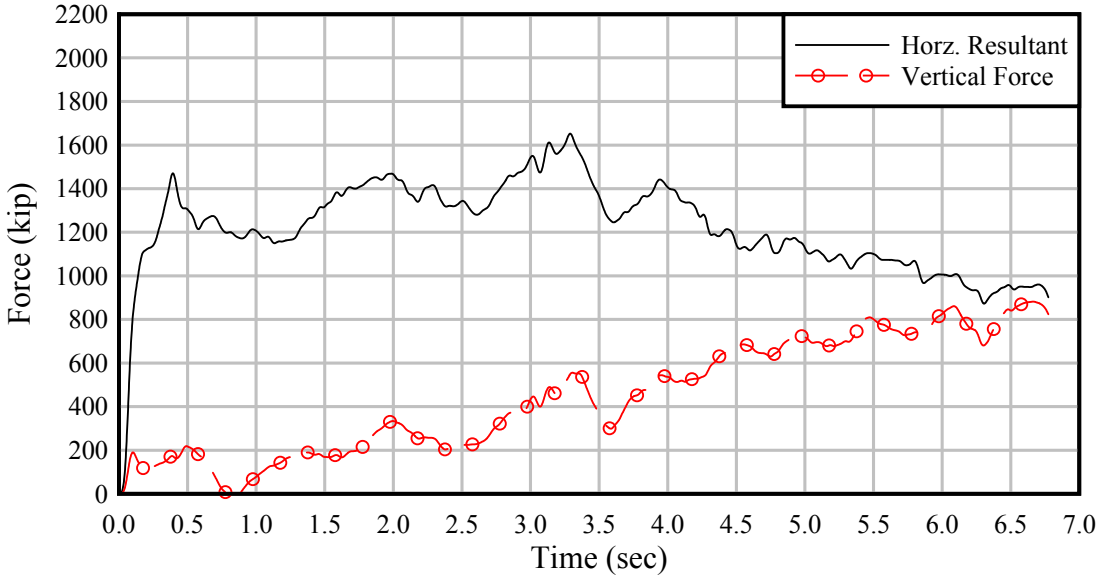

Figure A.53. 3x5 – 6 FPS – 10’ ∅ – Bow – Exterior

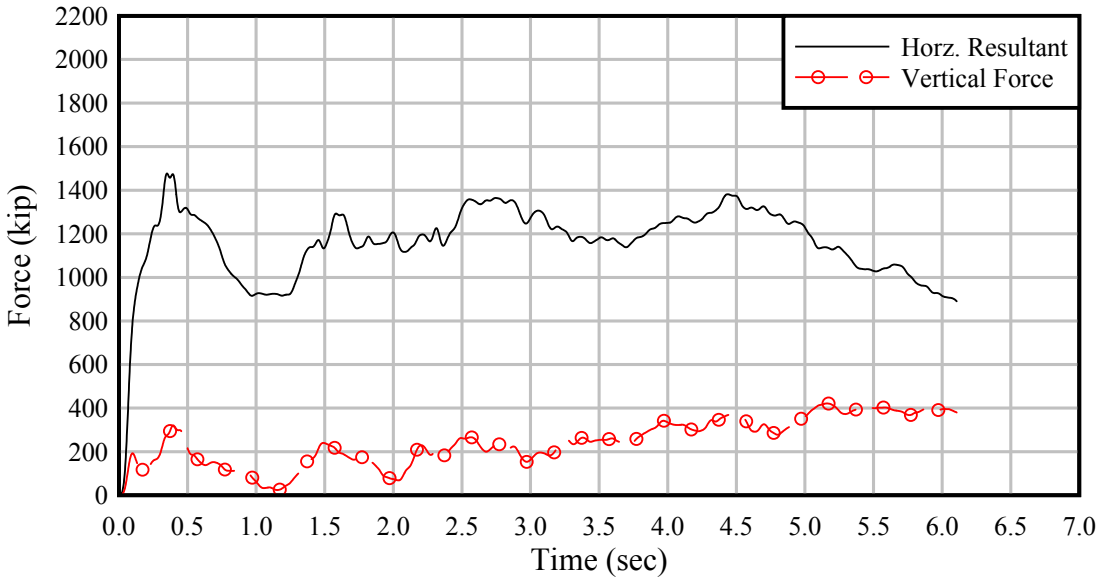

Figure A.54. 3x5 – 6 FPS – 10’ ∅ – Bow – Interior

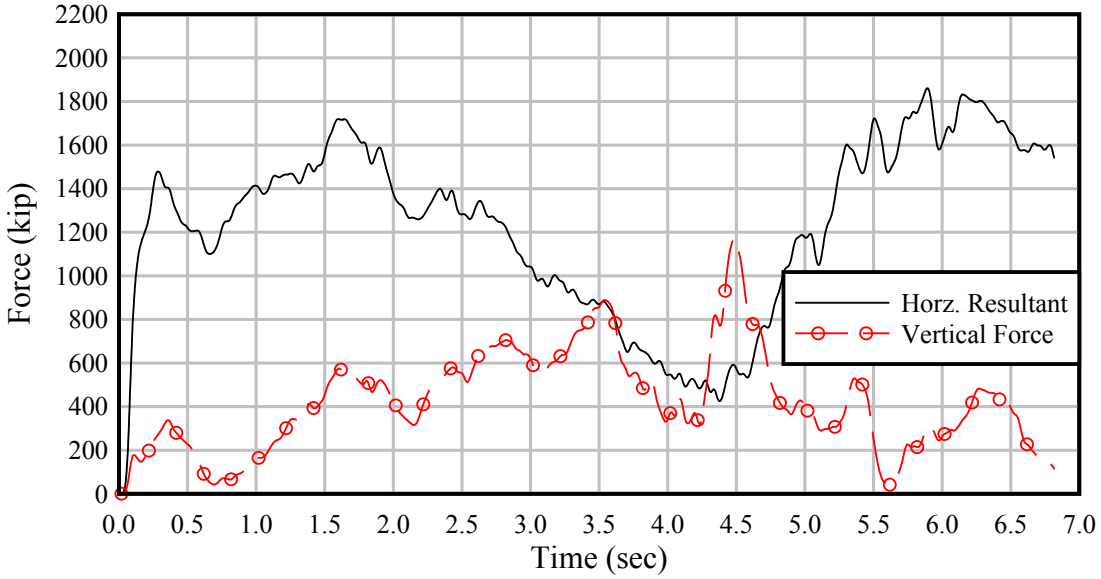

Figure A.55. 3x5 – 9 FPS – 10’ ∅ – Bow – Exterior

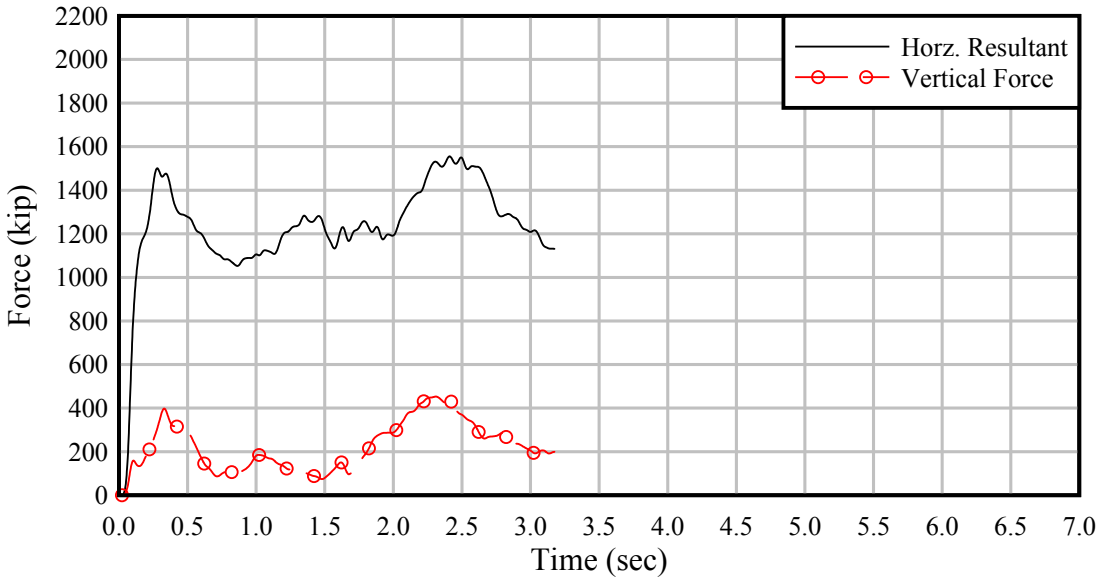

Figure A.56. 3x5 – 9 FPS – 10’ ∅ – Bow – Interior

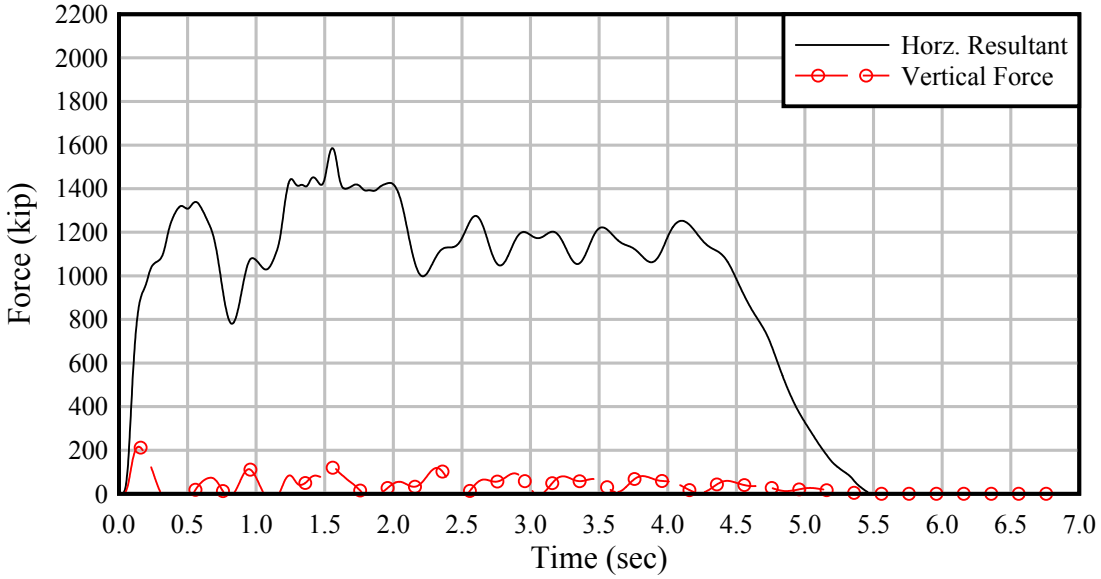

Figure A.57. 3x5 – 2 FPS – 35’ ∅ – Bow – Exterior

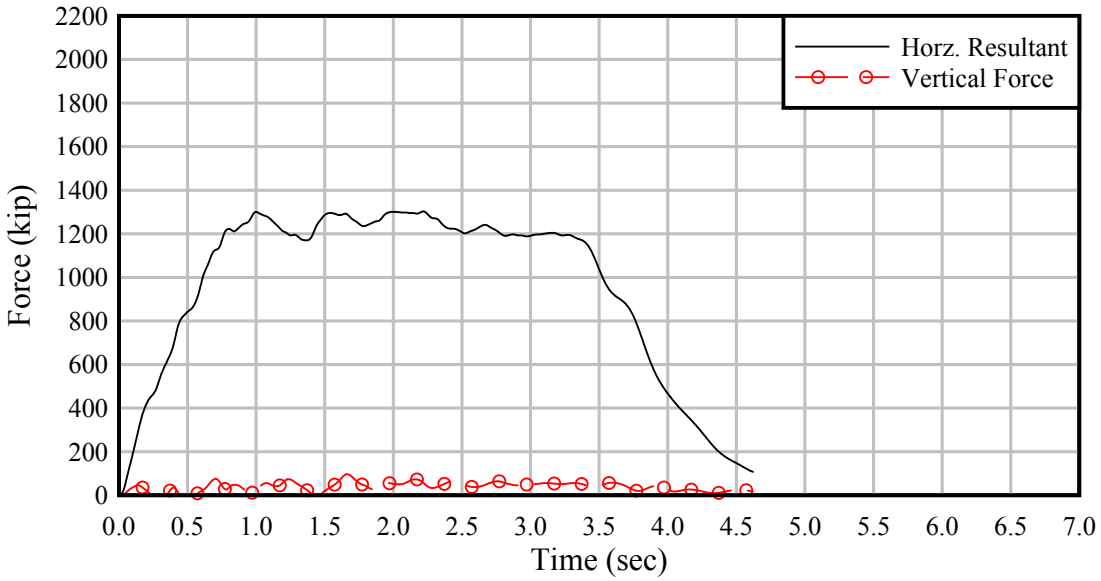

Figure A.58. 3x5 – 2 FPS – 35’ ∅ – Stern – Exterior

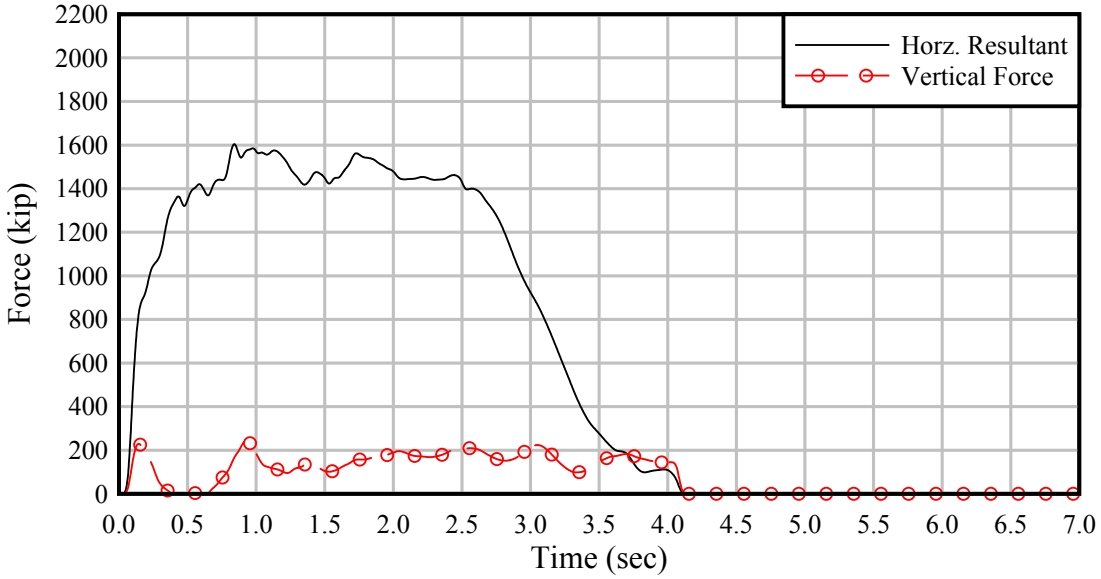

Figure A.59. 3x5 – 2 FPS – 35’ ∅ – Bow – Interior

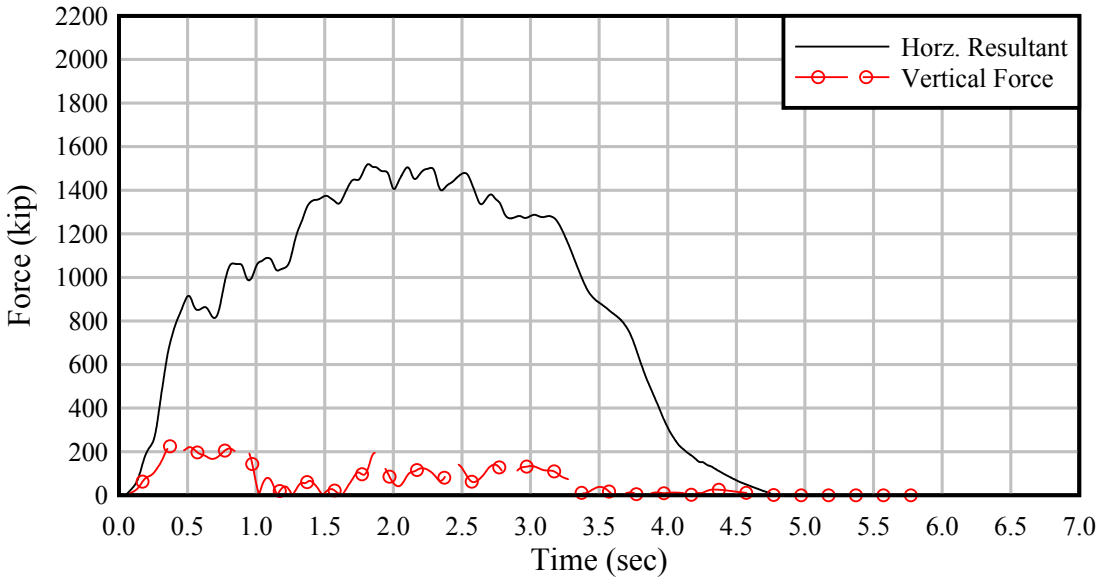

Figure A.60. 3x5 – 2 FPS – 35’ ∅ – Stern – Interior

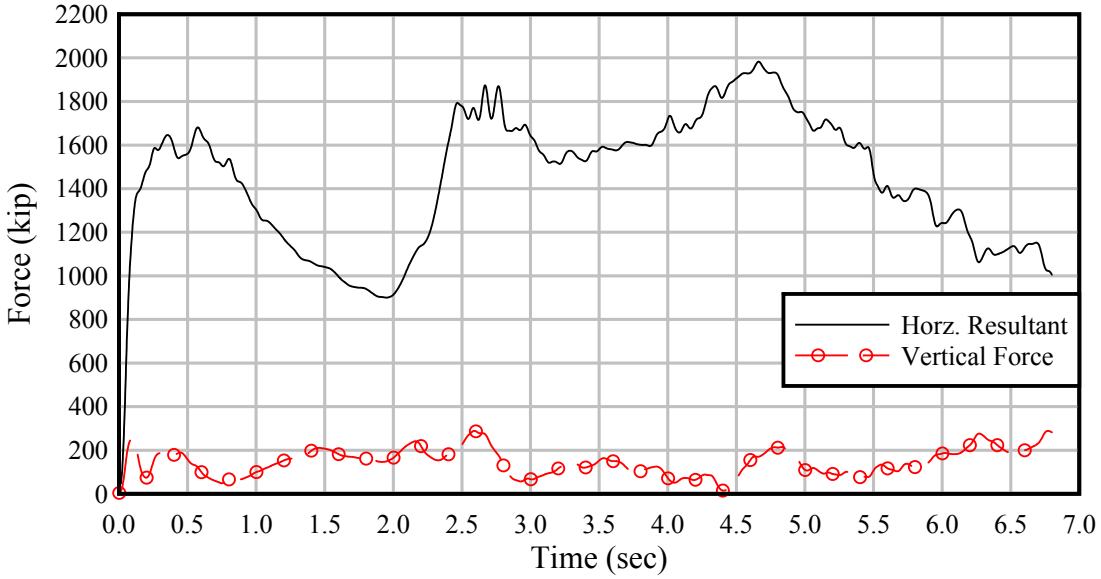

Figure A.61. 3x5 – 6 FPS – 35’ ∅ – Bow – Exterior

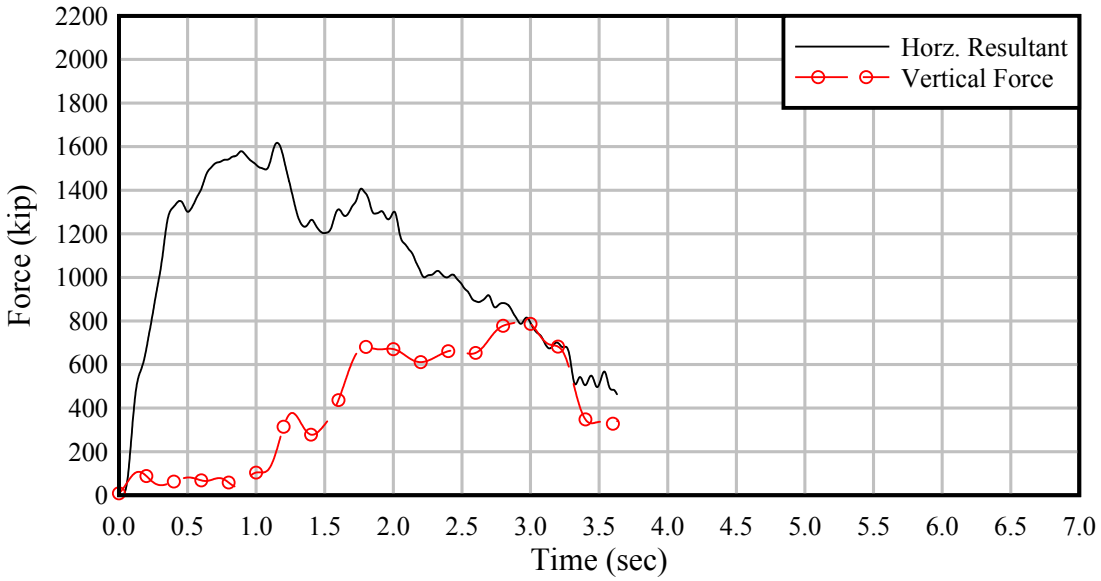

Figure A.62. 3x5 – 6 FPS – 35’ ∅ – Stern – Exterior

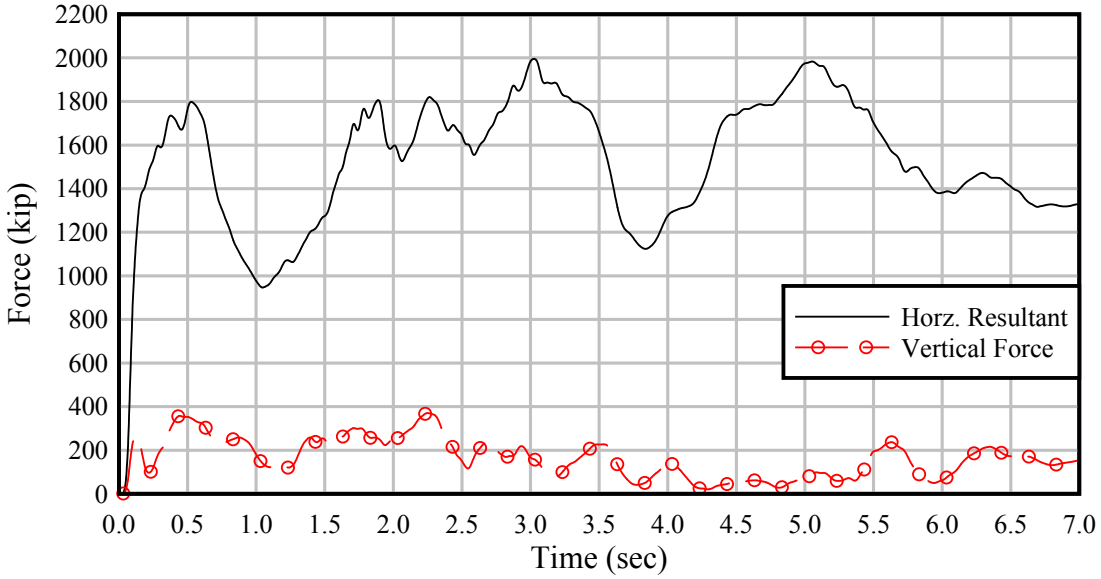

Figure A.63. 3x5 – 6 FPS – 35’ ∅ – Bow – Interior

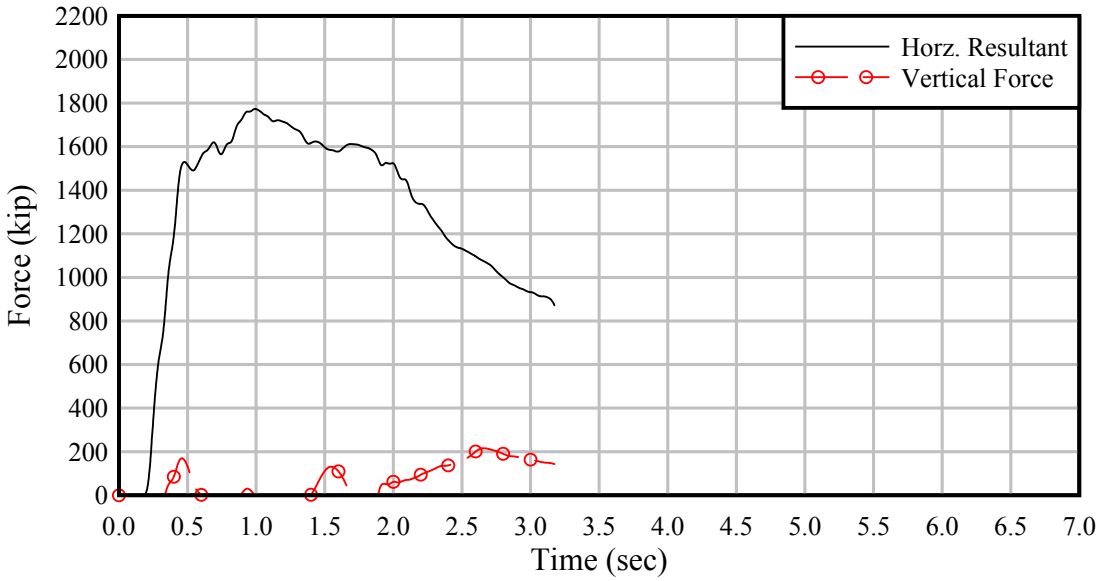

Figure A.64. 3x5 – 6 FPS – 35’ ∅ – Stern – Interior

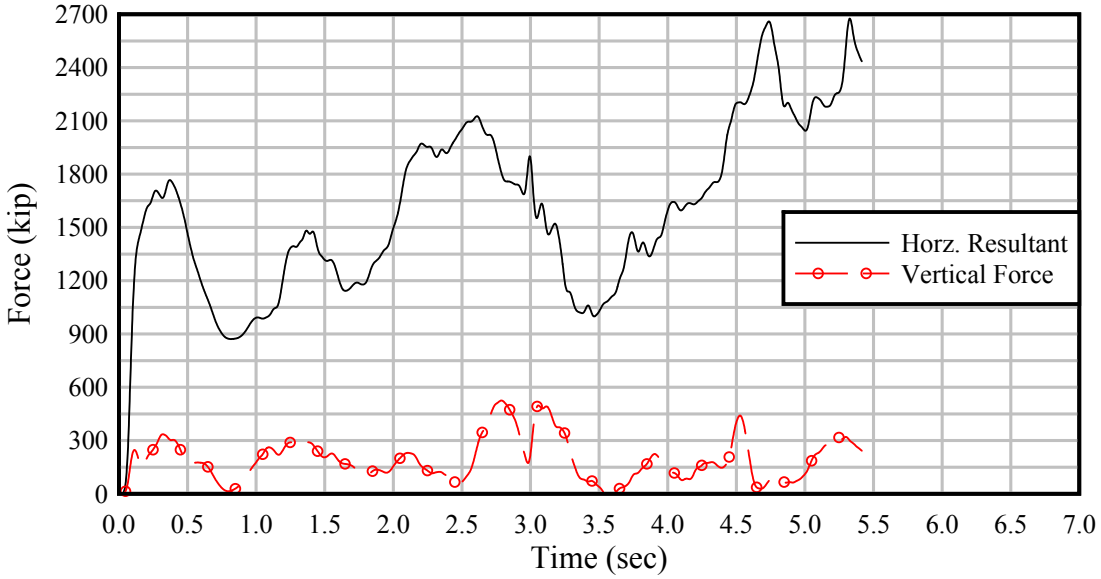

Figure A.65. 3x5 – 9 FPS – 35’ ∅ – Bow – Exterior
(Note: range of force scale unique to this time history)

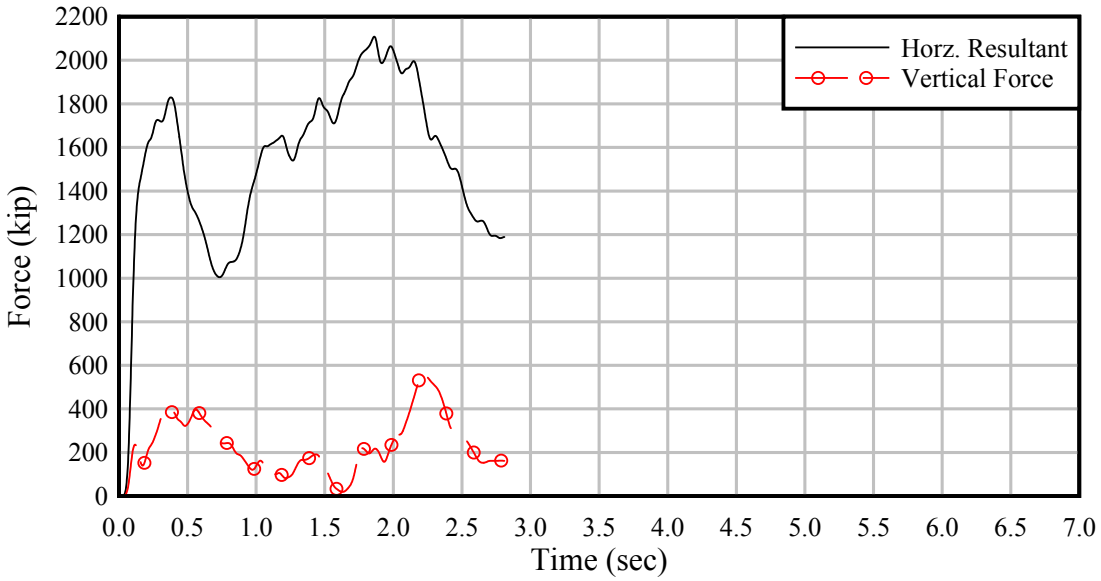

Figure A.66. 3x5 – 9 FPS – 35’ ∅ – Bow – Interior

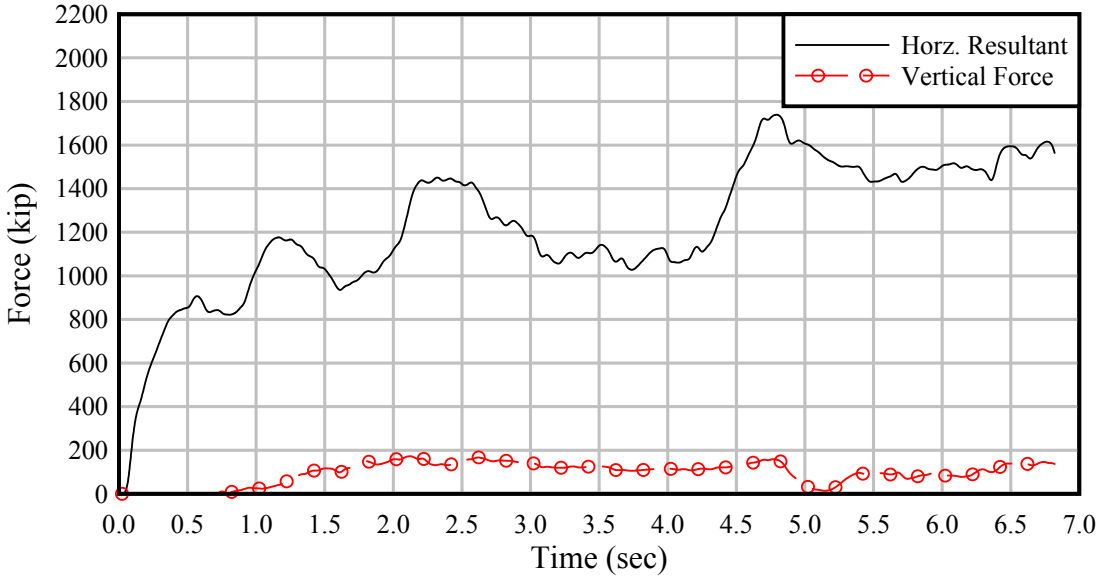

Figure A.67. 3x5 – 6 FPS – 2:1 Sloped-V – Bow – Exterior – 5 ft off center

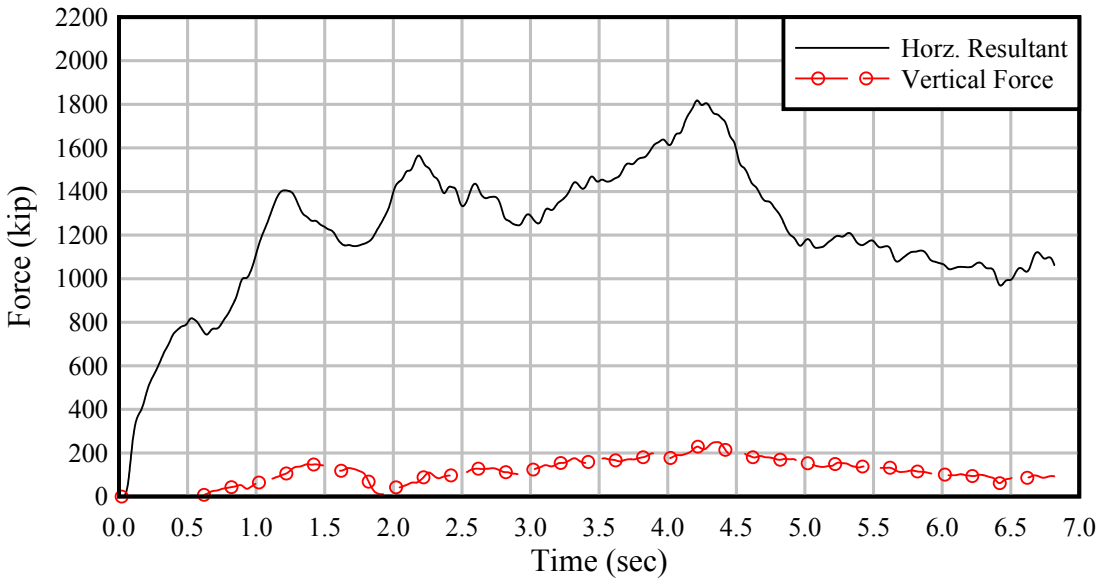

Figure A.68. 3x5 – 6 FPS – 2:1 Sloped-V – Bow – Exterior – 10 ft off center

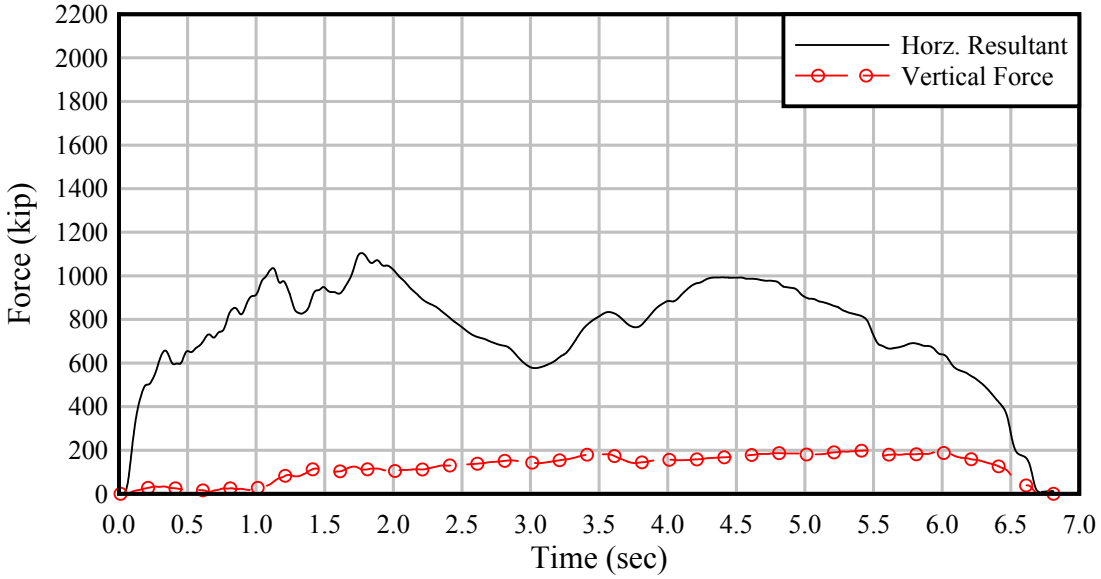

Figure A.69. 3x5 – 6 FPS – 2:1 Sloped-V – Bow – Exterior – 15 ft off center

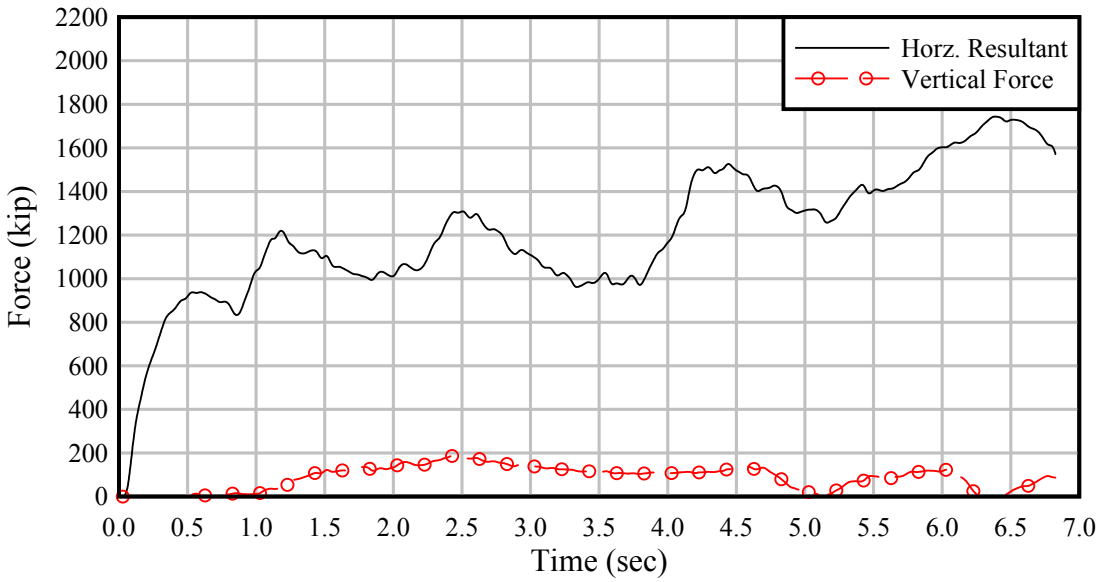

Figure A.70. 3x5 – 6 FPS – 2:1 Sloped-V – Bow – Exterior – 10° impact angle

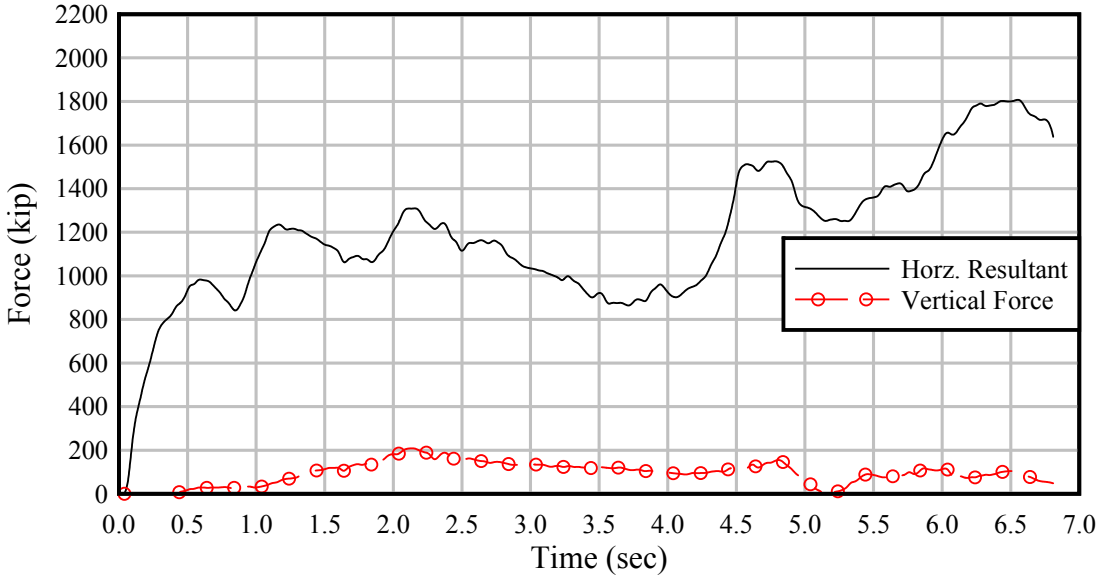

Figure A.71. 3x5 – 6 FPS – 2:1 Sloped-V – Bow – Exterior – 20° impact angle

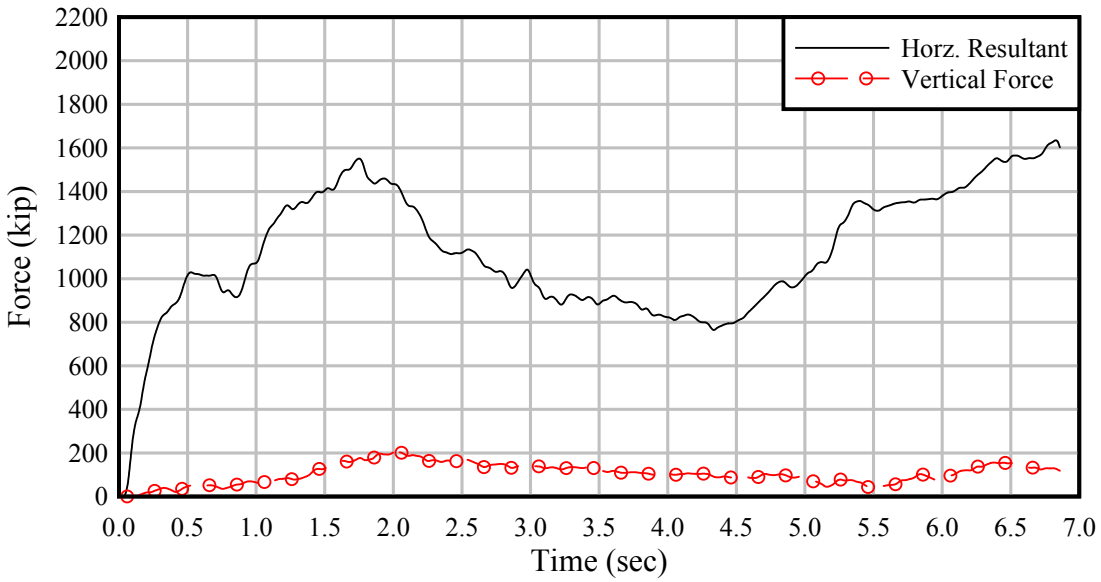

Figure A.72. 3x5 – 6 FPS – 2:1 Sloped-V – Bow – Exterior – 30° impact angle

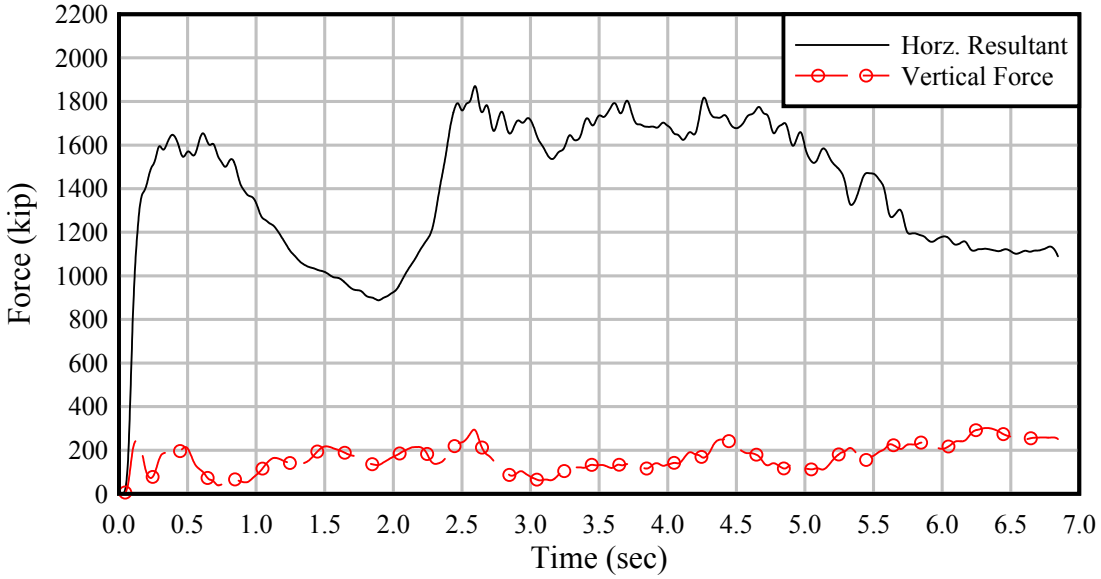

Figure A.73. 3x5 – 6 FPS – 35’ ∅ – Bow – Exterior – 30° impact angle

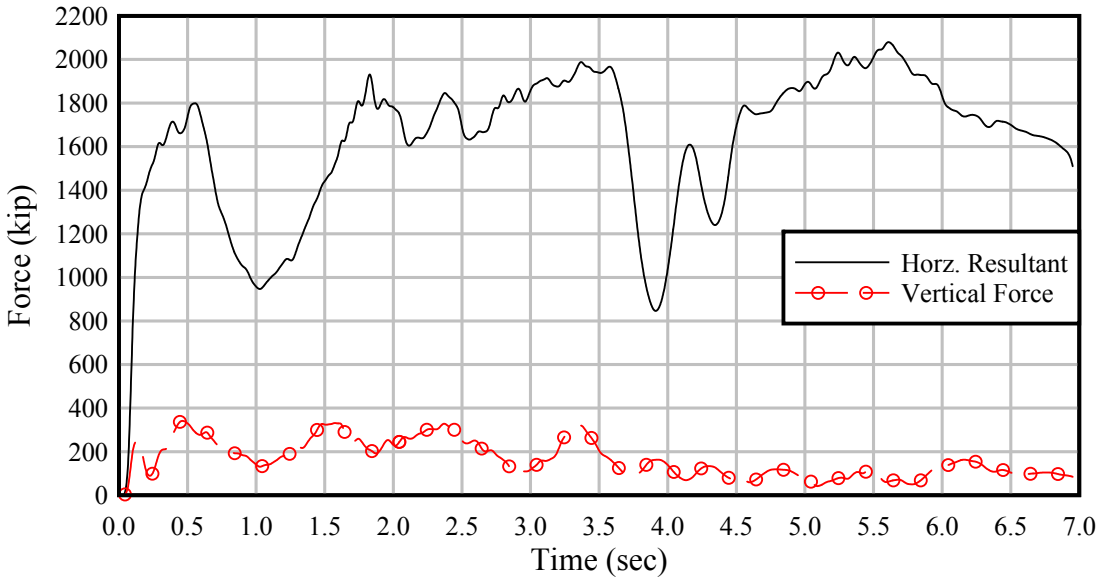

Figure A.74. 3x5 – 6 FPS – 35’ ∅ – Bow – Interior – 30° impact angle

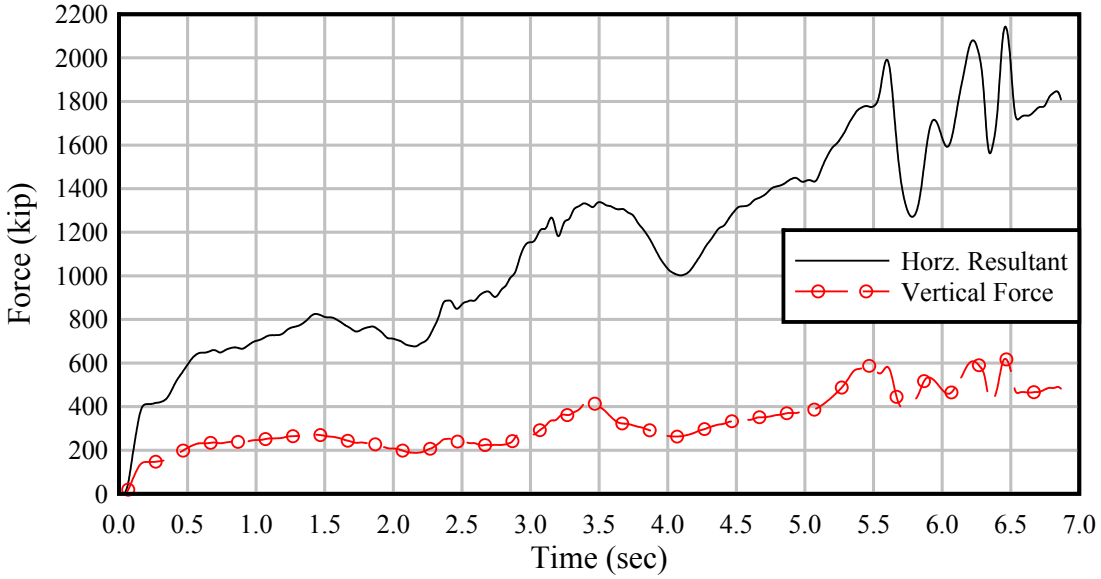

Figure A.75. 3x5 – 6 FPS – 1:1 Sloped-V – Bow – Exterior

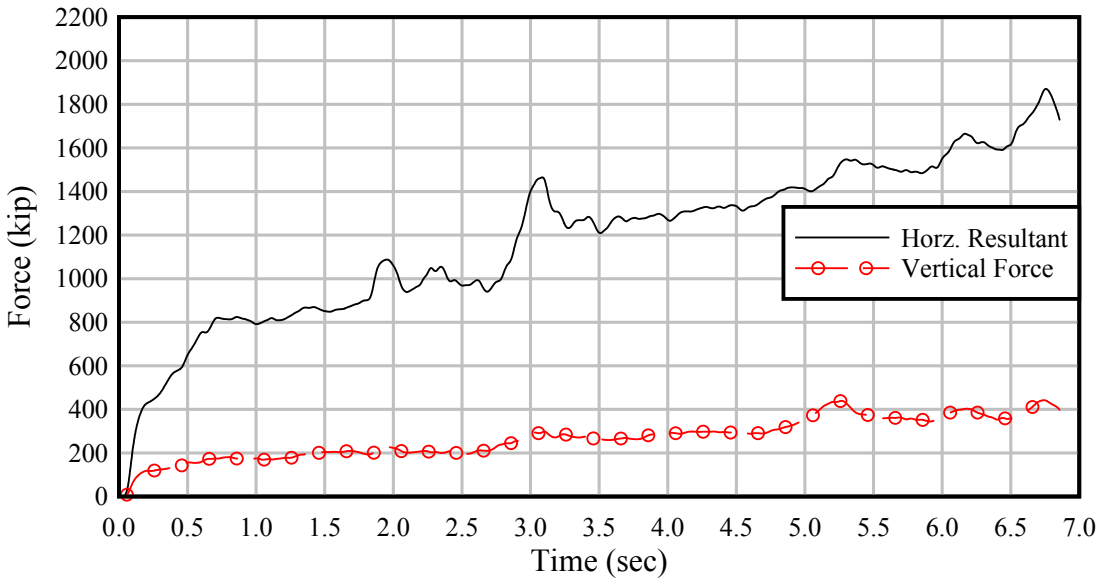

Figure A.76. 3x5 – 6 FPS – 1:1 Sloped-V – Bow – Exterior – 30° impact angle

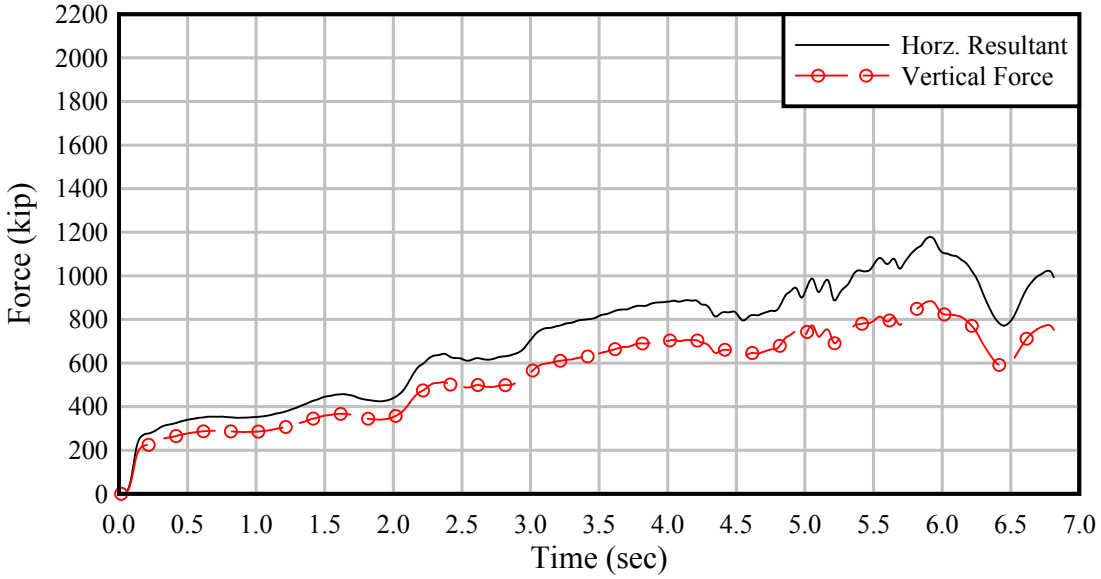

Figure A.77. 3x5 – 6 FPS – 1:2 Sloped-V – Bow – Exterior

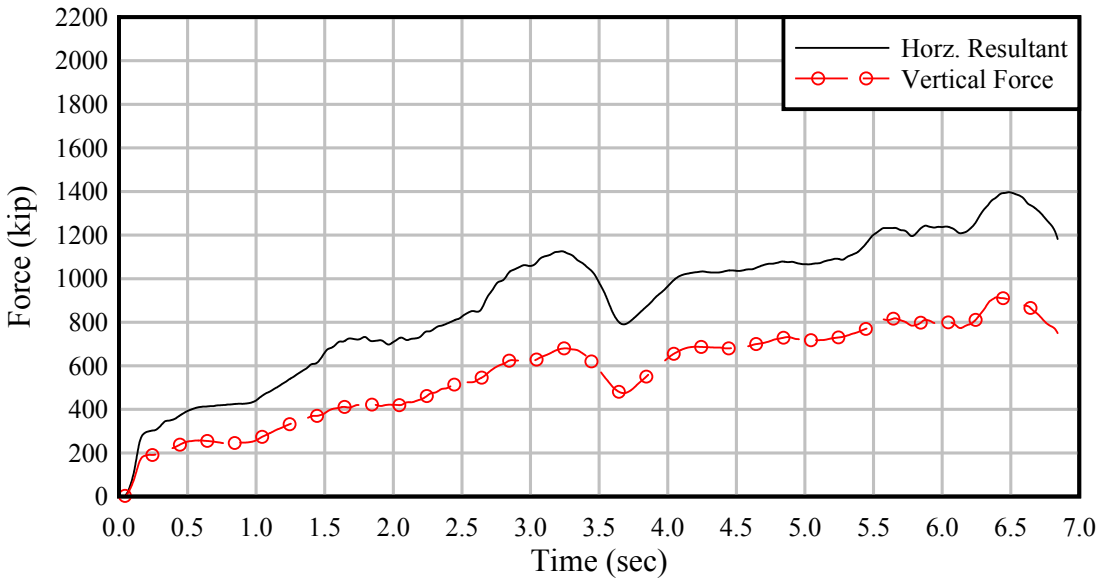

Figure A.78. 3x5 – 6 FPS – 1:2 Sloped-V – Bow – Exterior – 30° impact angle

APPENDIX B
IMPACT FORCE-TIME HISTORIES FROM FLEXIBLE TIMBER GUIDE WALL SIMULATIONS

Individual force-time histories for all flexible timber guide wall impact simulations conducted in this study are plotted on the following pages. Each plot includes separate traces for the *horizontal component of impact force that is normal to (perpendicular to) the impacted surface of the structure* (either the end flare, or the primary wall), and the vertical component of impact force. All impact forces presented herein correspond to the contact force-time histories between the high-resolution impacting (deformable) barge model and the wall model. Also note that all forces presented in this appendix have been low-pass filtered using the procedure described earlier in this report.

The nomenclature used in each figure caption, to identify the impact condition that is plotted, is of the form:

NSxNR – SPEED FPS – ANGLE° – SOIL – LOC

where:

NS	=	number of barge strings (barge columns) in the flotilla
NR	=	number of barge rows in the flotilla
SPEED	=	impact speed in ft/sec. (FPS)
ANGLE°	=	impact angle (in degrees) relative to the impacted surface: WALL° for impacts on the primary wall FLARE° for impacts on the end flare
SOIL	=	soil condition used in model: SSx1: baseline soil stiffness (SS) (multiplied ('x') by 1) SSx2: doubled soil stiffness; baseline soil stiffness (SS) multiplied by 2
LOC	=	impact location on the structure (see Chapter 6 for additional details): Flare: Impact on flare at 4th pile line from the flare-to-wall connection Wall: Impact on wall at 1st pile line from the flare-to-wall connection

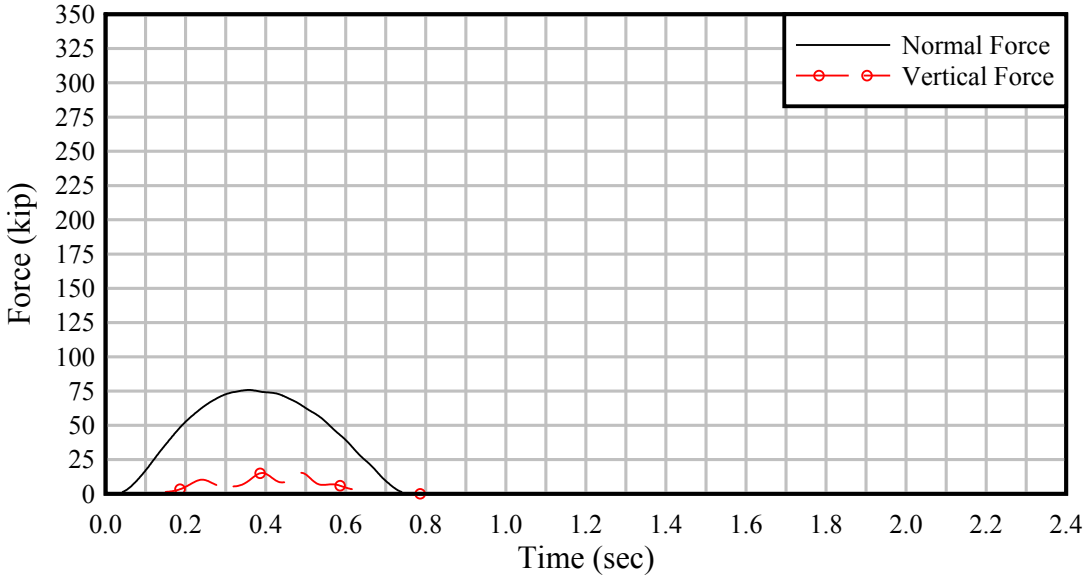

Figure B.1. 1x1 – 2 FPS – 25° – SSx1 – Flare

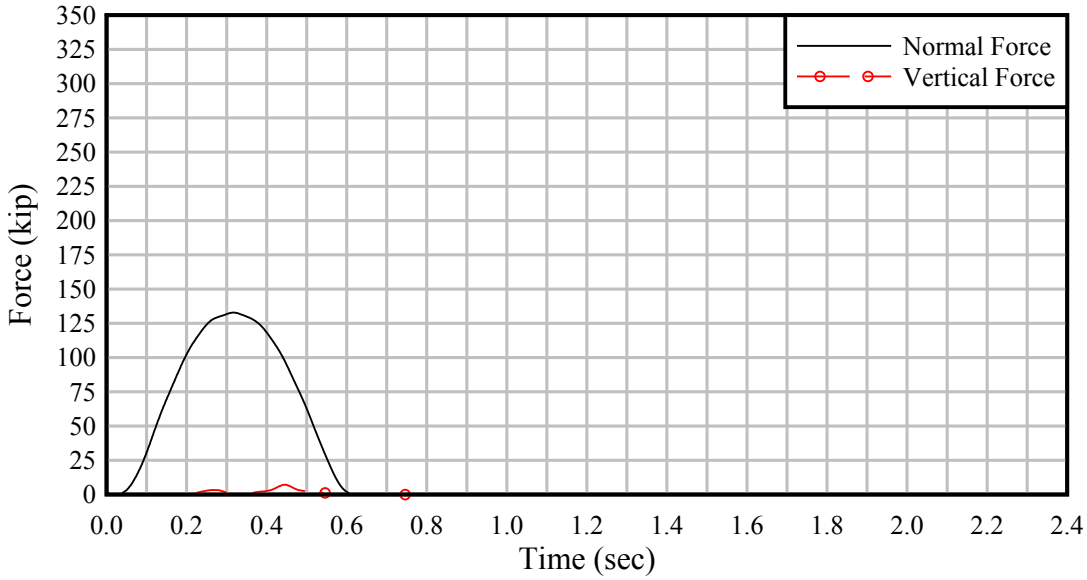

Figure B.2. 1x1 – 4 FPS – 15° – SSx1 – Wall

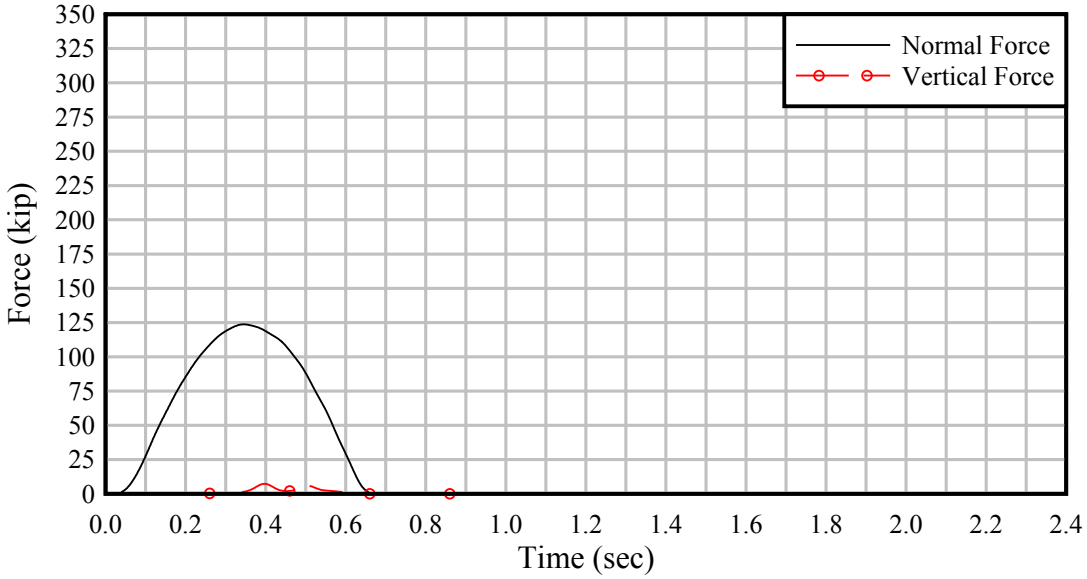

Figure B.3. 1x1 – 4 FPS – 15° – SSx2 – Flare

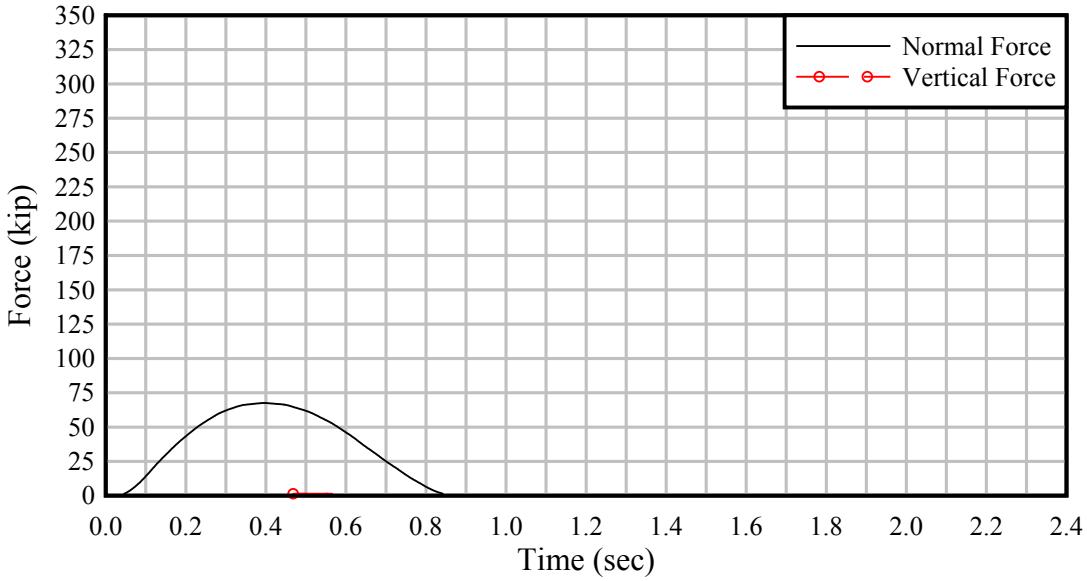

Figure B.4. 1x2 – 2 FPS – 15° – SSx1 – Flare

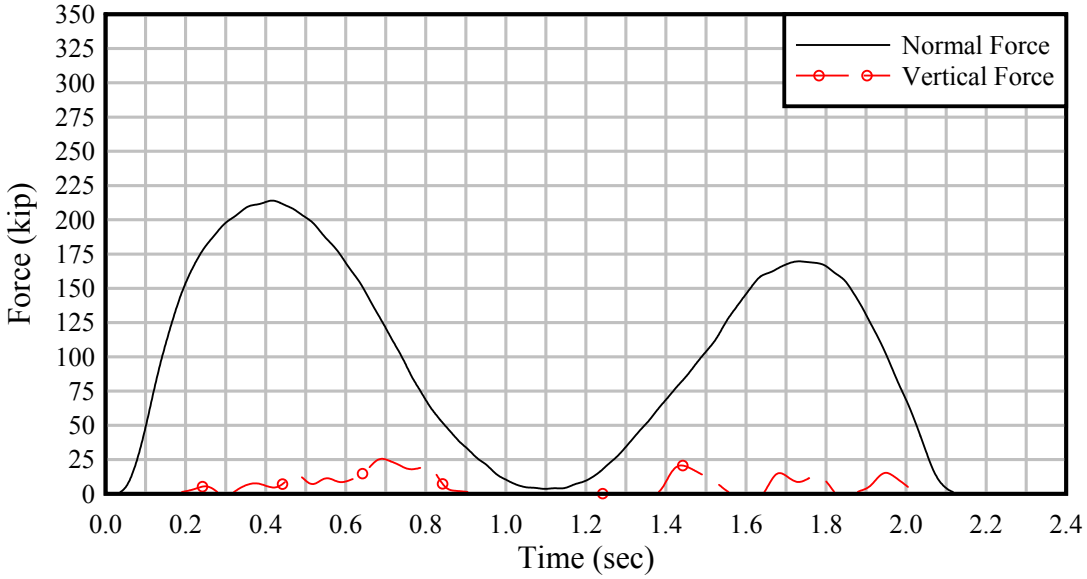

Figure B.5. 1x2 – 4 FPS – 25° – SSx2 – Flare

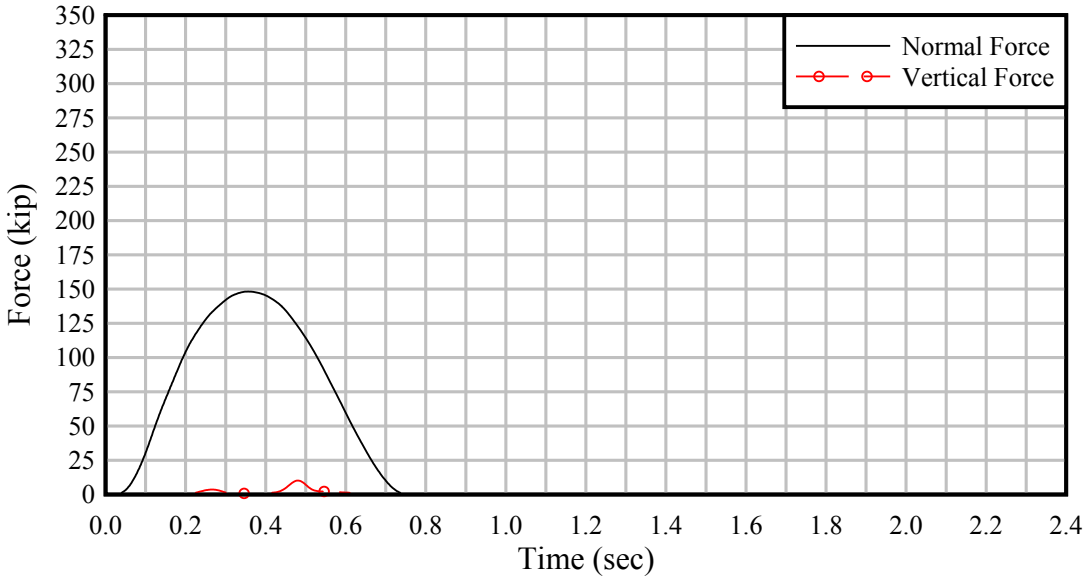

Figure B.6. 1x2 – 4 FPS – 15° – SSx1 – Wall

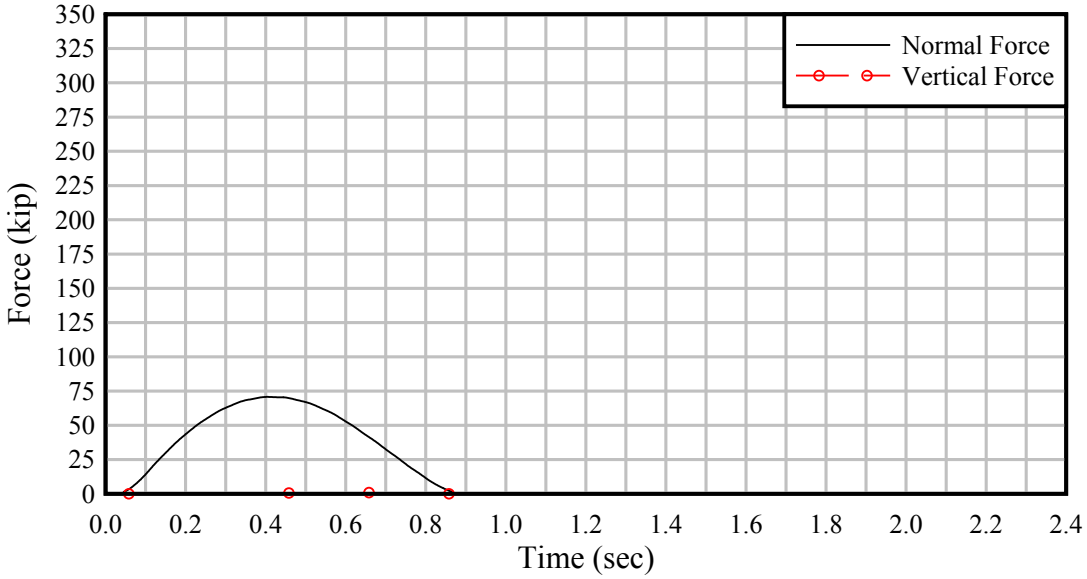

Figure B.7. 1x3 – 2 FPS – 15° – SSx1 – Flare

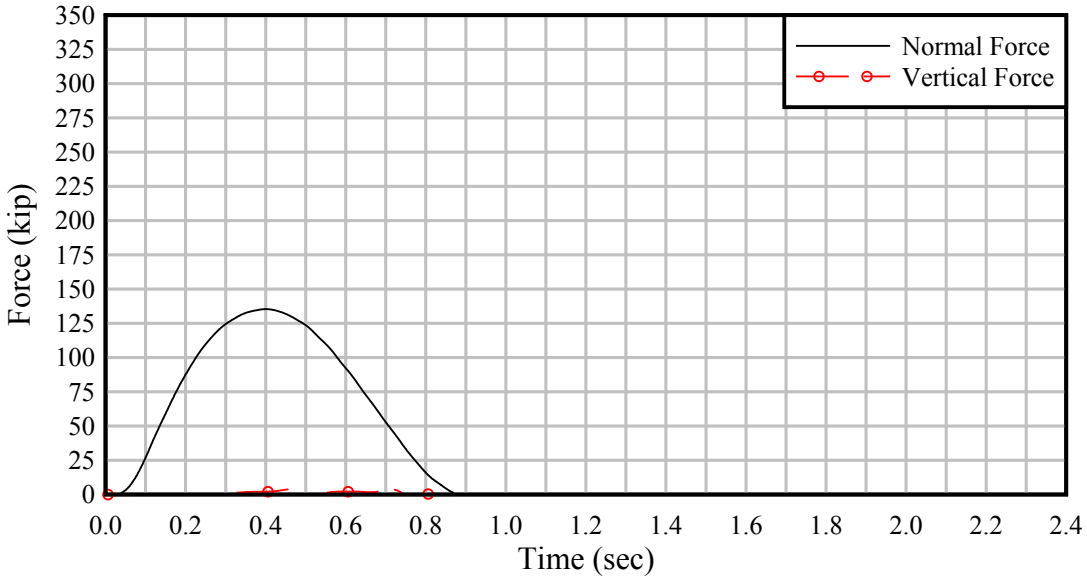

Figure B.8. 1x3 – 2 FPS – 25° – SSx2 – Flare

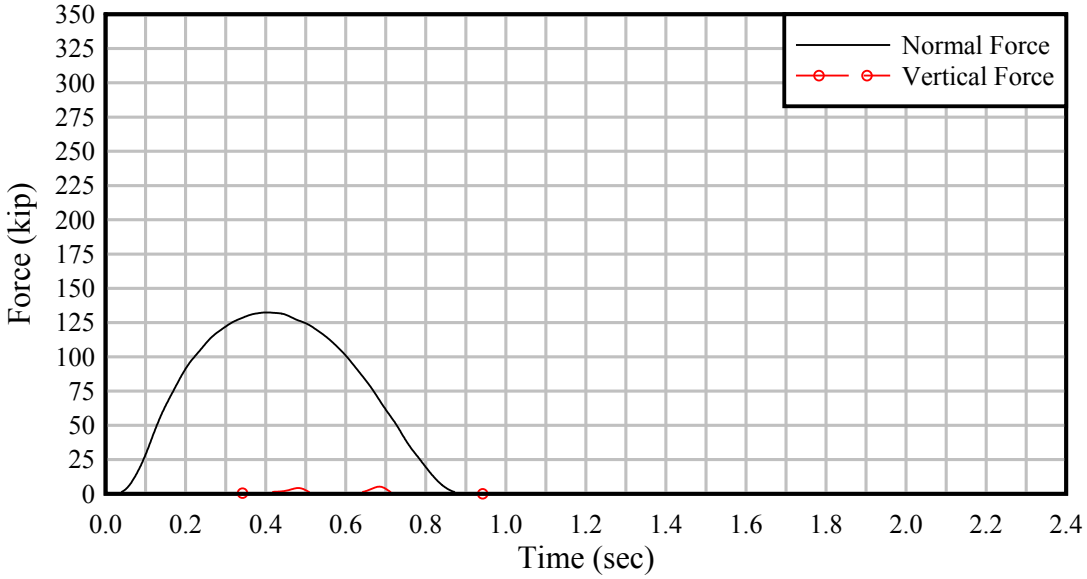

Figure B.9. 1x3 – 4 FPS – 15° – SSx1 – Wall

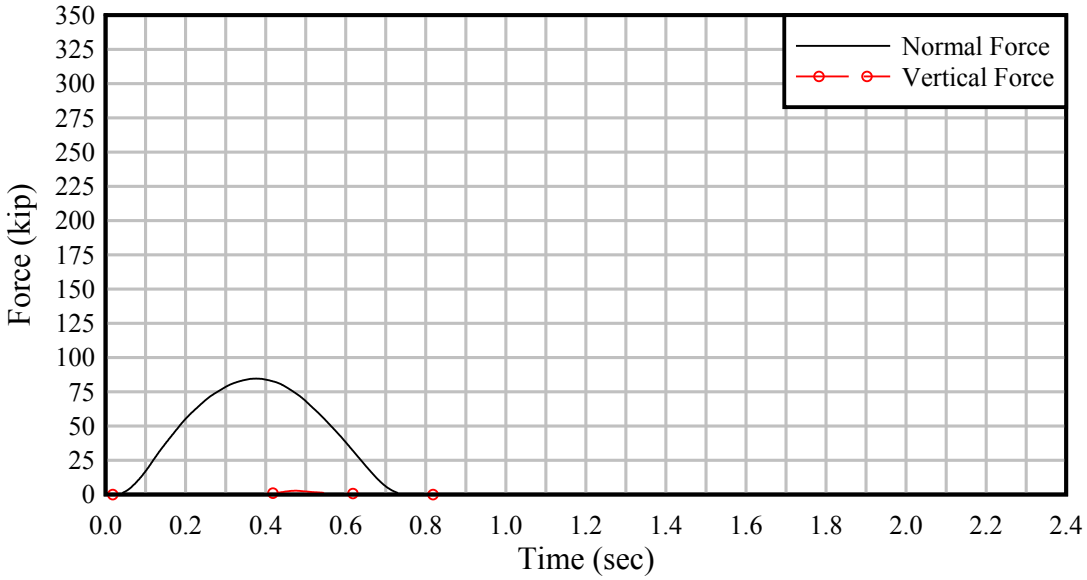

Figure B.10. 1x3 – 2 FPS – 15° – SSx2 – Wall

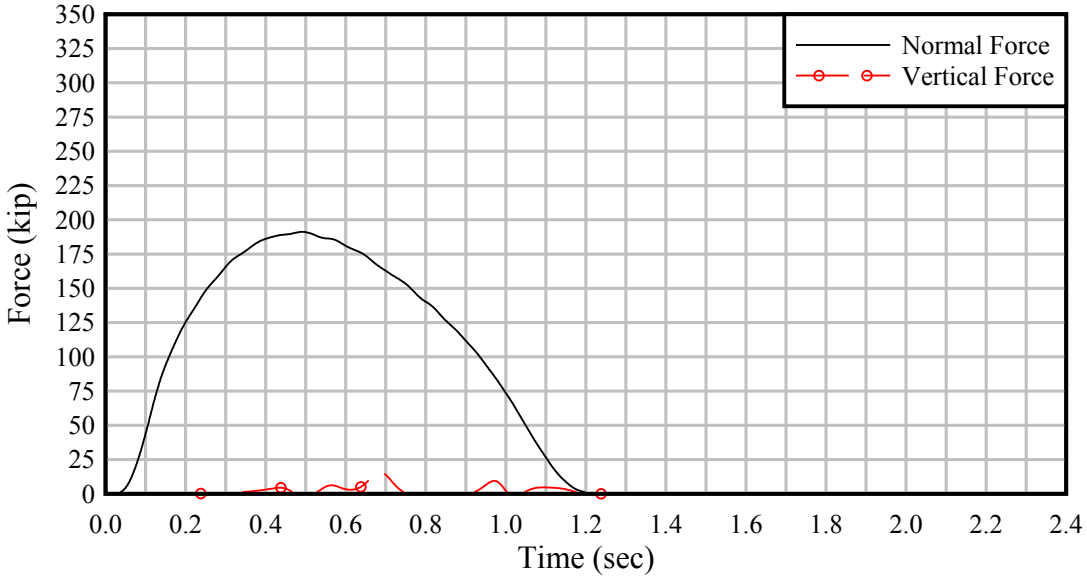

Figure B.11. 1x3 – 4 FPS – 25° – SSx1 – Flare

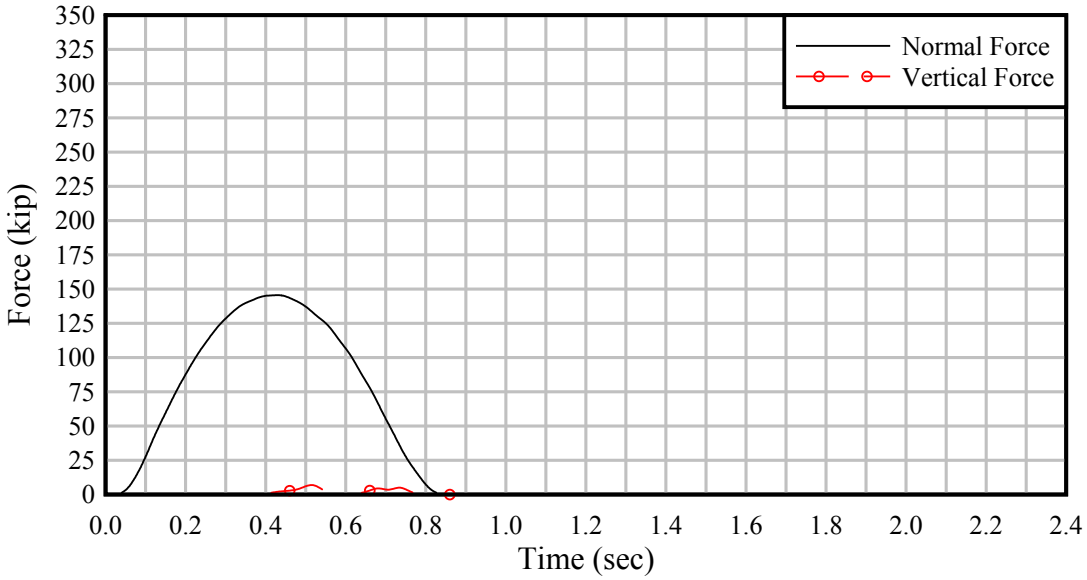

Figure B.12. 1x3 – 4 FPS – 15° – SSx2 – Flare

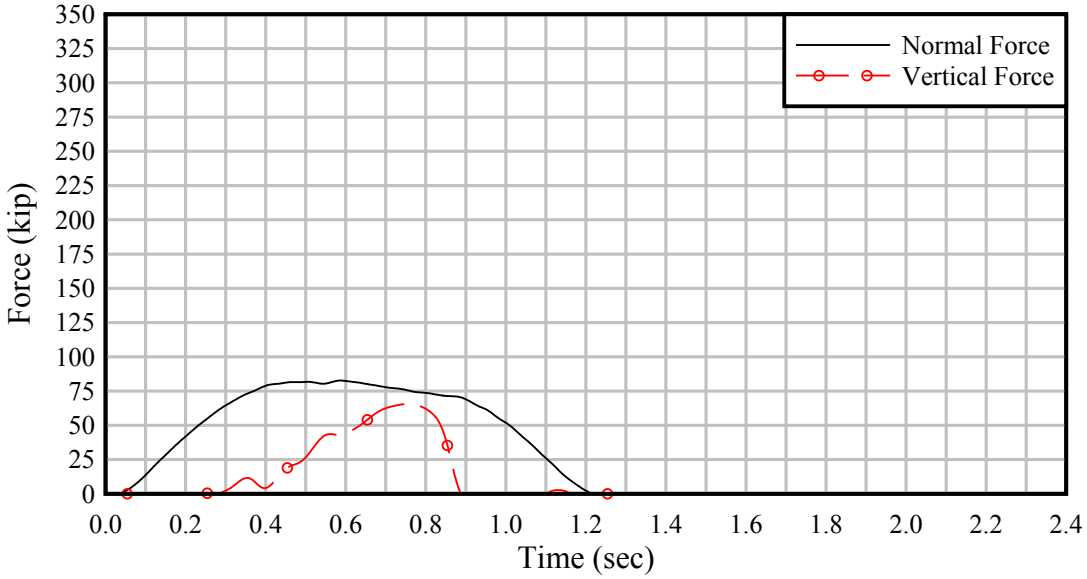

Figure B.13. 2x1 – 2 FPS – 15° – SSx1 – Flare

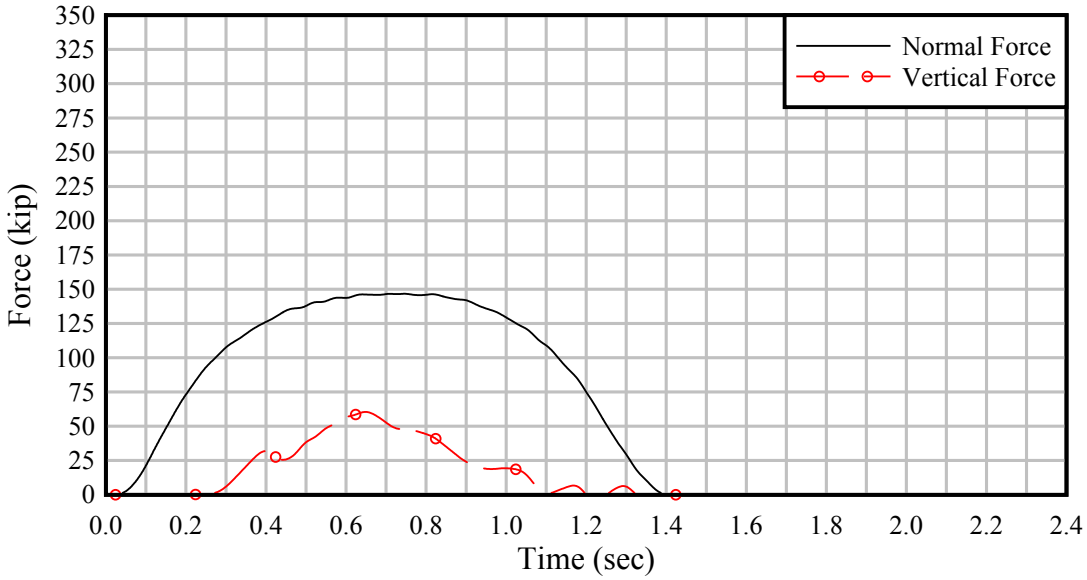

Figure B.14. 2x1 – 2 FPS – 25° – SSx1 – Flare

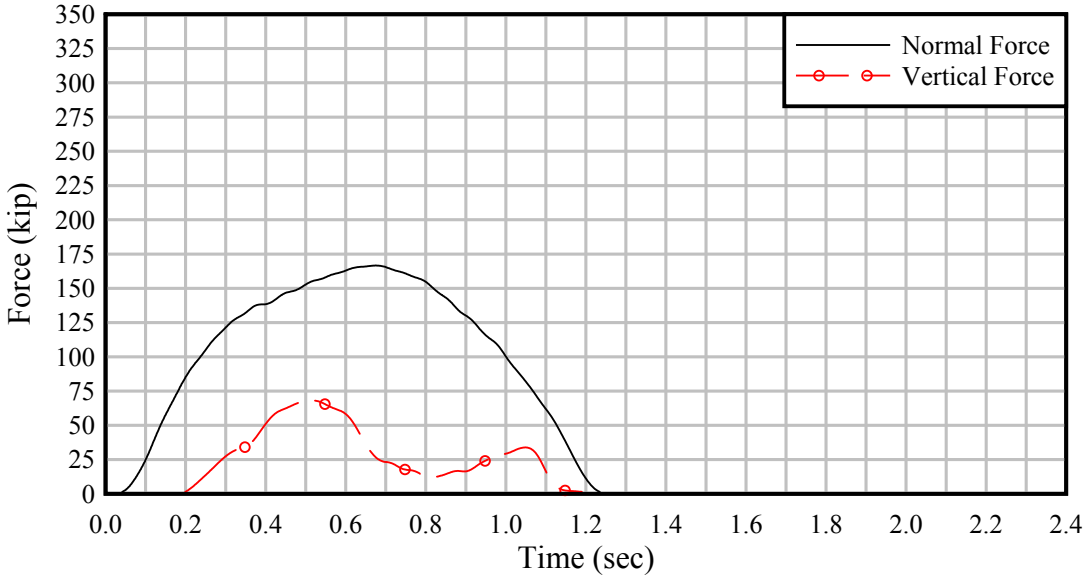

Figure B.15. 2x1 – 4 FPS – 15° – SSx1 – Wall

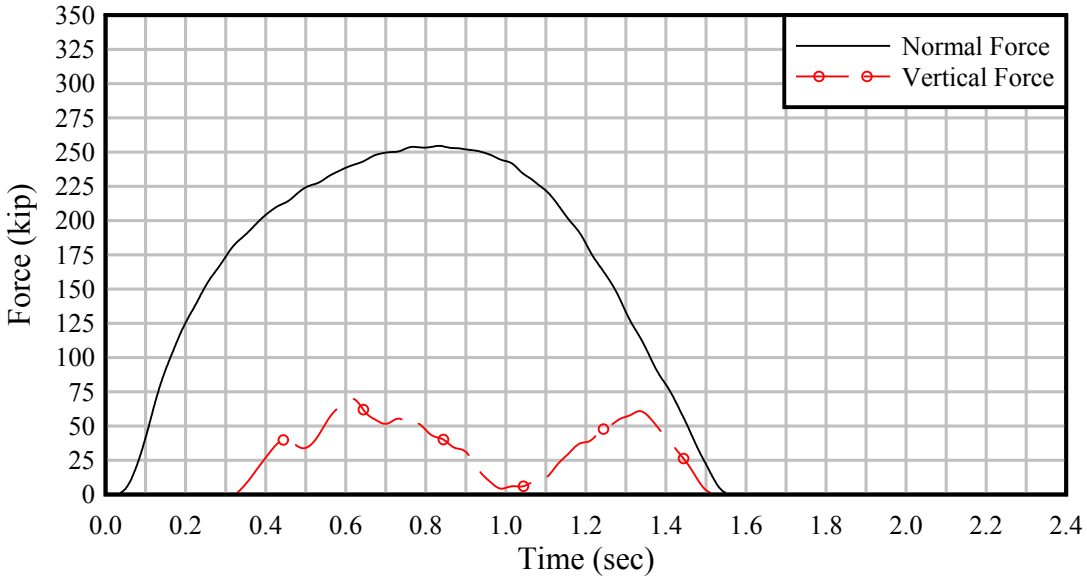

Figure B.16. 2x1 – 4 FPS – 25° – SSx1 – Flare

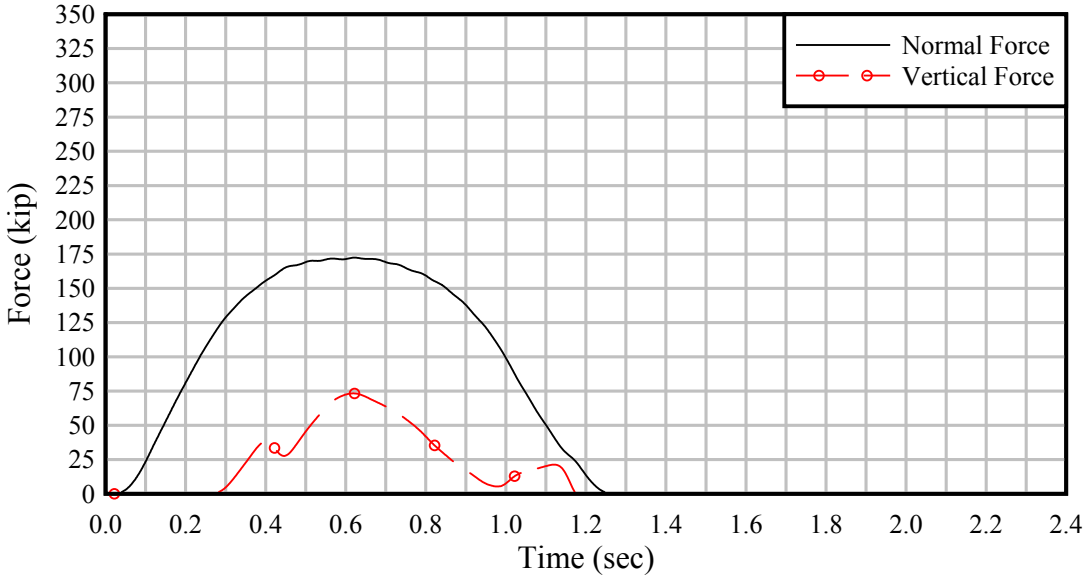

Figure B.17. 2x1 – 2 FPS – 25° – SSx2 – Flare

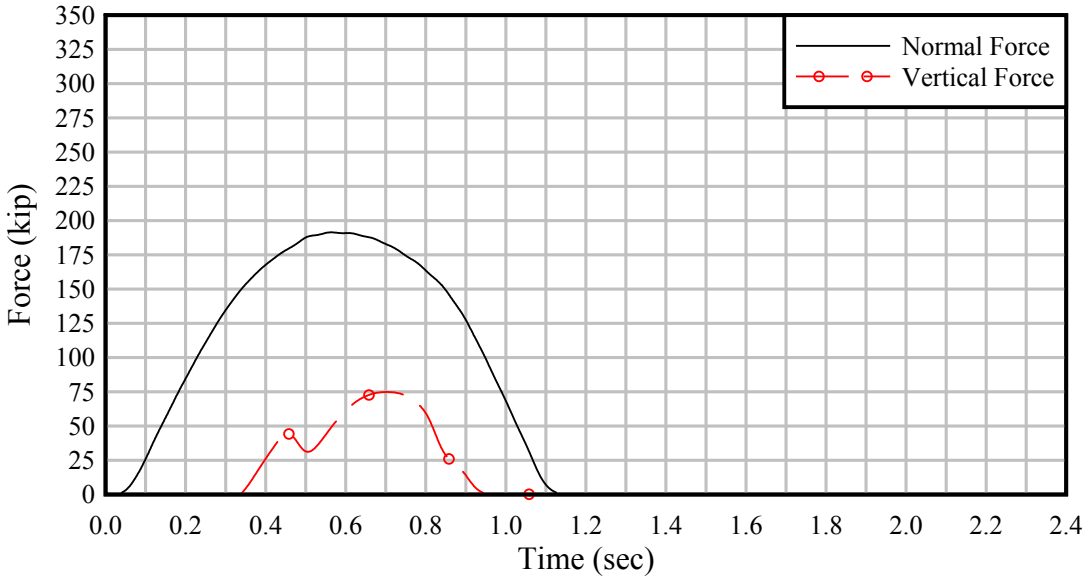

Figure B.18. 2x1 – 4 FPS – 15° – SSx2 – Flare

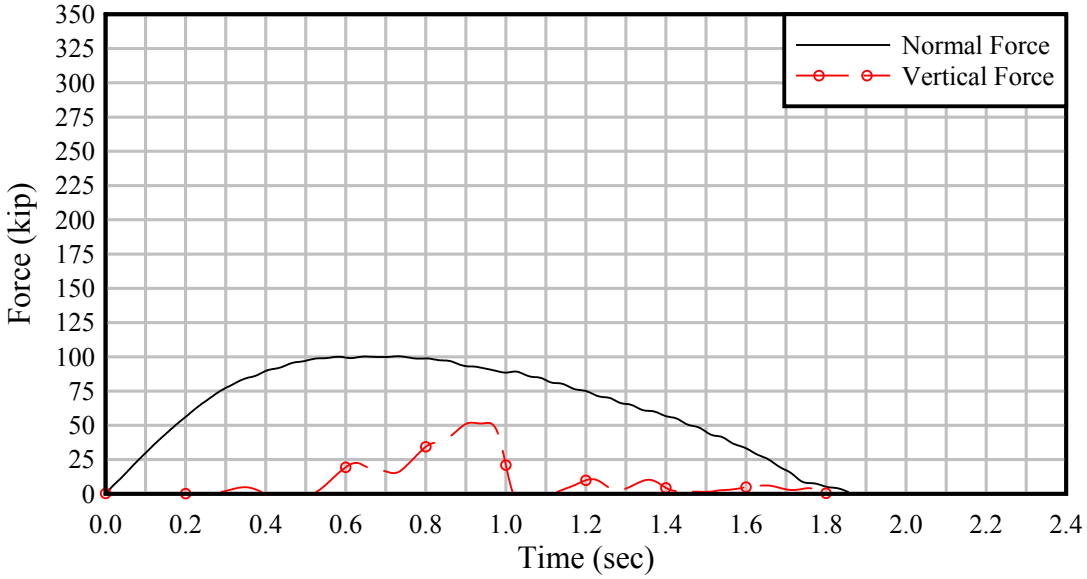

Figure B.19. 2x2 – 2 FPS – 15° – SSx1 – Flare

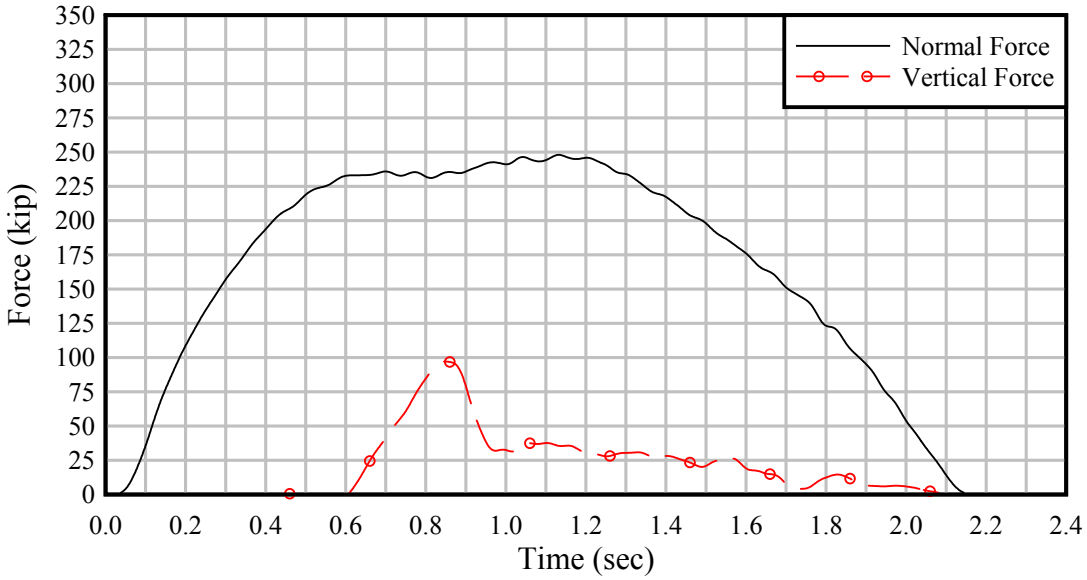

Figure B.20. 2x2 – 6 FPS – 15° – SSx1 – Flare

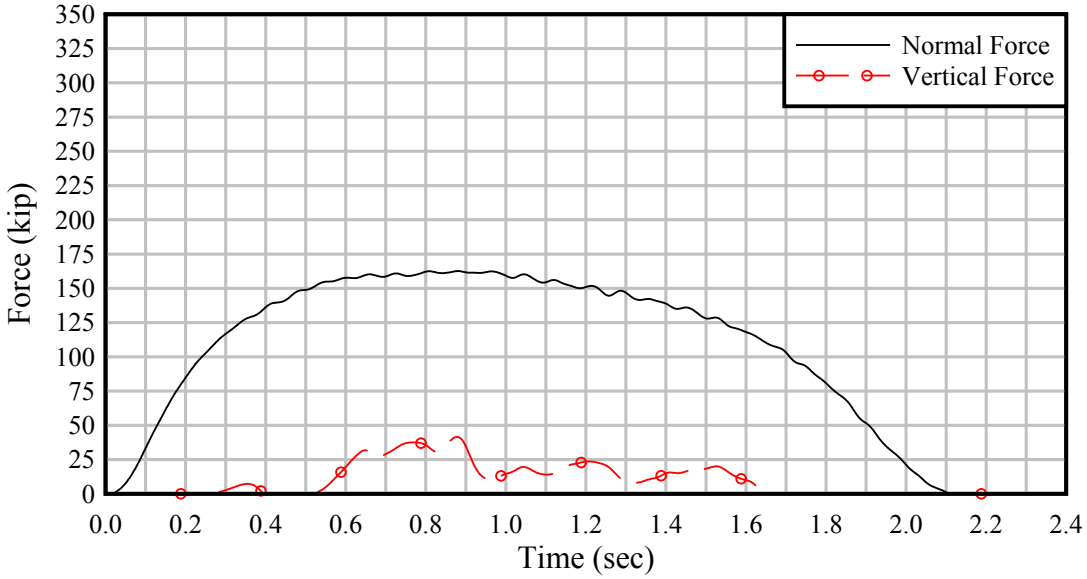

Figure B.21. 2x2 – 2 FPS – 25° – SSx1 – Flare

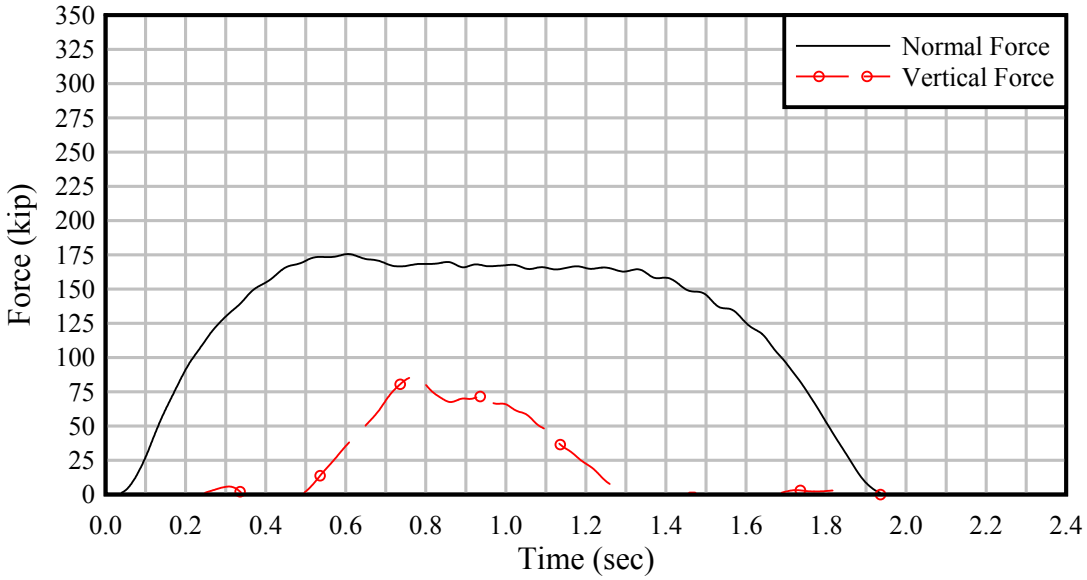

Figure B.22. 2x2 – 4 FPS – 15° – SSx1 – Wall

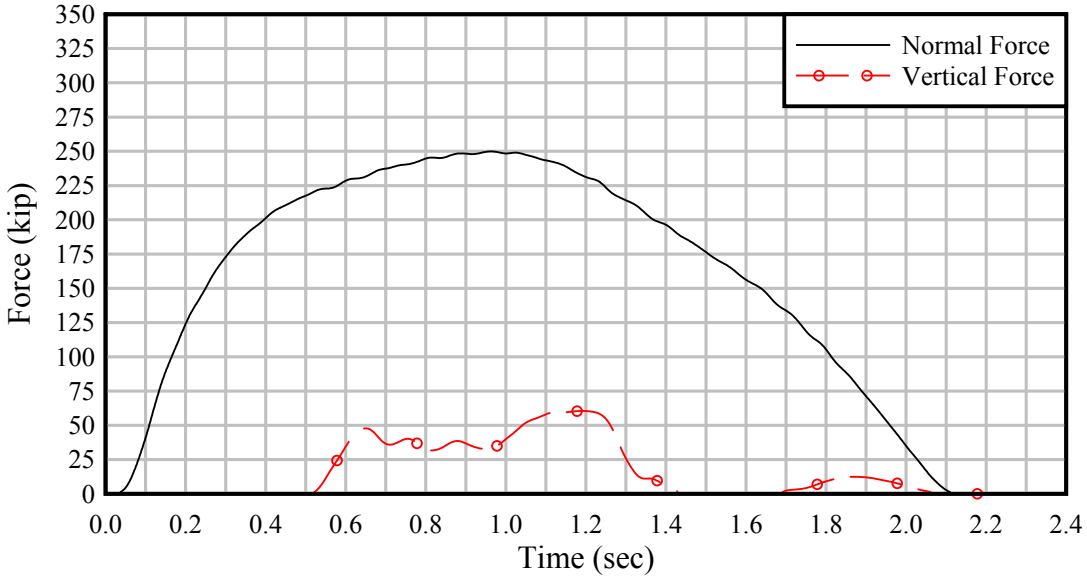

Figure B.23. 2x2 – 6 FPS – 15° – SSx1 – Wall

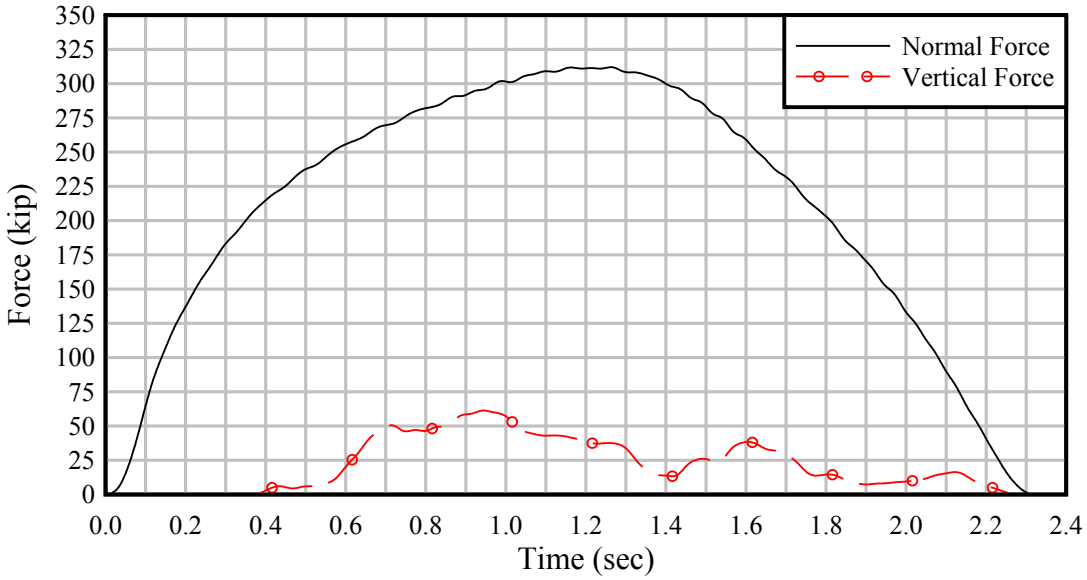

Figure B.24. 2x2 – 4 FPS – 25° – SSx1 – Flare

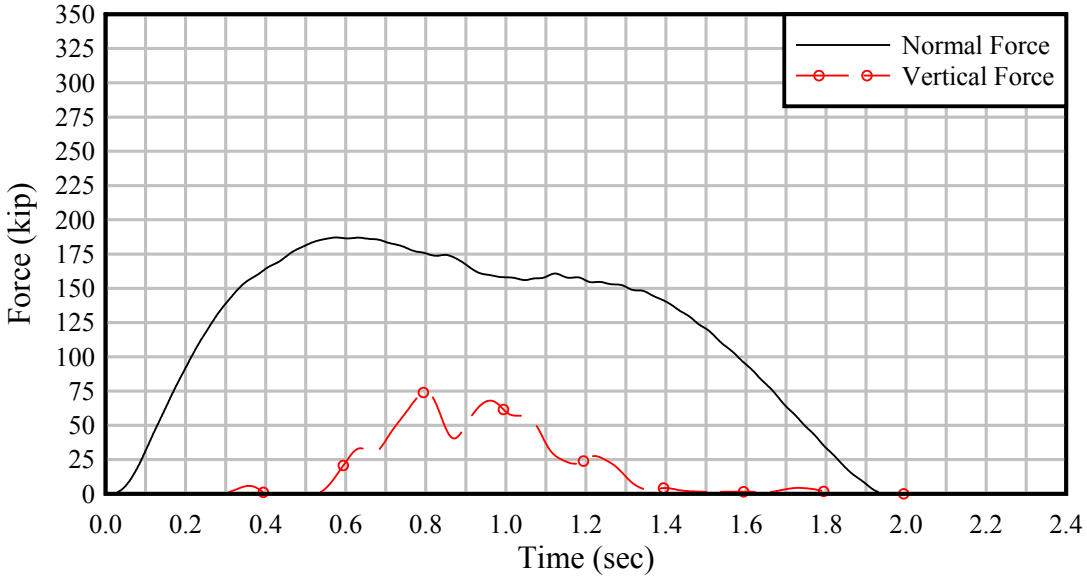

Figure B.25. 2x2 – 2 FPS – 25° – SSx2 – Flare

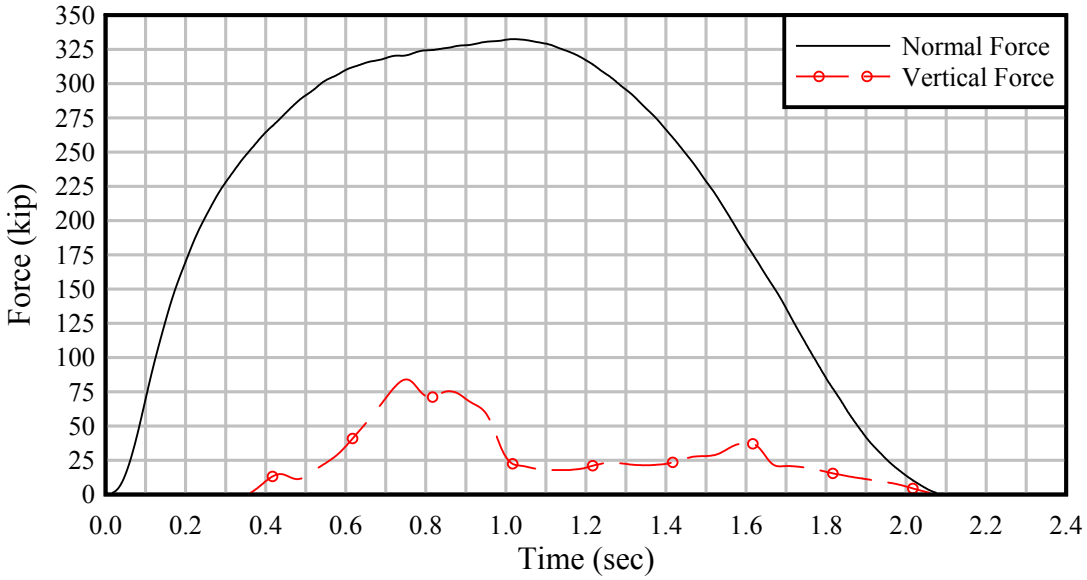

Figure B.26. 2x2 – 4 FPS – 25° – SSx2 – Flare

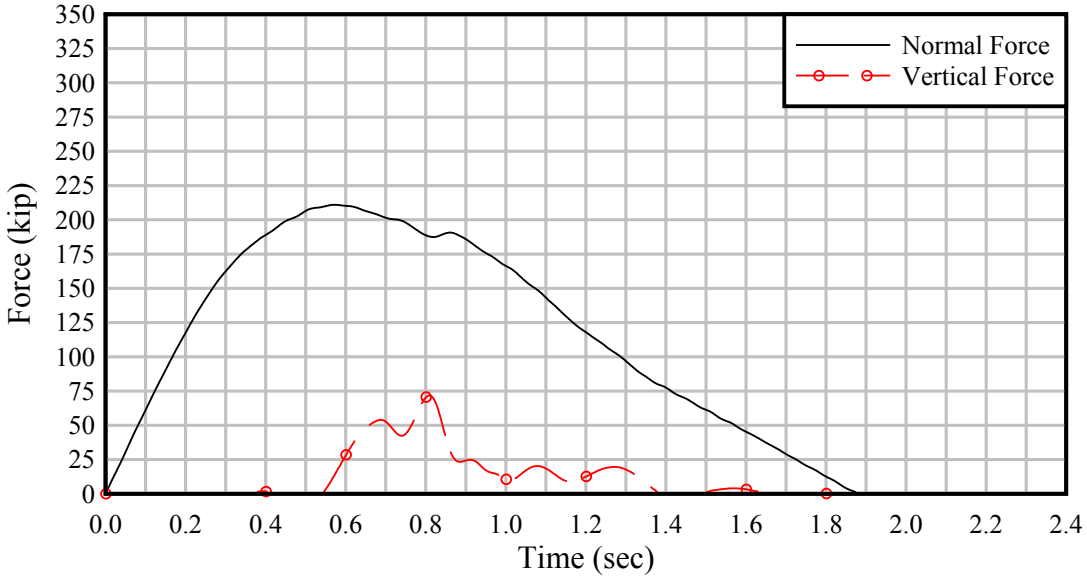

Figure B.27. 2x2 – 4 FPS – 15° – SSx2 – Flare

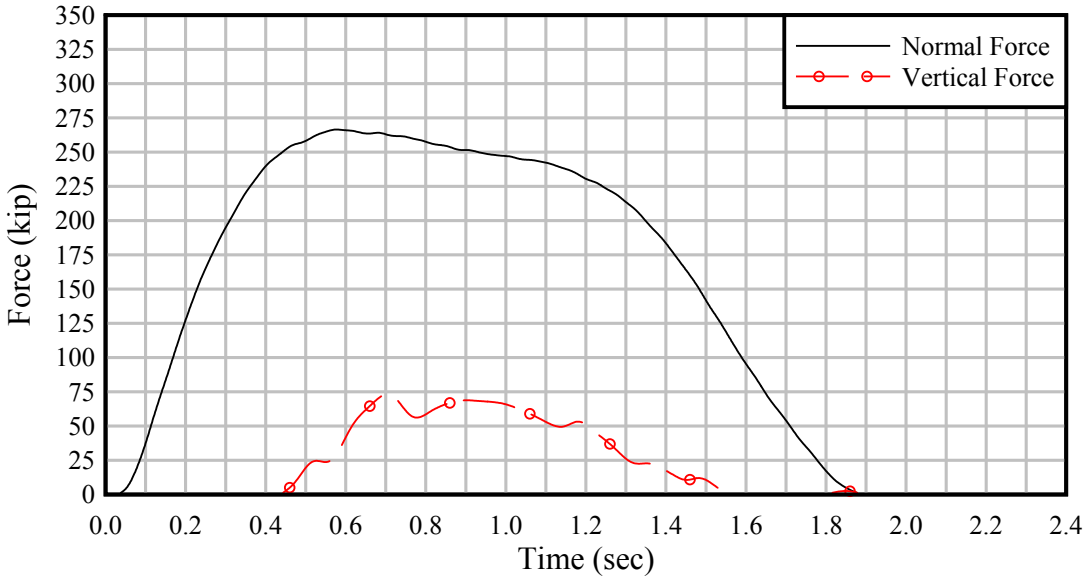

Figure B.28. 2x2 – 6 FPS – 15° – SSx2 – Flare

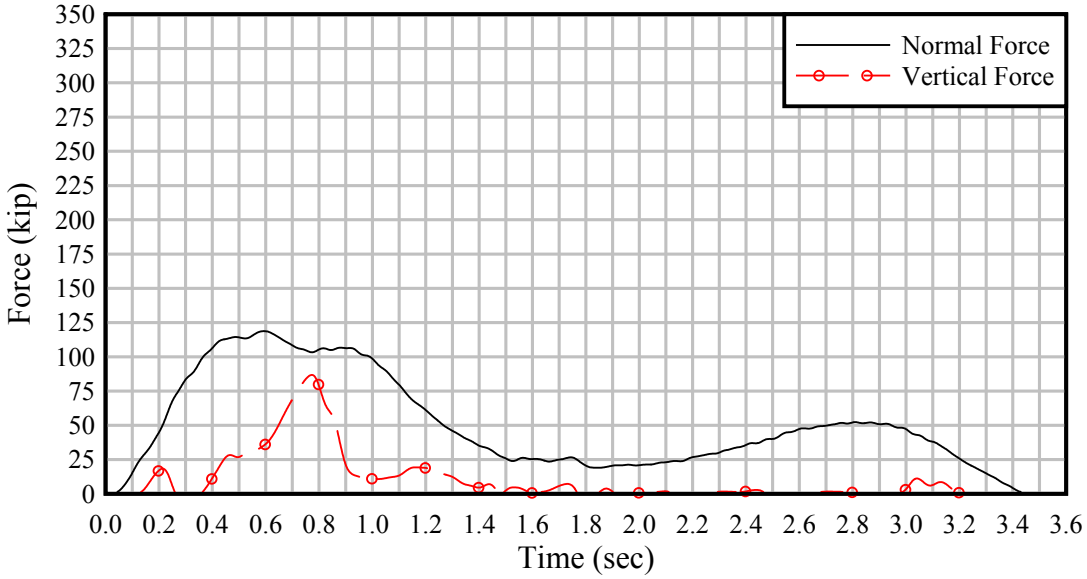

Figure B.29. 2x3 – 2 FPS – 15° – SSx2 – Wall

(Note: range of time-scale differs from previous plots)

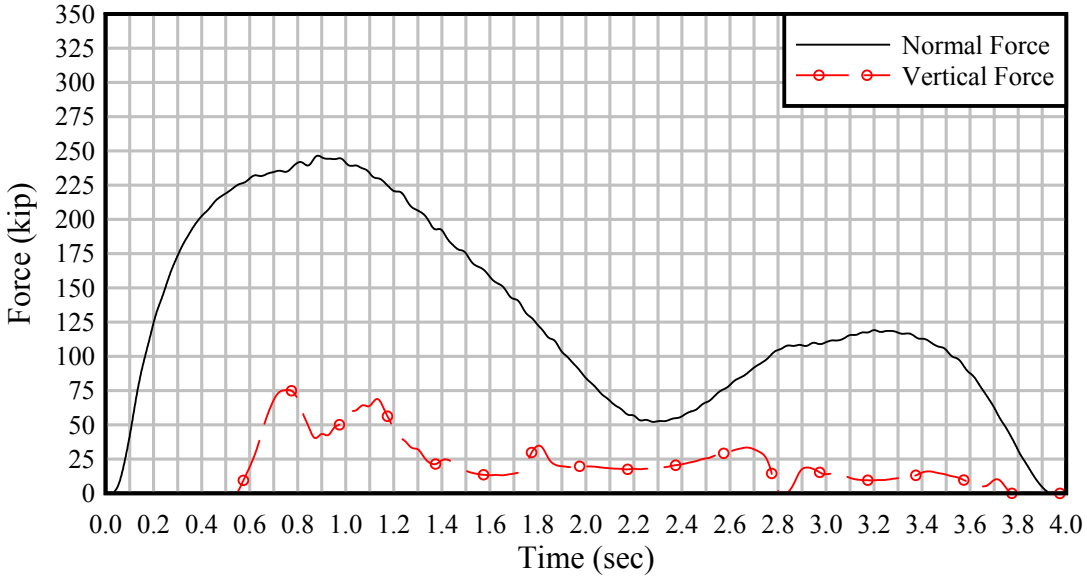

Figure B.30. 2x3 – 6 FPS – 15° – SSx1 – Wall

(Note: range of time-scale differs from previous plots)